ADENO-ASSOCIATED VIRUS 2 AS A VECTOR FOR DELIVERING CNTF AND SHRHOA TO THE VISUAL SYSTEM

by

JENNA TERI O'NEILL

A thesis submitted to the University of Birmingham for the degree of DOCTOR OF PHILOSOPHY

School of Clinical and Experimental Medicine
College of Medical and Dental Sciences
Institute of Biomedical Research (West)
University of Birmingham
September 2011

Abstract

Aims:

To fully characterise the RGC-5 cell line and determine whether it would be a suitable substitute for primary RGC cell culture. To optimise a CNTF Nogo-P4 inhibitory assay and establish whether (a) CNTF alone is capable of stimulating RGC neurite outgrowth and survival, or (b) an increase in intracellular cAMP is required for CNTF to be effective. To determine whether recombinant AAV2 viral constructs were capable of producing detectable levels of CNTF in HEK-293 transfected conditioned media. To optimise *AAV2-eGFP* delivery and establish whether *AAV2-CNTF-hrGFP* and *AAV2-CNTF-shRhoA-hrGFP* could promote RGC survival and regeneration after optic nerve crush surgery.

Methods:

The RGC-5 cell line was characterised using semi-quantitative PCR, sequencing and immunocytochemistry. RGC-5 cells were screened for a selection of neuronal, glial, progenitor, oligodendroglial lineages and cone photoreceptor cell markers to identify the cells origin. Retinal cultures were treated with recombinant CNTF and/or Forskolin to promote RGC neurite outgrowth and survival - this was quantified after 3 d. Retinal wholemounts were prepared to assess GFP transduction and survival after intravitreal delivery of *AAV2-eGFP*. Axonal regeneration and RGC survival were assessed through histological examination of optic nerves and retinal sections.

Results:

The RGC-5 cell line predominantly expressed oligodendroglial lineage markers and only weakly expressed ßIII-Tubulin mRNA. RGC-5 cells did not express mRNA for many of the phenotypic markers of RGC. CNTF was effective at stimulating RGC neurite outgrowth without the need for cAMP elevation - furthermore recombinant CNTF could disinhibit Nogo-P4 treated RGC in vitro. GFP transduction was low when injected alone, however, when administered with Pronase-E there was a significant increase in GFP expression. *AAV2-CNTF-hrGFP* and *AAV2-CNTF-shRhoA-hrGFP* did not promote RGC survival or regeneration 23 d post optic nerve crush.

Conclusions:

RGC-5 cells are not an appropriate substitute for primary retinal cell culture in vitro as they express many of the same markers as oligodendrocyte progenitors. CNTF is capable of stimulating RGC neurite outgrowth without an additional elevation of cAMP. AAV2-mediated GFP expression could be enhanced through the partial digestion of the inner limiting membrane - this seems to be the major obstacle in achieving optimal AAV2 transduction.

Acknowledgements

First and foremost I would like to thank my husband, Ben O'Neill, for his love and support throughout my PhD and write up — not to mention preparing copius amounts of tea.

I would also like to send a big thank you to all members of the Molecular Neuroscience Group (past and present) who have been there to discuss and troubleshoot with. Many thanks to Ann Logan, Martin Berry, Zubair Ahmed and Michael Douglas for their support and guidance throughout my PhD.

To Ruth Seabright and Barbara Lorber, you took the time to show me a variety of techniques and are some of the best scientists I've ever worked with. You were always happy to help and for that I am eternally grateful.

I'd like to offer my ~~condolences~~ thanks to Kevin Morrison, Steven Jacques and Samantha Prince for being extremely funny and great friends throughout my PhD. I will never forget some of our afternoon debates while waiting for experiments to run. I'd also like to thank Andy Thewles for introducing a whole new level of sarcasm to day to day life.

Finally, I'd like to thank Daljeet Bansal, Lisa Hill and everyone else from the Molecular Neuroscience Group for the support you've offered me over the past few years.

Eggs.

Dedication

In loving memory of Doris and Jack Carr

CONTENTS

List of Figures ix

List of Tables xii

List of Abbreviations xiii

1 General Introduction 1

1.1 Anatomy of the visual system 2

1.1.1 Organisation of the retina 2

1.2 RGC structure function and development 4

1.2.1 RGC cell fate 5

1.2.2 RGC morphology and classification 6

1.2.3 RGC receptive fields 7

1.2.4 Colour opponent RGC 8

1.3 Histology of the optic nerve 8

1.3.1 Anatomical differences between humans and rats 9

1.4 The ON as a model system to study CNS injury responses 10

1.4.1 The CNS injury response 12

1.5 Glia 14

1.5.1 Astrocytes 14

1.5.2 NG2 glia 14

1.5.3 Microglia 15
1.6 Why doesn't the mammalian CNS regenerate? 16
1.6.0.1 Myelin inhibitory ligands 16
1.6.0.2 Myelin inhibitory ligand receptors 21
1.6.1 The growth cone 23
1.6.2 Myelin inhibitory signalling cascade 25
1.6.3 Targeting the inhibitory signalling cascade 26
1.6.4 Chondroitin sulphate proteoglycans and the glial scar 29
1.7 Cell death 30
1.7.1 The extrinsic pathway 31
1.7.2 The intrinsic pathway 31
1.7.3 Regulators of apoptosis 33
1.8 Neurotrophins 33
1.8.1 Neurotrophin receptors 34
1.8.2 $p75^{NTF}$ and apoptosis 35
1.8.3 Neurotrophin signalling pathways 37
1.8.3.1 Ras/MAPK signalling 37
1.8.3.2 Phospholipase C 38
1.8.3.3 PI3K/Akt signalling 38
1.9 Cilliary neurotrophic factor 39
1.9.1 CNTF Receptor Complex 42
1.9.2 The JAK-STAT signalling pathway 42
1.10 Non-viral mediated gene transfer 43
1.10.1 Naked DNA 43
1.10.2 Electroporation and shotgun gene delivery 43

1.10.3 Cationic polymers . . . 45
1.11 Viral mediated gene transfer . . . 45
1.11.1 Adenoviruses . . . 46
1.11.2 Lentiviruses . . . 47
1.12 Structure of wild type adeno-associated virus . . . 48
1.13 The lytic pathway . . . 48
1.14 The lysogenic pathway . . . 49
1.15 Recombinant AAV virus as a gene delivery vector . . . 51
1.15.1 Advantages and disadvantages of using AAV as a viral vector . . . 53
1.16 RNA interference . . . 53
1.16.1 Mechanisms of RNA interference . . . 55

2 Materials and Methods 56

2.1 *In vitro* Techniques . . . 57
2.1.1 Retinal culture . . . 57
2.1.1.1 Retinal culture quantification . . . 58
2.1.2 RGC-5 cell culture . . . 59
2.1.2.1 Morphological analysis of RGC-5 cells . . . 59
2.1.3 Immunocytochemistry and Immunohistochemistry . . . 60
2.1.3.1 Immunocytochemistry . . . 60
2.1.3.2 Immunohistochemistry . . . 61
2.1.3.3 Antibodies . . . 62
2.1.4 Haematoxylin and Eosin staining of frozen retinal sections . . . 63
2.1.5 AAV2 constructs . . . 64
2.1.6 Lipofectamine 2000 Transfection . . . 65
2.1.7 Enzyme linked immunosorbent assay . . . 66

2.1.8 Cell viability assay 68
2.1.9 RNA extraction 70
2.1.9.1 RGC-5 cell RNA extraction 70
2.1.9.2 Mouse brain RNA extraction 71
2.1.9.3 Mouse eye RNA extraction 71
2.1.10 RNA quantification 71
2.1.11 cDNA Libraries 72
2.1.12 Primer Design 73
2.1.13 Semi-quantitative PCR and densitometry 76
2.1.13.1 Densitometry 77
2.1.14 Sample preparation for sequencing 79
2.1.14.1 Gel extraction 79
2.1.14.2 DNA quantification 80
2.1.14.3 Sample preparation 80
2.1.14.4 Sequencing 81
2.2 *In vivo* techniques 82
2.2.1 Animal surgery 82
2.2.1.1 Optic nerve crush 82
2.2.2 Intravitreal injections 83
2.2.3 *AAV2-CNTF-hrGFP*, *AAV2-eGFP* and *AAV2-CNTF-shRhoA-hrGFP* delivery and RGC survival counts 83
2.2.4 Tissue Preparation for Histology 84
2.2.5 Retinal wholemount counts 85
2.2.6 Retinal ganglion cell transduction 85
2.2.7 Quantification of RGC axon regeneration *in vivo* 87
2.2.8 Statistical Analysis 90

3 Characterisation of the RGC-5 Cell Line **91**

3.1 The use of cell lines in biological research 92

3.2 RGC-5 cell line 92

3.3 Aims 94

3.4 Results 94

3.4.1 Staurosporine treatment induces process extension 95

3.4.2 The impact of Staurosporine treatment on process number . . . 99

3.4.3 Process branching is dose dependent 100

3.4.4 RGC-5 cell viability assay after Staurosporine treatment 102

3.4.5 Representative images of the Staurosporine dose response experiment 104

3.5 The RGC-5 cell line is derived from *Mus musculus* and not *Rattus norvegicus* 107

3.5.1 New aims 107

3.5.2 Primer Optimisation 112

3.5.3 Determining the exponential phase of the PCR reaction 114

3.5.3.1 Neuronal marker expression 114

3.5.3.2 Expression of glial markers 114

3.5.3.3 Developmental Marker Expression 115

3.5.4 RGC-5 cells are derived from the oligodendroglial lineage 117

3.5.5 RGC-5 cells are not derived from cone photoreceptors 120

3.5.6 Densitometry 121

3.6 Discussion 123

3.6.1 Morphological analysis of Staurosporine treated RGC-5 cells . . . 123

3.6.2 RGC-5 sequencing 127

3.6.3 RGC-5 expression profile 127

3.7 Conclusions 130

4 *In vitro* Effects of CNTF in Primary Retinal Culture 131

4.1 Testing the effectiveness of CNTF in primary retinal culture 132

4.2 Aims 133

4.3 Results 134

4.3.1 Primary retinal cultures 134

4.3.2 Forskolin and recombinant CNTF promotes retinal ganglion cell neurite outgrowth *in vitro* 136

4.3.3 CNTF and Forskolin treatment has a minimal affect on neurite number 139

4.3.4 10 ng ml^{-1} and 50 ng ml^{-1} CNTF caused minor toxicity 141

4.3.5 100 ng ml^{-1} CNTF increases neurite number and abolishes the Nogo-P4 induced inhibitory effect 144

4.3.6 100 ng ml^{-1} CNTF disinhibits Nogo-P4 treated retinal ganglion cells 146

4.3.7 Nogo-P4 treatment had no effect on RGC survival 149

4.3.8 Summary of results 151

4.4 Discussion 152

4.4.1 Forskolin was effective at stimulating RGC neurite outgrowth when administered alone or in combination with a low dose of CNTF . . 152

4.4.2 100 ng ml^{-1} CNTF significantly increased mean neurite length . . 154

4.4.3 Treatment with Forskolin led a to a small reduction in RGC number 156

4.4.4 CNTF and Forskolin had a minimal effect on mean neurite number 156

4.4.5 25 µM Nogo-P4 peptide significantly inhibited RGC neurite outgrowth 157

4.4.6 Treatment with 25 µM Nogo-P4 peptide had no impact on RGC survival 158

4.4.7 Treatment with 100 ng ml^{-1} CNTF disinhibited Nogo-P4 peptide treated RGC 158

4.5 Conclusions 158

5 AAV2 as a Vector for Delivering CNTF to the Visual System 160

5.1 Introduction . . . 161

5.1.1 Barriers to AAV2 transduction . . . 162

5.2 Hypothesis . . . 166

5.3 Aims . . . 166

5.4 Results . . . 166

5.4.1 Design and validation of shRhoA containing constructs . . . 166

5.4.2 HEK-293 cells transfected with *AAV2-CNTF-hrGFP*, *AAV2-CNTF-shRhoA-hrGFP* and *AAV2-CNTF-FLAG* produced detectable levels of CNTF . 167

5.4.3 Co-injection with 0.0002% Pronase-E significantly enhanced *AAV2-eGFP* transduction, but caused some cell death . . . 169

5.4.4 RGC survival was not enhanced by *AAV2-CNTF-hrGFP* + Pronase-E or *AAV2-CNTF-shRhoA-hrGFP* + Pronase-E treatment . . . 172

5.4.5 *AAV2-CNTF-hrGFP* and *CNTF-shRhoA* did not promote extensive RGC axonal regeneration . . . 175

5.5 Discussion . . . 181

5.5.1 Conditioned media collected from *AAV2-CNTF-hrGFP*, *AAV2-CNTF-shRhoA-hrGFP* and *AAV2-CNTF-FLAG* transfected HEK-293 cells contained detectable levels of CNTF . . . 181

5.5.2 *AAV2-eGFP* + Pronase-E significantly enhanced *AAV2-eGFP* transduction . . . 181

5.5.3 *AAV2-eGFP* + Pronase-E significantly reduced RGC number in retinal wholemount preparations . . . 182

5.5.4 *AAV2-CNTF-hrGFP* and *AAV2-CNTF-shRhoA-hrGFP* did not promote extensive axonal regeneration . . . 184

5.5.5 *AAV2-CNTF-hrGFP* and *AAV2-CNTF-shRhoA-hrGFP* did not protect RGC from cell death . . . 185

5.6 Conclusions . . . 185

6 General Discussion 186

6.1 Main Findings and Future Work . . . 187

6.1.1 Viral Delivery 188
6.2 Conclusions 190

References **191**

Appendices **205**

A Characterisation of the RGC-5 Cell Line **205**

LIST OF FIGURES

1.1 Organisation of the retina 3

1.2 Diagrammatic representation of the optic nerve 9

1.3 Diagrammatic representation of the ON crush model 11

1.4 Diagramatic representation of MAG structure 17

1.5 Structure of OMgp 19

1.6 Structural arrangement of Nogo-A, Nogo-B and Nogo-C 20

1.7 Growth cone structure 24

1.8 Inhibitory signalling diagram 27

1.9 Diagrammatic representation of the intrinsic and extrinsic apoptotic signalling pathways 32

1.10 Neurotrophic factor signalling through Trk receptors 36

1.11 Structure of wild type AAV 50

1.12 Recombinant AAV virus 52

2.1 Diagrammatic representation of sampling technique 59

2.2 *pAAV-IRES-hrGFP* expression plasmid supplied in the AAV Helper Free System 65

2.3 Example of how the exponential phase of the PCR reaction was determined 78

2.4 Image illustrating the sampling technique used to calculate RGC survival and GFP transduction efficiency 86

2.5 Quantification of RGC axon regeneration 89

3.1 Staurosporine treatment induces process extension 97

3.2 Process number after Staurosporine dose response 99

3.3 Process branching is dose dependent 101

3.4 RGC-5 cell viability assay 103

3.5 Representative images of Staurosporine dose response experiment . . . 105

3.6 Rat CNTF primers do not anneal to RGC-5 cDNA 110

3.7 NG2 and CD44 PCR products and sequence alignments 111

3.8 Optimisation of annealing temperature 113

3.9 Semi-quantitative PCR analysis of selected neuronal, glial and progenitor cell mRNA markers in RGC-5 cells 116

3.10 Semi-quantitative PCR shows that RGC-5 cells express markers of the oligodendroglial lineage 118

3.11 Immunocytochenistry shows that RGC-5 cells express markers of the oligodendroglial lineage 119

3.12 RGC-5 cells are not derived from cone photoreceptor cells 120

3.13 Densitometric analysis of PCR products 122

4.1 Representative bright field images of control primary retinal cultures . . . 135

4.2 CNTF and Forskolin promotes neurite outgrowth *in vitro* 138

4.3 CNTF and Forskolin had a minimal affect on neurite number 140

4.4 Minor cytotoxicity was seen after treatment with 15 µM Forskolin compared to untreated controls 142

4.5 CNTF dose response experiment 143

4.6 100 ng CNTF increased neurite number and abolished the Nogo-P4 induced inhibitory effect 145

4.7 Effect of CNTF on Nogo-P4 treated primary retinal culture. 147

4.8 Nogo-P4 treatment had no effect on RGC survival 149

4.9 Nogo-P4 inhibitory assay 150

5.1 Localisation of Cy3-labelled AAV2 particles at the ILM of the retina 163

5.2 Pronase-E punches holes in the ILM of the retina 164

5.3 Design and validation of shRhoA containing constructs 167

5.4 CNTF ELISA on HEK-293 Conditioned Media 168

5.5 *AAV2-eGFP* transduction 170

5.6 *AAV2-eGFP* transduction representative wholemount images 171

5.7 RGC survival was not enhanced by *AAV2-CNTF-hrGFP* or *AAV2-CNTF-sRhoA* treatment 173

5.8 Representative images of H&E stained retinal sections 174

5.9 Quantification of RGC axon regeneration 177

5.10 Intravitreal injection of *AAV2-eGFP* + 0.0002% Pronase-E did not promote RGC axon regeneration 23 d post-ONC 178

5.11 Intravitreal injection of *AAV2-CNTF* + 0.0002% Pronase-E did not promote RGC axon regeneration 23 d post-ONC 179

5.12 Intravitreal injection of *AAV2-CNTF-shRhoA* + 0.0002% Pronase-E did not promote RGC axon regeneration 23 d post-ONC 180

A.1 RGC-5 neuronal marker expression 206

A.2 RGC-5 glial marker expression 207

A.3 RGC-5 developmental marker expression 208

A.4 RGC-5 oligodendroglial lineage marker expression 209

A.5 Blue-sensitive opsin expression 210

LIST OF TABLES

2.1 Immunocytochemistry / immunohistochemistry reagents. 62

2.2 Antibody details for immunocytochemistry and immunohistochemsitry. . 62

2.3 Reagents for CNTF ELISA. 68

2.4 2 x RT master mix (100 µl reaction volume). 72

2.5 Thermal cycler settings used for reverse transcription. 73

2.6 RGC-5 primer list. 74

2.7 PCR reaction volumes. 76

2.8 PCR thermal cycler settings. 76

2.9 PCR reaction volumes used to prepare samples for sequencing. 79

2.10 Sample preparation. 81

LIST OF ABBREVIATIONS

AAV	Adeno-associated virus
Ad	Adenoviruses
AIF	Apoptosis inducing factor
ANOVA	Analysis of variance
AP-1	Activator protein-1
ATCC	American Type Culture Collection
BDNF	Brain derived neurotrophic factor
Brn-3	Brain-3
C-domain	Central domain
C.elegans	Caenorhabditis elegans
CaMK	Calmodulin-dependent protein kinases
cAMP	Cyclic adenosine monophosphate
cDNA	Complementary DNA
ChaT	Choline acetyltransferase
CLC	Cardiotrophin like cytokine
CNS	Central nervous system
CNTF	Cilliary neurotrophic factor
CNTFRα	CNTFα receptor
CR3	Complement type 3 receptor
CREB	cAMP responsive binding element binding protein
CSPG	Chondroitin sulphate proteoglycan

CSPGs	Chondroitin sulphate proteoglycans
CT-1	Cardiotrophin-1
DAG	Diaglycerol
DAPI	4’,6-diamidino-2-phenylindole
DIABLO	Direct inhibitor of apoptosis binding protein with low PI
DMEM	Dulbecco's Modified Eagle Medium
DMSO	Dimethyl Sulfoxide
DNA	Deoxyribonucleic acid
DNase I	deoxyribonuclease I
dpi	Days post-injury
DREZ	Dorsal root entry zone
dsRNA	double-stranded RNA
EBSS	Earle's Balanced Salt Solution
ELAV	Equine infectious anaemia virus
ELISA	Enzyme-linked immunosorbent assay
EtBr	Ethidium bromide
F-actin	Filamentous-actin
FBS	Foetal bovine serum
FG	Flourogold
FG+	Flourogold positive
FGF2	Fibroblast growth factor 2
FIV	Feline immunodeficiency virus
GAG	Glycosaminoglycan chain
GAP	GTPase-activating protein
GAP-43	Growth-associated protein-43
GAPDH	Glyceraldehyde 3-phosphate dehydrogenase
GCL	Ganglion cell layer
GDI	GDP dissociation inhibitors

GDP	Guanosine diphosphate
GEF	Guanine nucleotide-exchange factor
GFAP	Glial fibrillary acidic protein
GFP	Green fluorescent protein
GPCR	G protein coupled receptors
GPI	Glycosyl phosphatidylinositol
Grb2	Growth factor receptor binding protein 2
H&E	Haematoxylin and eosin
HEK-293	Human embryonic kidney 293 cells
HIV	Human immunodeficiency virus
HSPG	Heparin sulphate proteoglycan
HSV	Herpes simplex virus
HtrA2	High-temperature requirement protein A2
IAP	Inhibitor of apoptosis
Ig	Immunoglobulin
IHC	Immunohistochemistry
IL-11	Interleukin-11
IL-6	Interleukin-6
INL	Inner nuclear layer
IP3	Inosital-trisphosphate
IPL	Inner plexiform layer
IRES	Internal ribosome entry site
ITR	Inverted terminal repeats
JAK	Janus-kinase
JAK-2	Janus-kinase 2
K252a	9,12-epoxy-1H-diindolo[1,2,3-fg:3',2',1'-kl]pyrrolo[3,4-i][1,6]benzodiazocine-10-carboxylic acid, 2,3,9,10,11,12-hexahydro-10-hydroxy-9-methyl-1-oxo-, methyl ester, (9S,10R,12R)-

K252b	(5R,6S,8S)-6-hydroxy-5-methyl-13-oxo-6,7,8,13,14,15-hexahydro-5H-16-oxa-4b,8a,14-triaza-5,8-methanodibenzo[b,h]cycloocta[jkl]cyclopenta[e]-as-indacene-6-carboxylic acid
K252c	Staurosporine aglycone
L-MAG	Large MAG
LCA	Leukocyte common antigen
LGN	Lateral geniculate nucleus
LIF	Leukemia inhibitory factor
LIFRβ	Leukemia inhibitory factor receptor β
Lingo-1	Leucine rich repeat and Ig domain containing 1
LRR	Leucine rich repeat
LV	Lentivirus
MAG	Myelin associated glycoprotein
MAP2	Microtubule-associated protein 2
MAPK	Mitogen-activated protein kinase
MEK	Map kinase kinase
MHC I	Major histocompatibilty complex I
MHC II	Major histocompatibilty complex II
MIL	Myelin inhibitory ligand
MMPs	Matrix metalloproteases
mRNA	Messenger RNA
NDPase	Nucleoside diphosphatase
NFL	Nerve fibre layer
NG2	Neuron-glial antigen 2
NGF	Nerve growth factor
NgR	Nogo receptor
NMDA-R1	*N*-Methyl-D-aspartic acid
Nogo	Neurite outgrowth inhibitor
NP	Neuropoietin

NT3	Neurotrophin 3
NT4	Neurotrophin 4
NT5	Neurotrophin 5
Olig-1	Oligodendrocyte transcription factor-1
Olig-2	Oligodendrocyte transcription factor-2
OMgp	Oligodendrocyte myelin glycoprotein
ON	Optic nerve
ONC	Optic nerve crush
ONL	Outer nuclear layer
OPL	Outer plexiform layer
OSM	Oncostatin M
P-domain	Peripheral domain
P/S	Penicillin/streptomycin
$p75^{NTR}$	Low-affinity p75 neurotrophin receptor
PAX-6	Paired box gene-6
PBS	Phosphate buffered saline
PFA	Paraformaldehyde
PI3K	Phosphoinositide 3-kinases
PIP2	Phosphatidylinositol-4,5-bisphosphate
PKA	Protein kinase A
PKC	Protein kinase C
PKC-412	4'-N-benzoylstaurosporine
PKG	Protein kinase G
PLC	Phospholipase C
PN	Peripheral nerve
ppNGF	prepro-Nerve growth factor
RGC	Retinal ganglion cells
RISC	RNA-induced silencing complex

RNAi	RNA interference
ROCK	Rho-associated kinase
RPF-1	POU-domain factor-1
RT	Room temperature
S-MAG	Small MAG
SC	Superior colliculus
SEM	Standard error of the mean
SHC	SH2 containing protein
Shh	Sonic hedgehog
siRNA	Short-interfering RNA
SIV	Simian immunodeficiency virus
Smac	Second mitochondria-derived activator of caspase
SOS	Son of sevenless
SOX-1	Sex determining region Y box-1
STAT	Signal-transducer and activator of transcription
STAT1	Signal transducers and activators of transcription 1
STAT3	Signal transducers and activators of transcription 3
T-domain	Transition domain
TGFβ	Transforming growth factor beta
Thy-1	Thymocyte differentiation antigen 1
TIMP	Tissue inhibitors of MMP
TNF	Tumour necrosis factor
Trk	Tropomyosin receptor kinase
TrkA	Tropomyosin receptor kinase A
TrkB	Tropomyosin receptor kinase B
TrkC	Tropomyosin receptor kinase C
Troy	Tumour necrosis factor receptor 19
UCN-01	7-hydroxystaurosporine

CHAPTER 1

GENERAL INTRODUCTION

1.1 Anatomy of the visual system

The visual system has a single population of neurons within the retina (Retinal ganglion cells) that extend their axons to form the optic nerves. The optic nerve (ON) decussates at the optic chiasm to form the optic tracts which synapses at the lateral geniculate nucleus (LGN) and superior colliculus (SC) (Berry, et al. 2008). Visual information is directed from these structures to the visual neocortex for processesing, the motor nuclei in the brain stem and cord for visually guided movement and the accessory oculomotor nucleus for accommodation reflexes (Berry et al. 2008). Interestingly, not all axons in the ON originate from retinal ganglion cells (RGC). A small subpopulation of retinopetal axons originate from peptidernergic neurons in the hypothalamus (and other limbic structures) and terminate in the retina (Vereczki, et al. 2006).

1.1.1 Organisation of the retina

The retina is a highly organised structure which can be described in terms of its layers (see figure 1.1). The ganglion cell layer (GCL) contains the cell bodies of RGC, and their unmyelinated axons make up the nerve fibre layer (NFL) — this layer is also occupied by astrocytes which become re-active after injury (Berry et al. 2008). The NFL layer is isolated from the vitreous by an inner limiting membrane which is composed primarily of basal lamina, plus Müller cell and astrocyte end feet (Berry et al. 2008). The inner nuclear layer (INL) contains the cell bodies of amacrine, horizontal, bipolar and Müller cells, whilst the outer nuclear layer (ONL) contains the cell bodies of both rods and cones (Berry et al. 2008). The ratio of rods to cones varies within the retina — there is a higher

ratio of rods to cones in the periphery as well as a higher proportion of photoreceptors to ganglion cells. At the back of the retina there is a layer of retinal pigmented epithelium which acts as a protective barrier and prevents the reflection of light striking the back of the retina to maintain image integrity. Synaptic connections between interneurons occur in the inner plexiform and outer plexiform layers (Berry et al. 2008).

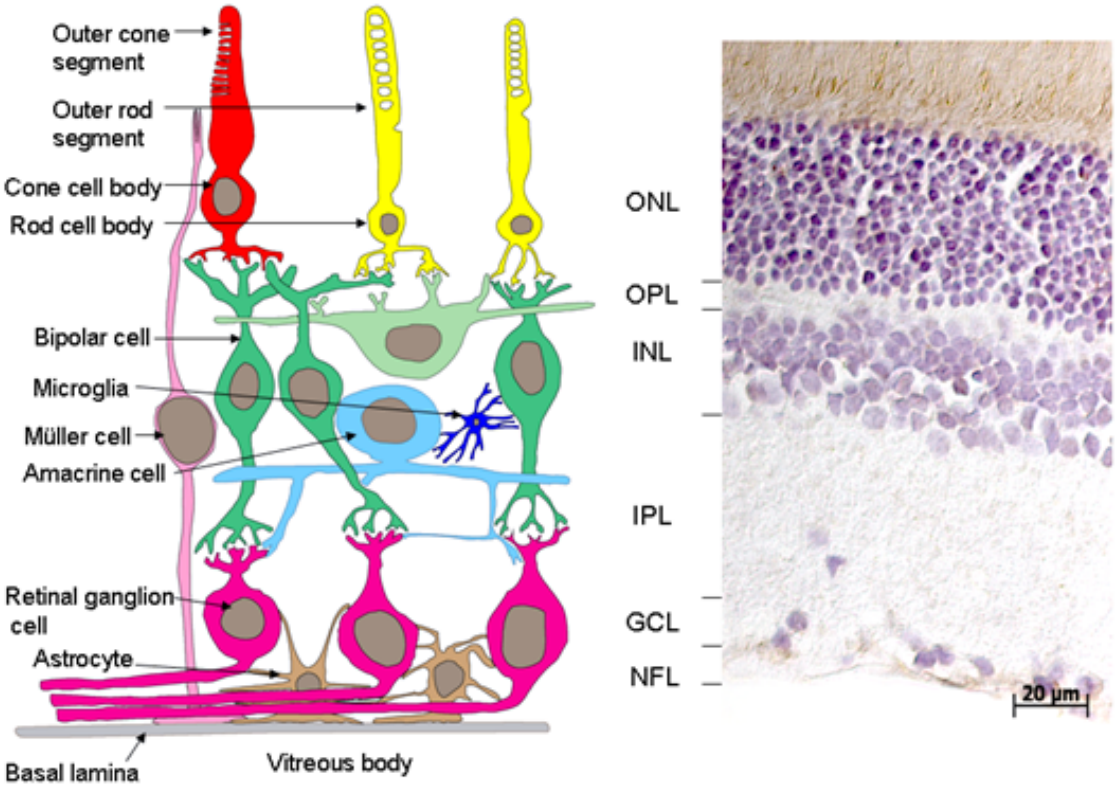

Figure 1.1: Organisation of the retina. The retina is a highly organised structure which can be described in terms of its layers. RGC lie within the GCL and their unmyelinated axons lie within the NFL. This layer also contains astrocytes which become reactive after injury. The NFL is separated from the vitreous by the inner limiting membrane. Bipolar, amacrine and horizontal cells reside within the INL. Rod and cone photoreceptors occupy the ONL. Synaptic connections between interneurons occur in the inner plexiform layer (IPL) and outer plexiform layer (OPL). (Reproduced with permission from Prof. Ann Logan) (Berry et al. 2008).

1.2 RGC structure function and development

The ON and eye are highly specialised central nervous system (CNS) structures which are formed from the neural tube. Eye development in vertebrates is characterised by bilateral evagination of the diencephalon (optic vesicle). The optic vesicle then makes contact with the surface ectoderm and folds back on its self to form the optic cup. The thin outer region of the optic cup forms the retinal pigmented epithelium whilst the inner region forms the retina (Chow & Lang 2001).

In the retina, cell differentiation from retinal precursors occurs in the inner layer of the optic cup and gradually expands out towards the peripheral edge of the retina. Cell differentiation from retinal precursors tends to occur in a very specific order. In the rat generation of all the major cell types commences between Embryonic day 14 and 20 (E14-E20) (Reese & Colello 1992).

RGC differentiation commences at around E14, these cells then migrate towards the inner limiting membrane (ILM) of the retina to form the GCL (Werner & Chalupa 2004). Amacrine cells emerge shortly afterwards, although this process overlaps considerably with RGC neurogenesis and does not occur sequentially (Reese & Colello 1992). At this point, synaptic connections are established between the RGC and amacrine cells to form the IPL of the retina (Werner & Chalupa 2004). Cone photoreceptors migrate at this point, but do not differentiate until much later (Werner & Chalupa 2004). This is immediately followed by the generation and differentiation of bipolar cells and Müller glia (Werner & Chalupa 2004). At this stage, cone and rod photoreceptors of the ONL mature

and form synaptic connections with bipolar and horizontal cells in the OPL (Werner & Chalupa 2004).

1.2.1 RGC cell fate

For the most part, the way in which cell fate is determined remains unclear — however, there are some studies which have provided insight. Progenitor cells which are destined to become RGC express transcription factors such as brain-3 (Brn-3) and retina derived POU-domain factor-1 (RPF-1) (Wang & Kim 2001). Sonic hedgehog (Shh) also appears to be an important determinant of RGC cell fate – as its expression leads to the generation and differentiation of new RGC (Isenmann & Kretz 2003). Furthermore, Shh has been shown to regulate paired box gene-6 (PAX-6) (a gene which plays a pivotal role in eye development) gene expression, for example, downregulation of PAX-6 directs retinal progenitors towards an amacrine cell fate whilst overexpression of PAX-6 increases the rate of RGC differentiation and decreases photoreceptor cell number (Isenmann & Kretz 2003).

Like many other neuronal populations, once differentiated, RGC loose the property of self renewal and can't be replaced after death. Newly established RGC extend their axons through the ON, decussate at the optic chiasm and continues on through the optic tracts to make contact with their midbrain targets (e.g. LGN and SC) (Berry et al. 2008).

1.2.2 RGC morphology and classification

RGC can be sorted into subcategories based on their dendritic morphology, dendritic field, cell size and location of dendritic arborisation. In 1974 Boycott and Wassle proposed a classification system for the cat. RGC of the cat were subdivided into alpha, beta, gamma and delta types based on their size and morphology (Boycott & Wassle 1974). Alpha cells have large cell bodies and wide dendritic fields, making up approximately 3% of cat RGC (Kolb 1981). In the centre of the retina the density of alpha cell bodies is high and the dendritic field is small, whilst in the periphery the reverse is true (Wassle 2004). Alpha cells are not confined to the retina of cats, they can also be found in a variety of mammals (rats, ferrets, guinea pigs, mice and ox) cited in (Wassle 2004). Beta cells have small dendritic fields making up approximately 50% of cat RGC (Kolb 1981).

Another commonly used classification system for the cat was based on their physiological responses to visual stimuli (Y, X and W types). Since then it's been found that there was a correlation between alpha, beta, gamma and delta morphologies with Y, X and W type physiological responses (Bear, et al. 2001). There are two additional classifications which should also be mentioned, namely M-type (or Midget RGC) and P-type ganglion cells (or Parasol RGC). These ganglion cell subtypes have been identified in the monkey and human retina (Bear et al. 2001). M-type RGC are thought to be the human equivalent of cat alpha cells and P-type RGC are thought to be the human equivalent of cat beta cells(Wassle 2004). M-type RGC are typically larger and account for approximately 5% of the total ganglion cell population, whilst P-type RGC are significantly smaller making up the majority (≈90%), of the total cell population (Bear et al. 2001). The remaining 5% of

ganglion cells are made up of a completely different class of ganglion cells (non-M and non-P subtypes) (Bear et al. 2001).

The functional properties of each of these subtypes differs considerably, for example, M-type RGC have larger receptive fields, propagate action potentials more rapidly and are sensitive to low contrast stimuli (Bear et al. 2001). Furthermore, stimulation of their receptive fields induces a transient burst of action potentials (Bear et al. 2001). In contrast stimulation of P-type RGC leads to the sustained firing of action potentials – in fact this period of sustained activity continues until the stimulus has ceased (Bear et al. 2001). As a result, M-type RGC are thought to be important in terms of detection of movement, whilst P-type RGC are more important in terms of visual acuity (Bear et al. 2001).

1.2.3 RGC receptive fields

RGC can be further categorised based on their branching location, for example RGCs which branch at different depths of the sublamina. The sublamina of the retina can be divided into (A) RGC with ON receptive fields and (B) RGC with OFF centre receptive fields (Nelson & Famiglietti 1978). A receptive field is an area of retina that can be stimulated to fire action potentials (through changes in RGC membrane potential) in response to light (Bear et al. 2001). ON-centre RGC fire action potentials when light strikes the centre of their receptive fields, whereas OFF-centre RGC are activated when a shadow falls on the centre of its receptive field (Bear et al. 2001). The majority of RGC in the retina display this property and have either ON or OFF centre receptive fields. The way in which this characteristic distribution is established is believed to occur through cell death. Axons

compete for a limited number of trophic factors at their designated post-synaptic targets – those which receive more trophic support typically survive and those that are outcompeted die through apoptotic mechanisms (Sernagor & Eglen 2001). The overall purpose of this type of configuration is so that RGC can respond to changes in light intensity.

1.2.4 Colour opponent RGC

A small population of RGC are also sensitive to specific wavelengths of light, namely colour opponent RGC. This means that the response to one wavelength (e.g. red), striking the centre of the receptive field can be cancelled out by the response of another (e.g. green), striking the perimeter of the receptive field (Bear et al. 2001). The central region of RGC receptive field receives inputs from mainly red cones, whilst the periphery receives inputs from green cones – therefore the response to red wavelengths can only be cancelled out by the response of green wavelengths (Bear et al. 2001). This type of configuration is typically seen in P-type RGC, whereas blue/yellow colour opponency is often found in non-M non-P type RGC (which works the same way). M-type RGC do not exhibit this property, since the centre and periphery of the receptive field are fed into by multiple types of cones (Bear et al. 2001).

1.3 Histology of the optic nerve

The ON is occupied by four types of glia, namely: oligodendrocytes, astrocytes, microglia and neuron-glial antigen 2 (NG2) glia. Within the retina RGC axons are unmyelinated,

upon entering the lamina cribrosa these axons are myelinated by resident oligodendrocytes. RGC axons are separated by rows of myelinating oligodendrocytes (Berry et al. 2008). These rows are occasionally interrupted by astrocytes, NG2 glia or microglia (Berry et al. 2008).

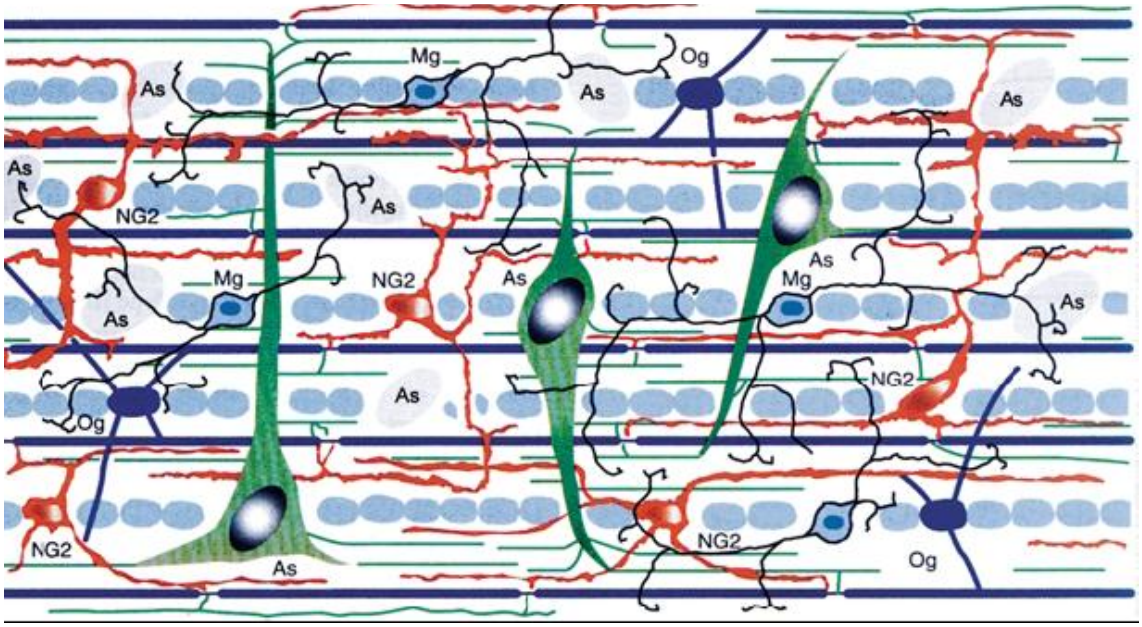

Figure 1.2: Diagrammatic Representation of the ON. The ON is predominantly composed of myelinated RGC axons. These axons are separated by rows of myelinating oligodendrocytes. These rows are occasionally interrupted by astrocytes, NG2 glia and microglia. This diagram reproduced with permission from Prof. Ann Logan (University of Birmingham) (Berry et al. 2008).

1.3.1 Anatomical differences between humans and rats

In animals with monocular visual fields, i.e. rats, 90% of RGC axons decussate at the chiasm — whereas in mammals with stereoscopic vision, i.e. humans, 60% of fibres project contralaterally to the visual cortex (Berry et al. 2008). In rats the retinal artery runs through the dural sheath, as such we can fully transect the ON whilst maintaining the retinal blood supply.

1.4 The ON as a model system to study CNS injury responses

The ON can be used as a model to study the cellular and molecular mechanisms underlying neuro-regenerative failure. The anatomical simplicity and accessibility of the ON allows us to dissect out basic mechanisms which inhibit or promote axon growth within the CNS as a whole. With this model it is possible to completely transect RGC axonal projections from their target cells. As the eye is a relatively enclosed system, specific cells can be targeted and drug dose can be regulated more effectively. Axon regeneration can be assessed by intravitreal injection of anterograde tracers e.g. cholera toxin or through growth-associated protein-43 (GAP-43) immunohistochemistry (IHC) (Berry et al. 2008). Retrograde tracers e.g. Fluorogold, can be injected proximal to the crush to assess RGC survival through the use of retinal wholemount preparations. Furthermore, functional recovery can be assessed through the measurement of visually evoked potentials, pupillary reflexes and visually guided behaviour (Berry et al. 2008).

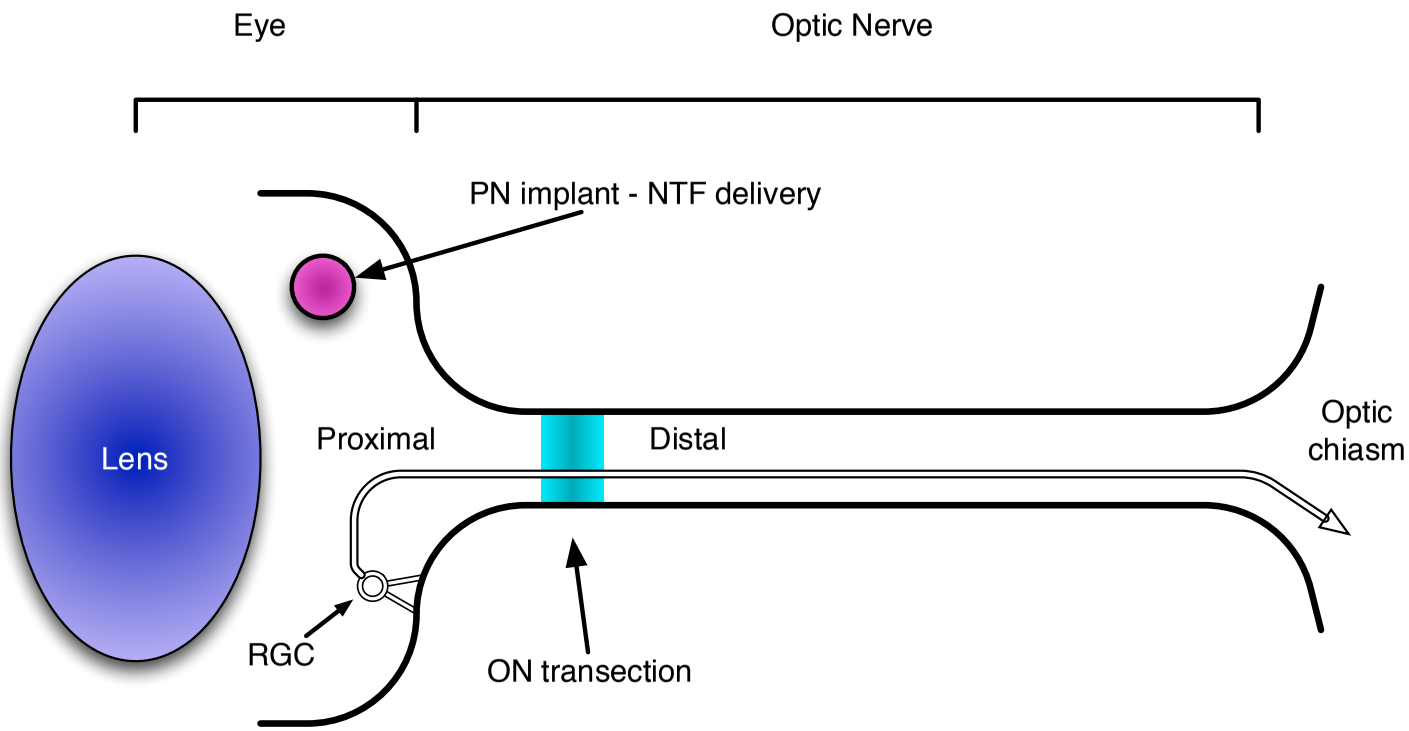

Figure 1.3: Diagrammatic Representation of the ON Crush Model. The ON is crushed ≈2 mm distal to the optic disc, transecting all RGC axons. Therapeutics (NTFs, siRNAs, viruses) are delivered to RGC somata by intravitreal injection. Alternatively, segments of peripheral nerve (PN) can be implanted in to the vitreous through an incision in the caudal surface of the eye. Schwann cells present within these PN segments secrete NTFs to promote RGC survival and axonal regeneration. Injection of retrograde tracers proximal to the crush site labels all surviving RGC, whilst injection distal to the crush site labels all regenerating axons. Diagram reproduced with permission from Prof. Ann Logan (University of Birmingham) (Berry et al. 2008).

1.4.1 The CNS injury response

The extent of CNS damage can vary depending on the type of injury, the spread of damage and the extent of secondary reactions. CNS injuries typically sever axons, damage myelin sheaths and blood vessels and can cause catastrophic damage to the CNS through both primary and secondary reactions. It is also important to note that cellular responses can vary depending on damage location and developmental age.

The primary responses to CNS injuries are typically initiated by mechanical damage and lead to apoptosis and necrosis of cells in the immediate vicinity, for example, membranes and myelin sheaths may be injured leading to the release of myelin inhibitory ligands (see section 1.6.0.1) and other extracellular matrix molecules (see section 1.6.4). In addition to this, the vasculature is commonly disrupted leading to infiltration of a variety of haematogenous cells (macrophages, monocytes, neutrophils, platelets and serum) (Berry 1998).

After the initial insult a whole host of secondary reactions occur. Platelets commence a clotting reaction to stem the haemorrhage from severed blood vessels and monocytes differentiate into macrophages to phagocytose necrotic debris and blood clots (Berry 1998). Infiltrating neutrophils, monocytes and lymphocytes stimulate the release of a whole host of chemokines which potentiates the inflammatory response (Berry 1998) and macrophages sequester erythrocytes from the haemorrhagic core, reducing its overall volume (Berry 1998). The macrophages, monocytes and neutrophils secrete a whole host of trophic cytokines (tumour necrosis factors, interleukins, TGFβ's, fibroblast growth factors and insulin-like growth factors) and stimulate the release of a variety of endoge-

nous trophic factors from both neurons and glia (Berry 1998). Resident microglia also play an important role in debris clearance by accumulating around the injury site and phagocytosing any cellular debris (Berry 1998). This is also accompanied by a change in morphology and upregulation of major histocompatibilty complex antigens (MHC I and II), leukocyte common antigen (LCA), nucleoside diphosphatase (NDPase) and complement type 3 receptor (CR3) (Berry 1998).

Reactive astrocytes proliferate around the injury site and release axon growth inhibitory molecules (CSPG, keratin sulphate proteoglycan and tenascin) which contribute towards regenerative failure (see section 1.6.4). This gliosis is typically identified by a change in cell morphology and upregulation of glial fibrillary acidic protein (GFAP) (Berry et al. 2008).

The numbers of haematogenous cells are reduced 3 to 8 days post-injury (dpi) as endogenous gliosis is amplified. Wound margins are established and a basal lamina is formed at the astrocyte end feet boundary (Berry 1998). This structure comprises the glia limitans and forms a continuous barrier against the infiltration of unwanted cells and molecules (Berry 1998). The lesion core continues to shrink between 8 dpi to 20 dpi — this structural change is accompanied by compaction of astrocytic processes and GFAP down regulation (Berry 1998).

1.5 Glia

Glial cells make up approximately 90% of cells present within the CNS - although glial cells were originally thought to purely have a structural role (Weigert 1895), it has become increasingly clear that glial cells have a variety of different functions, and are essential for normal CNS function and development. Four populations of glia exist in the CNS, namely, astrocytes, microglia and NG2 glia and oligodendrocytes.

1.5.1 Astrocytes

Astrocytes have a stellate morphology consisting of multiple processes which interact with numerous neurons to provide stability and support. Astrocytes have a number of different functions in health and disease. Neuronal damage and changes in the extracelluar environment triggers the upregulation of GFAP (Berry 1998). Astrocytes are a major source of matrix and adhesion molecules e.g. laminin, fibronectin, cytotactin-J1. Astrocytes also secrete pro-survival factors such as nerve growth factor (NGF), cilliary neurotrophic factor (CNTF) and S100-protein which have been shown to promote neurite outgrowth (Berry 1998).

1.5.2 NG2 glia

NG2 glia or `synantocytes' are highly abundant in the CNS and are distributed evenly throughout grey and white matter, making up approximately 8-9% of all white matter cells and 2-3% of grey matter cells (Dawson & Polito 2003). NG2 glia has a stellate mor-

phology and can be identified by their expression of platelet derived growth factor receptor alpha (PDGFRα), A2B5 and NG2 (Verkhratsky & Butt 2007). During development NG2 glia generate myelinating oligodendrocytes (Rivers, et al. 2008). NG2 glia persist in adulthood and retain some stem cell characteristics (Verkhratsky & Butt 2007).

1.5.3 Microglia

Microglial cells constitute the resident phagocytic cells of the CNS, making up approximately 10% of the total glial population (Hanisch & Ketterman 2007, Barres 2008). Microglia are derived from blood borne monocytes and mesenchymal progenitor cells, to a lesser extent (Guillemin & Brew 2003).

Under normal conditions microglia are thought to act as environmental sensors which are able to rapidly respond to extracellular cues (microbes, serum, intracellular components, protein aggregates) induced by trauma or infection (Hanisch & Ketterman 2007). To fulfil this role they continuously rebuild their processes to allow them to efficiently monitor the CNS environment (Hanisch & Ketterman 2007).

After injury microglial cells assume a `reactive' profile and temporarily cease their surveillance activity. This change in reactive state can be identified morphologically (processes become shorter and thicker) and histologically (through the up regulation of phagocytic makers such as CD68 and CD11b)(Ransohoff & Perry 2009).

1.6 Why doesn't the mammalian CNS regenerate?

Injury to the mammalian CNS has catastrophic functional consequences, often resulting in paralysis, loss of sensation, chronic pain and loss of bladder control (Donovan 2007). For many years the mammalian CNS was deemed to be incapable of regeneration. As a result, research in this area was impeded for almost a century (Cajal 1928). This assumption was first challenged by a series of early experiments which demonstrated that some injured axons were capable of regenerating long distances in the permissive environment of a PN graft (David & Aguayo 1981). Unfortunately regeneration was short lived, with axons being unable to re-enter the CNS environment. This phenomenon has also been documented in the retina, where axons were unable to enter the ON head (McConnell & Berry 1982) unless a PN implant was present (Cotman 1985, Berry, et al. 1986). Regeneration was halted when axons encountered CNS myelin. CNS myelin is formed by oligodendrocytes and its primary purpose is to increase the speed at which action potentials are propagated along myelinated fibres by saltatory conduction – it is essential for normal CNS function (Zalc & Colman 2000). These observations led researchers to investigate the environmental factors which play an important role in regenerative failure.

1.6.0.1 Myelin inhibitory ligands

CNS myelin was first implicated as a potential inhibitor of neurite outgrowth after a series of experiments showed that dissociated neurons could invade and extend neurites along sciatic nerve explants, but not ON explants (Schwab & Thoenen 1985). Further evidence came from experiments performed by Huang *et al* which showed that mice im-

munised with central myelin extract 3 weeks before spinal cord injury showed significant axonal regeneration across the lesion site (Huang, et al. 1999). Success was attributed to the production of polyclonal antibodies which specifically blocked myelin associated inhibitors and prevented growth cone collapse.

Myelin associated glycoprotein

Myelin associated glycoprotein (MAG) is a 100 kDa transmembrane glycoprotein which is a member of the immunoglobulin (Ig) family of proteins. MAG has two isoforms, large MAG (L-MAG) and small MAG (S-MAG), each of which have different cytoplasmic domains (Filbin 2003).

MAG has five extracellular Ig-like domains, a V-set Ig domain which binds to sialic acid and an intracellular C-terminus (Profyris et al. 2004, Filbin 2003). The primary function of MAG is to maintain axon-myelin stability and cytoskeletal integrity and although MAG has many roles in axon-myelin maintenance, it is not required for myelination (Schnaar & Lopez 2009). Found in both PNS and CNS myelin, MAG has a relatively low abundance, making up only 1% of CNS myelin and 0.1% of PNS myelin (Schnaar & Lopez 2009). Despite its

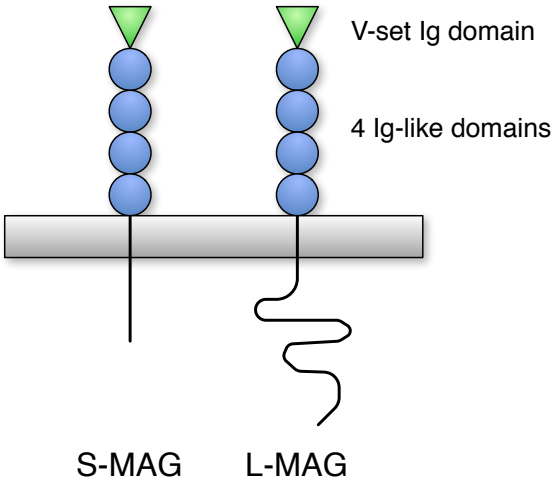

Figure 1.4: Diagramatic Representation of MAG Structure. Diagramatic representation of the two MAG isoforms. Diagram modified from (Profyris et al. 2004)

low abundance, MAG has potent inhibitory properties and is capable of inducing growth cone collapse both *in vitro* (Huang et al. 1999, Filbin 2003) and *in vivo* (Mukhopadhyay, et al. 1994). These inhibitory properties were first revealed in 1994 when MAG was isolated from PNS myelin extract and applied to neuronal cells to inhibit neurite outgrowth (Mukhopadhyay et al. 1994, McKerracher, et al. 1994). Interestingly, the inhibitory properties of MAG are cyclic adenosine monophosphate (cAMP) dependent, being inhibitory in the mature CNS where cAMP levels are low, and permissive in the embryonic CNS where cAMP levels are elevated (Cai, et al. 2001).

Oligodendrocyte myelin glycoprotein

OMgp is a 120 kDa GPI linked protein. It was first identified as a minor component of myelin and is expressed by both neurons and oligodendrocytes. Expression is localised primarily to the paranodal loops next to the Nodes of Ranvier where it is ideally placed for axonal interaction (Filbin 2003). OMgp has 8 LRR domains at its N-terminus, followed by a serine/threonine rich domain which is required for nogo receptor (NgR) binding (Profyris et al. 2004). Like both MAG and neurite outgrowth inhibitor (Nogo), OMgp is capable of inhibiting neurite outgrowth *in vitro* (Filbin 2003).

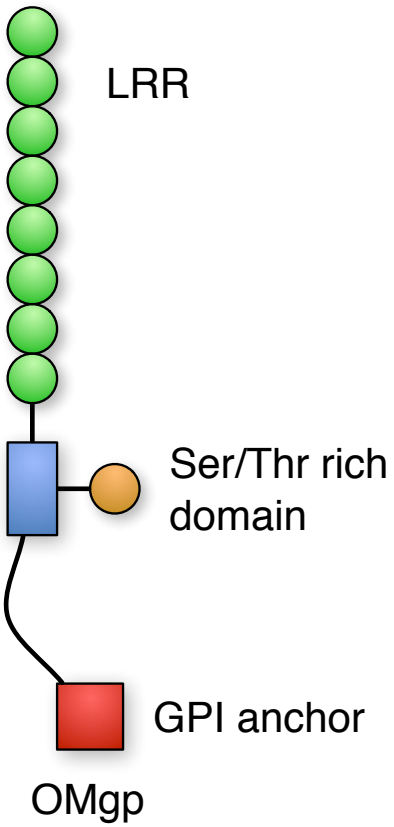

Figure 1.5: Structure of oligodendrocyte myelin glycoprotein (OMgp). OMgp has 8 leucine rich repeat (LRR) domains followed by a serine/threonine rich domain and is attached to the membrane through a glycosyl phosphatidylinositol (GPI) anchor. Figure modified from (Profyris et al. 2004)

Neurite outgrowth inhibitor

Nogo is a member of the reticulon family of proteins and is localised primarily to the endoplasmic reticulum (Filbin 2003). The first indication that Nogo was inhibitory came from studies performed by Schwab *et al* in the late 1980 s (Caroni & Schwab 1988). In this study, the IN-1 monoclonal antibody was raised against a fraction of CNS myelin which was known to inhibit neurite outgrowth. Appli-

cation of this antibody resulted in disinhibited neuronal growth both *in vitro* (Caroni & Schwab 1988) and *in vivo* (Schnell & Schwab 1990). Despite this breakthrough, it was not until the year 2000 that the antigen for this antibody was cloned and identified (Prinjha 2000, Chen, et al. 2000, GrandPre, et al. 2000). Nogo exists in three isoforms, (Nogo-A, Nogo-B and Nogo-C) all of which share a common carboxyl (C) terminal domain (Filbin 2003). The inhibitory properties of Nogo are attributed to two extracellular domains: Nogo-66, which is common to all three isoforms, and amino-Nogo, which is specific to Nogo-A (Filbin 2003). The topology of Nogo-A remains unclear, but two structural conformations have been proposed. The first proposal places Nogo-66 in the extracellular compartment and amino-Nogo in the cytoplasm, whilst the alternative suggestion places amino-Nogo in the extracellular compartment and Nogo-66 in the cytoplasm (Filbin 2003). Numerous studies have suggested that both topologies may co-exist in the CNS environment (Chen et al. 2000, GrandPre et al. 2000).

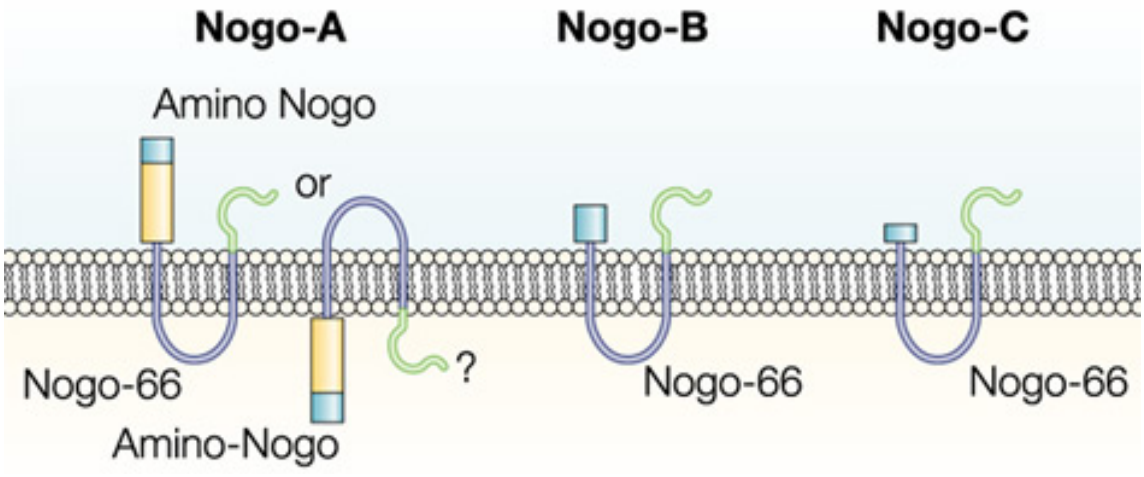

Figure 1.6: Structural Arrangement of Nogo-A, Nogo-B and Nogo-C. Nogo exists as 3 isoforms – Nogo-66 is common to all three isoforms, however amino-Nogo is specific to Nogo-A. There has been some debate over the structural conformation of Nogo-A, one proposal places amino-Nogo in the extracellular compartment whilst the other places it in the cytoplasm. Figure reproduced from (Filbin 2003).

1.6.0.2 Myelin inhibitory ligand receptors

Nogo-66 Receptors

MAG, Nogo and OMgp all bind to the Nogo-66 receptor (NgR1+2) to elicit their Rho mediated biological effects. A member of the LRR superfamily (Fournier, et al. 2001), NgR1 is a glycosyl phosphatidylinositol-linked membrane protein which is expressed primarily by neurons of the CNS (Fournier et al. 2001). As this receptor is GPI-linked it does not possess an intracellular signalling domain and requires a co-receptor to transduce inhibitory signals. This prompted researchers to identify NgR and several co-receptors, namely: low-affinity p75 neurotrophin receptor ($p75^{NTR}$), tumour necrosis factor (TNF) receptor 19 , and LRR and Ig domain containing 1.

$p75^{NTR}$, Tumour necrosis factor receptor 19 (Troy) and Lingo-1

$p75^{NTR}$ is a glycosylated membrane protein and a member of the TNF receptor superfamily. In addition to its role as a low affinity neurotrophin receptor, numerous lines of study have identified $p75^{NTR}$ as a co-receptor for NgR1 (Yamashita, et al. 2002, Wong, et al. 2002). $p75^{NTR}$ was first implicated as an interacting partner of NgR1 after neurons isolated from $p75^{NTR}$ knockout mice only exhibited a limited response to MAG, Nogo and OMgp treatment (Yamashita et al. 2002, Wang, et al. 2002). This was followed by co-immunoprecipitation studies which revealed that $p75^{NTR}$ formed a receptor complex with NgR1 (Wong et al. 2002, Wang et al. 2002). Interestingly $p75^{NTR}$ is not expressed universally, being present in only a small subpopulation of neurons (Park, et al. 2005). It may be

that $p75^{NTR}$ has a more prominent role in the developing CNS, as messenger RNA (mRNA) expression rapidly declines with maturity (Shao, et al. 2005).

In contrast, Troy mRNA is broadly expressed in the mature CNS and may act as the predominant co-receptor postnatally (Shao et al. 2005). Its function as an NgR1 co-receptor was confirmed after a series of binding and co-immunoprecipitation assays (Shao et al. 2005). COS-7 cells were treated with OMgp, MAG and Nogo after transfection with various combinations of Troy, NgR1 and leucine rich repeat and Ig domain containing 1 (Lingo-1). Rho activation was used as a functional readout of receptor activation (Shao et al. 2005). They found that only the combination of Troy, NgR1 and Lingo-1 activated Rho, and concluded that Troy could be used as a substitute for $p75^{NTR}$ (Shao et al. 2005). As Troy alone was incapable of transducing the inhibitory signalling, the requirement for an NgR1 receptor complex was also confirmed (Shao et al. 2005). Neurons isolated from Troy knockout mice only exhibited a limited response to MAG, OMgp and Nogo, and were able to extend neurites over myelin inhibitory ligand (MIL) coated slides (Shao et al. 2005). Higher concentrations were able to inhibit neurite outgrowth, but this was attributed to the presence of $p75^{NTR}$ (Shao et al. 2005).

To form a functional receptor complex with NgR, Lingo-1 is also required. Lingo-1 belongs to the TNF receptor superfamily and is expressed exclusively by neuronal tissue (Mi, et al. 2004). Lingo-1 has a 12 leucine-rich repeat domain which commences at the N terminus. This is followed by an Ig and transmembrane domain, as well as a short cytoplasmic tail (Mi et al. 2004). COS-7 cells transfected with NgR1 are able to directly interact with Lingo-1 fusion proteins (Mi et al. 2004). However, cells transfected with NgR1 and $p75^{NTR}$ were

insensitive to OMgp treatment. Only cells triple transfected with NgR1, $p75^{NTR}$ and Lingo-1 were capable of activating Rho and transducing the inhibitory signal (Mi et al. 2004).

1.6.1 The growth cone

To be able to understand how these inhibitory molecules induce growth cone collapse it is important to first describe the molecular machinery which underlies axon guidance. The growth cone is a specialised structure (see figure 1.7) at the end of an axon which senses environmental cues and guides the axon through the developing CNS to its correct target. The leading edge (or peripheral domain) of the growth cone contains finger-like structures called filopodia which are separated by membrane sheets of lamellipodia (Lowery & Vactor 2009). Long filamentous-actin (F-actin) bundles reside beneath this structure and make up the filopodia whilst branched F-actin networks make up the lamellipodia. The transition domain (T-domain) resides between the central and peripheral regions of the growth cone and is flanked by an F-actin arc. Peripheral domain (P-domain) microtubules are thought to act as guidance sensors, whilst central domain (C-domain) microtubules provide stability to the overall structure (Lowery & Vactor 2009).

Growth cone protrusion and advancement is highly reliant on the dynamic properties of actin. F-actin bundles are elongated through polymerisation at the leading edge of the growth cone — this process effectively pushes the plasma membrane forward. Concomitantly, polymerised sections of F-actin are severed at the proximal end of filopodia/lamellipodia and recycled as monomers. Growth cone advancement requires a careful balance between F-actin polymerisation and recycling.

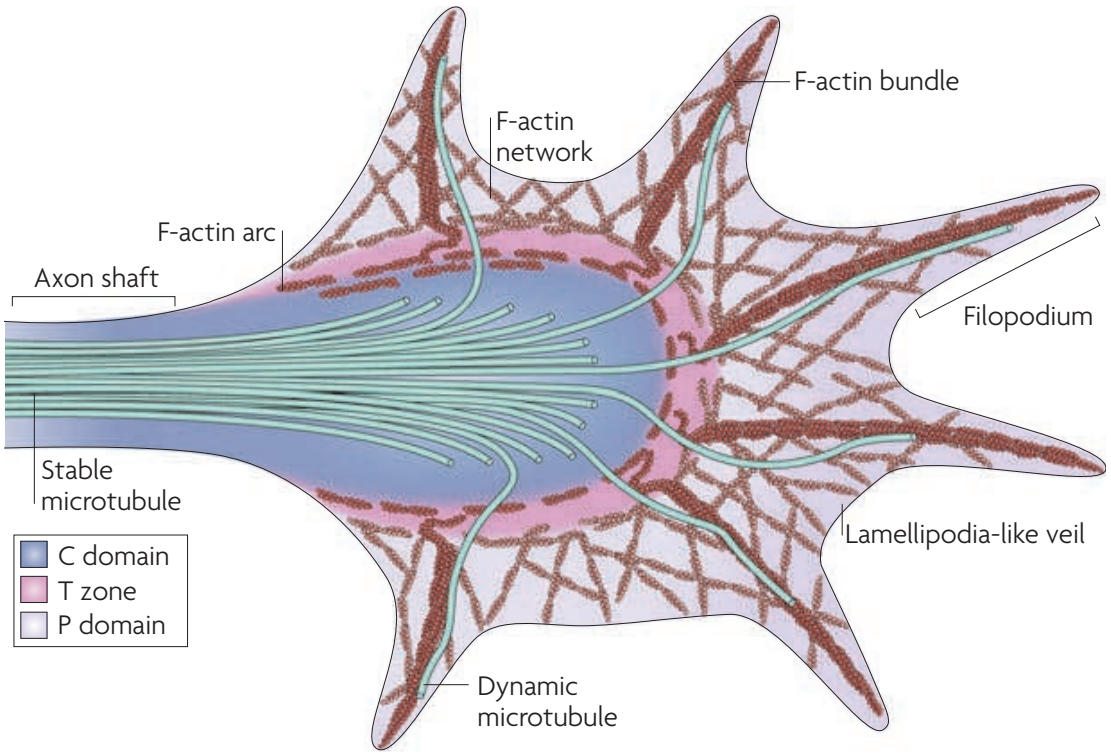

Figure 1.7: Growth cone structure. Growth cone advancement is mediated by the continuous polymerisation and movement of F-actin. Polymerisation of F-actin occurs at the leading edge of the growth cone, the growing chain is eventually severed in the transition zone, where it is eventually recycled and transported back to the leading edge for re-use. Protrusion occurs when the F-actin polymerisation occurs at a higher rate than F-actin depolymerisation. P-domain microtubules explore the filopodial environment and are thought to act as guidance sensors whilst C-domain microtubules stabilise the overall structure. Figure reproduced from (Lowery & Vactor 2009).

When the rate of F-actin polymerisation is higher than that of F-actin recycling, the leading edge of the growth cone advances. On the other hand, if the rate of actin depolymerisation is higher than that of actin polymerisation, the leading edge of the growth cone retracts. However, when F-actin monomers are polymerised and recycled at the same rate, protrusion at the leading edge does not occur and the growth cone is said to be arrested (Lowery & Vactor 2009).

When F-actin polymerisation occurs predominantly at the front of the growth cone, the axon advances in a relatively straight line. However, if F-actin depolymerisation occurs locally at one side of the growth cone, the axon turns in the opposite direction.

The last process that will be discussed is growth cone collapse. Importantly, growth cone retraction and growth cone collapse are two entirely separate entities. Whilst growth cone retraction is characterised by F-actin depolymerisation and lamellipodia shortening, growth cone collapse occurs as a result of lamellipodial disassembly (Gallo & Letourneau 2004). Growth cone collapse often occurs after CNS injury, where it encounters a variety of inhibitory ligands and is mediated by a number of different receptors and signalling molecules — which is discussed in section 1.6.2.

1.6.2 Myelin inhibitory signalling cascade

Rho GTPases are small (≈21 kDa) G proteins which regulate a whole host of cellular processes (gene transcription, vesicle trafficking, cell morphology and actin polymerisation) (Ellenbroek & Collard 2007). RhoA belongs to this family of proteins and is a key mediator of myelin based inhibition and growth cone collapse (Yamashita et al. 2002). RhoA

activity is regulated by guanine nucleotide exchange factors, GTPase activating proteins and guanosine diphosphate (GDP) dissociation inhibitors (GDI). GDP-bound (inactive) Rho is sequestered in the cytoplasm by GDI and prevented from interacting with guanine nucleotide-exchange factor (GEF) (Ellenbroek & Collard 2007). Upon phosporylation, Rho is released from GDI induced inhibition and allowed to translocate to the plasma membrane where it can interact with GEF (Ellenbroek & Collard 2007). Upon interaction with GEF, Rho is able to exchange GDP (inactive) for GTP (active) and interact with a variety of downstream effectors. GEF induced signalling is terminated by GTPase-activating protein (GAP) which renders Rho inactive once more through GTP hydrolysis (Ellenbroek & Collard 2007). Rho-associated kinase (ROCK), a serine threonine kinase, is a major downstream effector of GTP-bound Rho. Activation of ROCK and LIM kinase-1 leads to F-actin disassembly, inhibition of lamellipodea extension and growth cone collapse (see figure 1.8 for an overview of inhibitory signalling) (Yang, et al. 1998).

1.6.3 Targeting the inhibitory signalling cascade

Over the years various strategies have been used to overcome myelin induced growth cone collapse. The inhibitory signalling cascade can be targeted at multiple levels and since all myelin derived ligands signal through a common receptor complex, this is an obvious place to start. The NgR receptor complex can be targeted through the administration of antibodies or peptides to prevent ligand binding and/or receptor interaction (Chaudhry & Filbin 2006). However, targeting the inhibitory signalling pathway at this level is problematic since there is a degree of functional redundancy in the system

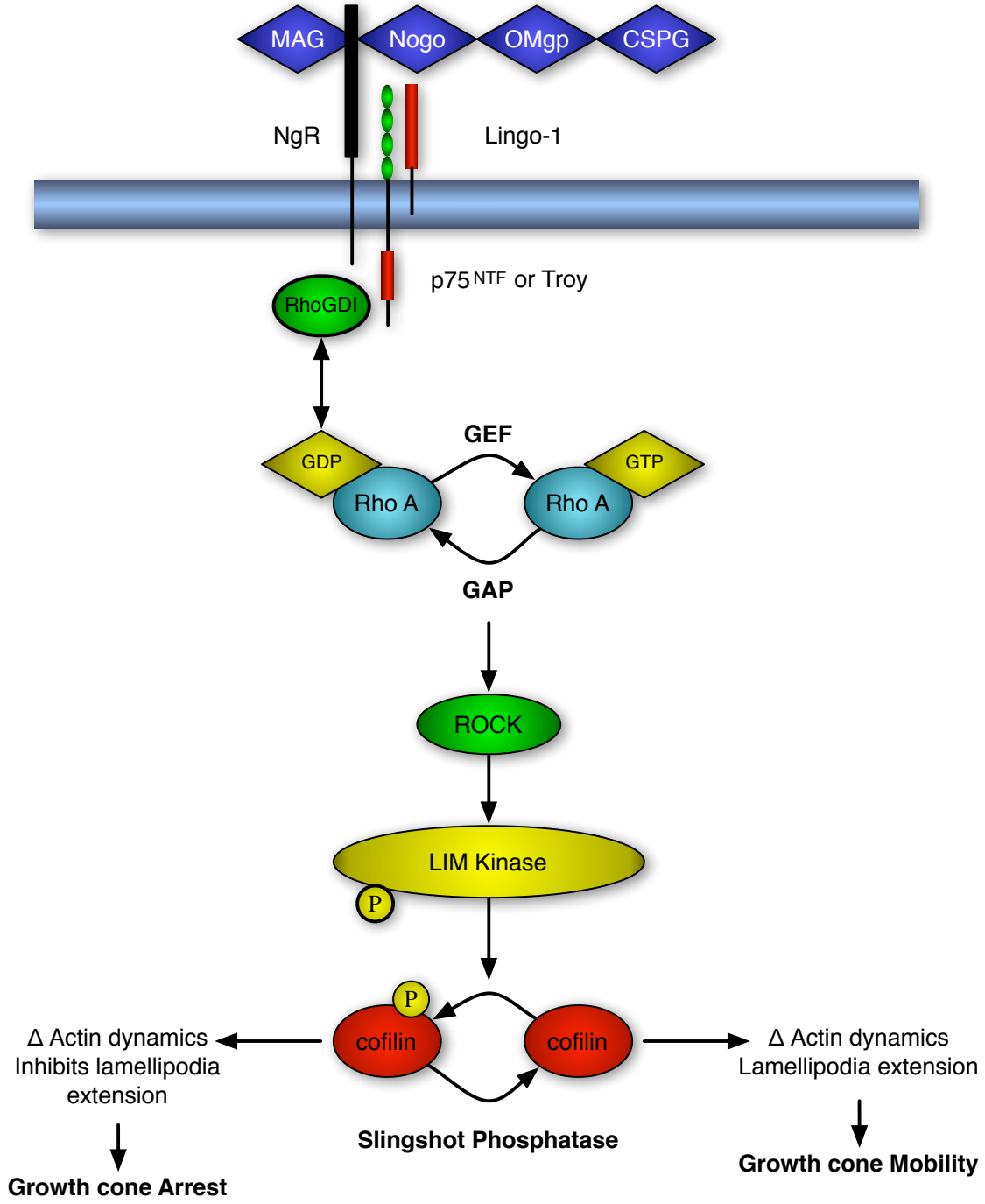

Figure 1.8: Inhibitory Signalling Diagram. Myelin derived inhibitory ligands, namely, MAG, Nogo and OMgp bind to NgR to elicit their biological response. As NgR lacks an intracellular signalling domain, association with $p75^{NTR}$/Troy and Lingo-1 are required to potentiate the signal. The inhibitory signalling cascade impinges on both Rho and ROCK and ultimately leads to growth cone collapse through F-actin disassembly, inhibition of lamellipodea extension and growth cone collapse. (Diagram adapted from version provided by Prof. Ann Logan, University of Birmingham).

(Filbin 2003), meaning targeting myelin inhibitory ligands is inefficient; as you would need to target multiple myelin derived elements (Filbin 2003). Furthermore knockdown of any one of these components may lead to a compensatory increase in protein expression – this is certainly true in the case of Nogo (Simonen, et al. 2003).

Nogo knockout experiments revealed that when Nogo-A was knocked down there was a compensatory increase in Nogo-B expression (Simonen et al. 2003). Furthermore the injured CNS environment is also littered with other inhibitory molecules (e.g. Chondroitin sulphate proteoglycans (CSPGs), semaphorins) which could induce growth cone collapse (Berry et al. 2008). Targeting the NgR receptor complex is also problematic since it associates with multiple proteins (Lingo-1, $p75^{NTR}$/Troy), as a result, it is possible that any inhibition (or knockdown) of Troy may result in a compensatory upregulation in $p75^{NTR}$ (Mandemakers & Barres 2005). It is also possible that NgR has some, as of yet, unidentified interacting partner which could also transduce the inhibitory signal (Mandemakers & Barres 2005).

An alternative would be to target signalling molecules which lie downstream of the NgR receptor complex. Since both Rho and ROCK are integral to the inhibitory signalling pathway their potential as a therapeutic target has received much attention (Dergham, et al. 2002, Lehmann, et al. 1999). For example C3-transferase (a bacterial enzyme derived from Clostridium Botulinum) can be used to specifically inhibit Rho activity and promote significant RGC neurite outgrowth in the presence of MIL (Lehmann et al. 1999). It has been shown that C3-transferase suppresses Rho activity through ADP-ribosylation (the addition of ADP-ribose moieties to a protein) of asparagine-41 (Paterson, et al. 1990). Moreover, treatment with the ROCK inhibitor Y-27632 enabled cortical neurons to extend

neurites on a myelin or chondroitin sulphate proteoglycan (CSPG) substrate (Dergham et al. 2002). Treatment with each of these inhibitors also resulted to improved functional recovery following spinal cord injury (Dergham et al. 2002).

1.6.4 Chondroitin sulphate proteoglycans and the glial scar

After injury, matrix molecules (fibronectin, collagen, laminin, tenascin and chondroitin sulphate proteoglycans) are deposited by reactive astrocytes at the lesion site (Berry 1998). In the developing CNS, CSPGs are expressed at glial boundaries such as the dorsal root entry zone (DREZ) (Pindzola, et al. 1993), optic tectum and spinal cord roof plate (Snow, et al. 1990). After injury, scar deposition appears to serve a similar purpose through the formation of the glia limitans accessories (Berry 1998). CSPG rich scar tissue was previously thought to act as a physical barrier to axon regeneration (Berry et al. 2008) — however this is not entirely the case. Neurons do not lack the intrinsic capability to regenerate axons as previously thought (Berry et al. 2008) — in fact if you can stimulate neurons to grow they can modulate their surrounding environment to dissolve scar tissue (Ahmed, et al. 2005a). This event is thought to occur by the upregulation of matrix metalloproteases (MMPs) and concomitant downregulation of tissue inhibitors of MMP (TIMP) (Ahmed et al. 2005a).

CSPGs comprise of a large family of glycosylated core proteins attached to a long chain of polysaccharides, namely, N-acetylgalactosamine and glucoronic acid. Members of this family include neurocan, brevican, versican, NG2, phosphocan and aggrecan, all of which have been shown to inhibit neurite outgrowth (Morgenstern, et al. 2002). The inhibitory

properties of CSPGs are mediated primarily by glycosaminoglycan chain (GAG) chains and in some instances by their core proteins (e.g. NG2) (Ughrin, et al. 2003). This inhibition can be partially reversed, and neurite outgrowth promoted *in vitro* and *in vivo* by Chondroitinase ABC treatment (an enzyme which cleaves sugar chains) (Bradbury, et al. 2002, Houle, et al. 2006). Although the CSPG receptor has recently been identified as PTPσ (a heparin sulphate proteoglycan (HSPG) receptor) (Shen, et al. 2009), its precise signalling mechanism remains unclear. However, there is some evidence to suggest that CSPG signalling may exert its actions through the Rho inhibitory pathway (see figure 1.8) (Monnier, et al. 2003). In this study they found that treatment with C3 transferase or Y-27632 disinhibited RGC neurite outgrowth (Monnier et al. 2003).

1.7 Cell death

After ON injury, axotomized RGC initiates a transitory sprouting reaction, however this growth ultimately fails (Cajal 1928), leading to RGC death through both apoptotic and necrotic mechanisms. During necrosis cells swell and burst, releasing their cellular contents into the surrounding environment – this can lead to a potentially damaging inflammatory responses (Alberts 2002). In contrast, cells undergoing apoptosis die in a regulated way – cells shrink and condense, the cytoskeleton collapses and the nuclear envelope loses structural integrity (Alberts 2002). As a result of this, nuclear deoxyribonucleic acid (DNA) is exposed to endogenous DNases and RNases and DNA fragmentation occurs (Alberts 2002). The apoptosome is then phagocytosed by surrounding cells before any of the cellular contents can be released into the surrounding environment (Alberts 2002).

This process is regulated by a highly conserved family of proteases known as Caspases (Cysteine-dependent Aspartate-directed protease). Caspases are initially manufactured as inactive precursors (pro-caspases) which require cleavage by other caspases to become active (Alberts 2002). Once activated these caspases interact with adaptor proteins to bring about activation of initiator pro-caspases (Alberts 2002).The apoptotic signalling pathways are typically activated through either an intrinsic or extrinsic mechanism (see figure 1.9).

1.7.1 The extrinsic pathway

The extrinsic signalling pathway is typically activated by a receptor mediated process. Upon ligand binding (Fas) death receptors of the of the TNF receptor superfamily aggregate and recruit intracellular adaptor proteins (FADD, NRAGE) (Fulda & Debatin 2006). These adaptor proteins bind and aggregate pro-caspase 8 molecules, which cleave and activate one another (Alberts 2002). Once activated these molecules initiate apoptosis through the direct cleavage of downstream effector caspases, such as Caspase-3 (Alberts 2002).

1.7.2 The intrinsic pathway

When a cell is damaged or stressed the intrinsic signalling pathway is activated. Stress signals induce the release of pro-apoptotic factors (cytochrome c, apoptosis inducing factor (AIF) (apoptosis inducing factor), second mitochondria-derived activator of caspase

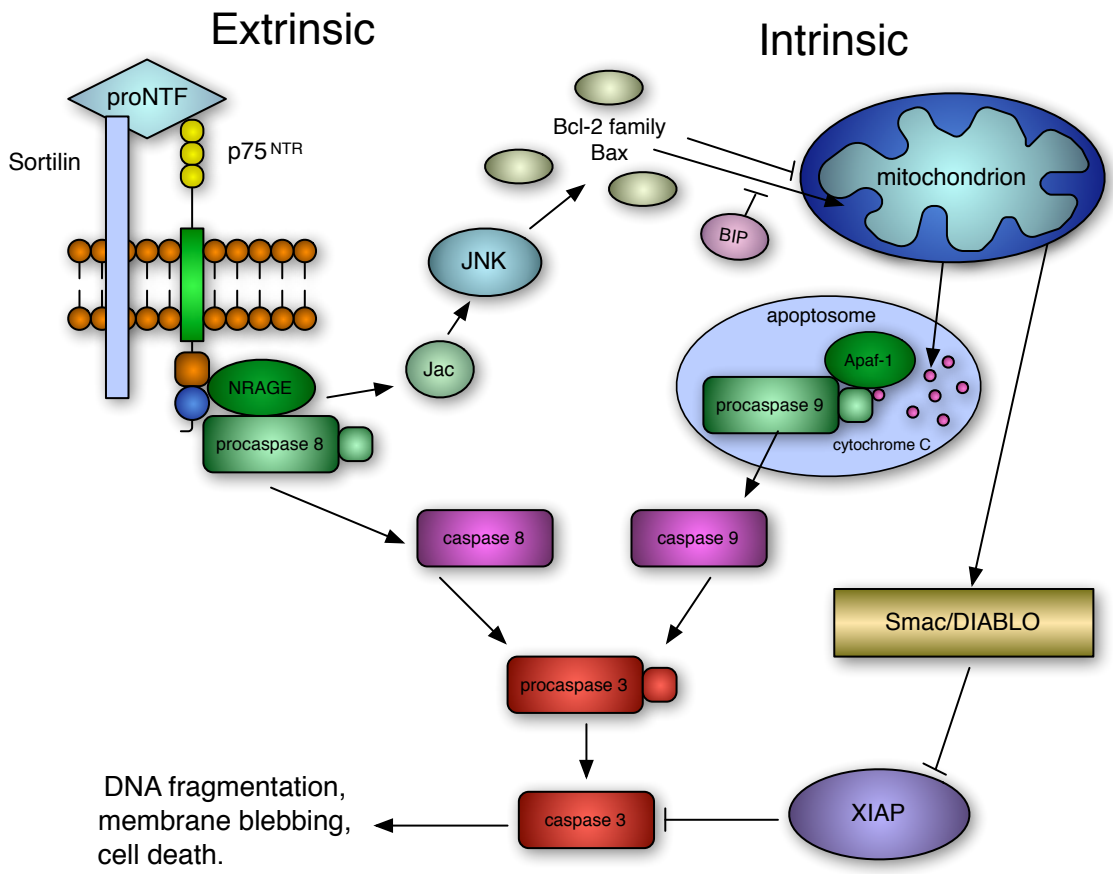

Figure 1.9: Diagrammatic representation of the intrinsic and extrinsic apoptotic signalling pathways. The intrinsic signalling pathway is activated by stress signals, these signals induce the release of cytochrome (as well as others) from the mitochondria into the cytosol. Once released cytochrome c binds to and activates Apaf-1. Pro-caspase-9 is bound by Apaf-1 to trigger its aggregation and cleavage. In contrast the extrinsic signalling pathway is activated through a receptor mediated process. Once active these death receptors recruit additional adaptor proteins. These adaptor proteins bind to aggregate pro-caspase-8 molecules which cleave and activated one another. Once active these molecules initiate apoptosis through the direct cleave of downstream effector caspases. Diagram reproduced with permission from Prof. Ann Logan (University of Birmingham).

(Smac) (second mitochondria-derived activator of caspase)/DIABLO (direct inhibitor of apoptosis (IAP) binding protein with low PI) or Omi/HtrA2 (high-temperature requirement protein A2)) from the mitochondria into the cytosol (Alberts 2002). Once released cytochrome c binds to and activates an adaptor protein called Apaf-1 (Alberts 2002). Pro-caspase-9 is then bound by Apaf-1, to trigger its aggregation and cleavage. Smac/DIABLO and Omi/HtrA2 regulates caspase activity through an alternative mechanism. Upon mitochondrial release Smac/DIABLO binds to and counteracts the inhibitory effects of IAPs (Alberts 2002).

1.7.3 Regulators of apoptosis

Apoptosis is regulated, in part, by the Bcl-2 family of proteins (Alberts 2002). This family contains pro- (e.g. Bax, Bak) and anti-apoptotic members (e.g. Bcl-2, Bcl-XL), each of which controls mitochondrial protein release by altering the permeability of the outer mitochondrial membrane (Alberts 2002). Another level of regulation is performed by inhibitors of apoptosis, these proteins bind to pro-caspases to prevent their activation, or interact directly with caspases to inhibit their activity (Alberts 2002).

1.8 Neurotrophins

Neurotrophins have numerous functions, both in the developing and mature CNS. They have roles in cell survival, synaptogenesis, growth cone guidance, synaptic plasticity, neurotransmitter turnover and differentiation (Tuszynski 2007). Members of this family in-

clude brain derived neurotrophic factor (BDNF) NGF, neurotrophin 3 (NT3), and Neurotrophin 4/5(NT4/NT5) (Tuszynski 2007). Neurotrophins are initially synthesized as proproteins (30-35kDa), which are proteolytically cleaved by convertases (convertase 1 and 2) to produce mature proteins (12-13kDa)which exist as non-covalently bound homodimers (Tuszynski 2007).

1.8.1 Neurotrophin receptors

tropomyosin receptor kinase (Trk) receptors are type I transmembrane proteins which are members of the receptor tyrosine kinase superfamily. Each neurotrophin binds with high affinity to their respective tropomyosin-related kinase receptor – NGF to tropomyosin receptor kinase A (TrkA), BDNF and NT4/NT5 to tropomyosin receptor kinase B (TrkB), and NT3 to tropomyosin receptor kinase C (TrkC) (Tuszynski 2007). Binding of neurotrophins to their corresponding Trk receptors causes receptor dimerisation and autophosphorylation of tyrosine residues within the activation loop, which leads to the phosphorylation of seven additional tyrosine residues (Roux & Barker 2002). These phosphotyrosine residues act as docking sites for SH2 containing secondary messengers which regulate cell growth and survival through Ras/MAPK, phospholipase C (PLC) and phosphatidylinositol 3-kinase / Akt signalling pathways.

As previously discussed in section 1.6.0.2, $p75^{NTF}$ is not solely a co-receptor for NgR1 and also plays an important role in neurotrophin signalling. In fact all neurotrophins (NGF, BDNF, and NT4/NT5) bind to $p75^{NTF}$ with almost equal affinity. Although $p75^{NTF}$ has been shown to bind to all neurotrophins with low affinity, its' exact function has been

the subject of much debate. There is substantial evidence to suggest that $p75^{NTF}$ enhances the responsiveness of Trk receptors to their corresponding ligands (Hantzopoulos & Suri 1994). For example Yancopoulus *et al* found that a truncated form of $p75^{NTF}$ significantly enhanced the ability of each of the Trks to respond to their cognate receptors (Hantzopoulos & Suri 1994). $p75^{NTF}$ may play a role in neuronal apoptosis, since neurotrophin pro-proteins are not have been found to bind to $p75^{NTF}$ with high affinity to initiate apoptosis (Volosin, et al. 2008).

1.8.2 $p75^{NTF}$ and apoptosis

The first indication that $p75^{NTF}$ had a role in inducing apoptosis came from the work of Rabizadeh *et al*. A selection of neuronal cell lines (CSM 14.1 and R2) were transfected with $p75^{NTF}$ and cultured in serum free or serum supplemented media. Cells which were cultured in serum free media had an increased rate of apoptotic cell death, however when these cells were cultured in serum supplemented media there was no effect on cell death. When NGF was added to the serum deprived cells the negative effect of the $p75^{NTF}$ transfected cells was abolished (Rabizadeh, et al. 1993). A similar effect was achieved by treating these cells with a monoclonal antibody targeted against $p75^{NTF}$. Since neither the R2 nor CSM 14.1 cell lines endogenously expressed detectable levels of TrkA or $p75^{NTF}$, the apoptotic effect was thought to be mediated by the $p75^{NTF}$ receptor (Rabizadeh et al. 1993).

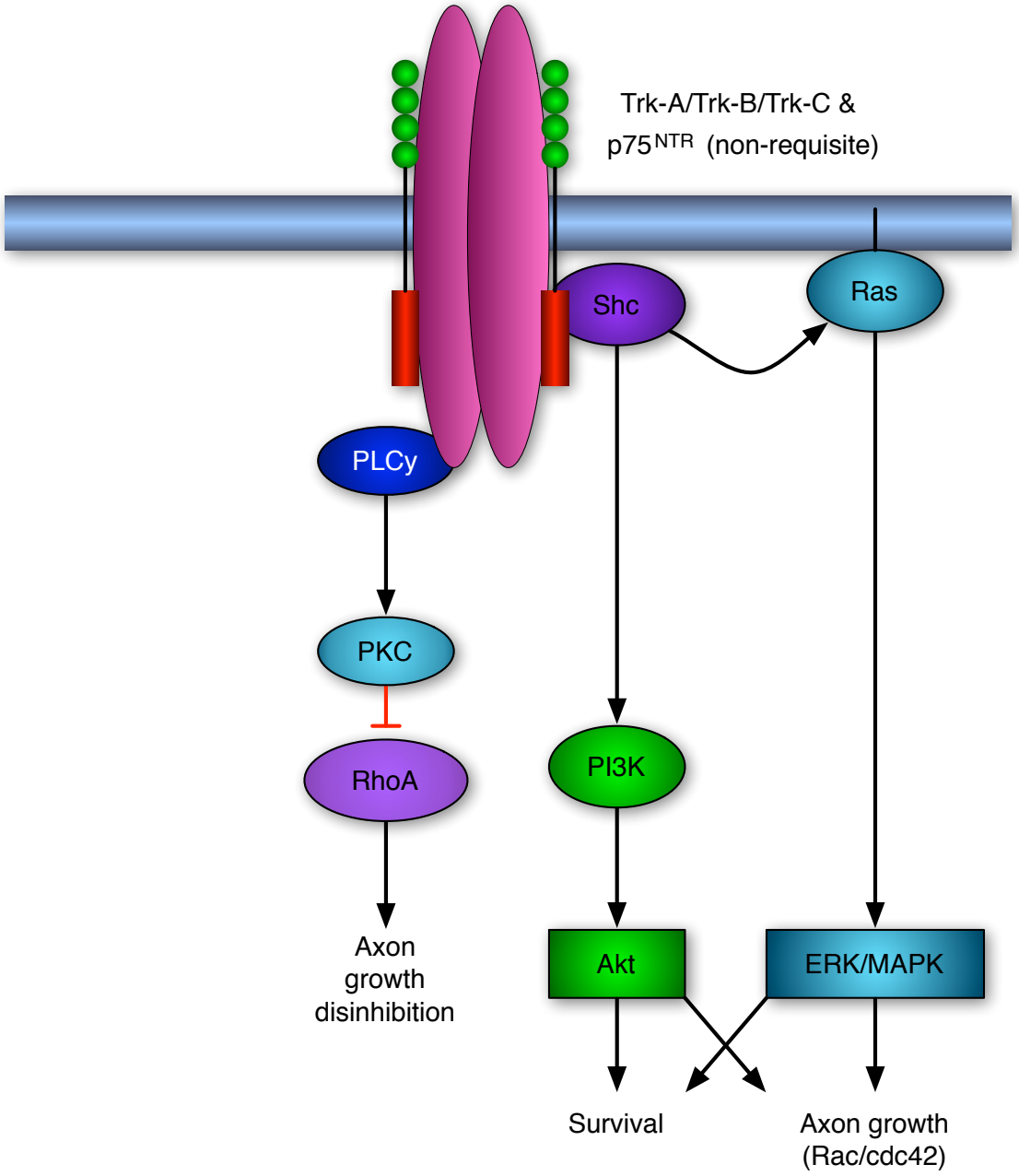

Figure 1.10: Neurotrophic factor signalling through Trk receptors. Neurotrophins signal through their corresponding Trk receptors to activate a number of interacting intracellular signalling pathways (PI3k/Akt, Ras/MAPK PLCɣ), ultimately leading to axon growth (through Rac/cdc42) and neuron survival. Figure modified with permission from Prof. Ann Logan (University of Birmingham).

1.8.3 Neurotrophin signalling pathways

1.8.3.1 Ras/MAPK signalling

Ras is a 21 kDa small GTPase which essentially acts as a molecular switch for a whole host of cellular processes (e.g. cell growth, differentiation, cytoskeletal organisation, membrane trafficking and apoptosis) (Huang & Reichardt 2003). Its role as a mediator of neurotrophin signalling was initially identified in 1986 (Huang & Reichardt 2003). Antibodies raised against Ras were micro-injected into PC12 cells, this resulted in neurite inhibition and partial reversal of neurite outgrowth following NGF treatment (Hagag, et al. 1986). Ras signalling is typically initiated through the activation of cell surface receptor tyrosine kinases (e.g. Trk receptors) (Ray 2009). Ligand binding induces receptor dimerization and autophosphorylation of three sites in the intracellular domain. SH2 containing protein (SHC) is phosphorylated at one of these sites, creating a binding site for growth factor receptor binding protein 2 (Grb2) (Huang & Reichardt 2003). This in turn interacts with son of sevenless (SOS) to activate Ras through the exchange of GDP for GTP (Huang & Reichardt 2003). Ras activation stimulates translocation of Raf (a 68 kDa to 72 kDa cytosolic protein) to the cell membrane where it can activate map kinase kinase (MEK) (Huang & Reichardt 2003). MEK then phosphorylates mitogen-activated protein kinase (MAPK) (ERK1 and ERK2) which translocates to the nucleus to activate a variety of transcription factors (e.g. c-Fos, Jun, activator protein-1 (AP-1), cAMP responsive binding element binding protein (CREB), c-myc, and signal transducers and activators of transcription 1 (STAT1) / 3 (STAT1/STAT3) which modulate gene expression (Huang & Reichardt 2003).

1.8.3.2 Phospholipase C

PLC is recruited to an alternative site of the intracellular domain after TrK receptor phosphorylation (Huang & Reichardt 2003). PLC catalyzes the formation of inositol-trisphosphate and diaglycerol (DAG) through the cleavage of phosphatidylinositol-4,5-bisphosphate (PIP2) (Huang & Reichardt 2003). DAG activates protein kinase C (PKC) whilst inosital-trisphosphate (IP3) induces the release of calcium from intracellular stores (Huang & Reichardt 2003). Cytosolic calcium can then go on to stimulate a variety of downstream enzymes (e.g activation of calmodulin-dependent protein kinases), whilst PKC can activate the Erk-1 signalling pathway (Huang & Reichardt 2003).

1.8.3.3 PI3K/Akt signalling

Phosphoinositide 3-kinases (PI3K) are a family of highly conserved lipid kinases that phosphorylate the 3'hydroxyl (3'-OH) group of phosphatidylinositides. Class 1 PI3Ks are heterodimeric molecules which contain a regulatory (p85) and a catalytic (p110) subunit (Vanhaesebroeck & Guillermet-Guibert 2010).

This class of PI3Ks can be further subdivided into class 1A and class 1B. Class 1A PI3Ks are typically activated by growth factors and their associated receptors (e.g. Trk receptors) whilst class IB PI3Ks are usually activated by G protein coupled receptors (GPCR) (Vanhaesebroeck & Guillermet-Guibert 2010).

PI3K/Akt signalling pathway

Trk receptor activation leads to receptor autophosphorylation of tyrosine residues and subsequent recruitment of PI3K to the plasma membrane. The regulatory subunit of PI3K interacts with the receptor through its SH2 containing domains leading to subsequent activation of its catalytic subunit (Vanhaesebroeck & Guillermet-Guibert 2010). This ultimately leads to the generation of phosphoinositol-3, 4, 5-triphosphate (PtdIns(3,4,5)P3) and PtdIns-3,4-bisphosphate (PtdIns-(3,4)P2) at the inner side of the cell membrane. Akt is then recruited to the cell membrane where it is phosphorylated by PDK1 and PDk2 (Vanhaesebroeck & Guillermet-Guibert 2010). Akt then translocates to the cell nucleus where it can interact with a variety of transcription factors to bring about changes in gene expression to influence a whole host of cellular processes (e.g. cell proliferation, growth and survival).

1.9 Cilliary neurotrophic factor

CNTF is a 22 kDa cytosolic protein which belongs to the interleukin-6 family of cytokines. This family consists of interleukin-6 (IL-6) together with leukemia inhibitory factor (LIF), interleukin-11 (IL-11), oncostatin M (OSM) and cardiotrophin-1 (CT-1) (Dutta, et al. 2007). Some more recent members include cardiotrophin like cytokine (CLC) and neuropoietin (NP) (Rousseau, et al. 2008).

CNTF has a tertiary structure which is similar to that of other cytokines and consists of a four alpha helix bundle (Inoue, et al. 1996). CNTF does not possess a classical secretory

signal sequence and it's unclear how the protein is released from cells. One potential explanation is that it is released from cells (e.g. astrocytes) through an induced mechanism (Sleeman, et al. 2000).

CNTF was first described as a protein which could enhance chick cilliary ganglionic neuron survival *in vitro* (Adler, et al. 1979). Further research has revealed that CNTF has a much broader effect and is capable of promoting sensory, motor, cerebral and hippocampal neuron survival (cited in (Sleeman et al. 2000)).

In the retina, CNTF is endogenously expressed by astrocytes and Müller glia while it's corresponding receptor, CNTFRα, can be found on RGC, horizontal cells and a subpopulation of amacrine cells (Adel, et al. 2005). It is generally believed that CNTF is an injury inducible factor which is released by glia, in response to trauma or cellular stress, to protect neurons from cell death (Adler 1993). Several lines of evidence indicate that this is the case. After injury, endogenous levels of CNTF, CNTFR α and leukemia inhibitory factor receptor β (LIFRβ) are substantially elevated (Adel et al. 2005). This compensatory up regulation of CNTF, CNTFR α and LIFRβ may be in place to enhance neuronal survival through JAK-STAT signalling and/or other neuroprotective signalling pathways e.g. MAPK and PI3K . Exogenous application of CNTF at this point may further enhance RGC survival, since more receptors are available for protein binding and propagation of the extracellular signal (Adel et al. 2005).

CNTF mediated activation of these pathways may also protect RGC from glutamate induced excitotoxic damage through modification and/or downregulation of glutamate receptors (Petersén & Brundin 1999). This is important since excitotoxic damage has been

shown to be a major contributor of RGC cell death after axotomy (cited in (Adel et al. 2005)).

Alternatively, CNTF may protect neurons from injury through an indirect mechanism, for example, CNTF release from glia can be stimulated through the application of exogenous protein (Adel et al. 2005). Several studies shown that exogenous CNTF can directly activate glia (Müller glia, astrocytes) to bring about changes in gene expression via the Ras-MAPK and JAK-STAT signalling pathways (Adel et al. 2005).

Intravitreal injection of CNTF has a neuroprotective effect after ON transection and — after multiple injections — promotes RGC axon regeneration through both the ON and a PN graft (Cui & Harvey 2000, Cui, et al. 2003). Long term CNTF gene expression has also been demonstrated using Adenoviral vectors. In 2000, Weise et al found that intravitreal injection of Ad-CNTF rescued approximately 31% of RGC from cell death 14 d after optic nerve crush (ONC) injury (Weise, et al. 2000). Interestingly, Ad-CNTF was more effective at rescuing RGC from cell death when Ad-CNTF was applied to the severed end of the transected ON – this resulted in a 41% increase in RGC survival. Although Ad-CNTF promoted significant RGC survival, axon regeneration was not evident(Weise et al. 2000). Lentiviral and AAV2 vectors have also been used to deliver CNTF to the visual system – this ultimately resulted in RGC survival and axonal regeneration (Leaver, et al. 2006b, van Adel, et al. 2003, Leaver, et al. 2006a).

1.9.1 CNTF Receptor Complex

CNTF binds to a tripartite receptor complex to elicit its biological effects. Initially it binds to the GPI-linked CNTFα receptor (CNTFRα), which in turn associates with gp130 and LIF receptor β to form a tripartite receptor complex (Tuszynski 2007). Ligand binding ultimately leads to activation of the JAK-STAT, PI3-Akt and Ras-MAPK signalling pathways (see figure 1.10).

1.9.2 The JAK-STAT signalling pathway

The JAK-STAT signalling pathway can be activated by a variety of cytokines (IL-6, IL-11, CNTF) and growth factors. Cytokines such as CNTF, IL-6, IL-11, bind to their respective receptors (CNTFRα, IL-6Rα, IL-11Rα) which stimulates association with co-receptors such as gp130 and LIF to form a tripartite receptor complex (Tuszynski 2007). Receptor activation leads to tyrosine phosphorylation of Janus kinase – the activated receptor complex provides docking sites for SH2 containing signalling molecules such as signal-transducer and activator of transcription (STAT) (Signal Transducer and Activator of Transcription) and Grb2 (Tuszynski 2007) (to activate the JAK-STAT and Ras/MAPK signalling pathways respectively). Once docked STAT proteins are phosphorylated by JAKS and undergo a process of homo- or heterodimerisation (Aaronson & Horvath 2002). At which point STAT dimers translocate to the nucleus and interact with specific DNA sequences to bring about changes in gene expression (Tuszynski 2007, Aaronson & Horvath 2002). CNTF signalling through this receptor complex has also been shown to activate the PI3k/AKt, Ras/MAPKand PLCɣ signalling pathways (Boulton, et al. 1994). The JAK-STAT signalling

pathway can interact with a variety of different signalling pathways. Cross-talk between these signalling pathways is complex and can occur at multiple points throughout the JAK-STAT signalling cascade.

1.10 Non-viral mediated gene transfer

1.10.1 Naked DNA

Delivering naked, unpackaged plasmid DNA to the visual system is extremely inefficient. The ability to transfect mammalian cells using naked, unpackaged plasmid DNA is extremely limited. Naked DNA is unable to cross biological membranes (e.g. plasma, endothelium and nuclear membranes) -this is thought to be a result of the repulsive forces generated between the negatively charged cell surface and the naked DNA (Niidome & Huang 2002). Another contributing factor to their poor efficacy is that endonucleases present within the extracellular space can rapidly degrade naked, unpackaged DNA rendering them ineffective (Niidome & Huang 2002). Several techniques have been developed to tackle the problem of poor DNA uptake.

1.10.2 Electroporation and shotgun gene delivery

Electroporation is a technique which is commonly used in vitro to facilitate DNA uptake — it has also been used in vivo with varying degrees of success. An electric pulse is applied

to temporarily permeabilise the cell membrane and overcome the repulsive forces by driving the negatively charged DNA into the cell (Vry, et al. 2010).

In vivo delivery is achieved when the electric field is applied directly after a bolus injection of DNA. The effectiveness of this technique was first demonstrated in vivo by Titomirov et al. In this study electroporation was successfully used to deliver plasmid DNA (containing a neomycin resistant cassette) into the skin of newborn mice (Titomirov, et al. 1991).

Since then electroporation has been extensively used as a method of gene transfer. Its usefulness has also been demonstrated in the eye to transduce RGC (Mo & Yokoyama 2002), pigmented epithelial cells (RPE cells) and the cornea (Mo & Yokoyama 2002). Retinal transduction was achieved by placing a hemisphere cathode on the cornea and a hemisphere anode around the ON. This technique was used to successfully transduce RGC with a plasmid encoding BDNF after an intravitreal injection, and rescued ≈38.7% of RGC from cell death 6 weeks after ON transection. Despite this promising outcome, this technique has a number of limitations (Mo & Yokoyama 2002).

One of the limitations of electroporation is that the electric pulse needs to be carefully calibrated to ensure that the pulse is strong enough to temporarily permeabilise the cell membrane, but not so strong that it causes irreversible cell damage (Niidome & Huang 2002). It is also very difficult to target specific cell types since electroporation increases the permeabilisation of all cell membranes. As a result, electroporation doesn't seem to be a very translatable technique in terms of delivery therapeutics to patients.

Gene gun can be used as an alternative to electroporation. Gold particles are coated with DNA and shot into the tissue or cell of interest. As a result DNA penetrates the

cell membrane and is transported directly into the cell cytoplasm or nucleus (Niidome & Huang 2002). One of the limiting factors of this technique is that the level of tissue penetration is often poor (Niidome & Huang 2002).

1.10.3 Cationic polymers

Cationic polymers are often used to increase the transduction efficiency of non-viral mediated gene transfer. Some cationic polymers (e.g. poly-L-lysine) form linear chains, whilst others have a highly branched structure (e.g. poly (ethyleneimine), fractured dendrimers) (Smedt & Demeester 2000). Cationic polymers are able to accommodate larger genes (Smedt & Demeester 2000). In the presence of cationic polymers and multivalent cations, plasmid DNA condenses to occupy a much smaller space (Smedt & Demeester 2000). This process is thought to protects DNA from degradation by extracellular nucleases and prolongs their half-life (Bielinska & Kukowska-Latallo 1997).

1.11 Viral mediated gene transfer

A variety of viral vectors have been tested for their ability to transfect RGC of the visual system. To be an effective therapeutic, the viral vector needs to be able to transduce post mitotic cells without eliciting a harmful immune response. This can be accomplished directly through the transduction of RGC or indirectly through the transduction of other retinal cell types. One of the main advantages of using a viral mediated gene transfer

strategy is that long term transgene expression can be achieved from a single injection of virus.

1.11.1 Adenoviruses

Adenoviruses (Ad) are polyhedral, non-enveloped viruses which contain a double-stranded DNA genome (Harvey, et al. 2006). Although Ad infection has been linked to a number of human diseases (Chanock 1974), Adenoviral vectors have become a popular choice for delivering therapeutic genes to the visual system. Ad exhibit a high degree of cellular tropism, in fact over 50 types of Ad has been identified in recent years.

One of the advantages of using Ad as a viral vector is that it is able to transduce both dividing and non-dividing cells – as a result both neuronal and glial cell populations can be targeted using this kind of viral vector (Harvey et al. 2006). Moreover infection can be achieved without incorporation of viral DNA into the host cells genome reducing the likelihood of causing random oncogenic events. Ads can also accommodate much larger inserts (≈8 kb), making it possible to deliver a wider range of therapeutic transgenes (Harvey et al. 2006).

Another important factor to consider when developing therapeutic gene vectors is the ease of production and purification. In the case of Ad this does not appear to be a problem, as high viral titres can be achieved through well established manufacturing techniques (Harvey et al. 2006).

Although the onset of gene expression is rapid, transgene expression is often short-lived and is rapidly cleared by the immune system (Isenmann, et al. 2001). As a result, adenoviral vectors are not typically suitable for long term therapeutic regimes and may be more suitable for short term use. Another important factor to consider is the impact of using such an immunogenic viral vector, as this may cause harmful adverse effects. To overcome this problem, several groups have developed ways to evade the immune response e.g. by encapsulating viral particles in polymers (Fasbender & Zabner 1997) or gold particles (Sims, et al. 2009).

1.11.2 Lentiviruses

Like other retroviruses, lentivirus (LV) has an RNA genome that is surrounded by core proteins and a lipid envelope (Verma & Weitzman 2005). Once the vector is taken up by the cell the RNA strand is reverse transcribed and incorporated randomly into the host genome (Verma & Weitzman 2005). As a result the transgene can be inherited by the cells progeny allowing long term gene expression to occur in dividing cells (e.g. glia) without the need for repeat administration (Davidson & Breakefield 2003). In addition to this, Lentiviral vectors can transduce non-dividing cells making it possible to also transduce neuronal cell populations. Although random integration is advantageous in some respects (see above) it can also increase the likelihood of gene inactivation or oncogene activation. LV has similar packaging capabilities to that of Ad and can accommodate an insert of approximately 8 kb (Davidson & Breakefield 2003). Furthermore LV does not typically induce a significant immune response (Davidson & Breakefield 2003).

A number of lentiviral variants are currently available for use as therapeutic vectors including the human immunodeficiency virus (HIV), equine infectious anaemia virus (ELAV), simian immunodeficiency virus (SIV) and feline immunodeficiency virus (FIV) (Verma & Weitzman 2005).

1.12 Structure of wild type adeno-associated virus

Wild type adeno-associated virus (AAV) was initially identified as a contaminant of adenovirus preparations (Atchison, et al. 1965). Wild type AAV has a single stranded DNA genome consisting of ≈4700 bases which is flanked by identical 145base inverted terminal repeats (ITR) (Vasileva & Jessberger 2005). Wild type AAV contains REP and CAP genes which are responsible for replicating and packaging viral DNA and producing the capsid proteins needed for successful infection (Vasileva & Jessberger 2005). The virus can enter either a lytic (see section 1.13) or lysogenic (see section 1.14) pathway after host cell infection.

1.13 The lytic pathway

The lytic pathway occurs when the virus infects a cell in the presence of a helper virus such as Ad or herpes simplex virus (HSV). The virus enters the cell via a receptor mediated process (e.g. HSPG or laminin receptor), replicates and packages its viral genome

(Vasileva & Jessberger 2005). The host cell then undergoes helper virus induced cell lysis followed by the release of infective virion particles (Vasileva & Jessberger 2005).

1.14 The lysogenic pathway

The virus enters the lysogenic pathway when the virus infects the cell in the absence of a helper virus. If this occurs gene expression is repressed and the AAV integrates its genome into the host cell at chromosome 19 (Vasileva & Jessberger 2005). The viral DNA remains there latently until a helper virus comes along. If a latently infected cell is then infected with a helper virus, viral gene expression is activated, viral DNA is excised from the chromosome and the cell enters the lytic pathway (Vasileva & Jessberger 2005) (see section 1.13).

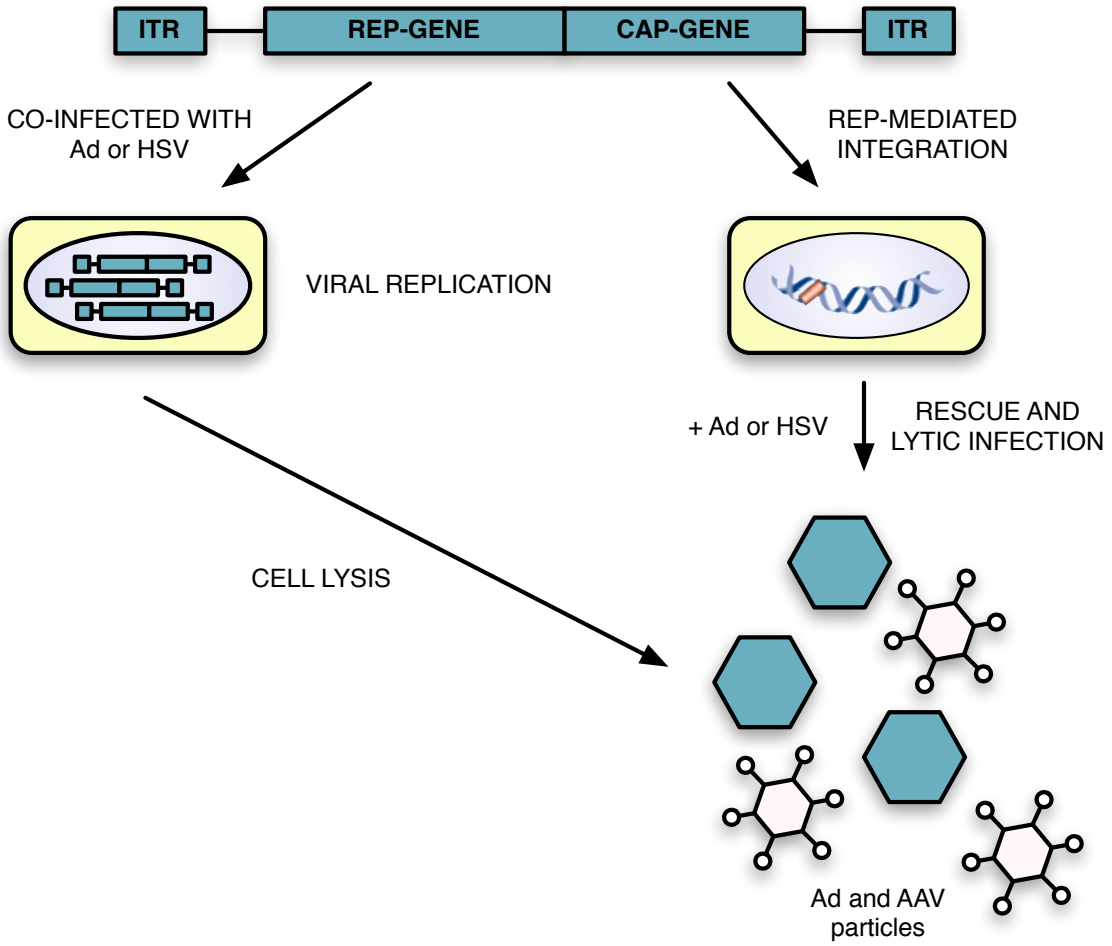

Figure 1.11: Structure of Wild Type AAV. Wild type AAV has a single stranded DNA genome which is flanked by palindromic ITRs. It also contains two open reading frames which encode rep and cap genes which are required for packaging viral DNA and producing the capsid proteins needed for infection. In the absence of a helper virus (e.g. Ad or HSV) AAV integrates at chromosome 19 of the host cells genome and resides there until a helper virus comes along. The lytic pathway occurs when AAV infects a host cell in the presence of a helper virus. The virus enters the cell through a receptor mediated process, replicates and packages its viral genome. The host cell undergoes helper virus induced cell lysis and virion particles are released. Figure modified from (Vasileva & Jessberger 2005).

1.15 Recombinant AAV virus as a gene delivery vector

The replication defective and non-pathogenic nature of this virus prompted researchers to rapidly develop recombinant vectors. These recombinant vectors exhibit many of the desirable features of wild type AAV (low pathogenicity and immunogenicity) whilst preventing the undesirable properties of chromosomal integration, and the requirement of a helper virus. The REP and CAP genes are replaced with a gene of interest (e.g. CNTF) together with a strong promoter (Cytomegalovirus, CMV) and a reporter gene, such as green fluorescent protein (GFP) (Vasileva & Jessberger 2005). The REP and CAP genes, together with Ad elements (Ad Va, E2A, E4), are supplied on separate plasmids (pAAV RC and pHelper plasmids, Stratagene) which contain all the genes required for the production of infective recombinant AAV particles (rAAV). Since these plasmids do not share any homology with the REP/CAP gene the risk of producing wild type virus (through recombination) is reduced. Triple transfection of these plasmids enables rAAV particles to be produced and released from the host cell. After purification and titration these viruses can then be used to deliver shRhoA and/or CNTF to RGC of the retina.

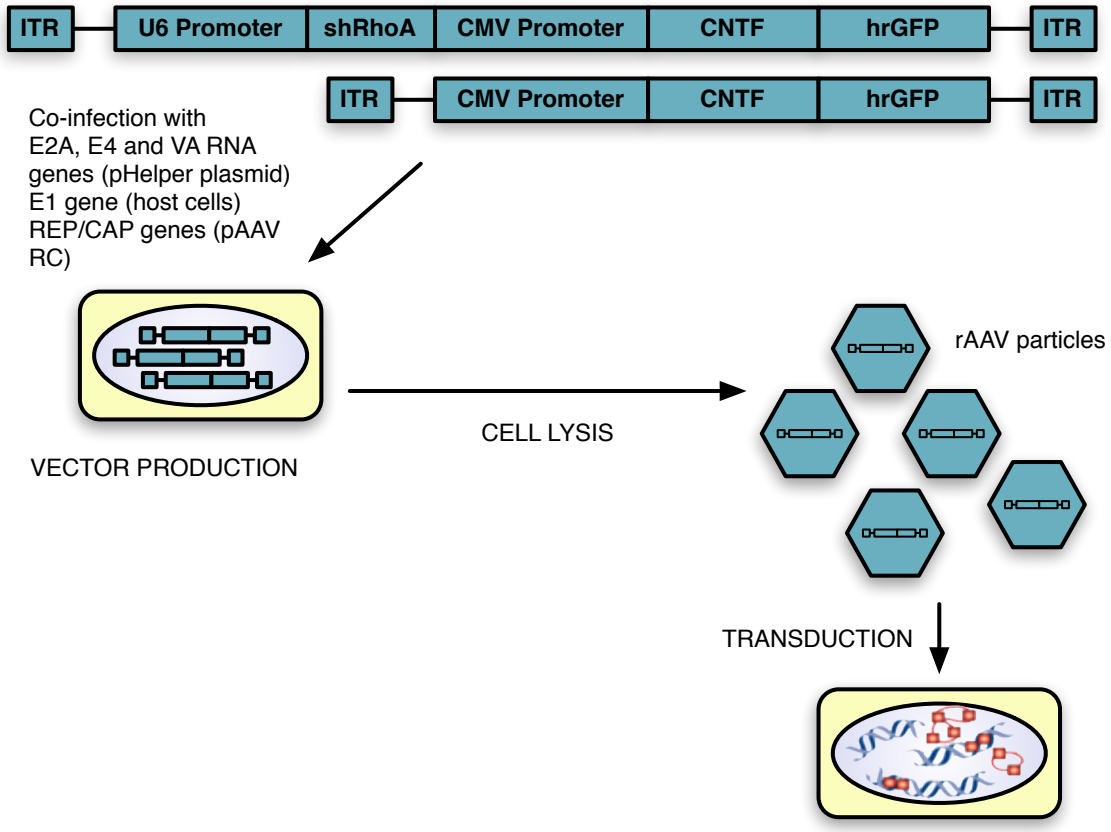

Figure 1.12: Recombinant AAV Virus. The REP and CAP genes of wild type AAV are replaced with a gene of interest (e.g. CNTF). This insert contains a strong promoter (CMV) to drive gene expression and a reporter gene which allows the visualisation of AAV2 transfected cells. Like the wild type virus, the transgene insert is flanked by ITR to allow viral replication to occur. Figure modified from (Vasileva & Jessberger 2005).

1.15.1 Advantages and disadvantages of using AAV as a viral vector

AAV viruses are ideal for retinal gene transfer since they are able to transduce both dividing and non-dividing cells. Furthermore they exert low pathogenicity and immunogenicity, in fact approximately 80% of the human population test seropositive for AAV2 without any overt pathology (Goncalves 2005). Moreover, rAAV vectors are particularly effective at promoting long term gene expression in the eye (Dudus, et al. 1999), making the requirement for repetitive protein injections redundant. One of the major limiting factors of using rAAV2 as a gene delivery vector is the transduction process. First AAV2 needs to be able to enter the cell of interest through a receptor mediated process (Surace & Auricchio 2008), this is problematic when virus is administered through an intravitreal injection and is discussed in section 5.1.1. Once internalised the AAV virus needs to be trafficked to the nucleus where it can initiate second strand DNA synthesis and express the desired transgene (Surace & Auricchio 2008). All of these processes are very time consuming; in the case of AAV2 it can take up to 30 d for transgene expression to be seen after delivery (Surace & Auricchio 2008, Zincarelli, et al. 2008). Furthermore AAV has a limited packaging capacity and is only able to accommodate a ≈4.7 kb insert (Surace & Auricchio 2008) — however this is sufficient to house our gene of interest.

1.16 RNA interference

RNA interference (RNAi) is a highly conserved mechanism that co-ordinates the degradation of double-stranded RNA (dsRNA) molecules (Davidson & McCray 2011). This nat-

urally occurring defence mechanism has been observed in a number of organisms, including single cell fungi (Cogoni, et al. 1996), plants (Bernstein, et al. 2001), frogs (Oelgeschlager, et al. 2000) and insects (Kennerdell & Carthew 1998). The process of RNAi was initially observed in transgenic plants (Bernstein et al. 2001). Transgenes coding for chalcone synthase were introduced into pertunia plants to enhance petal pigmentation (Bernstein et al. 2001); in spite of this they found that many of the plants had white or variegated petals — this outcome was indicative of gene silencing (Bernstein et al. 2001). Subsequent work on caenorhabditis elegans (C.elegans) (Fire, et al. 1998) revealed that the presence of double stranded RNA was a prerequisite for RNAi. They found that injection of single stranded sense or antisense RNAs led to moderate mRNA suppression, whilst introduction of dsRNA resulted in significant mRNA knockdown (Fire et al. 1998). Interestingly, many of the phenotypic changes associated with mRNA knockdown were displayed by injected adults, and inherited by their respective progeny (Fire et al. 1998). This was the first indication that RNAi could be used to cause heritable changes. This phenomenon was later recognised in a variety of mammalian cell lines (Human embryonic kidney-293, HeLa, COS-7 and NIH/3T3) (Elbashir, et al. 2001). They found that transfection of dsRNA caused significant mRNA knockdown without producing an interferon response. The outcome of this study brought with it the realisation that short-interfering RNA (siRNA) technology could be used to produce ``gene-specific'' therapeutics (Elbashir et al. 2001).

The mechanistic action of RNAi has recently been demonstrated in humans (during a phase I clinical trial) (Davis, et al. 2010). siRNA was administered systemically, using a nanoparticle delivery system, to treat patients with solid tumours. Analysis of patient

biopsies revealed a dose dependent accumulation of nanoparticles, together with mRNA cleavage and protein suppression (Davis et al. 2010).

1.16.1 Mechanisms of RNA interference

RNAi can be triggered by the presence of exogenous dsRNA (e.g. derived from viruses or transposable elements) and leads to the Dicer dependent generation of small (20 to 24 nucleotide pairs) siRNAs (Davidson & McCray 2011). Alternatively siRNAs can arise from endogenous loci that contain direct or indirect ITR (Davidson & McCray 2011). Transcripts arising from these loci form short hairpin loops which are cleaved by Dicer to produce siRNAs (Davidson & McCray 2011). The resultant siRNA duplex consists of two RNA strands, each of which has a 5' phosphate group and a 3' hydroxyl group (Davidson & McCray 2011). These strands are paired together to produce a 2 nucleotide overhang at each end (Davidson & McCray 2011). Once synthesized, one strand of the siRNA duplex (the guide strand) binds to the endonuclease Argonaut (AGO) and is incorporated into the RNA-induced silencing complex (RISC), whilst the other strand (the passenger) is discarded (Davidson & McCray 2011). The guide strand directs the RISC complex to a complementary region of mRNA. Gene silencing is achieved through the subsequent cleavage of the targeted mRNA, ultimately leading to mRNA degradation and translational arrest (Davidson & McCray 2011).

CHAPTER 2

MATERIALS AND METHODS

2.1 *In vitro* Techniques

Unless otherwise stated reagents were obtained from Sigma-Aldrich (Poole, UK).

2.1.1 Retinal culture

Adult Sprague-Dawley rats (150 g to 250 g) were killed by cervical dislocation, the eyes were removed and placed on ice in sterile phosphate buffered saline (PBS) (Gibco, Paisley, UK). Retinae were dissected from each eye and dissociated using a papain dissociation kit (Worthington Biochemicals, New Jersey, USA). The papain solution was prepared by adding 5 ml of earle's Balanced Salt Solution (EBSS) with bicarbonate and phenol red together with 20 U ml^{-1} papain and 100 U ml^{-1} deoxyribonuclease I (DNase I). Retinae were placed in this solution and incubated at 37 °C in a humidified atmosphere containing 5% CO_2 for 90 min. During this time, ovomucoid inhibitor was reconstituted in 32 ml EBSS to give a final concentration of 10 mg ml^{-1} ovomucoid inhibitor and 10 mg ml^{-1} albumin. After 90 min, any remaining tissue fragments were broken up by triturating with a 5 ml pipette, the solution was then centrifuged at 300 x g for 5 min at room temperature (RT). The supernatant was discarded and the remaining pellet was resuspended in a solution containing 1.35 ml EBSS, 150 µl reconstituted albumin ovomucoid inhibitor and 125 µl DNase. The cell suspension was then layered on top of a discontinuous density gradient (containing 2.5 ml of albumin ovomucoid inhibitor) to separate intact retinal cells from cell membrane components. The cell suspension was then passed through this gradient by centrifugation (70 x g for 6 min). The supernatant (containing cell membrane components) was discarded and the remaining cell pellet (containing retinal cells) was

resuspended in 1 ml of supplemented Neurobasal-A. Cell suspension (10 µl) was mixed with 10 µl of trypan blue and added to a haemocytometer. The number of live cells in the 25 squares located in the centre of the haemocytometer were counted, retinal cell number was calculated and the appropriate number of cells plated. Cells were plated on laminin coated chamber slides (BD Biosciences, Oxford, UK) and incubated at 37 °C in a humidified atmosphere containing 5% CO_2 for 3 d.

2.1.1.1 Retinal culture quantification

RGC were visualised by βIII-Tubulin immunostaining and identified by their distinctive morphology (see section 4.3.1). Retinal cultures were prepared as in section 2.1.1 and plated on laminin-coated chamber slides at a density of 130 000 retinal cells per well (0.7 cm^2).

Each well was divided into a grid of 9 squares. Within each grid square, 4 random fields of view were captured using an upright microscope (Carl Zeiss Meditec, Dublin CA) — 36 images/well were captured in total. RGC cell number was determined by counting βIII-Tubulin positive cells and neurite length was measured using Image Pro® 6.2 (Media Cybernetics, MD, USA). Neurites were classified as projections that originated at the cell body and were at least the diameter of the cell soma in length.

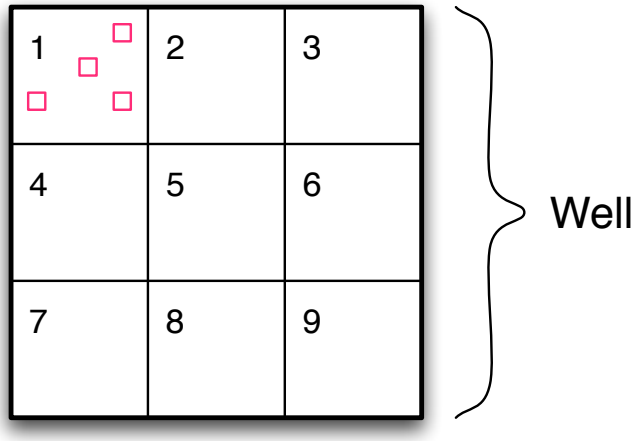

Figure 2.1: Diagrammatic representation of sampling technique. Each well was divided into a grid of 9 squares. 4 random fields of view were captured within each grid square. Diagram reproduced from (Morrison 2011).

2.1.2 RGC-5 cell culture

RGC-5 cells were kindly provided by Dr. Neeraj Agarwal (Department of Pathology and Anatomy, The University of north Texas Health Science Centre, Fort Worth, Texas, USA). RGC-5 cells were grown in dulbecco's Modified Eagle Medium (DMEM) supplemented with 100 U ml^{-1} penicillin/streptomycin (P/S) and 10% heat-inactivated foetal bovine serum (FBS). RGC-5 cells were incubated at 37 °C in a humidified environment containing 5% CO_2 and were passaged at a ratio of 1:20. The RGC-5 cells were grown in T175 flasks during general cell maintenance.

2.1.2.1 Morphological analysis of RGC-5 cells

RGC-5 cells were treated with Staurosporine using concentrations ranging from 0 nM to 3.16 µM for 24 h to induce differentiation. The extent of process outgrowth, expression and branching were assessed after 24 h exposure to the reagent. The extent of process

expression and branching per cell were expressed as mean ± standard error of the mean (SEM) from 60 cells. The length of each process was measured from soma to end using Image Pro® 6.2 (Media Cybernetics, MD, USA). Mean process length and longest process per cell were expressed as ± SEM from 60 cells. For the purpose of quantification a process was defined as any cellular projection longer than the diameter of one cell soma.

2.1.3 Immunocytochemistry and Immunohistochemistry

IHC and immunocytochemistry are techniques which can be used to visualise particular antigens on tissues/cells of interest. This is accomplished by the application of a primary antibody targeted against a specific antigen, followed by addition of a secondary antibody conjugated to a fluorescent label — this allows visualisation when examined microscopically. The location of fluorescent label gives an indication as to the cellular location of the antibody-antigen interactions.

2.1.3.1 Immunocytochemistry

Cells were fixed with 4% formaldehyde (TAAB Laboratories, Berkshire, UK) in PBS (Oxoid, Ltd, Basingstoke, UK) at RT for 10 min. The formaldehyde solution was then removed with a pasteur pipette and the wells were washed three times with rinsing buffer. Blocking buffer was then added to each of the wells to eliminate non-specific binding. Primary antibody (200 µl) was then added to each of the wells and incubated at RT for 1 h. Primary antibodies were then removed by inverting chamber slides onto paper towels and the wells were washed three times with rinsing buffer. Secondary antibodies (200 µl)

were added to each of the wells and incubated for 1 h at RT in a dark environment to prevent bleaching. Secondary antibodies were removed by inverting chamber slides onto paper towels and each of the wells were washed three times in rinsing buffer. When the last wash was removed, the well dividers were removed from the chamber slides and coverslips were mounted using vectashield with',6-diamidino-2-phenylindole (DAPI) (Vector Labs, Peterborough, UK). The slides were then viewed with an upright microscope (Carl Zeiss Meditec, Dublin, CA) and images were captured using the Axiovision software (Axiovision; Carl Zeiss Meditec).

2.1.3.2 Immunohistochemistry

ON and eye sections were removed from the freezer, thawed for 30 min and washed in rinsing buffer (3 x 5 min). Excess rinsing buffer was aspirated and a hydrophobic pen was used to draw around each section. Blocking solution (100 µl) was then applied to each of the sections and slides were subsequently placed in a humidified chamber at RT for 1 h. After this, blocking buffer was removed and 100 µl of primary antibody was applied to each section and incubated in a humidified chamber for 1 h at RT. Slides were then washed in rinsing buffer (3 x 5 min) before applying the appropriate secondary antibody. Sections were then incubated in a humidified chamber at RT for 1 h in the dark to prevent bleaching of fluorescence. Sections were washed in rinsing buffer (3 x 5 min) and coverslips mounted using vectashield with DAPI (vector labs, Peterborough, UK). The slides were then viewed with an upright microscope (Carl Zeiss Meditec, Dublin CA) and images were captured using the Axiovision software (Axiovision; Carl Zeiss Meditec).

Table 2.1: Immunocytochemistry / immunohistochemistry reagents.

Reagents	Eye & optic nerve sections	Retinal culture & RGC-5 cell culture
10 mM PBS, ph 7.4	PBS tablets in milli-Q water	PBS tablets in milli-Q water
Rinsing buffer	0.1% Triton X-100 in PBS	0.1% Triton X-100 in PBS
Blocking buffer	10% NGS and 3% BSA in rinsing buffer	5% NGS and 3% BSA in rinsing buffer
Primary antibody dilution buffer	3% BSA in rinsing buffer	Prepared in blocking buffer
Secondary antibody dilution buffer	3% BSA in rinsing buffer	Prepared in blocking buffer

2.1.3.3 Antibodies

Antibody details for immunocytochemistry and immunohistochemsitry are listed in table 2.2.

Table 2.2: Antibody details for immunocytochemistry and immunohistochemsitry.

Antibody	Specificity	Source & Location	Species	Stock Concentration	Dilution
βIII-Tubulin	RGC somata, axons and neurites	Sigma-Aldrich, Poole, UK	Mouse	N/A (Ascites)	1/500 (IHC/ICC)
βIII-Tubulin	RGC somata, axons and neurites	Sigma-Aldrich, Poole, UK	Rabbit	200 µg ml^{-1}	1/500 (IHC/ICC)
GAP-43	Regenerating RGC axons	Invitrogen Ltd, Paisley, UK	Mouse	0.5 µg ml^{-1}	1/500 (IHC)

Continued on next page ...

Table 2.2 -- continued from previous page

Antibody	Specificity	Source & Location	Species	Stock Concentration	Dilution
NG2	NG2 positive glia	Abcam, Cambridge, UK	Rabbit	1 mg ml^{-1}	1/500 (ICC)
Carbonic anhydrase II (CAII)	Oligodendrocytes	Gift from Prof. Wilkinson, University College London, UK	Rabbit	N/A (Serum)	1/4000 (ICC)
eGFP	eGFP positive cells	Abcam, Cambridge, UK	Rabbit	0.5 mg ml^{-1}	1/1000 (IHC)
hrGFP	hrGFP positive cells	Agilent Tech., Wokingham, UK	Rabbit	N/A (Antiserum)	1/1000 (IHC)
Alexa Fluor 488	Mouse IgG	Invitrogen Ltd, Paisley, UK	Goat	2 µg ml^{-1}	1/500 (IHC, ICC)
Alexa Fluor 594	Mouse IgG	Invitrogen Ltd, Paisley, UK	Goat	2 µg ml^{-1}	1/500 (IHC, ICC)
Alexa Fluor 488	Rabbit IgG	Invitrogen Ltd, Paisley, UK	Goat	2 µg ml^{-1}	1/500 (IHC, ICC)
Alexa Fluor 594	Rabbit IgG	Invitrogen Ltd, Paisley, UK	Goat	2 µg ml^{-1}	1/500 (IHC, ICC)

2.1.4 Haematoxylin and Eosin staining of frozen retinal sections

Frozen retinal sections were washed in several changes of PBS (3 x 5 min) to remove OCT. All sections were then immersed in Mayer's Haematoxylin for 1 min to stain the cell nuclei and identify the GCL, INL and IPL of the retina. Slides were then washed for 20 min under

running water to remove excess Haematoxylin. Retinal sections were then submerged in Eosin for 5 min to counterstain, the sections were then washed in distilled water to prevent streaking. The retinal sections were then immersed in 50%, 70%, 90%, 100% and 100% ethanol for 1 min each. Immediately after this, the sections were transferred into 2 changes of histoclear for 1 min and 3 min respectively. Slides were then mounted using vectamount. Cover slips were applied to each slide and bright field images were captured.

2.1.5 AAV2 constructs

The four constructs used (*AAV2-eGFP*, *AAV2-CNTF-hrGFP*, *AAV2-CNTF-shRhoA-hrGFP* and *AAV2-CNTF-FLAG*) were kindly provided by Dr Mike Douglas (Molecular Neuroscience Group, University of Birmingham). All constructs were produced using the AAV Helper Free system (Stratagene). The gene of interest, CNTF, was cloned into the multiple cloning site of the *pAAV-IRES-hrGFP* plasmid. Prior to this, the CNTF sequence was modified to include an NGF signal sequence — this was achieved by fusing a sequence encoding of the first 20 amino acids from rat prepro-Nerve growth factor (ppNGF) to the rat CNTF sequence. This would allow CNTF to be released from RGC and dispersed throughout the retina. The *pAAV-IRES-hrGFP* plasmid allowed us to produce FLAG-tagged CNTF as it contains a 3x FLAG sequence at the C terminus of the multiple cloning site. Untagged CNTF was produced by inserting a stop codon after the CNTF sequence, but before the FLAG encoding region. Importantly this plasmid contains an internal ribosome entry site (IRES) which allows multiple genes (e.g. CNTF and hrGFP) to be translated from a single

plasmid. IRES sequences allow translation initiation to occur in the middle of an mRNA sequence by a cap-independent mechanism. As a result Ribosomes bind to the AUG start codon without scanning the 5' non-translated region of the transcript (Mizuguchi, et al. 2000). AAV2 viruses were manufactured, concentrated and titred by Gene Vector Core (University of Iowa). For a more complete explanation of this process (see section 1.15).

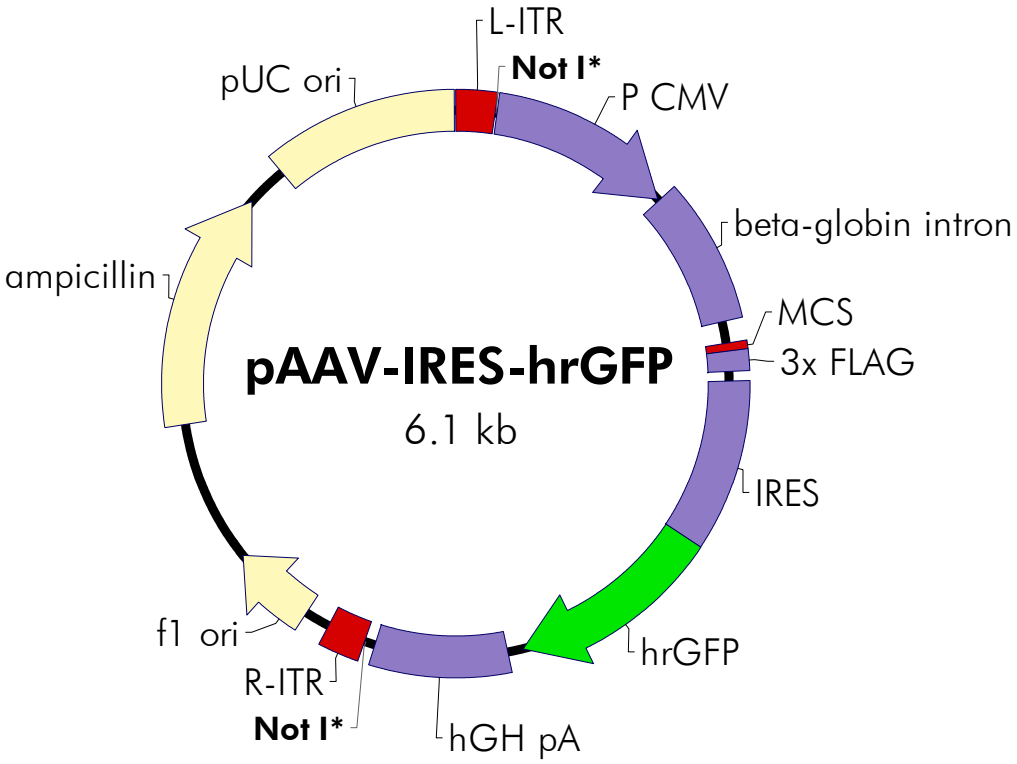

Figure 2.2: *pAAV-IRES-hrGFP* expression plasmid supplied in the AAV Helper Free System. Reproduced from `http://www.chem.agilent.com/Library/usermanuals/Public/240071.pdf`

2.1.6 Lipofectamine 2000 Transfection

Human embryonic kidney 293 cells (HEK-293) were plated in DMEM media at a density of 500 000 cells well^{-1} in a 6-well plate (Nunc, Loughborough, UK) to ensure that the

cells were 90-95% confluent at the time of transfection. The following day, transfection samples and reagents were prepared in separate tubes. In one tube, plasmid DNA was diluted in Opti-MEM media (2 ml well^{-1}) to give a DNA concentration of 4 µg well^{-1}. In the second tube, 10 µl of Lipofectamine 2000 (Invitrogen, Ltd, Paisley, UK) was diluted in Opti-MEM media (Invitrogen, Ltd, Paisley, UK) (2 ml well^{-1}) — both solutions were incubated at RT for 5 min. To form complexes, diluted plasmid DNA was combined with the diluted Lipofectamine solution, mixed gently and incubated at RT for 20 min. After this, 2 ml of complexes were added to each well and mixed gently. Cells were then incubated at 37 °C in a humidified atmosphere containing 5% CO_2 for 5 h, at which point the media was changed with DMEM (+ 100 U ml^{-1} P/S + 10% FBS). Treatment groups comprised of *AAV2-hrGFP*, *AAV2-CNTF-hrGFP*, *AAV2-CNTF-FLAG*, *AAV2-CNTF-shRhoA-hrGFP*, untreated control and Lipofectamine 2000 only. Conditioned media was collected 5 d after transfection.

2.1.7 Enzyme linked immunosorbent assay

A sandwich enzyme-linked immunosorbent assay (ELISA) was used to measure CNTF levels in HEK-293 conditioned media. The CNTF ELISA (R&D Systems) was performed in accordance with manufacturer's instructions and all reagents were supplied with the kit. A sterile 96-well plate (Nunc, Loughborough, UK) was coated with capture antibody, sealed with parafilm and incubated at RT overnight for 17 h. Following antibody removal, each well was rinsed three times with wash buffer (≈400 µl well^{-1}). After each wash step the buffer was removed by inverting the plate and blotting with clean paper towels.

To block, reagent diluent (300 µl) was added to each well and incubated at RT for 1 h. After repeating the aspiration wash step, CNTF standards and samples were prepared and added to each well (100 µl). The initial CNTF standard was diluted with reagent diluent to give a final concentration of 2000 pg ml^{-1}. A series of 1:2 dilutions (i.e. 1000 pg ml^{-1}, 500 pg ml^{-1}, 250 pg ml^{-1} etc) was then performed so that a standard curve could be constructed (each sample was initially diluted 1:5 to ensure that the concentration would fall within the standard curve). A series of 1:2 dilutions were then performed for each sample, as with the CNTF standard.

The plate was then covered with an adhesive strip and incubated at RT for 2 h on a shaker. After another round of washing, detection antibody (100 µl) was added to each of the wells. The plate was then covered with a new adhesive strip and incubated at RT for a further 2 h. Another aspiration wash step was performed and then a working solution of streptavidin-HRP was prepared and added to each well. The plate was incubated at RT for 20 min and covered with foil to avoid being placed in direct light – this was then followed by another aspiration wash step.

Substrate solution (100 µl) was added to each well and incubated at RT for 20 min. Stop solution (50 µl) was then applied to each well and mixed gently on a shaker. The optical density was measured using a microplate reader set to 450 nm (Victor3, Perkin Elmer). A standard curve of absorbance vs CNTF concentration was then plotted using Microsoft Excel. This curve was then used to determine the relative concentration of CNTF present within each sample.

Table 2.3: Reagents for CNTF ELISA.

Solution	Reagents
10 mM PBS, pH 7.4	PBS tablets in milli-Q water
Wash buffer	0.05% Tween-20 in PBS
Reagent diluent	1% BSA in PBS
Substrate solution	1:1 mixture of colour reagent A (H_2O_2) and colour reagent B (Tetramethylbenzidine)
Stop solution	2N H_2SO_4
Capture antibody	2 µg ml^{-1} prepared in PBS
Detection antibody	200 ng ml^{-1} prepared in reagent diluent
Streptavidin-HRP	Prepared in reagent diluent

2.1.8 Cell viability assay

The viability of RGC-5 cells was determined by the use of Cell Titer-Glo (Promega, Southampton, UK). The assay is based on a luciferase reaction which is used to measure the ATP levels of metabolically active cells. The Cell Titer-Glo reagent acts by lysing cell membranes to release ATP, inhibiting endogenous ATPase activity and providing the luciferin and luciferase needed to measure ATP in a bioluminescent reaction. The amount of ATP present following cell lysis is directly proportional to cell number.

This method of determining cell viability has a number of advantages over other methods. It takes a relatively short time to perform the assay and is incredibly sensitive at detecting intracellular ATP levels. The assay is performed in a single plate and does not involve any cell transfer or wash steps which could result in cell loss and inaccuracies. Further-

more, this assay gives reproducible bioluminescent readouts resulting in low standard deviation/error values.

One of the limitations of using this method is that it requires cells lysis to isolate and measure cellular ATP content. As a result, conclusions can only be drawn from whole populations of cells rather than from individual cells. Another potential limitation of having a cell lysis step is that it prevents further analysis from being carried out on the same population of cells (e.g.immunocytochemistry, PCR e.t.c.). This method relies on measuring the metabolic activity of cells (through ATP content) to determine cell viability. As a result this assay is potentially susceptible to additional factors which may rapidly influence ATP cell content (e.g. oxygen availability). Consequently, analysis is limited to gross changes in ATP content and does not allow for the analysis of contributing factors. It is also important that the right equipment is used to carry out these assays: Bioluminescent reactions require the use of a specialised microplates (opaque sides with a clear flat bottom) to prevent luminescent interference between wells. It's also essential that phenol red is not present within the media as it can reduce the luminescent signal.

RGC-5 cells were plated in a 96-well white opaque plate at a seeding density of 2500 cells well^{-1} in 180 µl of medium containing 10% FBS for 2 h at 37 °C in a humidified environment containing 5% CO_2. The CellTiter-Glo luminescent substrate was reconstituted with CellTiter-Glo buffer and equilibrated to RT. Cells were left at RT for 30 min before 100 µl of luminescent substrate was added. To ensure efficient cell lysis the plate was placed on a shaker for 5 min at RT and then left to stabilise for 10 min. The luminescence was then measured using a 96-well plate reader (Victor3, Perkin Elmer, MA, USA).

2.1.9 RNA extraction

RNA was extracted using the RNeasy mini kit (Qiagen) according to manufacturer's protocols.

2.1.9.1 RGC-5 cell RNA extraction

DMEM was removed from tissue culture flasks and cells were washed twice with sterile PBS. Trypsin (Gibco) in PBS (0.25%) was then added to detach cells from the flask — media (DMEM + 10% FBS + 1% P/S) was then added to inactivate the trypsin. The cell suspension was then transferred into a 50 ml Falcon tube and centrifuged at 300 x g for 5 min. The supernatant was carefully aspirated leaving the remaining cell pellet. The pellet was then re-suspended in denaturing buffer RLT (containing guanidine-thiocyanate) and homogenized using a rotor stator homogenizor. One volume of 70% ethanol was added to the homogenate to facilitate membrane binding. The solution was then transferred to a spin column and centrifuged at 8000 x g for 15 s, the flow through was collected in the tube supplied and discarded. Buffer RW1 (700 µl) was added to the spin column and centrifuged at 8000 x g for 15 s to wash the membrane. The membrane was then washed a further two times with buffer RPE (discarding the flow through each time) to remove contaminants. RNA was then eluted from the column in 50 µl of RNase free water. A Nanodrop was then used to measure RNA concentration.

2.1.9.2 Mouse brain RNA extraction

Mouse brain was dissected out and snap frozen in liquid nitrogen, ≈30 mg of brain tissue was disrupted in 600 µl buffer RLT using a rotor stator homogeniser (IKA ® T10 basic Ultra-Turrax) for 20 s to 40 s. The homogenate was centrifuged at full speed for 3 min and the supernatant was carefully removed using a pipette. The supernatant was then transferred into a clean eppendorf tube and one volume of 70% ethanol was added to aid membrane binding. The solution was then transferred to a spin column and centrifuged at 8000 x g for 15 s, the flow through was collected in the tube supplied and discarded. Buffer RW1 (700 µl) was added to the spin column and centrifuged at 8000 x g for 15 s to wash the membrane. The membrane was then washed a further two times with buffer RPE (discarding the flow through each time) to remove contaminants. RNA was then eluted from the column in 50 µl of RNase free water. A Nanodrop was then used to measure RNA concentration.

2.1.9.3 Mouse eye RNA extraction

RNA was extracted from 2 mouse eyes using the RNeasy mini kit as previously described (see section 2.1.9.2).

2.1.10 RNA quantification

RNA concentrations were determined by loading 2 µl of RNA solution into a Nanodrop spectrophotometer (ND-1000; Wilmington, DE, USA) and measuring the absorbance of

each sample at 260 nm. The Nanodrop machine was also used to estimate sample purity; this was achieved by measuring the 260 nm/280 nm absorbance ratio. RNA with a purity value of >1.8 was used in all experiments. RNA integrity was determined by gel electrophoresis — RNA samples were resolved in a 1% agorose gel, identified by ethidium bromide (EtBr) (EtBr) staining and analysed using multigenius imaging. RNA was deemed to be intact when sharp bands of 18 s and 28 s ribosomal RNA subunits were present at ≈2 kb and ≈4 kb.

2.1.11 cDNA Libraries

Purified RNA was reverse transcribed into single-stranded complementary DNA (cDNA) using the high capacity cDNA archive kit (Applied Biosystems). The RT master mix was prepared using the reagent volumes shown in table 2.4 and placed on ice. Once prepared, 50 µl 2 x RT master mix was combined with 50 µl of RNA (26.48 ng μl^{-1}) in a PCR tube (for each 100 µl reaction). PCR tubes were then transferred to the thermal cycler for reverse transcription to commence (for reaction conditions see table 2.5).

Table 2.4: 2 x RT master mix (100 µl reaction volume).

Component	**Volume (µl) per Reaction**	**Volume (µl) per 31 Reactions**
10X Reverse Transcription Buffer	10	310
25X dNTPs	4	124
10X Random Primers	10	310
Multiscribe Reverse Transcriptase, 50 U/µl	5	155
Nuclease-free H_2O	21	651
Total per Reaction	50	1550

Table 2.5: Thermal cycler settings used for reverse transcription.

Step	1	2	3	4
Temperature (°C)	25	37	85	4
Time	10 min	120 min	5 s	∞

2.1.12 Primer Design

Primers (Alta Bioscience) were designed with the help of Dr. Mike Douglas using the Primer 3 software package. Table 2.6 shows the DNA sequences of the forward and reverse primers used. All primers, with the exception of rat CNTF, were between 20 and 22 nucleotides in length. The rat CNTF primers were 31 nucleotides in length - although significantly longer than those generally believed to be optimal (18 to 24 nucleotides in length), these primers had previously been used and optimised by Dr. Mike Douglas. Primers were matched, as far as possible, for melting temperature (Tm) and PCR product size (see table 2.6). Care was taken to avoid primers which form stable secondary structures (hairpin loops) and primer dimers - this was done to ensure that cDNA amplification would be successful and specific. An annealing temperature of 55 °C was selected after visual inspection of amplified PCR products (see figure 3.8). An annealing temperature of 50 °C produced a high degree of smearing and non-specific amplification, whilst an annealing temperature of 55 °C produced significantly cleaner PCR products.

Table 2.6: RGC-5 primer list.

Cell Marker	Forward Primer	Tm (°C)	Reverse Primer	Tm (°C)	Accession No.
βIII-Tubulin	5′-TGA GGC CTC CTC TCA CAA GT-3′	56.8	5′-CGC ACG ACA TCT AGG ACT GA-3′	56.7	NM_023279.2
Neurofilament-H	5′-AGC CCA AGG ACT CTA CAG CA-3′	57.4	5′-CTT TGG CTT TTC CGT CTC TG-3′	57.7	NM_010904
Neurofilament-L	5′-GCC GAA GAG TGG TTC AAG AG-3′	57.2	5′-TGT CTG CAT TCT GCT TGT CC-3′	56.7	GI:76573285
Neurofilament-M	5′-GTC AGA CCA GGC AGA AGA GG-3′	56.8	5′-GAT TTG GGC ATA GGG GAT TT-3′	58.2	NM_008691
Tau	5′-CAG TCT CCA CAC CCC AGT TT-3′	56.8	5′-ACA AGC TAA CAG GGC GAA GA-3′	57.8	M18776
Thy-1	5′-AAG GCC TCT GCC TGT AGT GA-3′	57.4	5′-GAA GAG GCA GGT TGC AAG AC-3′	57.3	NM_009382
Nestin	5′-AGG AAC CAA AAG AGG CAG GT-3′	57.9	5′-TTG GGA CCA GGG ACT GTT AG-3′	57.2	GI:38173717
NeuroD	5′-CAA AGC CAC GGA TCA ATC TT-3′	57.6	5′-CCC GGG AAT AGT GAA ACT GA-3′	57.4	NM_010894.2
Neurogenin-1	5′-CGC TTC GCC TAC AAC TAC ATC-3′	58.0	5′-CTG AAG CCG AGG GAC TAC TG-3′	57.3	U67776
Neurogenin-2	5′-GAT GCC AAG CTC ACG AAG AT-3′	57.7	5′-ACG TGG AGT TGG AGG ATG AC-3′	56.6	GI:1666909
SOX1	5′-CAC AGT TCA GCC CTG AGT GA-3′	56.3	5′-GAT CAG CCC AGA GAG ACT GG-3′	56.7	NM_009233.3
SOX2	5′-AAG GGT TCT TGC TGG GTT TT-3′	58.1	5′-AGA CCA CGA AAA CGG TCT TG-3′	57.4	NM_011443.3
Mouse CNTF	5′-GAT GGC TTT CGC AGA GCA AAC-3′	55.38	5′-TCT GAT GAG AAG AAA TGA CAC G-3′	50.47	NM_170786
Rat CNTF	5′-GAT CGG ATC CTA GGG GAT GGC TTT CGC AGA G-3′	64.51	5′-GAT CCT CGA GCT ACA TCT GCT TAT CTT TGG C-3′	60.21	NM_013166
RALDH2	5′-TTG CAG ATG CTG ACT TGG AC-3′	56.7	5′-TCT GAG GAC CCT GCT CAG TT-3′	56.8	BC075704

Continued on next page ...

Table 2.6 -- continued from previous page

Cell Marker	Forward Primer	Tm (°C)	Reverse Primer	Tm (°C)	Accession No.
CD11b	5′-CAT CTG CCA AGA CGA TCT CA-3′	56.5	5′-TTC TGG CTT GCT GAA TCC TT-3′	57.6	NM_001082960.1
CD68	5′-TTC TGC TGT GGA AAT GCA AG-3′	57.2	5′-AGA GGG GCT GGT AGG TTG AT-3′	57.7	NM_009853.1
SOX1	5′-CAC AGT TCA GCC CTG AGT GA-3′	56.3	5′-GAT CAG CCC AGA GAG ACT GG-3′	56.7	NM_009233.3
CD44	5′-GGC AGA AGA AAA AGC TGG TG-3′	57.7	5′-GGA ATG ACG TCT CCA ATC GT-3′	56.9	BC005676
CD133	5′-GAA AAG TTG CTC TGC GAA CC-3′	57.7	5′-TCT CAA GCT GAA AAG CAG CA-3′	57.3	GI:20271425
ChAT	5′-CCT GCC AGT CAA CTC TAG CC-3′	57.4	5′-ATA CAG AGA GGC TGC CCT GA-3′	57.2	NM_009891.2
Pax6	5′-AAC AAC CTG CCT ATG CAA CC-3′	57.7	5′ACT TGG ACG GGA ACT GAC AC-3′	56.8	NM_013627.4
GFAP	5′-CAC GAA CGA GTC CCT AGA GC-3′	57.3	5′-ATG GTG ATG CGG TTT TCT TC-3′	57.4	NM_001131020.1
GalC	5′-TGC GCA GTT TGA CAA CTT TC-3′	57.3	5′-AGG ATC CAG CAA AAA TGC AC-3	57.7	NM_008079
NG2	5′-TGG GCT CAG GAG ATG CTA GT-3′	57.2	5′-CTG CGA TGT CTG GCT CAT AA-3′	57.1	NM_001081249
Olig1	5′-CTT GCT CTC TCC AGC CAA AC-3′	57.5	5′-GCG AGC CTG AAA AAC AGA AC-3′	57.7	NM_016968.4
Olig2	5′-ATA TGG GAA CCG AAG CAA TG-3′	57.6	5′-CAG GAA GTT CCA GGG ATG AA-3′	57.1	NM_016967.2
MBP	5′-CTT CAA AGA CAG GCC CTC AG-3	57.3	5′-CCT GTC ACC GCT AAA GAA GC-3′	57.8	NM_001025251
CNPase	5′-ACA CAG TGG CTA CCC TCC AC-3′	56.9	5′-GTA CGC CTC GGA GAA GTC TG-3′	57.3	AF332056.1
Blue sensitive opsin	5′-GCC TCA GTA CCA CCT TGC TC-3′	57.1	5′-CTG GCG ATG AAG ACT GTG AA-3′	56.6	NM_007538
GAPDH	5′-AAT-GCA-TCC-TGC-ACC-ACC-AA-3′	55.3	5′-GTA-GCC-ATA-TTC-ATT-GTC-ATA-3′	45.37	NM_017008

2.1.13 Semi-quantitative PCR and densitometry

For each gene, six PCR tubes were prepared. One tube was removed every 3rd cycle, starting from either the 16th or 25th cycle — these cycles were previously determined as the cycles where the exponential phase of the PCR reaction occurred (see appendix A). The intensity of the resultant PCR bands, resolved on agarose gels and stained with EtBr, were analysed using the Multigenius Gel Documentation System (Syngene, Cambridge, UK). The PCR thermal cycler conditions are shown in table 2.8 and the reaction volumes can be found in table 2.7.

Table 2.7: PCR reaction volumes.

40 µl **Reaction**	
Reagent	**Volume (µl)**
Biomix	20
H_2O	14
Mouse brain cDNA	2
Forward primer	2
Reverse primer	2
MgCl	1.5 mM

Table 2.8: PCR thermal cycler settings.

Step	1	2 (30 or 40 cycles)			3	4
Temperature (°C)	96	96	50	72	72	4
Time	2 min	30 s	30 s	30 s	5 min	∞

2.1.13.1 Densitometry

EtBr stained DNA bands from all genes that tested positive in the RGC-5 group were quantified by densitometry using the Phoretix 1D Software (Nonlinear Dynamics, Newcastle-upon-Tyne, UK) and normalised to the density of a glyceraldehyde 3-phosphate dehydrogenase (GAPDH) loading control. Unless otherwise stated, each experiment was performed on 3 independent occasions. Densitometry values were averaged for each primer and cycle number. The exponential phase of each PCR reaction was determined by plotting the densitometry readings on a line chart (see figure 2.3). This enabled me to establish which cycles fell within the exponential phase of the PCR reaction. A cycle was chosen where both PCR products fell within the exponential phase of the reaction (e.g. cycle 25 for mouse brain GalC and RGC-5 GalC), an example of this is shown below. Mean densitometry values at the selected cycle number were normalised by dividing the target gene (e.g. GalC) densitometry value by the GAPDH (internal control) densitometry value. The relative signal intensities could then be compared and plotted on a bar chart (see figure 2.3).

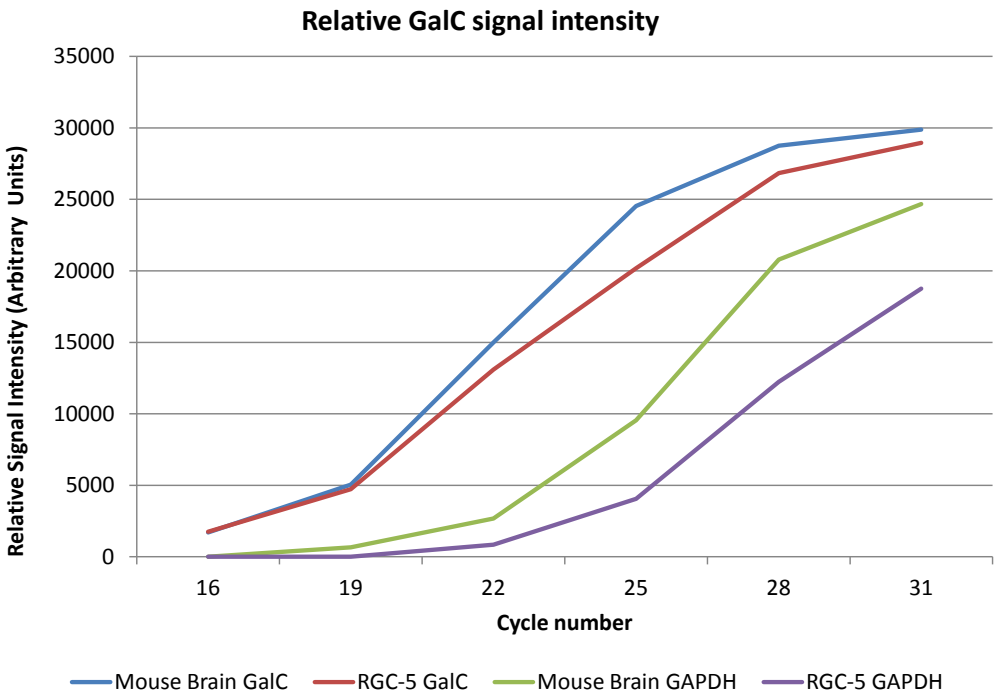

Figure 2.3: Example of how the exponential phase of the PCR reaction was determined. Mean desitometry readings were plotted on a line chart to determine which cycles fell within the exponential phase of the PCR reaction. A cycle was then chosen where both PCR products (RGC-5 mRNA and mouse brain positive control) fell within the exponential phase of the reaction. Mean densitometry readings at the selected cycle number (cycle 25 in this example) were then normalised by dividing the target gene densitometry value (GalC) by the internal control densitometry value. Relative signal intensities were then plotted on a bar chart (see figure 3.13).

2.1.14 Sample preparation for sequencing

PCR reactions were performed to prepare CD44, NG2 and GAPDH cDNA for sequencing.

PCR reactions were performed using the Phusion high-fidelity DNA polymerase. This enzyme was selected because of its 3' → 5' exonuclease activity — as a result, fewer errors should be made during the amplification process. For reaction volumes see table 2.9 and for thermal cycler conditions see table 2.8.

Table 2.9: PCR reaction volumes used to prepare samples for sequencing.

Reagent	**Volume (µl)**
Forward primer	2
Reverse primer	2
cDNA	4
dNTP	5
5x phusion HF buffer	10
Phusion DNA polymerase	0.5
H_2O	27

2.1.14.1 Gel extraction

Upon completion of the PCR reaction, each sample was resolved on a 0.7% agarose gel and visualised by EtBr staining. DNA bands were isolated using the QIAquick gel extraction kit (Qiagen). Protocols were performed in accordance with manufacturer's instructions — all reagents were supplied with the kit. Briefly: DNA bands were excised using a scapel blade and excess agarose was removed. Gel slices were weighed in a tube and 3 volumes of buffer QG was added to each sample. The tubes were incubated for 10 min

at 50 °C to dissolve the gel samples and 1 volume of isopropanol was added to each tube and mixed. Samples were then transferred into a QIAquick spin (with accompanying collection tube) and centrifuged for 1 min. The flow through was discarded and the spin column was placed back within the same collection tube. 500 µl of buffer QG was then added to the spin column and centrifuged for 1 min to remove all trace of agarose. Buffer PE (750 µl) was then added to the column and allowed to stand for 5 min, the column was then washed by centrifugation for 1 min. The flow through was discarded and the column was spun for an additional 1 min. The spin column was then placed within a new collection tube and the DNA was eluted by adding 50 µl of buffer EB and centrifuging for 1 min at maximum speed.

2.1.14.2 DNA quantification

DNA concentrations were determined by loading 2 µl of DNA into a Nanodrop spectrophotometer (ND-1000; Wilmington, DE, USA) and measuring the absorbance of each sample at 260 nm. The Nanodrop machine was also used to estimate sample purity — this was achieved by measuring the 260 nm/280 nm absorbance ratio. DNA with a purity value of <1.8 was used in all experiments.

2.1.14.3 Sample preparation

Two samples of each of the PCR products were made up with 50 ng of DNA (volume required to give 50 ng was calculated with the concentration measured using the Nanodrop machine). For each of the PCR product sample pairs, 1 µl of forward primer (10 pmol) was

added to one sample, and 1 µl reverse primer (10 pmol) to the other — water was then added to make a total volume of 12 µl (as shown in table 2.10).

Table 2.10: Sample preparation.

Sample	50 ng **DNA template volume (µl)**	**H_2O (µl)**	10 pmol **Forward Primer (µl)**	10 pmol **Reverse Primer (µl)**	**Total Volume (µl)**
NG2	6.3	4.7	1	—	12
NG2	6.3	4.7	—	1	12
CD44	3	8	1	—	12
CD44	3	8	—	1	12
GAPDH	3.5	7.5	1	—	12
GAPDH	3.5	7.5	—	1	12

2.1.14.4 Sequencing

All sequencing reactions were performed by the genomics lab sequencing service (University of Birmingham) using the Big Dye Terminator v3.1 Cycle Sequencing Kit (Applied Biosystems, Carlsbad, CA, USA), running a sequencing reaction, purifying samples and analysing the results on a 3700 DNA Analyzer.

2.2 *In vivo* techniques

2.2.1 Animal surgery

Adult male Sprague Dawley rats (150 g to 250 g) were used for AAV2 experiments to assess transfection rates, RGC survival and axon regeneration. All procedures were performed in accordance with the regulations of the UK Animals (Scientific Procedures) Act 1986 under a Home Office Licence. Surgeries were performed by Professor Martin Berry — anaesthesia and analgesia were administered by myself.

Inhalation anaesthesia was induced with an initial dose of 4% isoflurane (Abbott Laboratories Ltd, Kent, UK) and maintained at 3% during surgery. Animals received a subcutaneous injection of the analgesic Buprenorphine (National Vetinary Supplies, Stoke-on-Trent, UK) at the start of the procedure at a dose of 0.03 mg kg^{-1}. An ocular lubricant (Lacri-Lube, Allegan High Wycombe, UK) was also applied to prevent corneal dehydration.

2.2.1.1 Optic nerve crush

A midline cutaneous incision was made to access the ON intraorbitally, the skin was reflected over the upper lid to expose the orbital margin and the superficial fascia was removed. A vertical incision was made through the temporalis fascia and temporalis muscle and extended rostrally over the orbital margin without damaging the supraorbital vessels. The supraorbital neurovascular bundle was clamped using forceps and the Harderian gland exposed by making an incision in the orbital fascia between the clamp

sites. The gland was reflected rostrally to expose the superior and lateral rectus muscles. Retractors were placed between the superior rectus and ON as well as between the lateral rectus muscle and ON to allow easy access. The ON was exposed by excising the retractor bulbi muscle, dural sheath, and arachnoid. Care was taken not to sever the central retinal artery which runs through the dural sheath medially. The ON was crushed 2 mm from the laminal cribrosa using blunt forceps to transect all axons whilst leaving the sheath intact. The retractor bulbi, rectus muscles and Harderian gland were repositioned around the nerve and the skin margins sutured.

2.2.2 Intravitreal injections

A glass micropipette was loaded with a 10 µl volume of test reagent and inserted into the vitreous body via the sclera immediately posterior to the ora serrata. The pipette was positioned so that the tip was inserted between the lens and the retina. The micropipette was connected to a syringe before slowly injecting the appropriate solution into the vitreous. The pipette was then withdrawn slowly to prevent reflux — care was taken throughout the procedure not to damage the lens.

2.2.3 *AAV2-CNTF-hrGFP*, *AAV2-eGFP* and *AAV2-CNTF-shRhoA-hrGFP* delivery and RGC survival counts

Rats received an intravitreal injection of 1×10^{11} vg/10µl *AAV2-CNTF-hrGFP*, *AAV2-CNTF-shRhoA-hrGFP* or *AAV2-eGFP* in combination with 0.0002% Pronase-E 30 d prior to ONC

(see section 2.2.1.1). Eyes were prepared for histological examination as in section 2.2.4. To determine whether intravitreal injection of *AAV2-CNTF-hrGFP* or *AAV2-CNTF-shRhoA-hrGFP* could protect RGC from cell death, 10 retinal sections were randomly selected for histological examination. Retinal sections were stained with haematoxylin and eosin (H&E) and images were captured using an upright microscope (Carl Zeiss Meditec, Dublin CA). The number of RGC occupying a 550 µm $\times$ 500 µm field of view was counted and compared against an uninjured control. $n = 3$ for each treatment group (30 sections in total for each treatment group).

2.2.4 Tissue Preparation for Histology

Animals were killed by rising concentrations of CO_2 and the tissue fixed by perfusion with 4% paraformaldehyde (PFA) (TAAB Laboratories, Berkshire, UK). Eyes and optic nerves were removed and post fixed in PFA for 2 h at 4 °C. Tissue was then washed in PBS for 10 min and then passed sequentially through sucrose gradients (overnight at 4 °C in 10%, 20% and 30% sucrose in PBS) to cryoprotect. Eyes and ON were then blotted with filter paper (to remove excess PBS), embedded in OCT Embedding Medium (R.A. Lamb Laboratory), frozen rapidly on dry ice and stored at -80 °C. Eye and ON cryosections (15 µm) were cut on a cryostat (Bright Instrument Company, Huntingdon, UK) and mounted on either Superfrost Plus or Extra Adhesive slides microscope slides.

2.2.5 Retinal wholemount counts

To assess survival, RGC were retrogradely labelled with a 4% solution of flourogold (FG) (FG, hydroxystilbamidine, Cambridge Bioscience, Cambridge, UK). The ON was accessed intraorbitally and a 2 µl volume of tracer was injected into the ON proximal to the crush site 48 h prior to tissue harvesting. After the eyes had been harvested, the retina was exposed by carefully removing the cornea, iris diaphragm, lens and attached vitreous. The remaining eye cup was then submerged in 4% PFA for 2 h to post fix the tissue. The retina was then removed from the eye cup, cut into 4 quadrants and flattened out onto a slide using dry paintbrushes. Coverslips were mounted with Vectamount (without DAPI) to preserve immunoflourescence. Wholemounted retinae were viewed with an Axioplan-2 fluorescent microscope (Carl Zeiss Meditec, Dublin CA) and images were captured using Axiovision software (Axiovision; Carl Zeiss Meditec). The radial centre was determined for each quadrant and 4 images were captured along this axis. FG-positive RGC were counted and averaged per wholemount. Results were expressed as the mean number of RGC/mm^2 ± SEM of 3 retinae for each treatment group. For a diagrammatic representation of this sampling technique see figure 2.4.

2.2.6 Retinal ganglion cell transduction

To determine whether the addition of Pronase-E could increase AAV2 transduction efficiency, animals received a 10 µl intravitreal injection of *AAV-GFP* (1×10^{11} vg/10µl) with and without 0.0002% Pronase-E (see section 2.2.2). After the eyes had been harvested the retina was exposed by carefully removing the cornea, iris diaphragm, lens and at-

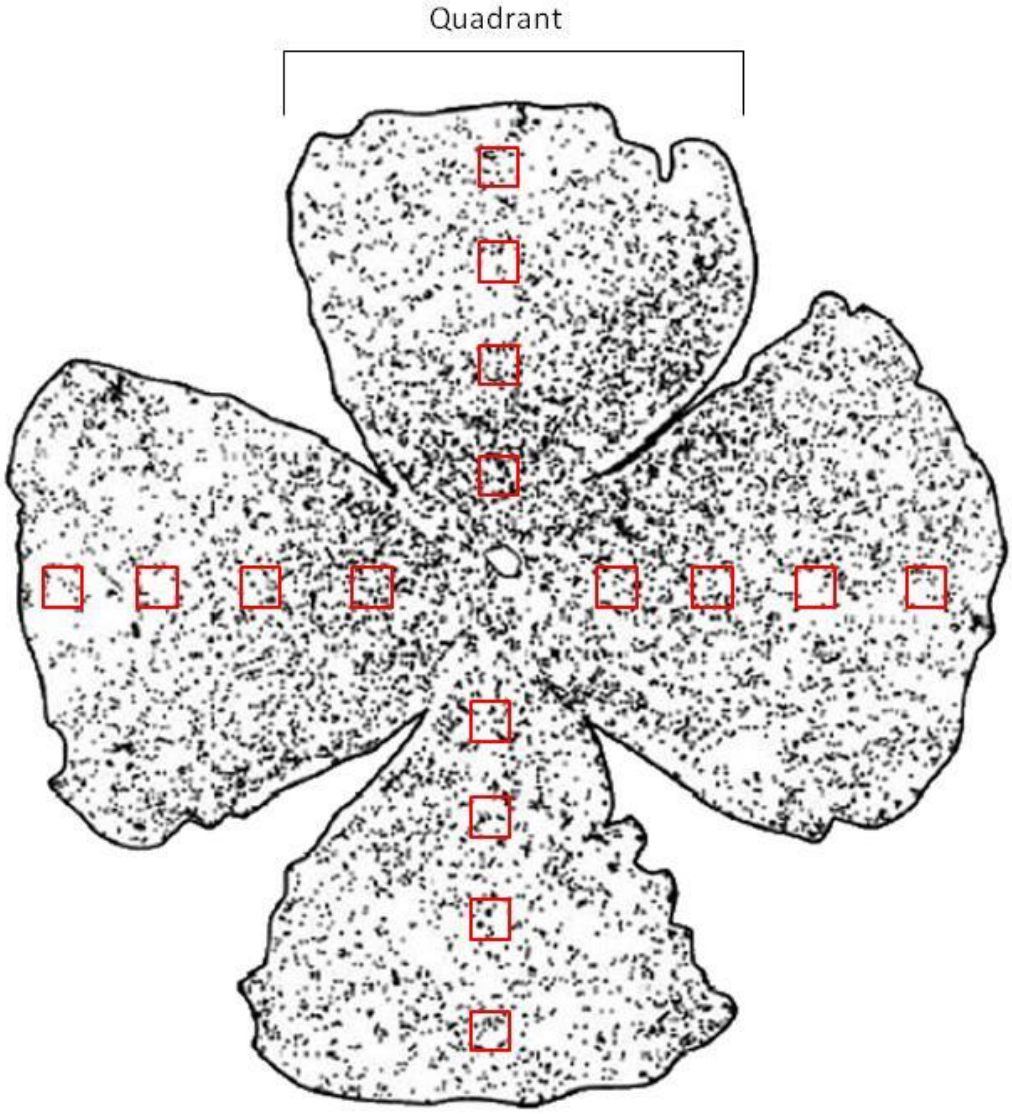

Figure 2.4: Image (not to scale) illustrating the sampling technique used to calculate RGC survival and GFP transduction efficiency. Retinal wholemount diagram modified from `http://goo.gl/Sq8Iy`

tached vitreous. The remaining eye cup was then submerged in 4% PFA for 2 h to post fix the tissue. The retina was then removed from the eye cup, cut into 4 quadrants and flattened out onto a slide using dry paintbrushes. Coverslips were mounted with Vectamount (without DAPI) to preserve immunoflourescence. Wholemounted retinae were viewed with an Axioplan-2 fluorescent microscope (Carl Zeiss Meditec, Dublin CA) and images were captured using Axiovision software (Axiovision; Carl Zeiss Meditec). The radial centre was determined for each quadrant and 4 images were captured along this axis. GFP positive RGC were counted and averaged per wholemount. Results were expressed as the mean number of RGC/mm^2 ± SEM of 3 retinae for each treatment group. For diagrammatic representation of this sampling technique see figure 2.4.

2.2.7 Quantification of RGC axon regeneration *in vivo*

Quantification of RGC axon regeneration was based upon a method described by others (Leon, et al. 2000, Lorber, et al. 2005). The number of GAP-43 positive axons extending 100 µm, 200 µm, 400 µm, 800 µm and 1200 µm from the lesion core was counted. The cross sectional width of the ON was measured at the point at which the counts were taken. This was used to calculate the number of axons/mm width. Unless otherwise stated, this value was averaged over 3 sections. $\sum ad$ (the total number of axons extending distance d in an ON with radius r) was calculated and results were expressed as the mean from 3 optic nerves per treatment group ± SEM.

$$\sum ad = \pi r^2 \times \frac{\text{average number of axons/mm width}}{t}$$

(t = section thickness (15 µm))

Figure 2.5 shows a diagrammatic explanation of the above formula.

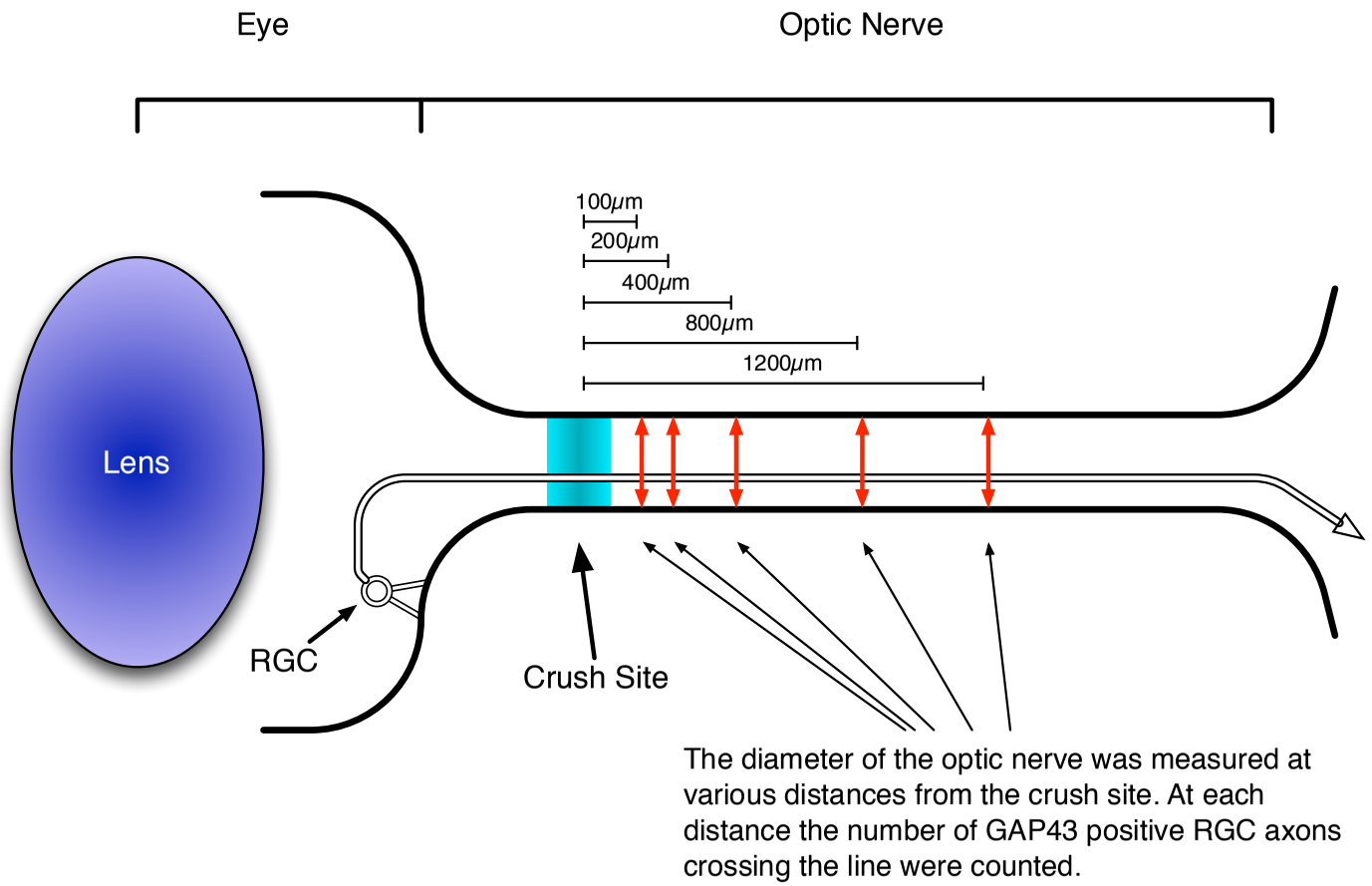

Figure 2.5: Quantification of RGC axon regeneration. The diameter of the ON was measured (red double ended arrows) at various distances (100 µm, 200 µm, 400 µm, 800 µm and 1200 µm) from the centre of the crush site. At each distance the number of GAP-43 positive RGC axons crossing the line was counted and this was used to determine the number of axons/mm width at each distance. This value was then averaged over 3 ON sections per animal. Results were then expressed as the mean from 3 optic nerves per treatment group ± SEM.

2.2.8 Statistical Analysis

All statistical analysis was performed using the SPSS (IBM) software package. Statistical analysis was performed to ascertain whether differences seen between treatment groups were real, due experimental error or random chance. An independent t-test was used to compare data from 2 experimental treatment groups. A one-way analysis of variance (ANOVA) in combination with the Gains Howell post-hoc test was used to compare data from multiple treatment groups. This test was performed to determine if the mean of 2 or more treatment groups was significantly different from that of the untreated controls. Parametric tests were chosen based on the assumption that the data followed a normal distribution. Data was considered to be statistically significant if the probability (p) was less than the specified significance levels (where $*p \geq 0.05$, $**p \geq 0.05$, $***p \geq 0.001$).

CHAPTER 3

CHARACTERISATION OF THE RGC-5 CELL LINE

3.1 The use of cell lines in biological research

Cell lines have many advantages over primary cell cultures. Cell lines tend to represent a homogeneous population of cells — giving them the advantage of generating more reproducible results. As cell lines are mitotically active they are relatively easy to maintain and can be passaged for a long, or indefinite, amount of time. This provides us with the means to produce and harvest high yields of cells. The use of cell lines can also limit the cost of using animals as a source of material which in turns minimises the variability inherent in using such animals.

Cell lines also have some disadvantages — they need to be fully characterised before they can be used as a substitute for primary cells. This involves determining whether the cells express the same transcription factors, signalling molecules, receptors, neurotrophic factors and proteins present in the primary cells. A further disadvantage is that with increasing time and passage number, cell lines may incur morphological changes as well as changes in gene expression.

3.2 RGC-5 cell line

The use of *in vitro* assays is an important tool for elucidating the mechanisms involved in regenerative failure. Primary retinal cultures are commonly used to achieve this, however RGC are notoriously difficult to purify making it difficult to distinguish between neuronal and glial based actions. The use of an RGC cell line would eliminate this complication and facilitate the analysis of neuronal specific responses.

The RGC-5 cell line was first introduced in 2001 as an immortalised cell line generated by isolating RGC from postnatal day 1 Sprague Dawley rats and transforming them using ψ2EIA virus (R.R.Krishnamoorthy, et al. 2000). The cell line was deemed to be of retinal ganglion cell origin based upon it testing positive for a number of markers associated with RGC e.g. Thymocyte differentiation antigen 1 (Thy-1), Brn-3C, Neuritin, NMDA receptor, GABA-B receptor, synaptophysin, neurotrophic factors and their respective receptors (R.R.Krishnamoorthy et al. 2000). They were not found to express GFAP which is a marker of astrocytes (R.R.Krishnamoorthy et al. 2000).

Since their introduction, more than 100 research reports have used RGC-5 cells as a substitute for primary RGC. Many of these reports use RGC-5 cells to model apoptotic events induced by hypoxia (Li, et al. 2011, Sato, et al. 2010), serum deprivation (Charles, et al. 2005), oxidative stress (Jung, et al. 2010, Koriyama, et al. 2009), glutamate excitotoxicity (Harper, et al. 2009, Bergen, et al. 2009, Tchedre & Yorio 2008) and hydrostatic pressure (Agar, et al. 2006). Other publications have used RGC-5 cells to investigate differentiation (R.R.Krishnamoorthy et al. 2000, Tchedre & Yorio 2008, Frassetto, et al. 2006, Lieven, et al. 2007, Schwechter, et al. 2007), calcium signalling (Tchedre & Yorio 2008, Luo, et al. 2005) and neuroprotection (Koriyama et al. 2009, Harper et al. 2009, Tchedre & Yorio 2008).

The purpose of this study was to characterise the RGC-5 cell line to determine whether it would be a suitable substitute for primary retinal cultures.

3.3 Aims

1. Characterise the RGC-5 cell line.
2. Establish whether the RGC-5 cell line can be used as a substitute for primary RGC.
3. Determine whether Staurosporine could be used to differentiate the RGC-5 cell line.
4. Look at the morphological dynamics of Staurosporine mediated RGC-5 differentiation.

3.4 Results

The use of cells lines in biological research can be a very useful tool for investigating the molecular mechanisms which underlie CNS injury. However, comparisons made between mitotic cell lines (e.g. the RGC-5 cell line) and post-mitotic neuronal cell populations (e.g. primary RGC) are often problematic, since they often don't have the same characteristics as primary neurones.

As a result it would be useful to find a means of differentiating the RGC-5 cell line so that more accurate comparisons can be made between these two cell populations. In recent years, several differentiating agents have been tested on the RGC-5 cell line. One such reagent is Staurosporine, a broad spectrum kinase inhibitor which is reported to cause cell cycle arrest, somal rounding and process extension (Frassetto et al. 2006). In addition to this, Staurosporine treated RGC-5 cells are believed to take on a more neuronal phe-

notype as evidenced by an increased expression of neuronal markers and establishment of outward rectifying channels (Frassetto et al. 2006).

To achieve this, a Staurosporine dose response experiment was performed and RGC-5 morphological measurements were taken (see section 2.1.2.1). The purpose of this was to find out which concentration was optimal in terms of process extension, process length (figures 3.1a and 3.1b), process number (figure 3.2), process branching (figure 3.3) and toxicity (figure 3.4). The evaluation of toxicity was particularly important since Staurosporine is commonly used to initiate apoptosis at high doses (Manns, et al. 2011).

3.4.1 Staurosporine treatment induces process extension

Approximately 5000 RGC-5 cells per well were plated and given 2 h to adhere. Once the 2 h had passed the reagents were added and left for a further 24 h to induce differentiation, finally the cells were fixed and analysed.

For the purpose of quantification a process was defined as any cellular projection greater than one soma in length. The length of each cellular projection was measured using Image Pro® and expressed for each treatment group as ± SEM from 60 cells.

Results demonstrate that increasing the concentration of Staurosporine led to increases in the length of the longest process (and processes length/cell), with a concentration of Staurosporine between 100 nM and 1.78 µM favouring optimum process outgrowth. There was a statistical significance between Staurosporine treatment groups and controls, ***$p \leq 0.001$. Dimethyl Sulfoxide (DMSO) treatment did not induce process out-

growth and there was no statistical significance between DMSO treatment groups and control.

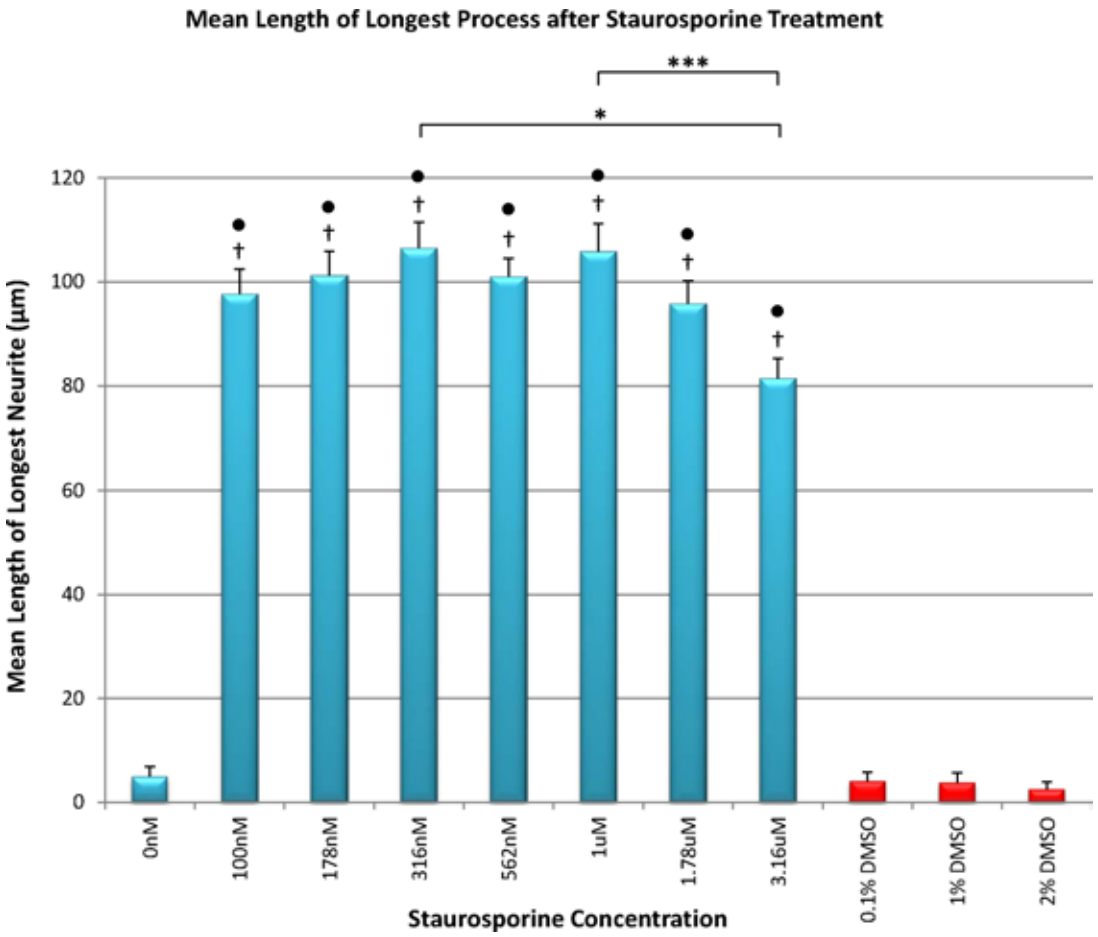

(a) Mean length of longest process after Staurosporine treatment

Figure 3.1: Staurosporine treatment induces process extension. RGC-5 cells (5000 cells well^{-1}) were treated (after being left to adhere for 2 h) with increasing concentrations of Staurosporine for 24 h. All concentrations induced similar levels of process extension, increasing mean length of longest neurite and process length/cell. All Staurosporine treatment groups are statistically significant from controls, ***p ≤ 0.001. $n = 3$ for all groups. Error bars represent the SEM from 3 independent experiments. † indicates ***p ≤ 0.001 when compared to 0 nM control. ● indicates ***p ≤ 0.001 when compared to DMSO controls (0.1%, 1% and 2% DMSO). ***p ≤ 0.001 and *p ≤ 0.05. Continued on next page.

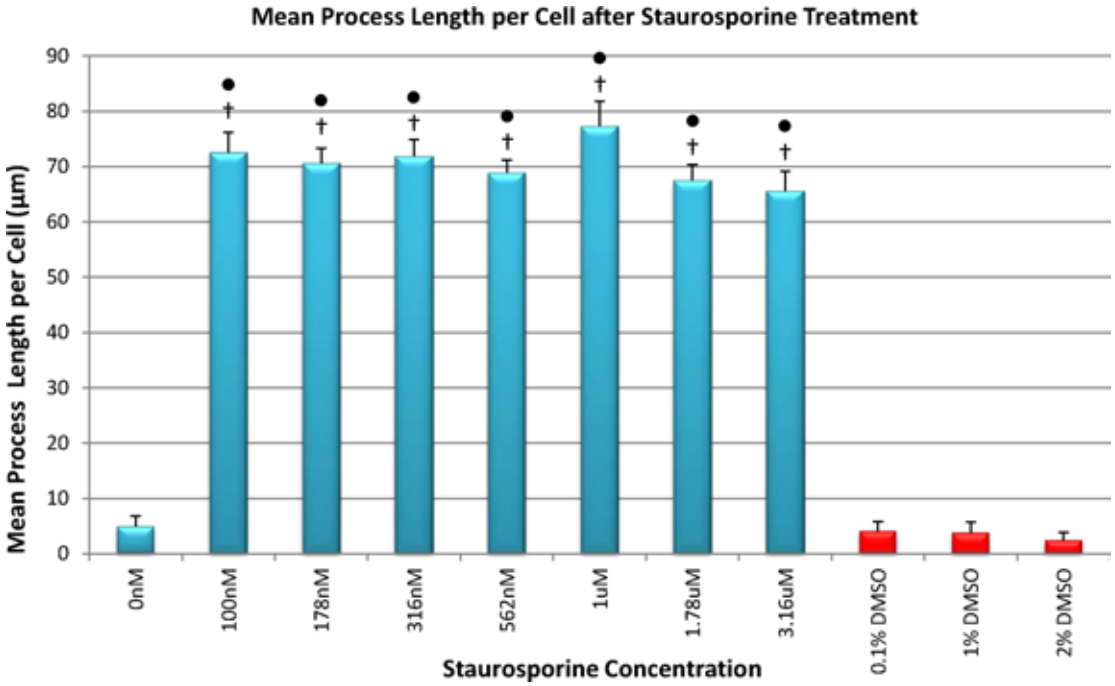

(b) Mean process length per cell after Staurosporine treatment

Figure 3.1: Staurosporine treatment induces process extension. Continued from previous page. Error bars represent the SEM from 3 independent experiments. † indicates ***p ≤ 0.001 when compared to 0 nM control. ● indicates ***p ≤ 0.001 when compared to DMSO controls (0.1%, 1% and 2% DMSO).

3.4.2 The impact of Staurosporine treatment on process number

Increasing Staurosporine concentration led to an increase in process number, with maximal process number being achieved at 562 nM. Process number declined between 1 µM to 3.16 µM, this may have been a result of increased cytoxicity (see figure 3.2). There is a statistical significance between Staurosporine treatment groups and control, ***p ≤ 0.001. DMSO treatment did not induce process outgrowth. There is no statistical significance between DMSO treatment groups and control.

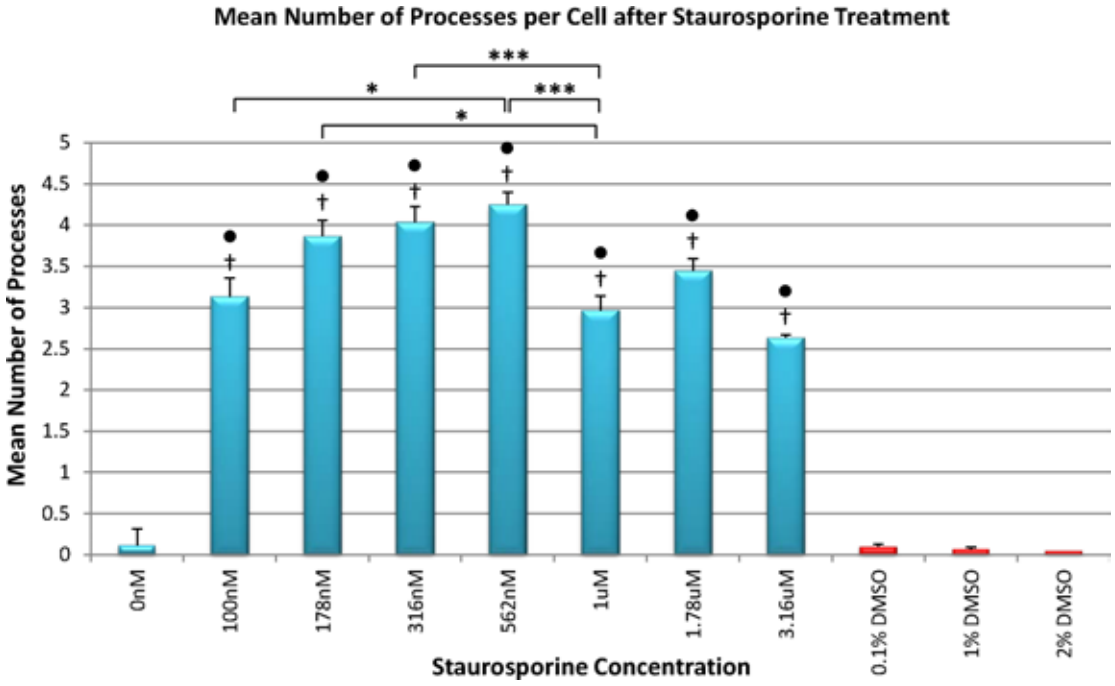

Figure 3.2: Process Number after Staurosporine Dose Response. RGC-5 cells (5000 cells well^{-1}) were treated with increasing concentrations of Staurosporine for 24 h (after being left for 2 h to adhere to the plate). Process number (a process was defined as any cellular projection greater than one soma in length) was significantly enhanced by application of 100 nM to 562 nM Staurosporine. This effect declined between 1 µM to 3.16 µM, presumably as a result of cytoxicity. All Staurosporine treatment groups are statistically significant from controls, ***p ≤ 0.001. Error bars represent the SEM from 3 independent experiments. † indicates ***p ≤ 0.001 when compared to 0 nM control. ● indicates ***p ≤ 0.001 when compared to DMSO controls (0.1%, 1% and 2% DMSO). ***p ≤ 0.001, **p ≤ 0.01 and *p ≤ 0.05.

3.4.3 Process branching is dose dependent

Results demonstrate that increasing concentrations of Staurosporine led to a dose dependent increase in process branching. Maximal branching was achieved at a dose of 1 μM to 1.78 μM, the extent of process branching was dramatically reduced by concentrations higher than this, presumably as a result of cytotoxicity (see figure 3.3). There was a statistically significant difference between Staurosporine treatment groups and controls. Branching was not observed in the untreated control and DMSO treatment groups.

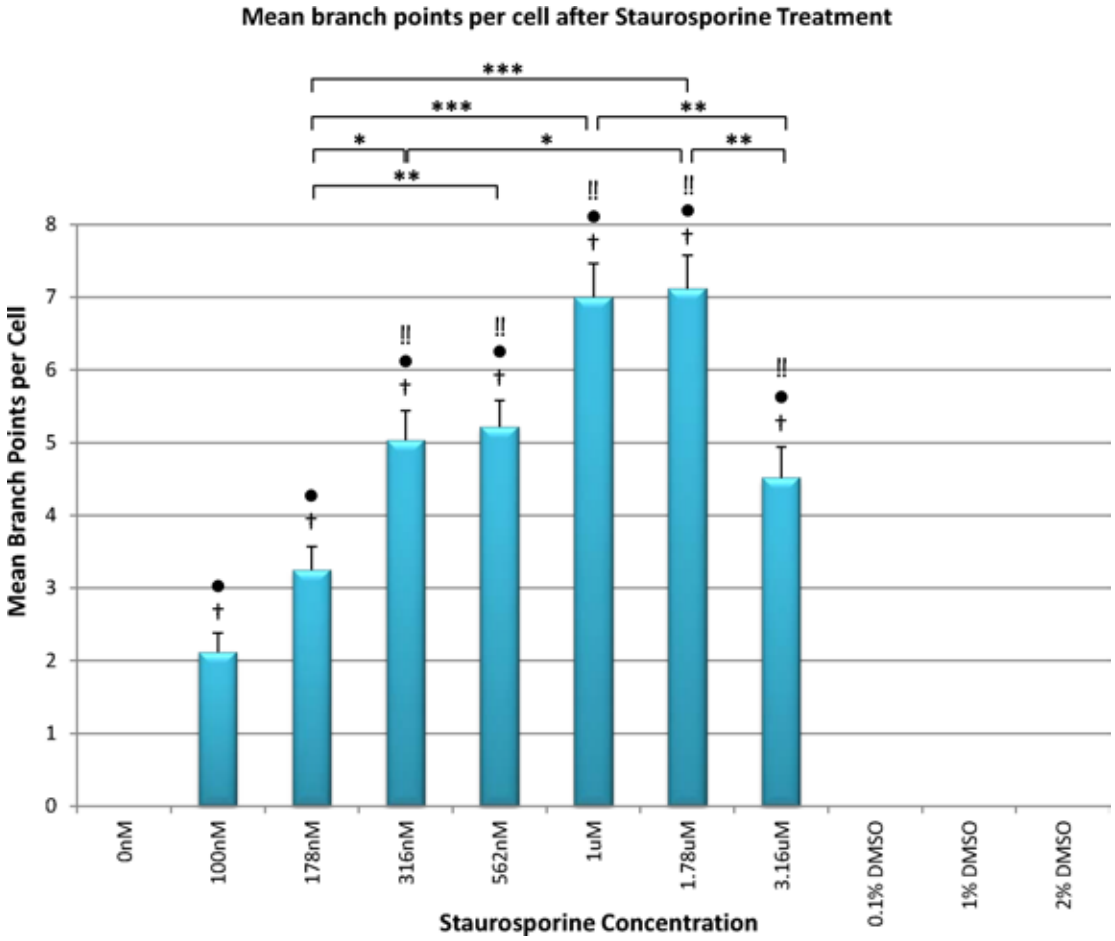

Figure 3.3: Process Branching is Dose Dependent. RGC-5 cells (5000 cells well^{-1}) were exposed to increasing concentrations of Staurosporine for 24 h (after being left for 2 h to adhere to the plate). The extent of process branching was positively correlated with Staurosporine concentration. Process branching (where a process was defined as any cellular projection longer than one soma) drastically declines after exposure to 3.16 µM. Branching is absent from the untreated control and DMSO groups. All Staurosporine treatment groups are statistically significant from controls. Error bars represent the SEM from 3 independent experiments. † indicates ***p ≤ 0.001 when compared to 0 nM control. ● indicates ***p ≤ 0.001 when compared to DMSO controls (0.1%, 1% and 2% DMSO). ‼ indicates ***p ≤ 0.001 when compared to 100 nM Staurosporine treatment group. ***p ≤ 0.001, **p ≤ 0.01 and *p ≤ 0.05.

3.4.4 RGC-5 cell viability assay after Staurosporine treatment

A cell viability assay was performed on RGC-5 cells to determine the extent of toxicity caused by increasing concentrations of Staurosporine.

At the start of the experiment, 2500 cells well^{-1} were plated in a 96 well plate. RGC-5 cells were allowed to adhere for 2 h, at which point the appropriate amount of Staurosporine (100 nM, 178 nM, 316 nM or 562 nM) was added. Cell viability assays were performed (as in section 2.1.8) 24 h later.

Treatment with 1 μM, 1.78 μM and 3.16 μM caused a statistically significant (***$p \leq 0.001$) reduction in mean ATP content after 24 h compared to all other treatment groups. Although this is indicative of RGC-5 cell death an accurate comparison can't be made without additional quantitative data (e.g. direct cell counts, BrdU and or Tunnel staining). There was no significant difference between DMSO treated controls (0.1%, 1% and 2%) and the untreated control group (0 nM) (see figure 3.4). DMSO controls were added to account for the small amount of compound present within the Staurosporine preparations.

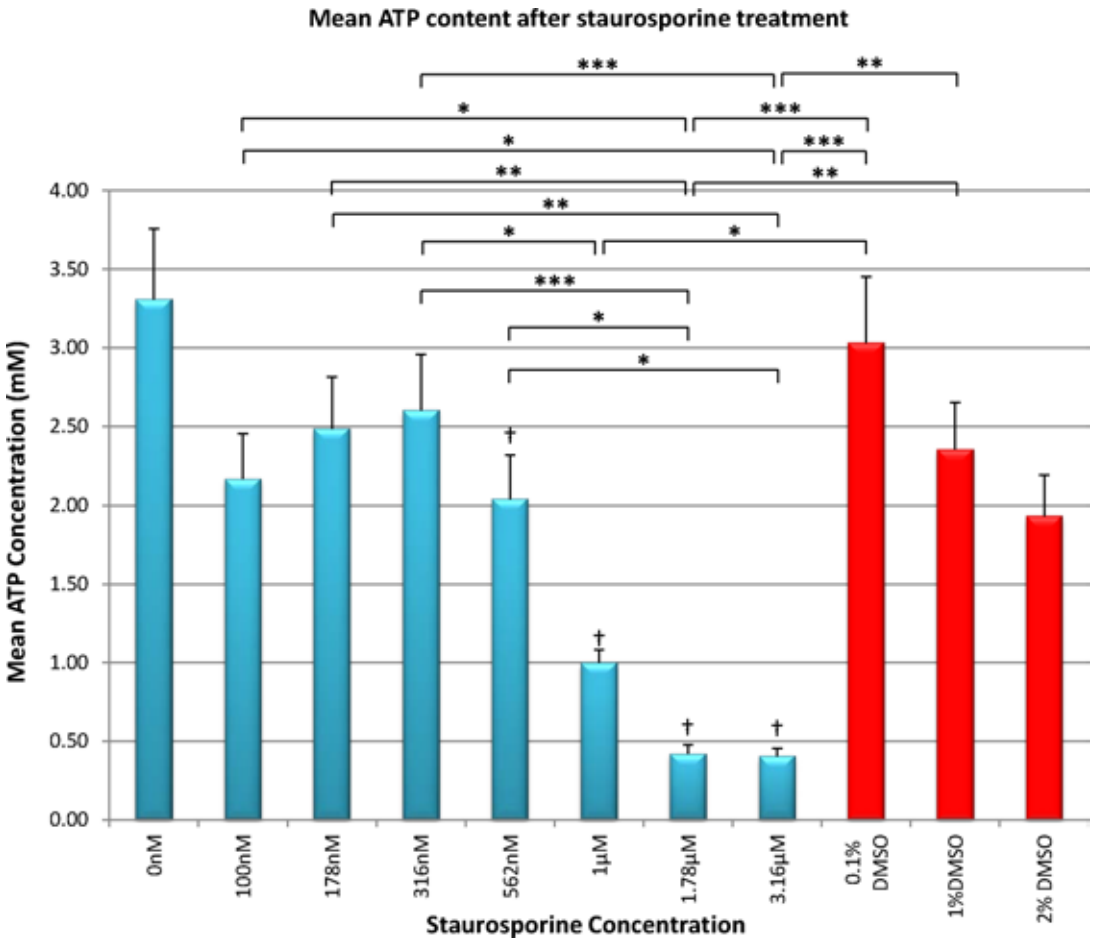

Figure 3.4: RGC-5 Cell Viability Assay. RGC-5 cells were plated, left 2 h to adhere and then treated with Staurosporine using concentrations ranging from 0 µM to 3.16 µM to induce differentiation. Cells were fixed and analysed 24 h after the reagent was added. Treatment with 1 µM, 1.78 µM and 3.16 µM caused a significant reduction in mean ATP content after 24 h compared to all other treatment groups. There was no significant difference between DMSO treatment groups and the untreated control group. Error bars represent the SEM from 3 independent experiments. † indicates ***p ≤ 0.001 when compared to 0 nM control. ***p ≤ 0.001, **p ≤ 0.01 and *p ≤ 0.05.

3.4.5 Representative images of the Staurosporine dose response experiment

RGC-5 cells were plated (5000 cells well^{-1}) onto chamber slides (BD Biosciences, Oxford, UK) and allowed to adhere for 2 h. The cells were then treated with increasing concentrations (0 nM, 100 nM, 178 nM, 562 nM, 1 µM, 1.78 µM, 3.16 µM) of Staurosporine to determine an optimal dose for differentiation. After 24 h the cells were fixed and visualised by βIII-Tubulin immunostaining (shown in figure 3.5 as green). Somal rounding and process extension was evident in all Staurosporine treatment (see figure 3.5B-H and figures 3.2, 3.3, 3.4 for quantification) groups after 24 h. In contrast, fewer processes (examples highlighted with a red arrow in figure 3.5) were present in all control groups (figure 3.5A, 3.5I-K) and the cell soma of these cells (examples highlighted with a white arrow in figure 3.5) were markedly flatter – DMSO was included as a control to account for the small amount of compound present within the Staurosporine solution. Increasing concentrations of Staurosporine led to a dose dependent increase in process branching (see figure 3.5A-H and figure 3.3, where a process was defined as any cellular projection which was longer than one cell soma. Fewer cells were present at higher Staurosporine concentrations - this was likely a result of toxicity. As expected no background staining was evident in the no primary control group (see figure 3.5L).

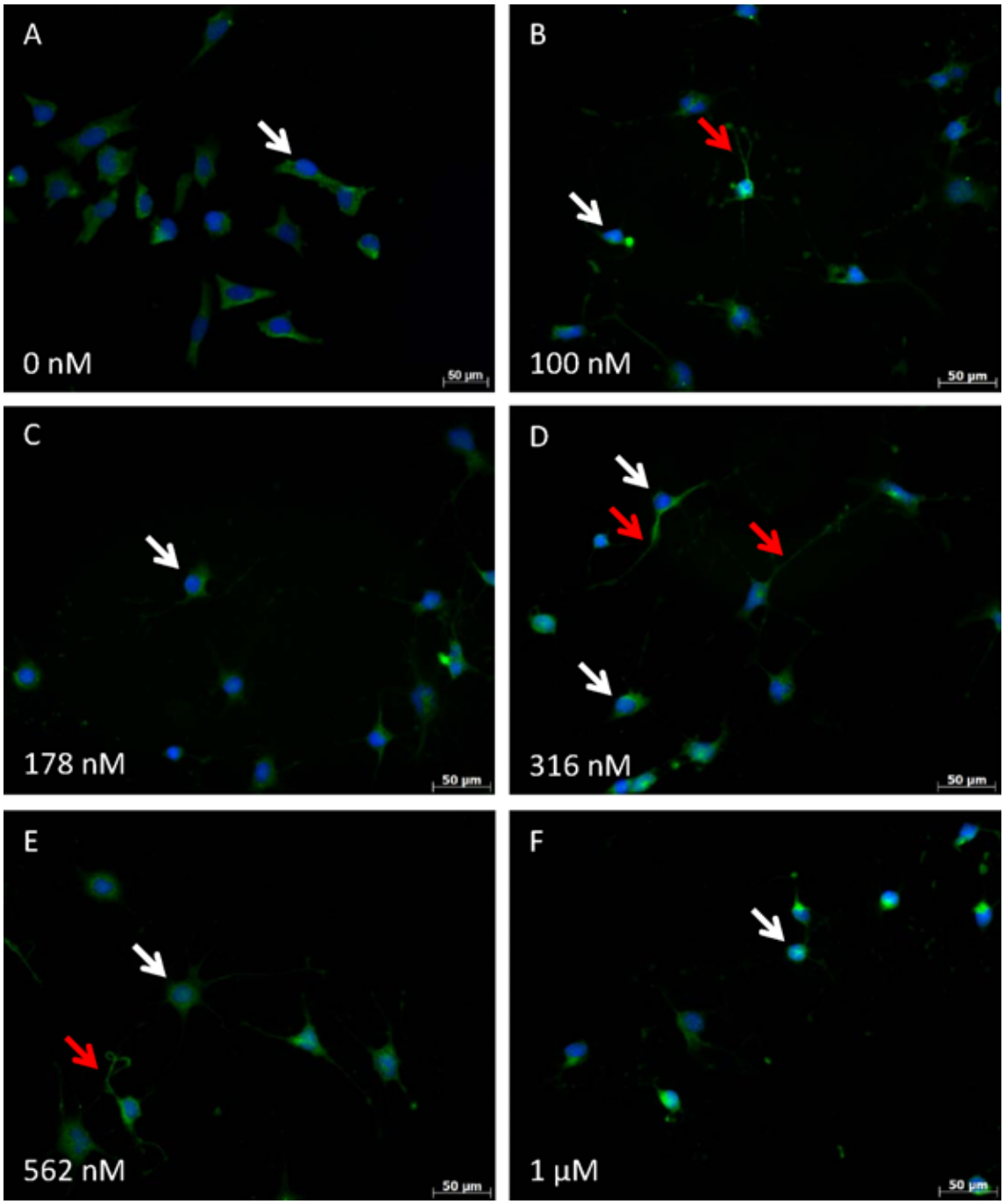

Figure 3.5: Representative images of Staurosporine dose response experiment. RGC-5 cells were treated with increasing concentrations of Staurosporine (0 nM, 100 nM, 178 nM, 562 nM, 1 µM, 1.78 µM, 3.16 µM) to determine an optimum dose for differentiation. 24 h later cells were fixed and visualised by βIII-Tubulin immunostaining (green). Process extension (red arrow) and somal rounding (white arrow) was evident in all Staurosporine treatment groups (A-H). Process branching became more apparent with increasing concentrations of Staurosporine. Controls consisted of 0.1% DMSO, 1% DMSO, 2% DMSO and an untreated control. DMSO was included as a control to account for the small amount present within Staurosporine preparations. Fewer processes were evident in all RGC-5 control groups and the cell soma was considerably flatter. DAPI stained nuclei are shown in blue. Continued on next page.

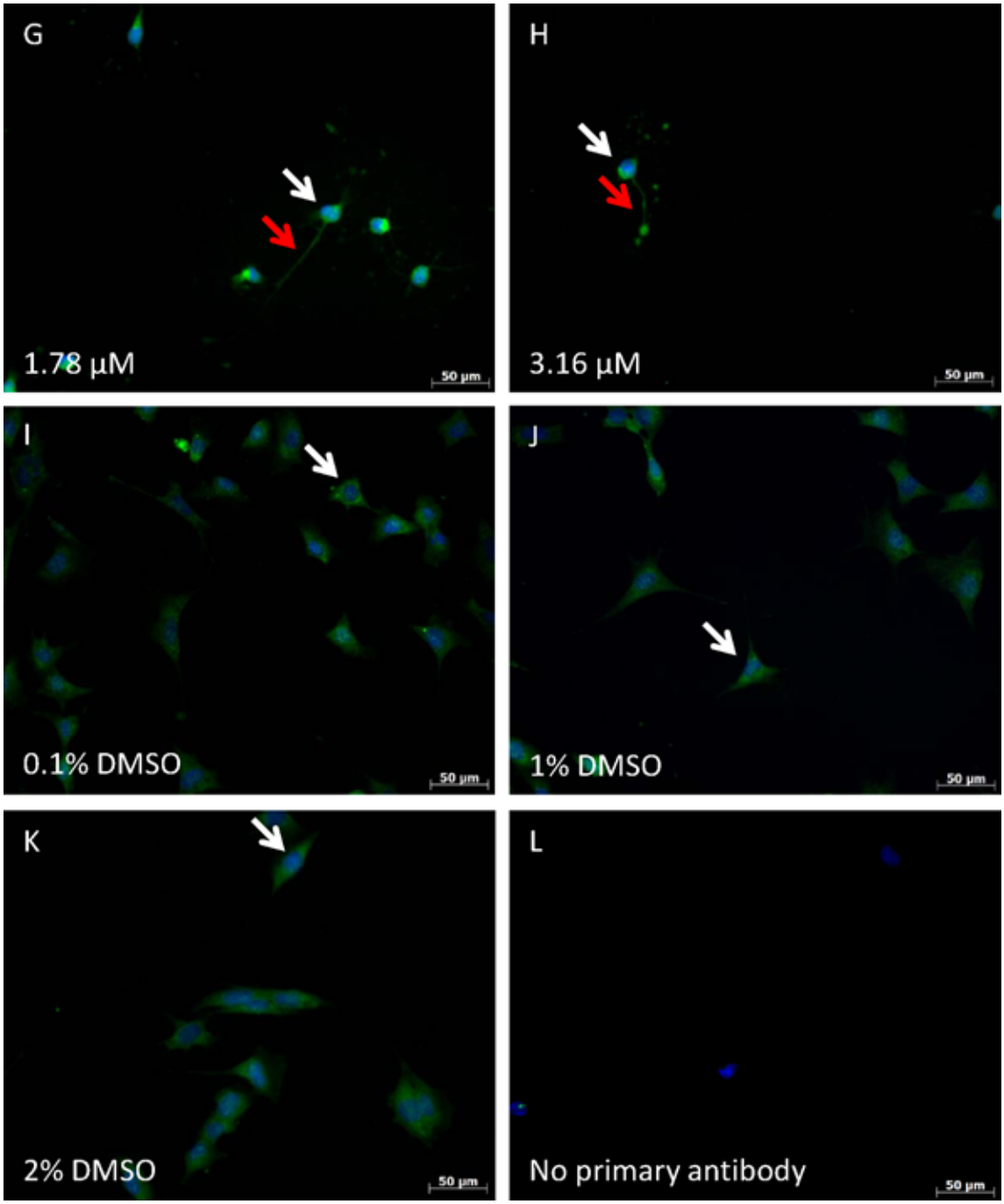

Figure 3.5: Representative images of Staurosporine dose response experiment. Continued from previous page. Red arrows point to process extensions, white arrows point to somal rounding. DAPI stained nuclei are shown in blue.

3.5 The RGC-5 cell line is derived from *Mus musculus* and not *Rattus norvegicus*

The primary aim of this chapter was to characterise the RGC-5 cell line and to determine whether the cells would be a suitable substitute for primary RGC.

In 2009 several batches of RGC-5 cells were found to be derived from *Mus musculus* rather than *Rattus norvegicus* (Bergen et al. 2009). Although all RGC-5 cells used in the studies listed in section 3.2 were derived from a common source, held by the Agarwal laboratory (R.R.Krishnamoorthy et al. 2000, Agarwal, et al. 2007), their origin was challenged when it was found that a number of batches were not derived from rats and were phenotypically unlike RGC (Bergen et al. 2009). Furthermore, a study re-characterised the RGC-5 cell line as a derivative of a mouse cone photoreceptor lineage (Wood, et al. 2010).

In light of this, all experiments from this point onwards were performed in the knowledge that this batch of cells may not be of rat origin as originally thought. As a result a new set of aims were planned:

3.5.1 New aims

1. Design and optimise primers for PCR and sequencing reactions.
2. Determine whether the RGC-5 cell line is derived from *Rattus norvegicus* or *Mus musculus*.

3. Establish whether the RGC-5 cell line expresses neuronal, glial or developmental cell markers.

Sequencing was performed to determine whether the RGC-5 cell line was derived from *Mus musculus* or *Rattus norvegicus*. PCR was performed on RGC-5 and rat brain cDNA using primers specific for rat CNTF. PCR products were run on a 0.7% agarose gel and visualised using EtBr staining. No band was present in the RGC-5 sample, whilst a band of the expected size (≈550 bp) was present within the control lane (see figure 3.6).

The primers were then re-designed to target the mouse CNTF sequence and included a GAPDH control for both rat brain and RGC-5 cDNA samples. The PCR reaction was repeated a second time, on this occasion no bands were present in the CNTF groups, but GAPDH positive bands (≈473 bp) were present in the control group (see figure 3.6). As the purpose of this exercise was not specifically to sequence CNTF, but to ascertain whether the RGC-5 cells were of mouse origin I decided to go ahead and sequence the GAPDH positive samples. Subsequent sequence alignments (see figure 3.6) confirmed that the RGC-5 cDNA was of mouse (*Mus musculus*) not rat (*Rattus norvegicus*) origin. Sequence alignment revealed that the GAPDH mouse homologue shared 97% identity with the RGC-5 sequence whilst the rat homologue shared 96% identity.

To confirm that RGC-5 cells were of mouse origin, a region of the NG2 and CD44 genes were selected for sequencing (see figure 3.7). Sequences were aligned using ClustalX and compared against published sequences for both NG2 (*Rattus norvegicus*: NM_001170558.1; *Mus musculus*: Mm: NM_001081249.1) and CD44 (*Rattus norvegicus*: M61875.1; *Mus musculus*: NM_009851.2). Sequence alignments revealed that the

NG2 mouse homologue was 99% identical to the RGC-5 sequence, whereas the rat homologue was only 87% identical. The CD44 sequence alignment revealed that the RGC-5 sequence was 100% identical to *Mus musculus* and shared 93% identity with *Rattus norvegicus* (see figure 3.7). All sequence alignments confirm that the RGC-5 cells in our possession are derived from mouse (*Mus musculus*) and not rat (*Rattus norvegicus*).

PCR and sequencing experiments were not performed on differentiated RGC-5 cells because this had already been investigated by Wood *et al* in 2010 (Wood et al. 2010). A full comparison between their results and mine is discussed in section 3.6.3.

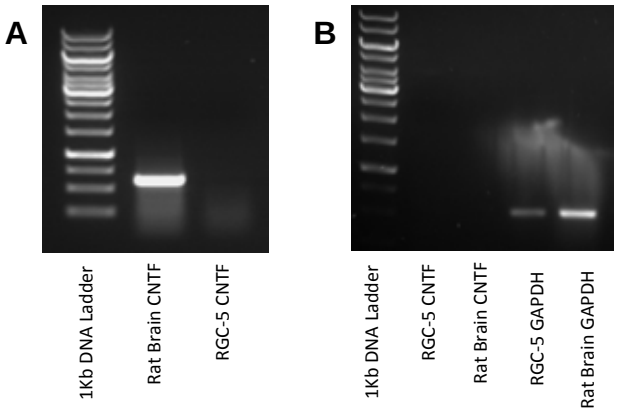

C

```
gi|37590766_Rn     GTCATCCATGACAACTTTGGCATCGTGGAAGGGCTCATGACCACAGTCCATGCCATCACT
Rat_brain_GAPDH    GTCATCCATGACAACTTTGGCATCGTGGAAGGGCTCATGACCACAGTCCATGCCATCACT
gi|126012538_Mm    GTCATCCATGACAACTTTGGCATTGTGGAAGGGCTCATGACCACAGTCCATGCCATCACT
RGC5               GTCATCCATGACAACTTTGGCATTGTGGAAGGGCTCATGACCACAGTCCATGCCATCACT

gi|37590766_Rn     GCCACTCAGAAGACTGTGGATGGCCCCTCTGGAAAGCTGTGGCGTGATGGCCGTGGGGCA
Rat_brain_GAPDH    GCCMCTCARAAGACTGTGGATGGCCCCTCTGGAAAGCTGTGGCGTGATGGCCGTGGGGCA
gi|126012538_Mm    GCCACCCAGAAGACTGTGGATGGCCCCTCTGGAAAGCTGTGGCGTGATGGCCGTGGGGCT
RGC5               GCCACCCARAAGACTGTGGATGGCCCCTCTGGAAAGCTGTGGCGTGATGGCCGTGGGGCT

gi|37590766_Rn     GCCCAGAACATCATCCCTGCATCCACTGGTGCTGCCAAGGCTGTGGGCAAGGTCATCCCA
Rat_brain_GAPDH    GCCCAGAACATCATCCCTGCATCCACTGGTGCTGCCAAGGCTGTGGGCAAGGTCATCCCA
gi|126012538_Mm    GCCCAGAACATCATCCCTGCATCCACTGGTGCTGCCAAGGCTGTGGGCAAGGTCATCCCA
RGC5               GCCCAGAACATCATCCCTGCATCCACTGGTGCTGCCAAGGCTGTGGGCAAGGTCATCCCA

gi|37590766_Rn     GAGCTGAACGGGAAGCTCACTGGCATGGCCTTCCGTGTTCCTACCCCCAATGTATCCGTT
Rat_brain_GAPDH    GAGCTGAACGGGAAGCTCACTGGCATGGCCTTCCGTGTTCCTMCCCCCAATGTATCCGTT
gi|126012538_Mm    GAGCTGAACGGGAAGCTCACTGGCATGGCCTTCCGTGTTCCTACCCCCAATGTGTCCGTC
RGC5               GAGCTGAACGGGAAGCTCACTGGCATGGCCTTCCGTGTTCCTACCCCCAATGTGTCCGTC

gi|37590766_Rn     GTGGATCTGACATGCCGCCTGGAGAAACCTGCCAAGTATGATGACATCAAGAAGGTGGTG
Rat_brain_GAPDH    GTGGATCTGACATGCCGCCTGGAGAAACCTGCCAAGTATGATGACATCAAGAAGGTGGYG
gi|126012538_Mm    GTGGATCTGACGTGCCGCCTGGAGAAACCTGCCAAGTATGATGACATCAAGAAGGTGGTG
RGC5               GTGGATCTGACGTGCCGCCTGGAGAAACCTGCCAAGTATKATGACATCWAGAAGGTGGTG

gi|37590766_Rn     AAGCAGGCGGCCGAGGGCCCACTAAAGGGCATCCTGGGCTACAC
Rat_brain_GAPDH    AA----------------------------------------
gi|126012538_Mm    AAGCAGGCATCTGAGGGCCCACTGAAGGGCATCTTGGGCTACAC
RGC5               AAKCAKGCWTCTGASGKCCCACTGAATGGY-TCTTGTSCTAC--
```

Figure 3.6: Rat CNTF primers do not anneal to RGC-5 cDNA. (**A.**) Rat CNTF primers were used to amplify rat brain and RGC-5 cDNA in a PCR reaction and samples were run on a 0.7% agarose gel. No band was present in the RGC-5 sample. However a band of the expected size (≈550 bp) was present within the rat brain positive control lane. (**B.**) Primers were re-designed and the experiment repeated to include GAPDH controls for both rat brain and RGC-5 samples. No bands were present within the CNTF groups — however bands (≈473 bp) were present in the GAPDH control groups. (**C.**) RGC-5 and rat brain PCR products were sequenced and aligned using ClustalX alignments for GAPDH. The sequence alignment also included the published genes for *Rattus norvegicus* (Rn) GAPDH (gi: 37590766) and *Mus musculus* (Mm) GAPDH (gi: 126012538). Areas highlighted in green indicate areas of rat homology, whereas regions highlighted in pink signify areas of mouse homology. Sequence alignments confirm that the RGC-5 cell line was not derived from rat.

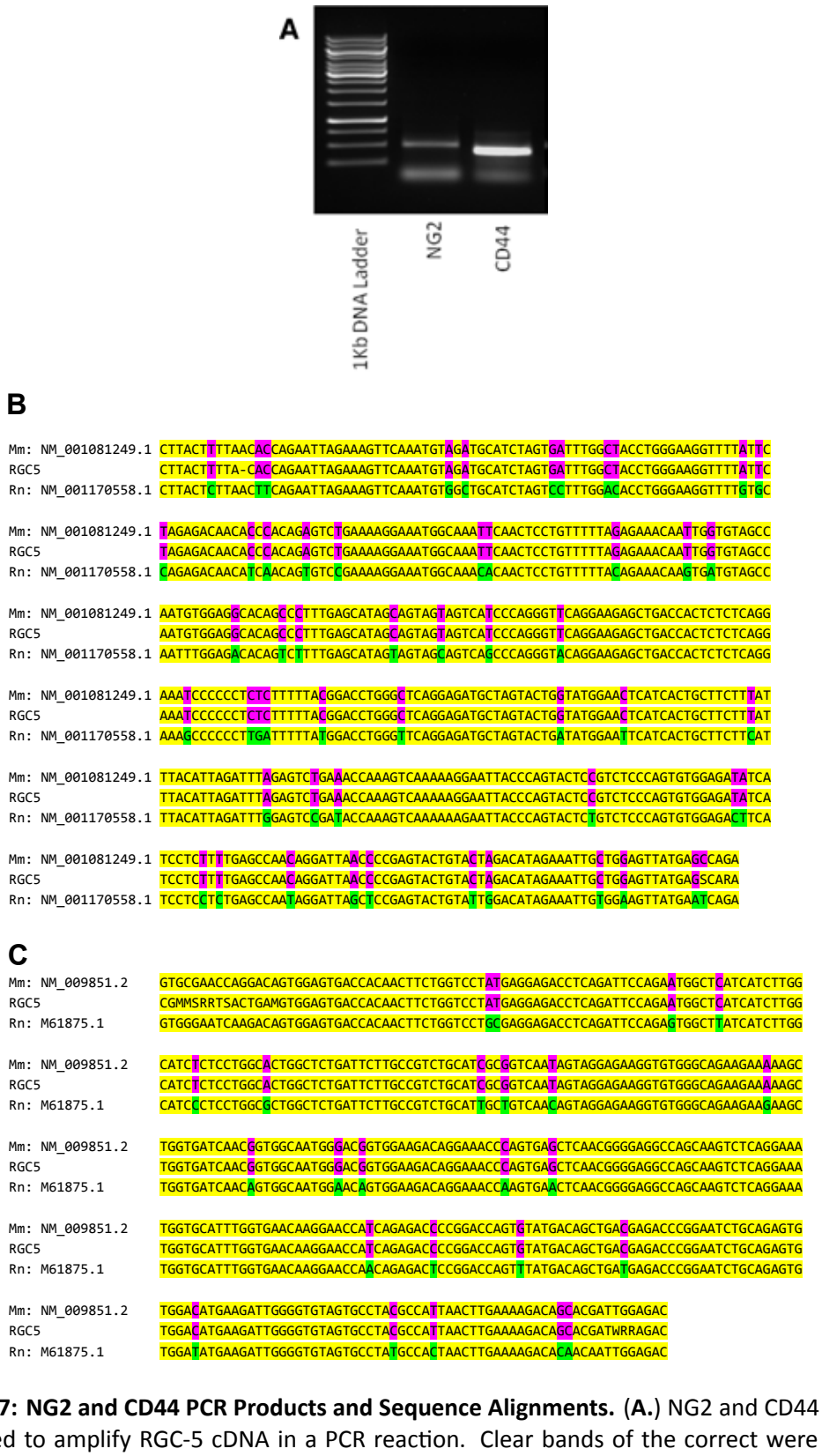

Figure 3.7: NG2 and CD44 PCR Products and Sequence Alignments. (**A.**) NG2 and CD44 primers were used to amplify RGC-5 cDNA in a PCR reaction. Clear bands of the correct were present for both NG2 (≈475 bp) and CD44 (≈381 bp). To confirm my original findings, RGC-5 PCR products were sequenced and aligned using ClustalX alignments for (**B.**) NG2 and (**C.**) CD44. Sequence alignment also included published genes for NG2 (Mm. NM_001081249.1) (Rn. NM_001170558.1) and CD44 (Mm. NM_009851.2) (Rn M61875.1). The sequencing data confirms that RGC-5 cells are derived from mouse. Areas highlighted in green indicate areas of rat homology whereas regions in pink signify areas of mouse homology.

3.5.2 Primer Optimisation

To determine primer specificity and optimum annealing temperature a series of PCR reactions were performed. The amplified products were separated on a 1% agarose gel and visualised by EtBr staining. A series of primers were designed to characterise the RGC-5 cell line and determine its origin. An annealing temperature of 50 °C produced a high degree of smearing and non-specific amplification. As a result, an annealing temperature of 55 °C was selected for all future experiments. Primers which were unsuccessful at amplifying the desired products were re-designed for use in future experiments.

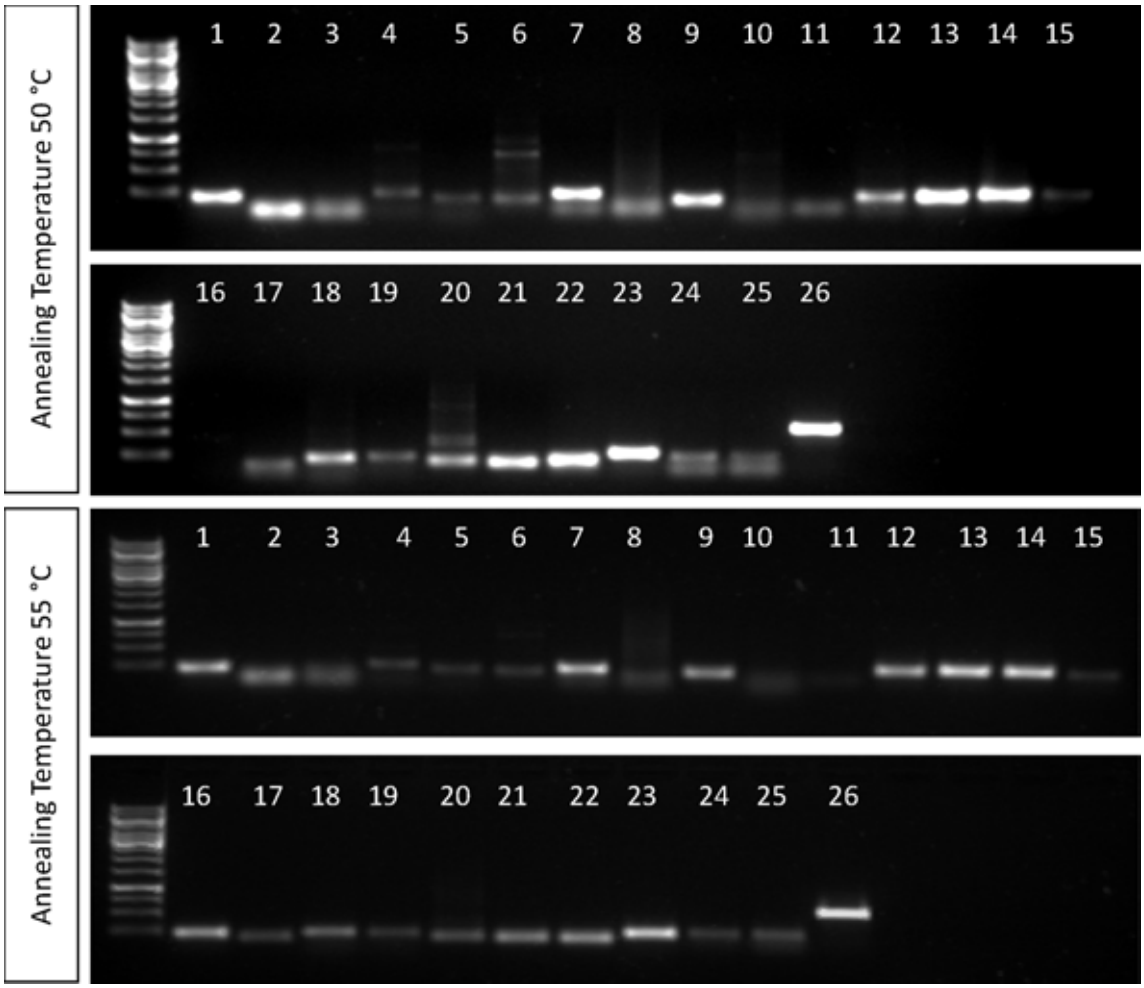

Figure 3.8: Optimisation of Annealing Temperature. Initial primer optimisation was performed on mouse brain cDNA (positive control). The genes of interest were amplified in a PCR reaction for 30 cycles (for reaction conditions see section 2.1.13) then separated on a 1% agarose gel. An annealing temperature of 50 °C produced a high degree of smearing and non-specific amplification. As a result an annealing temperature of 55 °C was selected for all future experiments. This temperature reduced non-specific annealing and produced clean bands. **1.** βIII-Tubulin **2.** CD11b **3.** CD44 **4.** CD68 **5.** CD113 **6.** ChAT **7.** GFAP **8.** Nestin **9.** NeuroD **10.** Neurogenin-1 **11.** Neurogenin-2 **12.** Neurofilament-H **13.** Neurofilament-L **14.** Neurofilament-M **15.** NG2 16.Oligodendrocyte transcription factor-1 (Olig-1) **17.** oligodendrocyte transcription factor-2 (Olig-2) **18.** Pax-6 **19.** RALDH2 **20.** sex determining region Y box-1 (SOX-1) **21.** SOX-2 **22.** Tau **23.** Thy-1 **24.** Tyrosine Hydroxylase **25.** UCLH **26.** GAPDH.

3.5.3 Determining the exponential phase of the PCR reaction

For each primer, the exponential phase of the PCR reaction was determined using cDNA from the positive control groups. The results of which are displayed in appendix A.

3.5.3.1 Neuronal marker expression

Semi-quantitative PCR was used to determine whether the RGC-5 cell line has a neuronal lineage, primers were designed for a selection of neuronal markers (NF-H, NF-M, NF-L, Tau, Thy-1 and βIII-Tubulin). Mouse brain cDNA was included as a positive control whilst GAPDH was included as an internal control. Clear bands of the correct size were present in all mouse brain control positive control groups (confirming primer specificity) for each set of markers. RGC-5 cells did not express mRNAs for NF-H, NF-M, NF-L, Tau and Thy-1, but weakly expressed βIII-Tubulin (see figure 3.9a).

3.5.3.2 Expression of glial markers

Semi-quantitative PCR was used to establish whether the RGC-5 cell line had a glial origin. Mouse brain cDNA was included as a positive control whilst GAPDH was included as an internal control. Clear bands of the correct size were present in all mouse brain control positive control groups (confirming primer specificity) for each set of markers. In contrast, RGC-5 cells did not express mRNAs for the astrocyte marker, GFAP, the fibroblast marker RALDH2 or the activated microglia marker CD11b (see figure 3.9b).

3.5.3.3 Developmental Marker Expression

RGC-5 cells strongly expressed CD44 mRNA (a marker of haematopoietic stem cell origin), Nestin (an intermediate filament protein commonly found in progenitors) and PAX-6 (Pax-6, a master control gene for the development of the eye and other sensory organs). RGC-5 cells did not express CD133 mRNA (a marker found in neuronal, endothelial, glial, glioblastoma and hematopoietic progenitor cells), nor choline acetyltransferase (ChaT) mRNA (ChaT, an enzyme synthesised by neurons and required for their normal function) (see figure 3.9c). However, RGC-5 cells did weakly express mRNA for SOX-1 (SOX-1, a marker of cells restricted to the neuroectoderm in embryos) (see figure 3.9c).

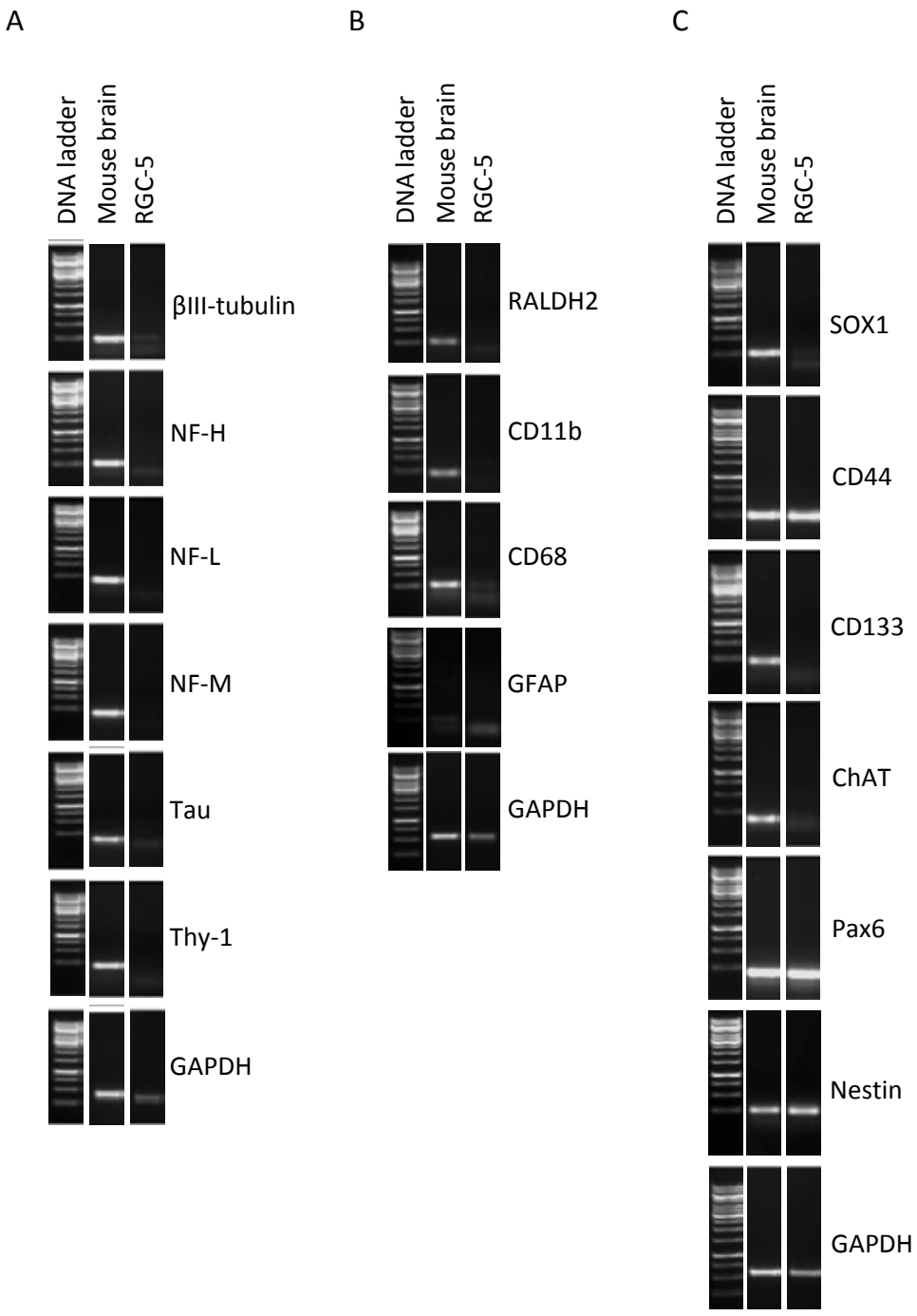

Figure 3.9: Semi-quantitative PCR analysis of selected neuronal, glial and progenitor cell mRNA markers in RGC-5 cells. Clear bands of the correct size were present in all mouse brain positive control groups for all mRNAs tested. (**A.**) RGC-5 cells expressed little or no mRNA for neuronal cell markers including βIII-Tubulin, Neurofilament-H, Neurofilament-L, Neurofilament-M, Tau and Thy-1. (**B.**) RGC-5 cells did not express mRNAs for the astrocyte marker, GFAP, the fibroblast marker RALDH2, or the activated microglia marker CD11b. (**C.**) RGC-5 cells were strongly positive for CD44, Nestin and Pax-6 – this was indicative of a early progenitor marker cell lineages. However, RGC-5 cells did not express mRNA for CD133 or ChAT and only very weakly expressed SOX-1. See figures A.1, A.2 and A.3 for the optimisation processes.

3.5.4 RGC-5 cells are derived from the oligodendroglial lineage

RGC-5 cells expressed mRNA markers consistent with those found in the oligodendroglial lineage. Clear bands of the correct size were present in all mouse brain positive control groups. Interestingly, RGC-5 cells co-expressed mRNA for markers of mature and immature oligodendrocytes (see figure 3.10). For example, RGC-5 cells expressed mRNAs for NG2, CNPase and GalC, but tested negative for MBP (a marker of mature myelinating oligodendrocytes). NG2 and CAII expression, was confirmed by immunocytochemistry (see figure 3.11) and sequencing (see figure 3.7b). Since strong immunoreactivivity was seen in all cells (not just a subpopulation) it is unlikely that this constitutes a mixed population of cells. RGC-5 cells also displayed strong homogeneous immunoreactivity for CAII (carbonic anhydrase II, typically expressed at all stages of oligodendrocyte development (Baumann & Pham-Dinh 2001)). RGC-5 cells did not express mRNA for Olig-1 or -2.

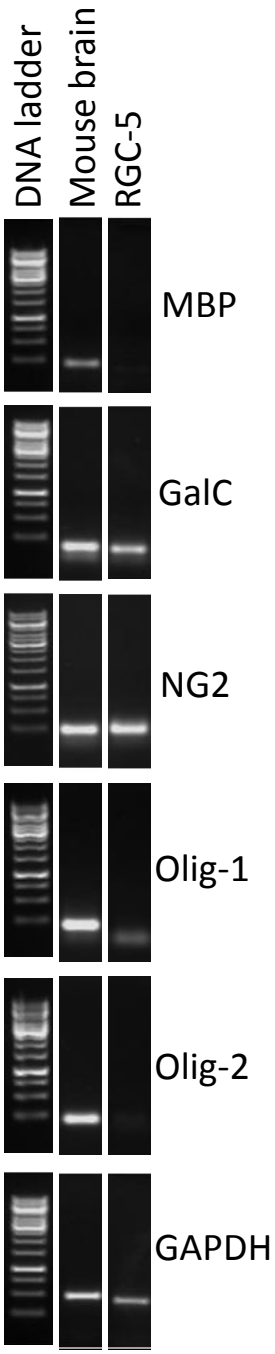

Figure 3.10: Semi-quantitative PCR shows that RGC-5 cells express markers of the oligodendroglial lineage. Clear bands of the correct size were present in all mouse brain positive control groups for all mRNAs tested. RGC-5 cells expressed mRNA markers of both mature and immature oligodendrocytes (GalC and NG2), but tested negative for Olig-1, Olig-2 and MBP. See figure A.4 for the optimisation process.

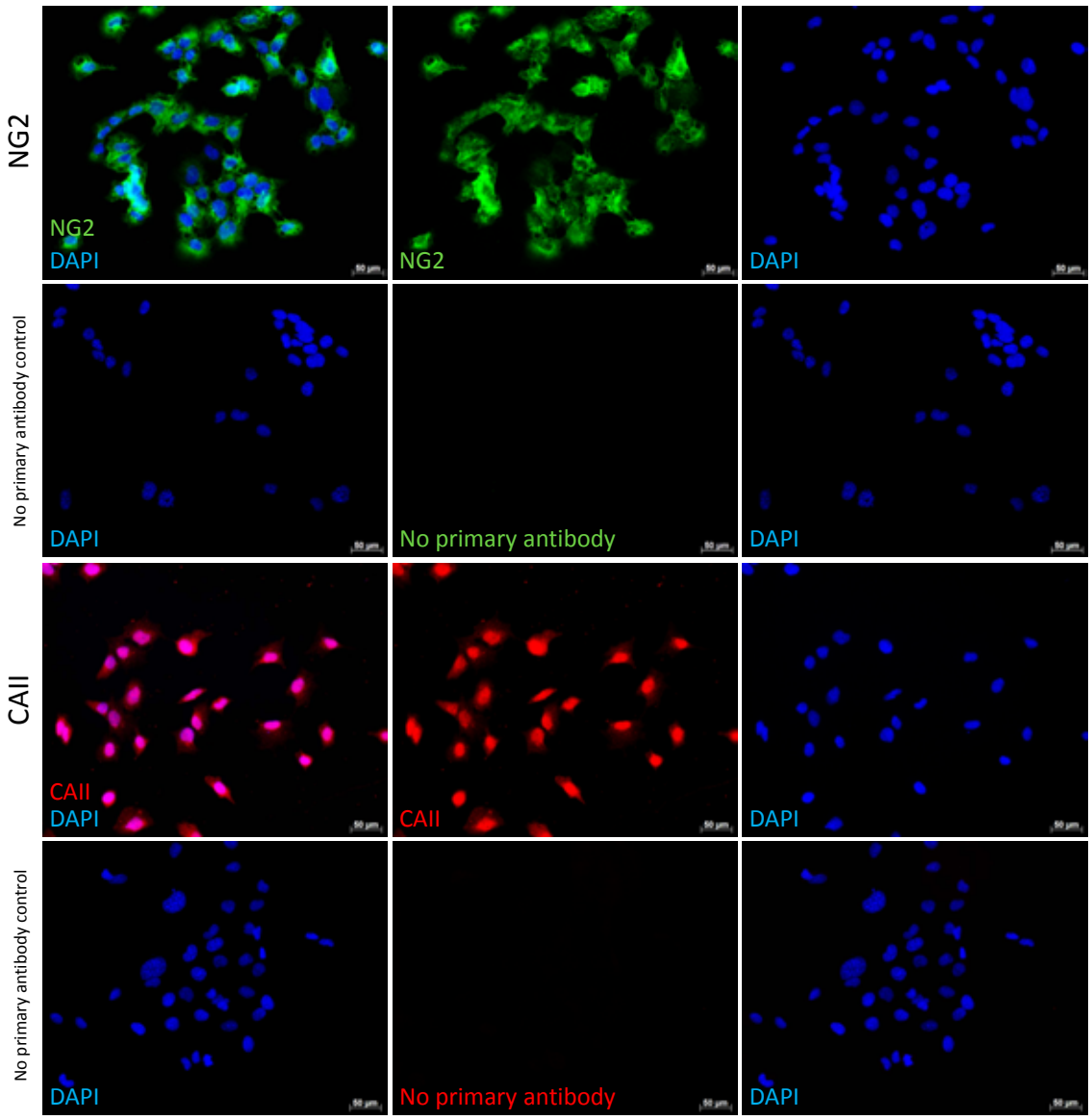

Figure 3.11: Immunocytochenistry shows that RGC-5 cells express markers of the oligodendroglial lineage. RGC-5 cells co-express NG2 (green), a CSPG and marker of NG2 glia, as well as CAII (red). Strong immunoreactivity was observed in all cells. DAPI stained nuclei are in blue. Scale bars = 20 µm.

3.5.5 RGC-5 cells are not derived from cone photoreceptors

To establish whether the RGC-5 cell line was derived from cone photoreceptors of the retina, as suggested previously (Wood et al. 2010), semi-quantitative PCR for blue-sensitive opsin was performed and compared with cDNA from mouse eyes (positive control). Clear bands of the correct size were present in all mouse eye control groups, but absent from the RGC-5 test group (see figure 3.12). This demonstrates that the RGC-5 cell line is not derived from blue sensitive cone photoreceptors.

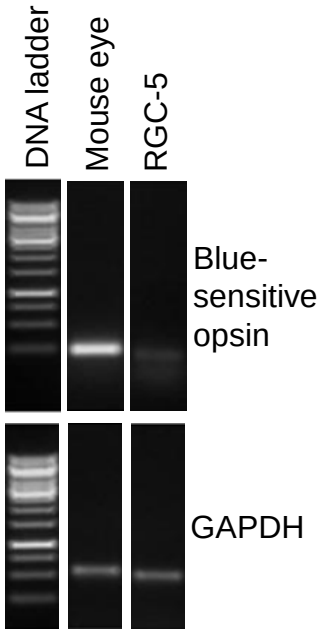

Figure 3.12: RGC-5 cells are not derived from cone photoreceptor cells. Semi-quantitative PCR analysis shows that RGC-5 cells did not express blue-sensitive opsin, a marker of cone photoreceptor cells. However, a clear band of the correct size was present in the mouse eye positive control group. See figure A.5 for the optimisation process.

3.5.6 Densitometry

Densitometric quantification was performed on all of the positive lineage markers expressed in RGC-5 cells and compared to that of the mouse brain positive controls. Apart from βIII-Tubulin, all mRNA markers were expressed in greater abundance than mouse brain positive controls (see figure 3.13). All the mRNA markers were expressed in greater abundance in RGC-5 cells than in the mouse brain positive controls (see figure 3.13). Moreover, RGC-5 cells expressed significantly more CD44, CNPase and Nestin mRNA than in the mouse brain positive controls. The only exception to this was βIII-Tubulin, which was weakly expressed in the RGC-5 cell line.

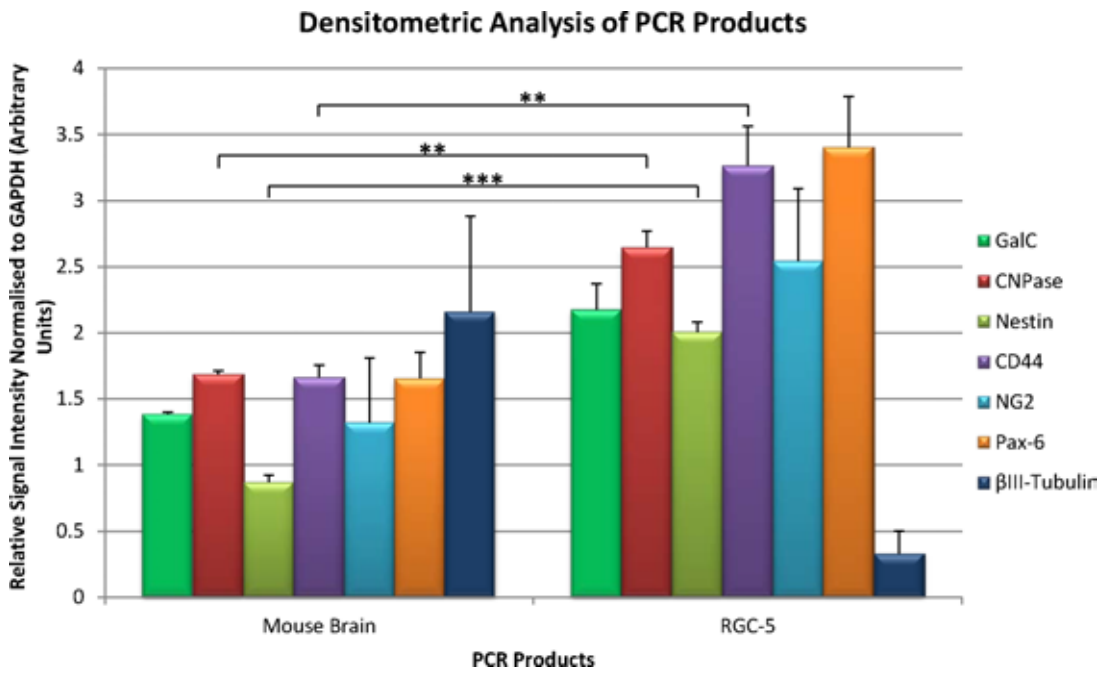

Figure 3.13: Densitometric Analysis of PCR Products. RGC-5 PCR products were compared against a mouse brain positive control. All measurements were normalised to GAPDH (internal control). All lineage markers were expressed in greater abundance than mouse brain positive controls. The only exception to this was βIII-Tubulin, which was weakly expressed in the RGC-5 cell line. Densitometric analysis was performed on PCR products from 3 independent experiments, apart from Pax-6 which represents $n = 2$. ***p ≤ 0.001, **p ≤ 0.01. Statistical test = independent T-test. Due to the low n number, statistics were not performed on Pax-6 densitometry measurements.

3.6 Discussion

3.6.1 Morphological analysis of Staurosporine treated RGC-5 cells

Previous studies (Frassetto et al. 2006) have suggested that Staurosporine, a broad spectrum protein kinase inhibitor, is capable of differentiating the RGC-5 cell line. According to the literature (Frassetto et al. 2006), Staurosporine treatment induces cell cycle arrest, morphological changes, upregulation of neuronal markers (Thymocyte differentiation antigen 1, microtubule-associated protein 2 (MAP2) and *N*-Methyl-D-aspartic acid (NMDA-R1) and establishment of outward rectifying channels.

Unfortunately the mechanism by which Staurosporine induces differentiation is not yet fully understood. Its mechanism of action is presumably related to kinase inhibition however, it's unclear as to which kinases are directly responsible. In 2006 Frassetto *et al* tested a variety of different kinase inhibitors to determine which were involved in the RGC-5 differentiation process (Frassetto et al. 2006). Although treatment with H-1152 (a Rho kinase inhibitor) and H-89 (a non-specific protein kinase-A inhibitor) resulted in some process formation, however the morphological changes induced were dissimilar from Staurosporine treated RGC-5 cells (Frassetto et al. 2006). Although each kinase inhibitor induced RGC-5 process formation, somal rounding was not evident, irrespective of whether the kinase inhibitors were added alone or in combination (Frassetto et al. 2006).

In 2009 Thompson *et al* took a different approach, by comparing Staurosporine against other structurally related molecules (K252a[1], K252b[2], K252c[3], UCN-01[4] and PKC-412[5]) (Thompson & Levin 2010). RGC-5 cells were treated with each of these compounds and morphological measurements (somal rounding, process formation, number of processes etc.) were taken. They found that only Staurosporine and-hydroxystaurosporine (UCN-01) (the most structurally similar) induced differentiation of the RGC-5 cell line – both of which induced somal rounding and process extension. Since Staurosporine and UCN-01 were the only compounds that contained an accessible methoxy group at the 3' carbon and a neighbouring amine group, they concluded that these structural groups were responsible for causing RGC-5 differentiation.

One of the limitations of using Staurosporine as a differentiating agent is that very little is known about its mechanism of action. As Staurosporine is a broad spectrum kinase inhibitor it has multiple targets, many of which have not yet been identified. As a result, Staurosporine should be used with care as it may be difficult to make direct comparisons between Staurosporine treated cell lines and primary cell cultures.

Although many targets have not yet been identified many have, and these include: PKC (see section 1.8.3.2), protein kinase A (PKA) and protein kinase G (PKG) (Tamaoki, et al. 1986). In addition to this Staurosporine also inhibits a variety of cell cycle regulators

[1]9,12-epoxy-1H-diindolo[1,2,3-fg:3',2',1'-kl]pyrrolo[3,4-i][1,6]benzodiazocine-10-carboxylic acid, 2,3,9,10,11,12-hexahydro-10-hydroxy-9-methyl-1-oxo-, methyl ester, (9S,10R,12R)-

[2](5R,6S,8S)-6-hydroxy-5-methyl-13-oxo-6,7,8,13,14,15-hexahydro-5H-16-oxa-4b,8a,14-triaza-5,8-methanodibenzo[b,h]cycloocta[jkl]cyclopenta[e]-as-indacene-6-carboxylic acid

[3]Staurosporine aglycone

[4]7-hydroxystaurosporine

[5]4'-N-benzoylstaurosporine

including cyclin dependent kinase 1 (regulates M phase), cyclin dependent kinase 2 (regulates G1/S phase) and cyclin dependent kinase 5 (regulates Transcription). Additional targets include: janus-kinase 2 (JAK-2) (see section 1.9.2), epidermal growth factor receptor kinase, platelet derived growth factor receptor, myosin-light chain kinase (regulates cellular morphology), ROCK (see section 1.6.2), MAP/ERK kinase (see section 1.8.3.1) and Akt (see section 1.8.3.3) (Bain, et al. 2003). Using this differentiation agent may present a number of problems when investigating growth and/or inhibitory signalling pathways, since staurosporine inhibits key mediators of many of these pathways.

To determine whether Staurosporine did indeed induce morphological changes consistent with that of an RGC phenotype, it was decided to perform a Staurosporine dose response experiment. In agreement with other published works (Wood et al. 2010, Frassetto et al. 2006), RGC-5 cells do exhibit distinctive morphological changes after Staurosporine treatment (see figures 3.1, 3.2 and 3.3). Staurosporine treatment led to increases in the length of the longest process, and processes length/cell, with a concentration of Staurosporine between 0.1 μM to 1.78 μM favouring optimum process outgrowth. In addition to this, Staurosporine treatment significantly enhanced process number (compared to controls), with maximal process number being achieved at 562 nM. Process number declined between 1 μM to 3.16 μM, this may have been a result of increased cytoxicity (see figure 3.4). Moreover, Staurosporine treatment led to a dose dependent increase in process branching. Maximal branching was achieved at a dose of 1 μM to 1.78 μM, the extent of process branching was dramatically reduced by concentrations higher than this, presumably as a result of cytotoxicity (see figure 3.4).

In order to establish a suitable concentration to induce differentiation whilst keeping toxicity to a minimum, a cell viability assay was performed. In retrospect this wasn't the best approach to take since comparisons can't be easily made between loss of viability and reduced cell number due to cell cycle arrest. Ideally I should have combined this approach with direct cell counts and BrdU or Tunnel immuno-labelling, as this would have allowed me to distinguish between mitotic and post-mitotic cells. This would have allowed me to more accurately distinguish between toxicity and cell cycle arrest.

The results show that there was a significant reduction in mean ATP content after treatment with high doses of Staurosporine (1 μM, 1.78 μM or 3.16 μM) compared to all other treatment groups (see figure 3.4). Although this indicates that Staurosporine could have caused some toxicity, additional experiments would need to be performed to confirm this (see previous). Interestingly, a number of other studies (Thompson & Levin 2010) (Frassetto et al. 2006) have shown that Staurosporine does indeed cause toxicity at doses higher than 316 nM, after direct cell counting. This suggests that the reduction of ATP seen in figure was likely a result of toxicity.

Treatment with 0.1%, 1% and 2% DMSO did not cause significant toxicity compared to the untreated control. I am fairly confident that this was the case, since all of the cells present within these groups were still actively dividing, however this would still need to be confirmed by additional experiments.

3.6.2 RGC-5 sequencing

Sequencing analysis of GAPDH (see figure 3.6), CD44 and NG2 (see figure 3.7) has revealed that the cells in my possession are derived from mice (*Mus musculus*) not rats (*Rattus norvegicus*). The distribution of this misidentified and/or cross-contaminated cell does not appear to be an isolated occurrence — two other laboratories have corroborated these findings (Bergen et al. 2009). However this in itself does not exclude the use of the RGC-5 cell line as an appropriate alternative for primary retinal culture. To assess this, it was necessary to look at the expression profile of the RGC-5 cell line.

3.6.3 RGC-5 expression profile

Semi-quantitative PCR analysis has revealed that the RGC-5 cell line does not express mRNA for markers of mature RGC, (Thy1, NF-M, NF-L, NF-H and Tau) and only weakly expressed the neuronal marker βIII-Tubulin (see figure 3.9a). As a result the RGC-5 cell line is unlikely to be derived from mature RGC. Furthermore, RGC-5 cells did not express markers of fibroblasts (RALDH2), activated microglia (CD11b) or macrophages (CD68) (see figure 3.9b).

Since the original report of the generation of the RGC-5 cell line (R.R.Krishnamoorthy et al. 2000), many discrepancies with primary RGC have been identified. For example, there has been marked decrease in glutamate sensitivity suggesting that the RGC-5 cells were pharmacologically less ganglion-cell like (Bergen et al. 2009, Fan, et al. 2005, Maher & Hanneken 2005).

Contrary to previously published works (Wood et al. 2010), the RGC-5 cell line does not express mRNA for blue-sensitive Opsin, a marker of cone photoreceptors. In this study (Wood et al. 2010), Opsin expression was determined through the use of western blotting and immunostaining. This discrepancy may have been due to a problem with antibody specificity. It is possible that the antibody exhibited cross-reactivity with an antigen present on the RGC-5 cell line.

However, in agreement with this study (Wood et al. 2010), RGC-5 cells expressed βIII-Tubulin but did not express Thy-1, NF-H, NF-M or NF-L – even after treatment with any of the known RGC-5 differentiating agents (Staurosporine, Succinyl-concanavalin A and Trichostatin).

RGC-5 cells expressed mRNAs for NG2, CNPase and GalC (oligodendroglial lineage markers) but tested negative for MBP (a marker of mature myelinating oligodendrocytes). NG2 expression (a marker of oligodendrocyte progenitors / NG2 glia) was further confirmed by immunocytochemistry and sequencing analysis (see figure 3.7). In light of this information, it seems unlikely that these cells were even derived from the eye, since oligodendrocyte progenitors are typically absent from the retina.

Interestingly, RGC-5 cells did not express oligodendrocyte transcription factor 1 and 2 (Olig- 1, Olig-2) (see figure 3.10). These genes encode basic helix-loop helix transcription factors and are expressed exclusively by oligodendrocytes and NG2 glia/oligodendrocyte progenitors. Furthermore, RGC-5 cells strongly express the neural stem cell marker Pax-6 (see figure 3.9c). This was surprising since RGC-5 cells express many markers consistent with an oligodendroglial lineage. This may in some way explain the absence of Olig-2

expression since It has been well documented that (Agarwal et al. 2007) there is an inverse correlation between Olig-2 and Pax-6 expression — over expression of Pax-6 generally leads to down regulation of Olig-2 and progression towards a neuronal fate (Jang & Goldman 2011). It is also possible that these cells may be derived from a subpopulation of NG2 glia which expresses Pax-6, or that these cells have not yet committed themselves to a particular cell fate.

Interestingly, RGC-5 cells highly expressed mRNA for both CD44 and Nestin (see figure 3.9c) — this was not surprising since both are markers of multilineage progenitors (Wiese, et al. 2004). Nestin is highly upregulated in proliferating oligodendrocyte progenitors (Gallo & Armstrong 1995). Moreover, Nestin and CD44 are upregulated in response to injury, so it is also possible that this may have been a consequence of the isolation process (Frisen, et al. 1995, Moon, et al. 2004).

The wide range of disparities in RGC-5 cell phenotypes, which encompass the original characteristics given by Agarwal and colleagues (R.R.Krishnamoorthy et al. 2000, Agarwal et al. 2007) and more recent re-evaluations (Bergen et al. 2009, Wood et al. 2010), are probably explained by inadequate isolation during passage (American Type Culture Collection Standards Development Organization Workgroup ASN-0002 2010), differential methods of screening and misidentification (MacLeod, et al. 1999, Masters, et al. 2001, Thompson, et al. 2004) through mislabelling (American Type Culture Collection Standards Development Organization Workgroup ASN-0002 2010) and cross-contamination with other cell lines. For example, phenotypic screening may yield divergent results when using specific antibody marker techniques compared to DNA amplification, restriction digest and sequencing analyses. Once contaminated, invading cells can swiftly over-ride

and eventually replace the resident cell line (Nims, et al. 1998). For example, a study conducted by the american Type Culture Collection (ATCC) found that 27 out of 56 cell lines were contaminated by the HeLa cell line (Lavappa, et al. 1976), while another found that ECV304 (Dirks, et al. 1999), a normal human endothelial cell line, had become contaminated by the bladder cancer derived T24 cell line, and two human prostate cancer cell lines, TSU-Pr1 and JCA-1 (van Bokhoven, et al. 2001). Despite the application of genotyping, karyotyping and cell marker identification, the use of misidentified and contaminated cell lines continues to invalidate results, waste time and resources, and make comparison between published works impossible.

3.7 Conclusions

The overall aim of this study was to establish whether the RGC-5 cell line could be used as a substitute for primary RGC. From the current data it is evident that the RGC-5 cell line is not what it was originally reported to be. The RGC-5 cells in our laboratory were derived from a mouse oligodendroglial lineage and were not ganglion or cone photoreceptor cells.

CHAPTER 4

IN VITRO EFFECTS OF CNTF IN PRIMARY RETINAL CULTURE

4.1 Testing the effectiveness of CNTF in primary retinal culture

Before a long term *in vivo* delivery strategy was undertaken, it was decided to look at the effectiveness of CNTF treatment on primary retinal cultures. It was also necessary to confirm that CNTF could disinhibit RGC neurite outgrowth whilst in an inhibitory environment. To this end, a dose response experiment was performed to determine the optimum CNTF concentration for RGC.

Having determined the optimum CNTF concentration, it was necessary to test this dose in the presence of a growth inhibitory ligand. To achieve this, the recombinant Nogo-P4 peptide was chosen to crudely mimic the inhibitory CNS environment after injury. Nogo-P4 was selected in preference to central myelin extract for a number of reasons. Firstly, the recombinant protein is soluble, allowing the dose to be easily modified if optimisation was required. In contrast, central myelin extract is lipid rich and contains an array of inhibitory ligands, therefore it would be necessary to fully characterise and titrate each batch of central myelin extract before use. This is a time consuming and expensive process which is further impeded by the presence of contaminating growth factors, such as fibroblast growth factor 2 (FGF2). Secondly, Nogo has a well defined signalling profile which has been extensively characterised — this would make it easier to monitor CNTF and/or Nogo dependent signalling mechanisms. Once optimised, this neurite growth inhibitory assay could be used to reproducibly inhibit RGC neurite outgrowth. Furthermore, this assay could be used to test a variety of neuritogenic and/or neuroprotective therapeutics *in vitro*.

Several studies suggest that CNTF is ineffective at directly stimulating RGC axon growth (Cui, et al. 2008), whilst others suggest that cAMP elevation is required for CNTF to be effective (Müller, et al. 2009). Furthermore, it was recently proposed that CNTF exerts its effects indirectly through the activation of macrophages/microglia (Cen, et al. 2007). As there has been some controversy regarding the effectiveness of CNTF *in vitro* (Müller et al. 2009) and *in vivo* (Müller et al. 2009). It was also necessary to establish whether an additional elevation in cAMP was required to stimulate neurite outgrowth. To establish this it was decided to test each CNTF dose in the presence of a cAMP elevator, namely Forskolin (an activator of adenylate cyclase).

As already discussed, cAMP is important both developmentally and after injury. cAMP levels not only modulate neuronal responsiveness to myelin inhibitory ligands, but can also influence their capacity for regrowth (Cai et al. 2001, Cai, et al. 1999). cAMP activates PKA to exert many of its biological effects and acts independently to that of the JAK/STAT, MAPK/ERK and PI3-K/Akt signalling pathways (Li, et al. 2000).

4.2 Aims

1. Develop an assay for assessing whether recombinant CNTF can disinhibit RGC neurite outgrowth *in vitro* in the presence of a growth inhibitory ligand.

2. Determine whether an elevation in cAMP is required for CNTF to effectively stimulate RGC neurite outgrowth.

3. Determine whether *AAV2-CNTF-hrGFP*, *AAV2-CNTF-FLAG* and *AAV2-CNTF-shRhoA-hrGFP* constructs produce biologically relevant levels of CNTF when transfected into HEK-293 cells.

4.3 Results

4.3.1 Primary retinal cultures

Primary retinal cultures were prepared as in section 2.1.1 and incubated for 4 d. Cultures contained a mixed population of cells comprising of both retinal neurons and glia. RGC make up approximately 1% of the total cell population in mixed retinal cultures. The remaining cell population is made up of retinal neurons (e.g. amacrine cells, photoreceptors, bipolar cells and horizontal cells), retinal glia (e.g. Müller glia and astrocytes), and endothelial cells. Primary RGC were identified from other cell types by size, morphology and βIII-Tubulin (a neuronal marker which is highly expressed in mature RGC) immunoreactivity (see figure 4.1). The size criterion was based on the assumption that RGC typically have a cell diameter of 12 µm or less (Guenther, et al. 1994) (see figure 4.1). Primary RGC were incubated for 24 h to allow the cells to adhere to the plate — the test reagents (Nogo-P4 peptide and CNTF) were then added. RGC survival and neurite extension were assessed 3 d later (96 h after plating). A yield of approximately 1×10^6 retinal cells were extracted from each retina and plated at a density of 130 000 cells well^{-1}.

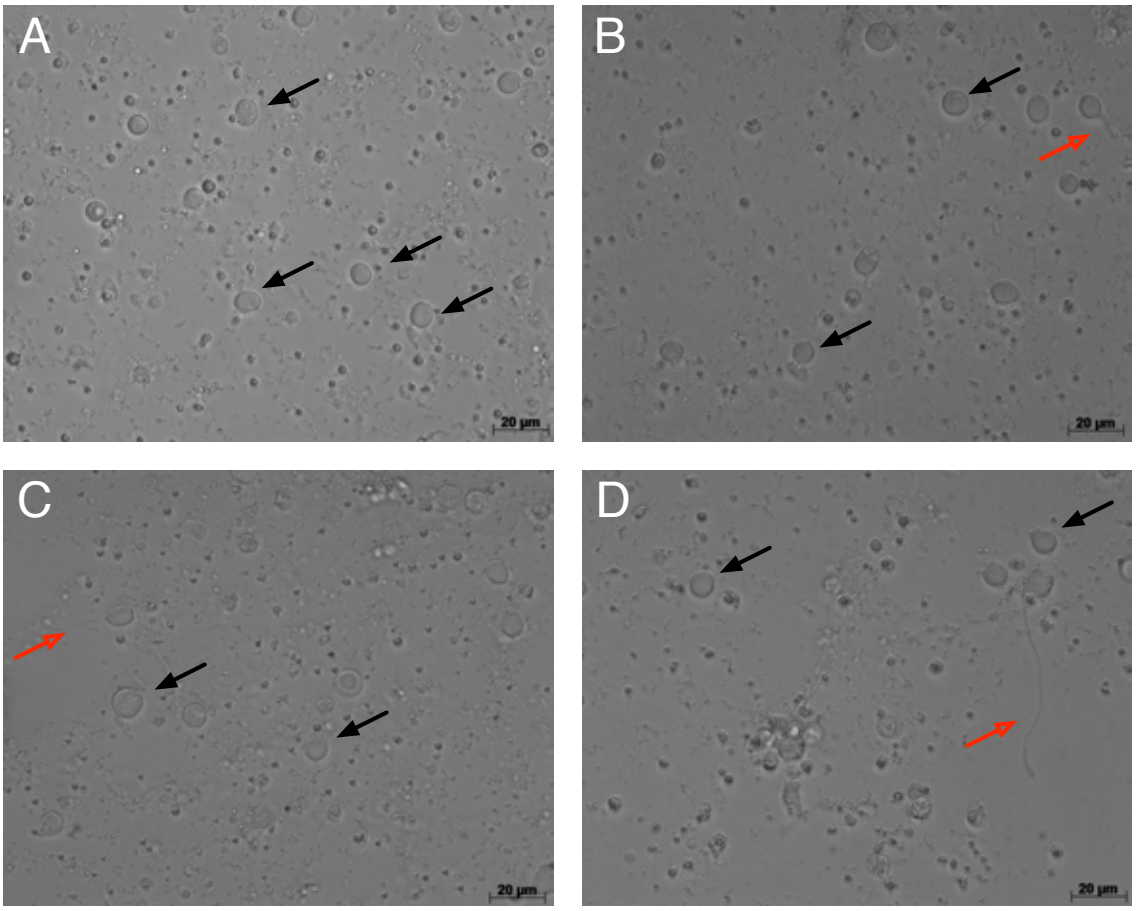

Figure 4.1: Representative bright field images of control primary retinal cultures. Primary RGC were identified in culture by their distinctive morphology and size. Retinal cells were incubated for 24 h to allow the cells to adhere to the plate, all test reagents were added at this time point. Primary RGC typically have a cell diameter of 12 µm or less (Guenther et al. 1994) and tend to extend neurites within 96 h of plating. Figture shows control retinal cultures (**A.**) 24h (**B.**) 48h (**C.**) 72h (**D.**) 96h after plating. Black arrows point to the soma of primary RGC, whilst red arrows point to the neurites.

4.3.2 Forskolin and recombinant CNTF promotes retinal ganglion cell neurite outgrowth *in vitro*

A range of CNTF concentrations was applied to adult rat primary retinal cultures to determine whether recombinant CNTF was capable of promoting RGC neurite outgrowth (see figure 4.2) and survival (see figure 4.4) *in vitro*.

Approximately 130 000 cells well^{-1} were plated and given 24 h to adhere to the plate after which treatment was applied. After a further 72 h the cells were fixed and analysed for mean length of longest neurite (figure 4.2a) and mean neurite length (figure 4.2b).

Results indicate that CNTF is capable of promoting neurite outgrowth in culture (see figure 4.2a) and that this effect can be augmented with increasing concentrations of protein. The optimal dose was deemed to be 100 ng ml^{-1} as application of this concentration elicited the greatest effect in terms of mean neurite length and mean length of longest neurite. Treatment with 100 ng ml^{-1} CNTF significantly increased the mean length of longest neurite from 18.83 µm ± 1.67 (untreated control) to 33.89 µm ± 2.41 (100 ng ml^{-1} CNTF) and mean neurite length from 17.3 µm ± 0.07 (untreated control) to 29.97 µm ± 0.07 (100 ng ml^{-1} CNTF). See figure 4.5 for representative images of this experiment.

Maximal RGC neurite outgrowth was achieved when Forskolin was added alone (Forskolin control). Treatment with 15 µM Forskolin significantly increased the mean length of longest neurite from 18.82 ± 1.67 (untreated control) to 33.66 ± 2.97 (15 µM Forskolin) and mean neurite length from 17.36 ± 1.43 (untreated control) to 28.21 ± 2.22 (15 µM Forskolin). Similar neurite outgrowth measurements (mean neurite length and mean length of longest

neurite) were obtained when CNTF (10 ng ml^{-1}, 50 ng ml^{-1} and 100 ng ml^{-1}) was added in combination with 15 μM Forskolin. However, there was no statistically significant difference in neurite length irrespective of whether Forskolin was added alone (Forskolin control) or in combination with CNTF (10 ng ml^{-1}, 50 ng ml^{-1} or 100 ng ml^{-1}, see figure 4.2b).

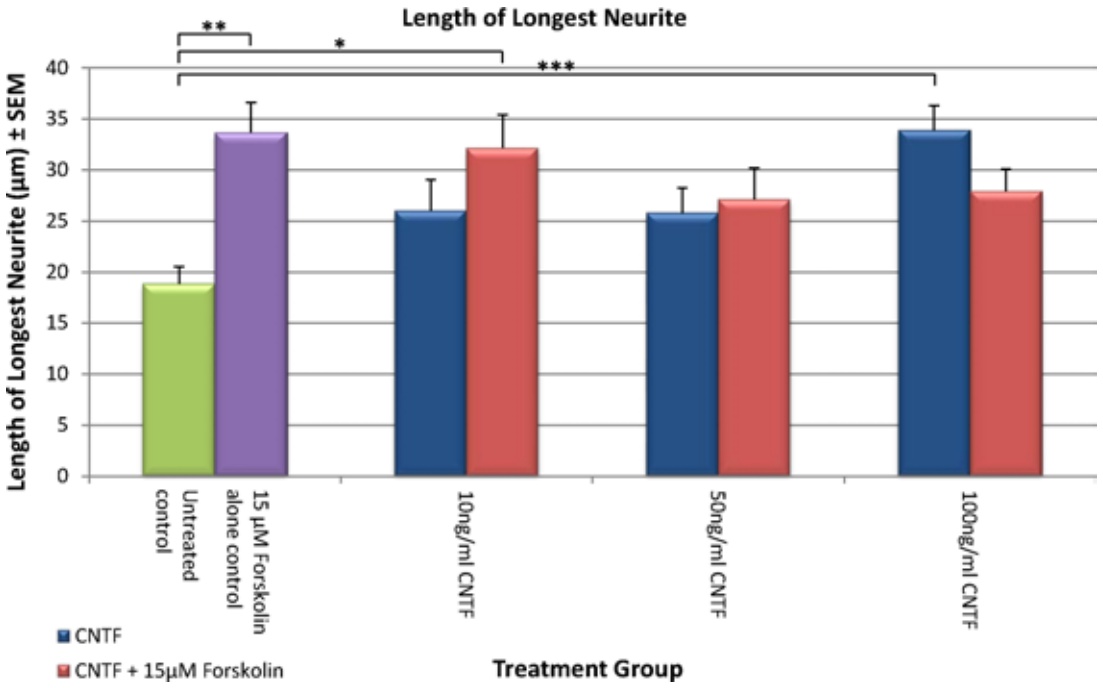

(a) Length of longest neurite

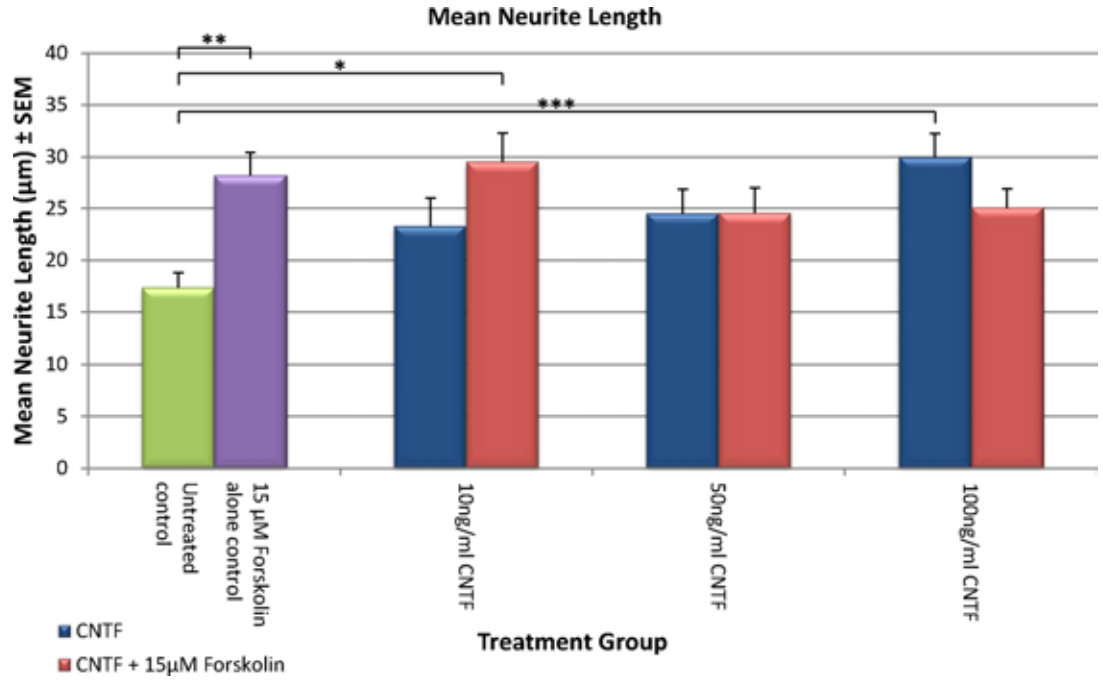

(b) Mean neurite length

Figure 4.2: CNTF and Forskolin promotes neurite outgrowth *in vitro*. Retinal cultures were treated with increasing doses of CNTF. Each dose was administered alone or in combination with 15 µM Forskolin after 24 h had passed (to allow the cells to adhere to the plate). The cells were fixed after a further 72 h for analysis. When CNTF was administered alone a dose of 100 ng ml^{-1} induced optimal neurite outgrowth — however, when given in combination with Forskolin a dose of 10 ng ml^{-1} was deemed to be optimal. Error bars represent the SEM. $n = 3$ for all treatment groups. ***p ≤ 0.001, **p ≤ 0.01, *p ≤ 0.05, statistical test = one-way ANOVA.

4.3.3 CNTF and Forskolin treatment has a minimal affect on neurite number

Forskolin (15 μM) treated RGC possessed more neurites both with and without CNTF as shown in figure 4.3. Primary retinal cells (130 000) were plated at the beginning of the experiment, CNTF (10 ng ml^{-1}, 50 ng ml^{-1} or 100 ng ml^{-1}) and/or Forskolin (15 μM) was added 24 h later (to allow time for the RGC to adhere to the plate) and cells were fixed and analysed 72 h after treatment was applied.

In most cases there was no significant change in neurite number (figure 4.3), irrespective of whether CNTF was administered alone or in combination with Forskolin. Cells treated with Forskolin alone (Forskolin control, 1.23 ± 0.10) had significantly more neurites than those treated with 100 ng ml^{-1} CNTF (0.82 ± 0.07). RGC were identified by morphology and βIII-Tubulin staining whilst neurite number was quantified by directly counting the number of RGC (section 2.1.1.1 describes the sampling technique used). Figure 4.5 shows representative images of this experiment.

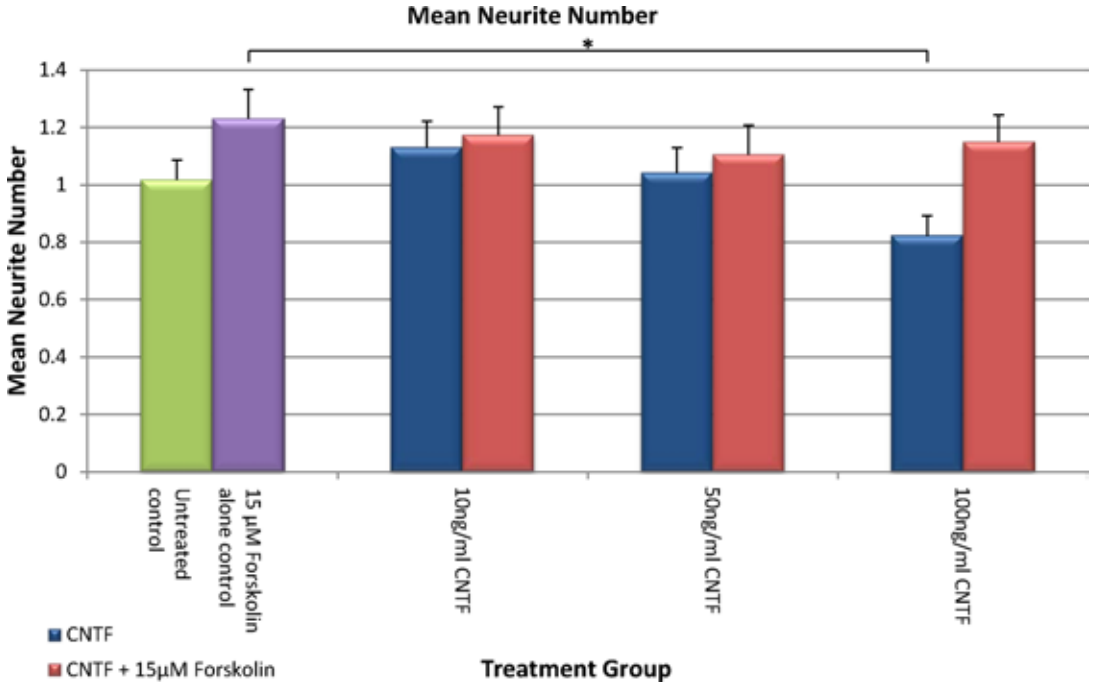

Figure 4.3: CNTF and Forskolin had a minimal affect on neurite number. In most cases, there was no significant change in neurite number. RGC within the 15 µM Forskolin treatment group (Forskolin control) had significantly more neurites than those in the 100 ng ml^{-1} CNTF treatment group. All Forskolin treatment groups possessed more neurites than their CNTF-treated counterparts. The control groups consist of an untreated (negative) control and a 15 µM Forskolin control. Error bars represent the SEM. $n = 3$ for all treatment groups. *p ≤ 0.05, statistical test = one-way ANOVA.

4.3.4 10 ng ml^{-1} and 50 ng ml^{-1} CNTF caused minor toxicity

Toxicity was seen 72 h after treatment with 15 µM Forskolin alone (Forskolin control) compared to the untreated (negative) control (RGC number was reduced by 23.96%). Similar levels of toxicity were observed when Forskolin was administered together with 10 ng ml^{-1} CNTF or 50 ng ml^{-1} CNTF — each of which had a 22.23% reduction in RGC cell number compared to untreated controls. There was no significant change in RGC cell number between 100 ng ml^{-1} CNTF treated and untreated controls. Primary retinal cultures were fixed and analysed 96 h after plating (72 hour after CNTF and/or Forskolin addition). RGC were visualised by βIII-Tubulin immunostaining and identified by their distinctive morphology (see section 4.3.1). Cell survival was assessed by directly counting the βIII-Tubulin positive (red) RGC (see section 2.1.1.1 for details of the sampling technique). As 100 ng ml^{-1} has been shown to be an optimal dose for RGC neurite outgrowth, survival and toxicity, I decided to use this dose for all future experiments. See figure 4.5 for representative images of this experiment.

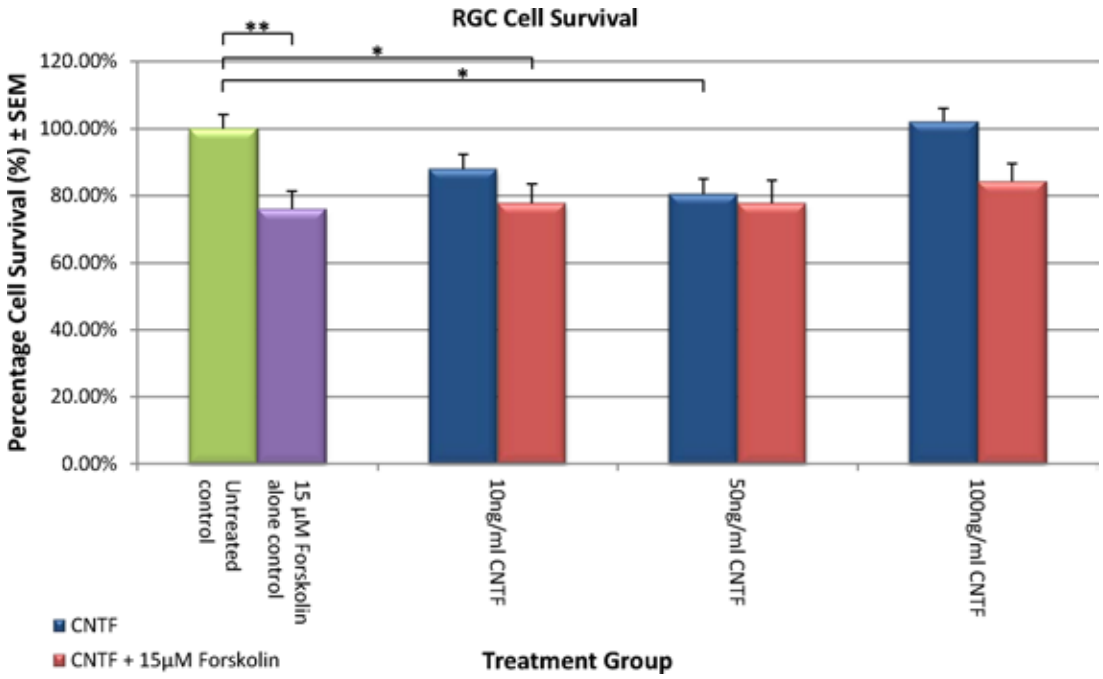

Figure 4.4: Minor cytotoxicity was seen after treatment with 15 µM Forskolin compared to untreated controls. 130 000 retinal cells were plated on day 0, treatment was applied 24 h after plating and cell number was then assessed 96 h after plating by directly counting βIII-Tubulin positive (red) RGC. There was no significant change in RGC number between 100 ng ml^{-1} CNTF treated and the untreated controls. The error bars represent the SEM from 3 independent experiments. **$p \leq 0.01$, *$p \leq 0.05$, statistical test = one-way ANOVA.

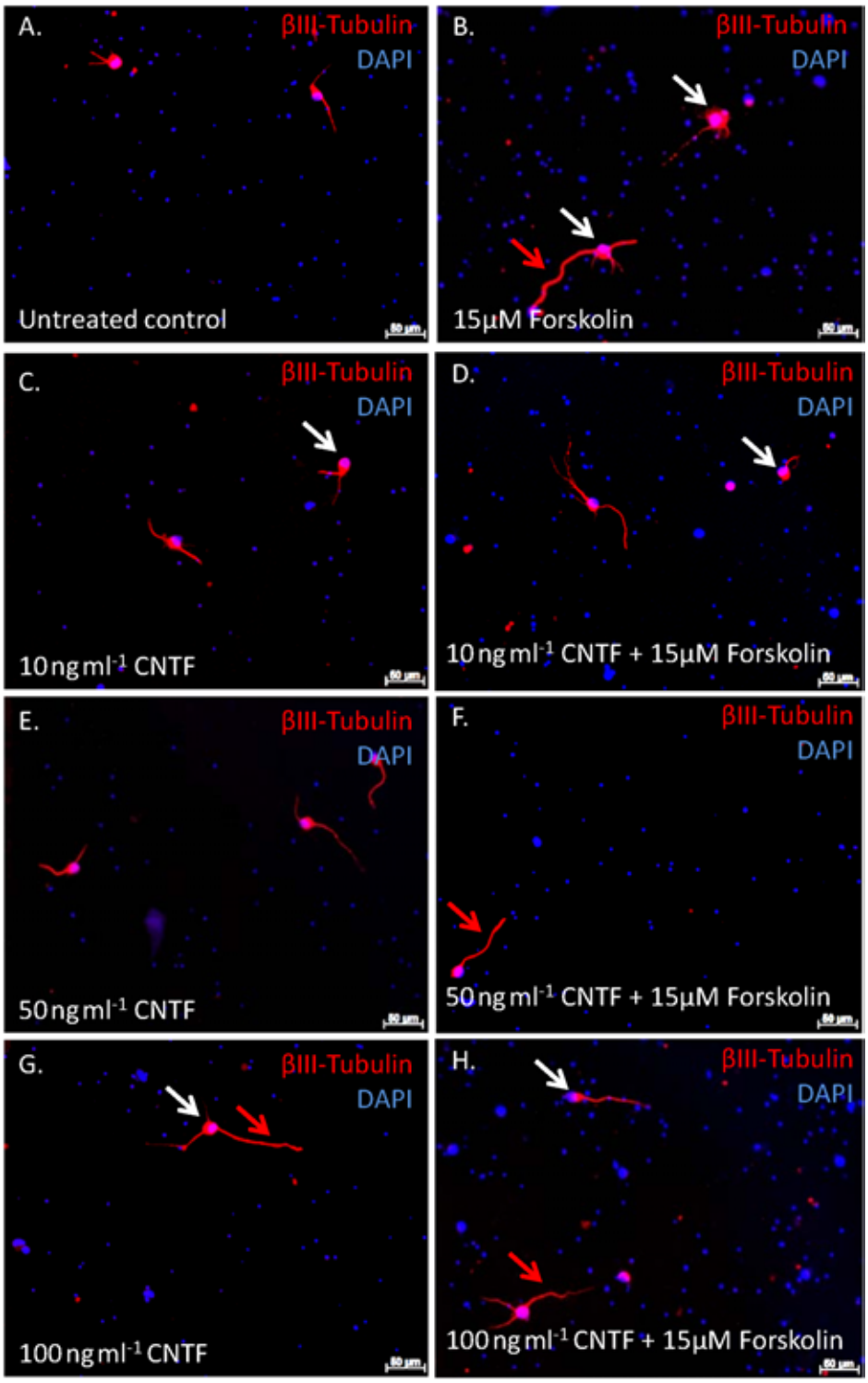

Figure 4.5: CNTF dose response experiment. Retinal cells (130 000) were treated with either Forskolin (15 µM) and/or increasing concentrations (10 ng ml^{-1}, 50 ng ml^{-1} and 100 ng ml^{-1}) of CNTF 24 hour after plating. Cells were fixed 72 h later for analysis and quantification of cell number, neurite number and neurite length (see section 2.1.1.1). Treatment with Forskolin and/or CNTF stimulated RGC neurite outgrowth (highlighted in figure with red arrows). RGC were identified by morphology, cell soma size and βIII-Tubulin immunoreactivity (red). DAPI stained nuclei are shown in blue (highlighted in figure with white arrows). Scale bar = 50 µm.

4.3.5 100 ng ml^{-1} CNTF increases neurite number and abolishes the Nogo-P4 induced inhibitory effect

Primary retinal cultures were treated with 25 μM Nogo-P4 peptide to inhibit neurite outgrowth (see figure 4.7) and neurite number (see figure 4.6). A positive control of 100 ng ml^{-1} CNTF was also included in the experiment. 25 μM Nogo-P4 significantly inhibited neurite number (0.61 ± 0.04) when compared to the untreated control (0.91 ± 0.04). A dose of 100 ng ml^{-1} CNTF abolished this effect, increasing neurite number from 0.61 ± 0.04 (Nogo-P4 treated) to 0.84 ± 0.06 (25 μM Nogo-P4 and 100 ng ml^{-1} CNTF treated). Interestingly, there was no significant difference between 100 ng ml^{-1} CNTF (0.93 ± 0.05) and untreated controls (0.91 ± 0.04). For consistency, 130 000 retinal cells were plated at the start of the experiment. Treatment with Nogo-P4 peptide and/or CNTF was applied after 24 h and cells were fixed and analysed 72 h later. Neurite number was established by directly counting βIII-Tubublin positive RGC. Figure 4.9 shows representative images of this experiment.

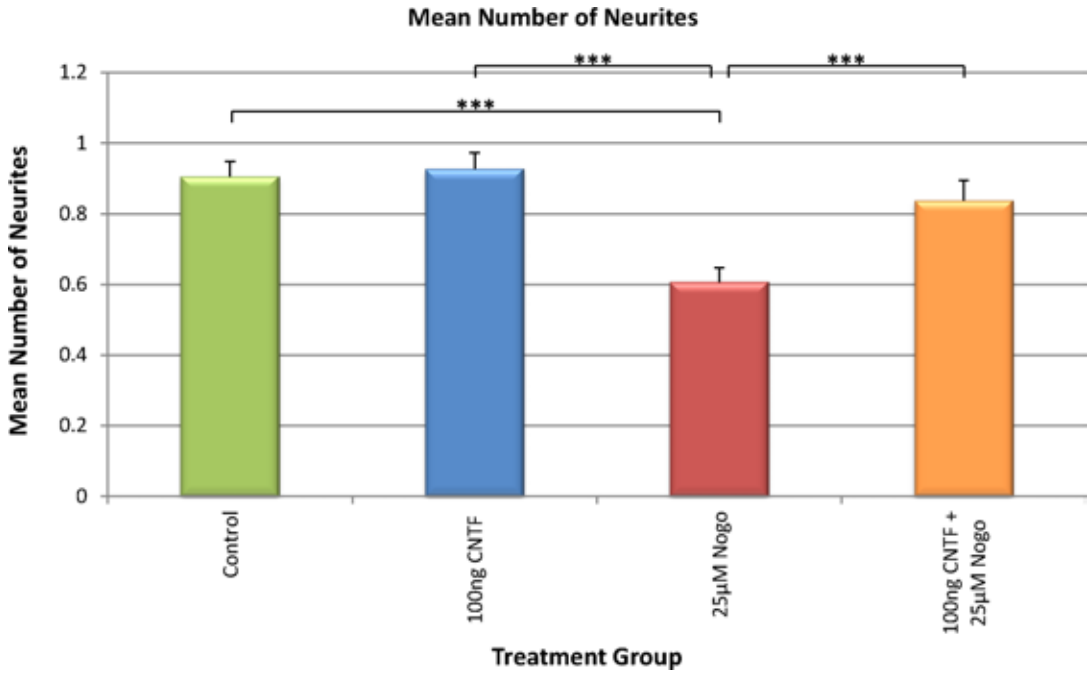

Figure 4.6: 100 ng CNTF increased neurite number and abolished the Nogo-P4 induced inhibitory effect. Treatment with 25 µM Nogo-P4 peptide significantly inhibited neurite number, whereas application of 100 ng CNTF reversed this effect. This reversal brought neurite number back in line with untreated controls. Control groups consisted of 100 ng ml^{-1} CNTF (positive control) and an untreated control (negative control, labelled as `Control' in figure). Error bars represent the SEM from 3 independent experiments. ***$p \leq 0.001$, statistical test = one-way ANOVA.

4.3.6 100 ng ml^{-1} CNTF disinhibits Nogo-P4 treated retinal ganglion cells

Primary retinal cultures were treated with a 25 μM Nogo-P4 inhibitory peptide to inhibit neurite outgrowth and to crudely mimic the inhibitory environment seen *in vivo*. This dose was previously optimised by Dr Kevin Morrison (personal communication) and the results obtained were consistent with his findings (see section 4.4.5). A dose of 100 ng ml^{-1} recombinant CNTF was capable of reversing Nogo-P4 induced inhibition (see figure 4.7), increasing mean length of longest neurite (see figure 4.7a) from 18.69 μm ± 1.44 (Nogo-P4 treated) to 39.46 μm ± 3.53 (25 μM Nogo-P4 and 100 ng ml^{-1} CNTF treated).

Furthermore, 100 ng ml^{-1} CNTF increased mean neurite length (see figure 4.7b) from 25.58 μm ± 1.26 (Nogo-P4 treated) to 53.29 μm ± 3.34 (25 μM Nogo-P4 and 100 ng ml^{-1} CNTF treated), bringing it in line with the value of the untreated control (47.07 μm ± 2.35). Interestingly, CNTF alone only caused a minimal increase in mean neurite length (40.16 μm ± 3.82) and mean length of longest neurite (45.17 μm ± 4.00) compared to untreated controls (34.84 μm ± 2.35 and 39.48 μm ± 2.71 respectively), although this effect did not reach statistical significance. See figure 4.9 for representative images of this experiment.

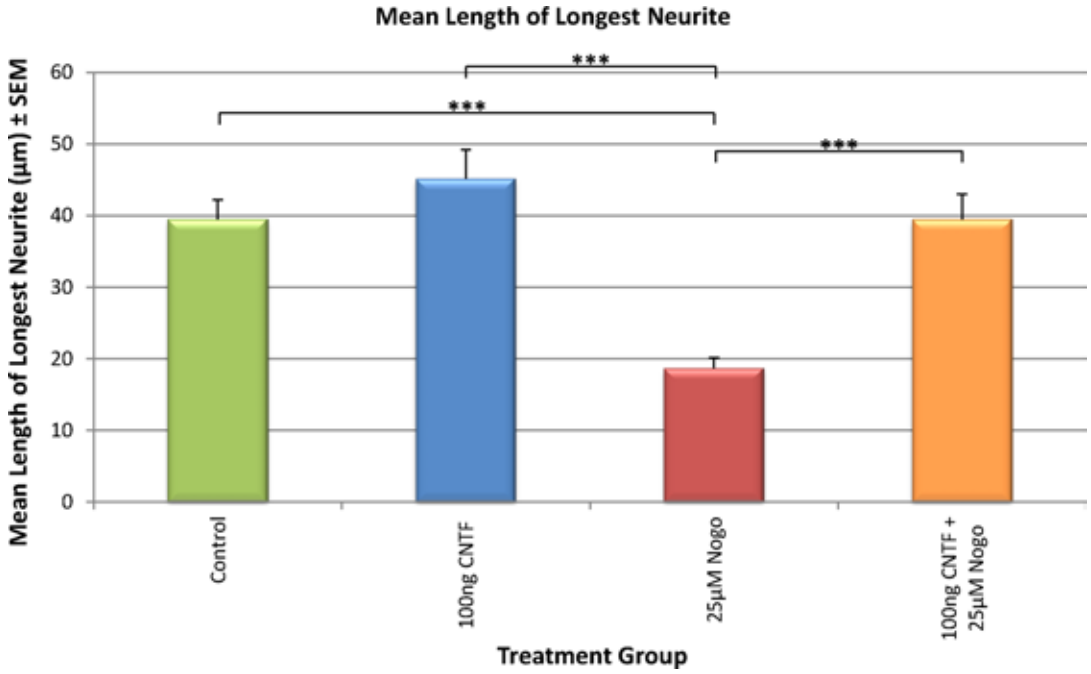

(a) Mean length of longest neurite

Figure 4.7: Effect of CNTF on Nogo-P4 treated primary retinal culture. 130 000 retinal cells were plated at the start of the experiment, 100 ng CNTF and/or 25 µM Nogo-P4 was added 24 h later and results were assessed 72 h post-treatment. Application of 25 µM Nogo-P4 peptide significantly inhibited mean length of longest neurite and mean neurite length. Application of 100 ng CNTF reversed this effect, bringing measurements back in line with untreated control values. βIII-Tubulin positive neurites were measured using Image Pro® software. Control groups consisted of 100 ng ml^{-1} CNTF (positive control) and an untreated control (negative control, labelled as `Control' in figure). Error bars represent the SEM from 3 independent experiments. Continued on next page. ***$p \leq 0.001$, statistical test = one-way ANOVA.

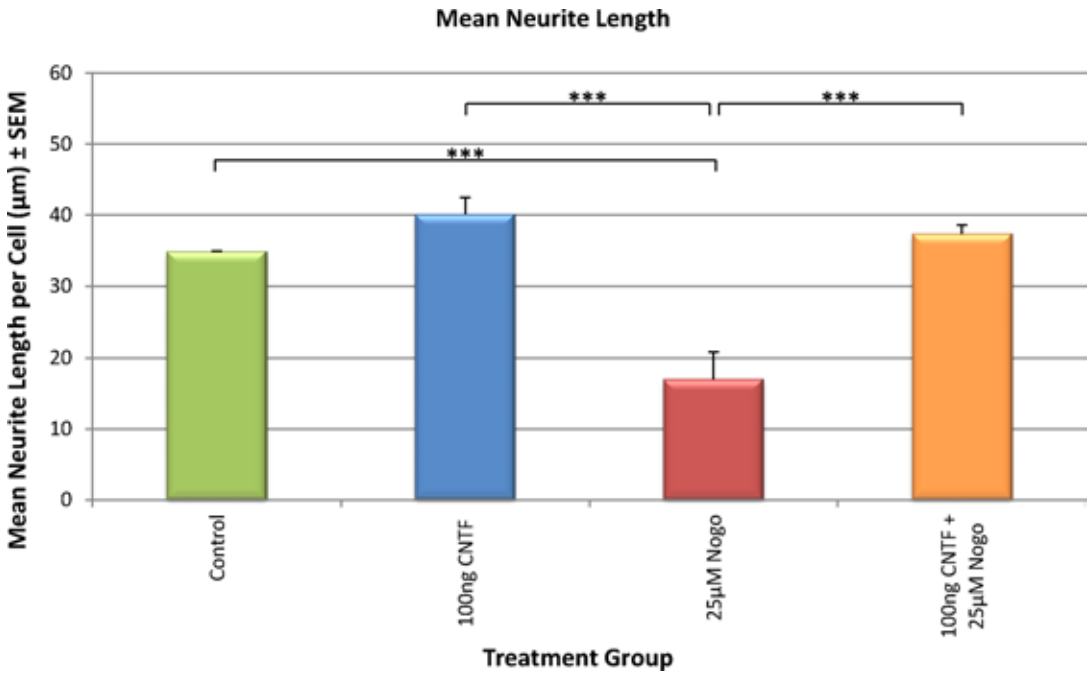

(b) Mean neurite length

Figure 4.7: Effect of CNTF on Nogo-P4 treated primary retinal culture. Continued from previous page. Control groups consisted of 100 ng ml^{-1} CNTF (positive control) and an untreated control (negative control, labelled as `Control' in figure). Error bars represent the SEM from 3 independent experiments. ***$p \leq 0.001$, statistical test = one-way ANOVA.

4.3.7 Nogo-P4 treatment had no effect on RGC survival

Results show that there was no significant difference in RGC survival between the untreated control (negative control) and each of the treatment groups after 72 h, see figure 4.8. RGC were visualised by βIII-Tubulin immunostaining and identified by their distinctive morphology (see section 4.3.1). Cell survival was assessed by directly counting βIII-Tubulin positive (red) RGC (see section 2.1.1.1 for details of the sampling technique). See figure 4.9 for representative images of this experiment.

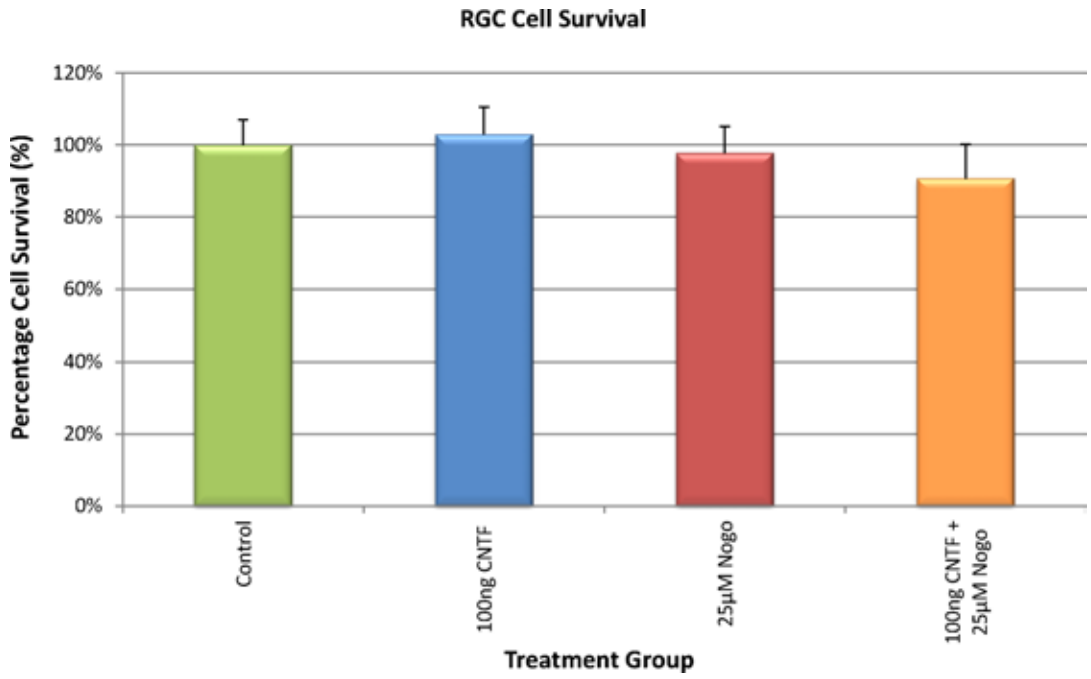

Figure 4.8: Nogo-P4 treatment had no effect on RGC survival. RGC were plated (at a density of 130 000 cells well^{-1}) and incubated for 24 h, treatment was then applied. After a further 72 h (96 h after plating) the cells were fixed and analysed. RGC survival was not affected by any of the treatment groups. No significant difference was observed in RGC number between treatment groups and the untreated control (negative control). Control groups consisted of 100 ng ml^{-1} CNTF (positive control, labelled as `Control' in figure) and untreated cells served as a negative control. Error bars represent the SEM from 3 independent experiments. Statistical test = one-way ANOVA.

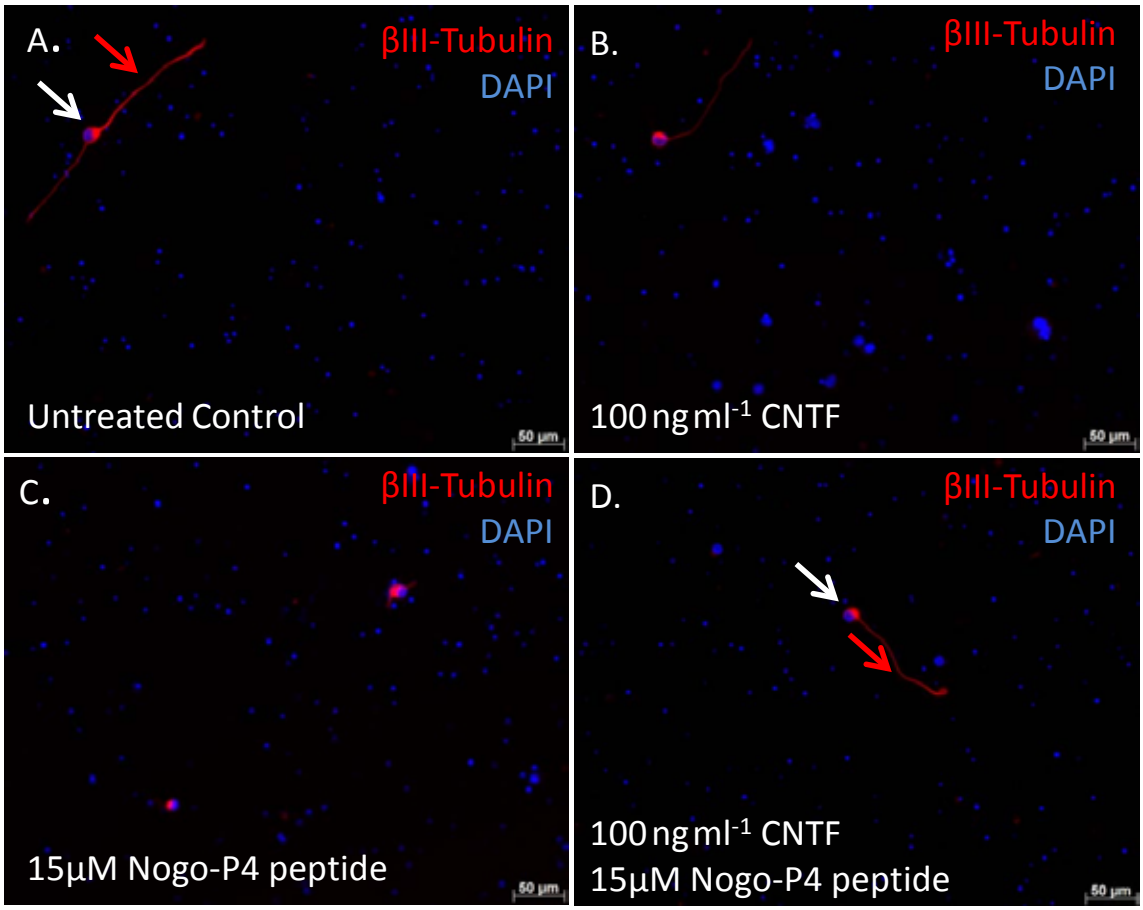

Figure 4.9: Nogo-P4 inhibitory assay. Immunostaining for the RGC marker βIII-Tubulin (red) in Nogo-P4 peptide and CNTF treated retinal cultures. DAPI stained nuclei are blue. Treatment with (C.) 25 µM Nogo-P4 significantly inhibited RGC neurite outgrowth. Scale bar = 50 µm

4.3.8 Summary of results

A range of CNTF concentrations (10 ng ml^{-1}, 50 ng ml^{-1} and 100 ng ml^{-1}) were applied to adult primary retinal cultures to determine whether recombinant CNTF could promote RGC neurite outgrowth and survival in vitro. A dose of 100 ng ml^{-1} CNTF was found to be optimum since this concentration induced maximal neurite outgrowth and survival.

In addition to this, each concentration of CNTF was tested in the presence of Forskolin (15 μM) – this was done to find out whether cAMP elevation was required to enhance the neuritogenic effects of CNTF. Interestingly, the addition of CNTF (10 ng ml^{-1}, 50 ng ml^{-1} or 100 ng ml^{-1}) did not significantly augment neurite outgrowth measurements compared to treatment with Forskolin alone (this is discussed in section 4.4.1). In most cases there was no significant change in neurite number, irrespective of whether Forskolin (15 μM) was administered alone or in combination with CNTF. Minor toxicity was induced by 15 μM Forskolin when given in combination with 10 ng ml^{-1} and 50 ng ml^{-1} CNTF.

The optimised dose of 100 ng ml^{-1} CNTF was then tested in a Nogo-P4 neurite outgrowth inhibitory assay. Nogo-P4 was added to primary retinal cultures to inhibit RGC neurite outgrowth. Results show that CNTF (100 ng ml^{-1}) was capable of disinhibiting RGC neurite outgrowth when given in combination with Nogo-P4 (25 μM). In this experiment, treatment with 100 ng ml^{-1} CNTF alone did not significantly enhance RGC neurite outgrowth compared to the untreated control.

4.4 Discussion

4.4.1 Forskolin was effective at stimulating RGC neurite outgrowth when administered alone or in combination with a low dose of CNTF

Treatment with Forskolin (a cAMP elevator) alone significantly enhanced mean RGC neurite length and mean length of longest neurite compared to untreated controls. This was hardly surprising since cAMP elevation can stimulate RGC neurite outgrowth *in vitro* (Cai et al. 1999) and can promote RGC axon regeneration *in vivo* (Monsul, et al. 2004). A similar effect was observed when Forskolin was applied in combination with 10 ng ml^{-1} CNTF.

Interestingly, when 10 ng ml^{-1} CNTF was added alone the neuritogenic effects were attenuated. This phenomenon is consistent with previous studies that suggest treatment with low doses of CNTF (e.g. 10 ng ml^{-1}) is insufficient to promote significant RGC neurite outgrowth (Jo, et al. 1999).

Maximal effects in terms of mean neurite length and mean length of longest neurite were achieved using Forskolin alone or 100 ng ml^{-1} CNTF alone. Supplementation with Forskolin caused a modest increase in RGC mean neurite length and mean length of longest neurite — however, this effect decreased with higher concentrations of CNTF (50 ng ml^{-1}, 100 ng ml^{-1}).

This result may have been a consequence of CNTF receptor saturation and/or CNTF receptor down-regulation/desensitisation. It is well documented that prolonged exposure

to agonists can lead to receptor down-regulation. This is certainly true in the case of BDNF, where it has been demonstrated that continuous stimulation with recombinant protein leads to a reduction in TrkB protein and mRNA levels in rat hippocampal neurons (Frank, et al. 1996).

Furthermore, after ON injury RGC begin to lose their ability to respond to NTFs, presumably through the loss of their respective receptors and/or perturbation of protein trafficking. Like BDNF, a similar decline in responsiveness has been seen after CNTF administration and this decline has been associated with a reduction in CNTFRα expression (Miotke, et al. 2007). This is important since CNTFRα is a major component of the CNTF tripartite receptor complex. Likewise, it is possible that CNTFRα expression may be affected by retinal dissociation, since this process effectively disconnects RGC from their respective targets. However this seems unlikely since all RGCs were isolated using the same process, and were responsive to CNTF treatment when given at the correct dose (100 ng ml^{-1} CNTF).

Alternatively, a lower concentration of Forskolin may be required to optimally stimulate neurite outgrowth when high concentrations of CNTF are present. Whilst 15 μM Forskolin may be adequate to stimulate significant neurite outgrowth when supplied alone, it may be too high when given in combination with 50 ng ml^{-1} or 100 ng ml^{-1} CNTF. It is also possible that this dose of Forskolin (15 μM) saturated the system, preventing further neurite outgrowth from being achieved. Ideally I should have performed a Forskolin dose response experiment to determine whether this was case, and to find out whether 15 μM Forskolin was indeed the optimum concentration.

Since retinal cultures contain a variety of different cell types one must also consider the resident glial population. CNTF and/or Forskolin treatment may, to a greater or lesser extent, have an effect on this population. This effect may manifest itself through changes in metabolism, energy consumption, neurotrophic factor production or neurotrophic factor release (Park, et al. 2004). Any of which may directly or indirectly have an effect on RGC neurite outgrowth.

4.4.2 100 ng ml^{-1} CNTF significantly increased mean neurite length

Optimal neurite outgrowth was achieved when 100 ng ml^{-1} CNTF was added alone. This suggests that CNTF treatment is capable of stimulating neurite outgrowth without the need for exogenous cAMP elevation, a finding consistent with that of Müller *et al* (Müller et al. 2009). Treatment with 100 ng ml^{-1} CNTF was deemed to be optimal in terms of mean neurite length and mean length of longest neurite.

Interestingly Müller *et al* tested much higher doses of recombinant CNTF compared to those tested in chapter 4 (10 ng ml^{-1}, 50 ng ml^{-1} and 100 ng ml^{-1}). Müller *et al* found that a concentration of 10 ng ml^{-1} CNTF was sufficient to promote significant RGC neurite outgrowth (Müller et al. 2009). In contrast, no significant increase in RGC neurite outgrowth was documented at this concentration in figure 4.2. This outcome could have been due to differences in retinal cell preparation or plating density. The enhanced neuritogenic effects, seen at 10 ng ml^{-1} CNTF, could be explained by differences in glial number and/or contact dependent neurotrophic support.

Müller *et al* found optimum RGC neurite outgrowth was achieved at much higher concentrations of CNTF (200 ng ml^{-1} CNTF) (Müller et al. 2009) — this was exactly double the concentration of my optimum (100 ng ml^{-1}). It is possible that recombinant CNTF is much more effective at stimulating RGC neurite outgrowth at higher concentration (e.g. at 200 ng ml^{-1} CNTF). However, higher doses (e.g. concentrations >100 ng ml^{-1}) of CNTF would need to be tested to determine whether this was the case. Unfortunately direct comparisons in RGC neurite outgrowth could not be made at 100 ng ml^{-1} CNTF, since this concentration was not tested in the publication.

Interestingly, Müller *et al* used the same concentration of Forskolin (15 μM) to determine whether a rise in cAMP was required for CNTF to be effective at stimulating RGC neurite outgrowth (Müller et al. 2009). In agreement with my results, Forskolin (15 μM) was capable of stimulating significant RGC neurite outgrowth, when administered alone. However, it was not required for CNTF to promote significant neurite outgrowth *in vitro*.

In terms of RGC survival Forskolin groups could not be compared since survival data was not shown in this study (for these groups) and as a result it's impossible to tell whether the same levels of RGC toxicity were observed. The CNTF-alone groups can be compared and agree with my data (see figure 4.4), there was no significant change in RGC number after treatment with increasing doses of CNTF (without Forskolin) (Müller et al. 2009).

4.4.3 Treatment with Forskolin led a to a small reduction in RGC number

Cytotoxicity was seen after treatment with 15 µM Forskolin, compared to untreated controls. Similar levels of toxicity were observed when Forskolin was administered together with 10 ng ml^{-1} or 50 ng ml^{-1} CNTF. Since cell counts were not performed for other retinal cell populations, it is unclear as to whether Forskolin caused the death of any other cell types. As a result, it is difficult to establish whether RGC cell death was induced directly through exposure to Forskolin or indirectly — through the loss of glial cells (and contact dependent neurotrophic support). It is possible that Forskolin had an adverse effect on glial cell function and that this may have contributed to the cytotoxicity seen. There was no significant change in RGC cell number between the 100 ng ml^{-1} CNTF treatment group and untreated controls. 100 ng ml^{-1} CNTF was deemed to be optimal in terms of RGC neurite outgrowth and survival. As a result this dose was used in all future experiments.

4.4.4 CNTF and Forskolin had a minimal effect on mean neurite number

Treatment with CNTF and/or Forskolin had no significant effect on RGC neurite number compared to untreated controls. The CNTF plus Forskolin treated groups tended to have more neurites than their CNTF alone treated counterparts, although this did not reach statistical significance. It is important to note that this experiment had a relatively low n number ($n = 3$) and it is possible that this trend may have reached statistical significance with further repetition. In the visual system RGC typically possess a single long axon which

degenerates after ONC. Consequently neurite length and RGC number were considered to be a more important measure of axogenic and/or survival response.

4.4.5 25 µM Nogo-P4 peptide significantly inhibited RGC neurite outgrowth

Treatment of RGC with 25 µM recombinant Nogo-P4 peptide significantly inhibited neurite outgrowth whilst causing minimal toxicity. This factor was important as we needed to be able to differentiate between cells lacking neurites as a consequence of apoptosis/necrosis and those lacking neurites as a result of Nogo-P4 induced inhibition. A dose of 25 µM Nogo-P4 was selected based upon previous work from our laboratory (Morrison 2011). In his 2010 study, Dr Kevin Morrison found that doses higher than 25 µM caused similar levels of RGC neurite inhibition, but induced significant cell death (Morrison 2011). In a similar study (Wang & Zhu 2008), Wang *et al* used Nogo-P4 to inhibit neuronal stem cell differentiation. They found that a dose of 4 µM Nogo-P4 was sufficient to significantly inhibit neurite outgrowth, however, it is important to note that the cells under investigation were neural stem cells that may be more susceptible to Nogo-P4 treatment than mature RGC.

4.4.6 Treatment with 25 µM Nogo-P4 peptide had no impact on RGC survival

There was no statistically significant difference in RGC number after treatment with 25 µM Nogo-P4, a finding that is consistent with previous work (Morrison 2011). As this dose did not cause significant cell death it was concluded that the growth inhibition observed was due to growth cone collapse and not a consequence of RGC necrosis and/or apoptosis.

4.4.7 Treatment with 100 ng ml^{-1} CNTF disinhibited Nogo-P4 peptide treated RGC

Treatment with 100 ng ml^{-1} recombinant CNTF abolished the inhibitory effects of Nogo-P4 peptide and brought neurite measurements back in line with untreated controls. Interestingly 100 ng ml^{-1} CNTF did not significantly stimulate neurite outgrowth above that of untreated controls. It is possible that significance may be achieved with further repetition since this experiment has a relatively low n number ($n = 3$).

4.5 Conclusions

The purpose of this chapter was to investigate the neuritogenic and/or neuroprotective effects of CNTF *in vitro*. To this end, a dose response experiment was performed to determine the optimum CNTF dose. A concentration of 100 ng ml^{-1} CNTF was deemed to be optimal since it significantly enhanced neurite outgrowth compared to other CNTF con-

centrations tested. Upon finding an appropriate concentration, the disinhibitory properties of CNTF could then be investigated. To accomplish this, Nogo-P4 peptide was used to inhibit RGC neurite outgrowth. Results show that Nogo-P4 peptide reproducibly inhibited RGC neurite outgrowth, this result was consistent with previous findings from our lab (Morrison 2011). The use of such an inhibitory assay has many applications and could be used to test a host of potential therapeutics *in vitro*. CNTF (100 ng ml^{-1}) was capable of enhancing RGC neurite outgrowth when administered alone (in some circumstances), but had a disinhibitory effect when given in combination with Nogo-P4 peptide. Forskolin significantly enhanced RGC neurite outgrowth when given alone or in combination with a low dose of CNTF, however it was not required to potentiate the neuritogenic effects of CNTF.

CHAPTER 5

AAV2 AS A VECTOR FOR DELIVERING CNTF TO THE VISUAL SYSTEM

5.1 Introduction

In the previous chapter it was established that recombinant CNTF could be used to disinhibit neurite outgrowth in Nogo-P4 treated primary RGC. It was also shown that 100 ng ml^{-1} CNTF could significantly enhance RGC neurite outgrowth in a dose response experiment.

Having established the effectiveness of recombinant CNTF *in vitro*, the next step would be to develop and test a viral vector CNTF gene delivery system. To accomplish this *AAV2-CNTF-hrGFP* constructs were provided by Dr. Michael Douglas (Molecular Neuroscience Group, University of Birmingham) to be used in a series of transfection experiments. As CNTF does not have a classical secretory sequence the CNTF transgene was modified to include the first 20 amino acids of the rat ppNGF. This region of the NGF gene contains a classical secretion sequence, allowing CNTF to be released from HEK-293 cells after transfection. CNTF ELISAs could then be performed on HEK-293 conditioned media to determine whether the constructs produce CNTF. It was decided to include a FLAG-tagged construct as it would allow discrimination between CNTF transgene products and endogenous CNTF levels *in vivo* (since the transgene was designed using a rat CNTF sequence). Secondly, the presence of a FLAG-tag would facilitate any purification attempts. The final CNTF construct included an shRNA to knockdown RhoA and silence the growth inhibitory signalling cascade (for details on RNAi see section 1.16). The aim of this was to launch a two pronged attack on RGC axons — driving growth through the secretion of CNTF whilst preventing growth cone collapse through the knockdown of RhoA.

The main objective of this chapter was to test each AAV2 virus *in vivo* and to determine whether *AAV2-CNTF-hrGFP* and *AAV2-CNTF-shRhoA-hrGFP* could promote RGC axonal re-generation and survival.

5.1.1 Barriers to AAV2 transduction

Targeting recombinant AAV2 can be difficult when the route of delivery is impeded by the presence of other structures.

This was clearly demonstrated by Dalkara *et al*, who identified the ILM as an important barrier of AAV retinal transduction after intravitreal injection. In 2009 a series of AAV targeting experiments were performed to identify any potential barriers and to improve AAV transduction efficiency (Dalkara, et al. 2009). To accomplish this, they injected Cy3-labelled AAV particles (Cy3-labelled AAV1, AAV2, AAV5, AAV8 and AAV9) into the vitreous of the eye and found that some of these serotypes accumulated at the ILM. Accumulation of AAV particles seemed to be serotype specific, with AAV2 and 9 showing the greatest level of accumulation in this region. In contrast accumulation at the ILM was not readily apparent after intravitreal injection of AAV1-Cy3 and AAV5-Cy3. Accumulation of AAV2 particles are shown in figure 5.1.

To overcome this barrier Dalkara *et al* used Pronase-E (a non-specific protease) to punch holes in the ILM (as shown in figure 5.2) and to increase AAV2 transduction efficiency. Laminin immunostaining was performed to identify the ILM and to monitor its' structural integrity. Pronase-E disintegration of the ILM was clearly apparent (see above). At high concentrations (0.01%) Pronase-E treatment perturbed normal retinal function (Dalkara

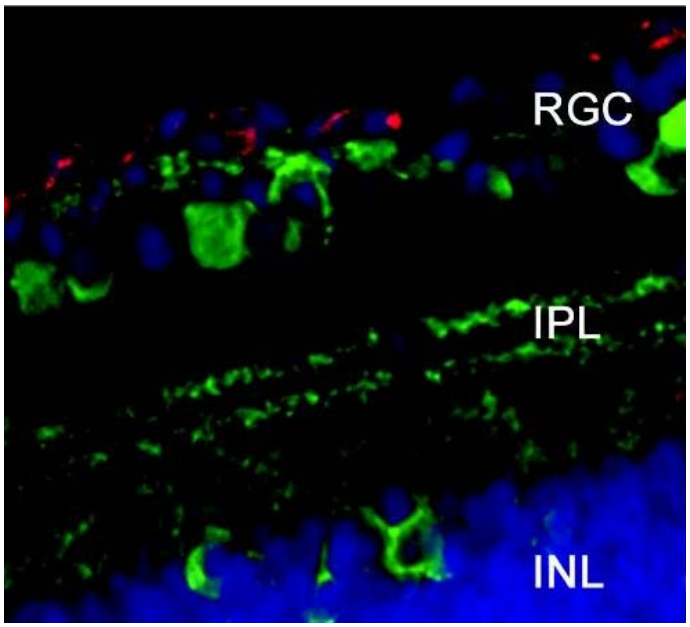

Figure 5.1: Localisation of Cy3-labelled AAV2 particles at the ILM of the retina. Dalkara *et al* injected Cy3-labelled AAV2 particles (2×10^{12} vg/µl to 5×10^{12} vg/µl) into the vitreous of Sprague Dawley rats. Animals were sacrificed 3 weeks later and frozen retinal sections were examined to determine AAV2 localisation. Clear accumulation of Cy3-labelled AAV2 (shown in red) was readily apparent at the vitreoretinal junction of the eye. Retinal neurons were visualised using a Calbindin antibody (shown in green) and cell nuclei were labelled with DAPI (blue). Figure reproduced from (Dalkara et al. 2009).

et al. 2009). A concentration of 0.0002% Pronase-E was found to be optimal as it increased AAV2 transduction efficiency whilst retaining normal retinal function.

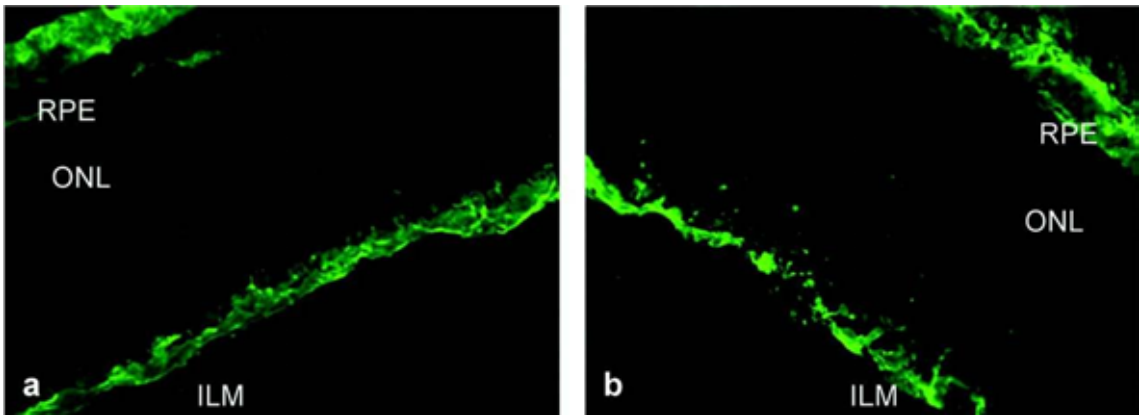

Figure 5.2: Pronase-E punches holes in the ILM of the retina. The ILM was visualised using an anti-laminin antibody (shown in green). **(a.)** Uninjured / untreated control, ILM can be seen to be intact **(b.)** after intravitreal injection of Pronase-E holes can be seen in the ILM. Figure reproduced from (Dalkara et al. 2009).

As a result it was decided to test whether *AAV2-eGFP* transduction efficiency could be improved by partially digesting the inner limiting membrane using Pronase-E at a concentration of 0.0002%.

Another potential barrier to viral transduction is the vitreous body – a transparent gel which occupies the posterior compartment of the eye and is located between the lens and the retina. Although the vitreous is primarily composed of water (99%) (Forrester, et al. 2002), it is also occupied by macromolecules (0.1%) such as collagen, hyaluronic acid and CSPGs, with salts (0.9%) making up the remaining element of the intravitreal environment (Forrester et al. 2002). Collagen (predominantly type-II) forms a complex network of fibrils (10 nm to 20 nm) and gives the vitreous body its characteristic gelatinous properties (Forrester et al. 2002). This collagen meshwork is surrounded by hyaluronic acid which can hinder (to a greater or lesser extent) the diffusion of substances throughout

the vitreous (Forrester et al. 2002). This largely depends on the size (which can vary) and the properties of the GAG (Forrester et al. 2002). The vitreous also contains a second type of collagen, type IX, which contains three collagenous and four non-collagenous domains. As a result of this it can interact with hyaluronic acid and collagen fibrils to provide structural support (Forrester et al. 2002). Since collagen is highly hydrophobic in nature these collagen fibres continually associate and dissociate to form protein aggregates (Bos, et al. 2001). Therefore, the structural makeup of the vitreous is constantly changing and this may also be a major impediment to AAV2 transduction. It is possible that this network of collagen fibres may entrap the AAV2 virus and prevent its diffusion and subsequent infection of RGC, as a result it is possible that partial digestion of these proteins might also aid AAV2 transduction.

The use of proteolytic enzymes to permeabilise the ILM may seem like an extreme course of action, considering that the intention is to eventually develop a therapeutic. Although the ILM is essential during development (Halfter 1998, Semina, et al. 2006), it is not needed during adulthood and is often removed by ophthalmic surgeons during macular hole surgery (Dalkara et al. 2009, Mester & Kuhn 2000). Since this procedure is unfeasible in rodents, proteolytic digestion may serve as an appropriate alternative and form the basis for a proof of concept experiment. Due to time constraints I was unable to optimise the dose of Pronase-E and so it was decided to use the dose which was optimised by Dalkara *et al* (Dalkara et al. 2009).

5.2 Hypothesis

1. Intravitreal delivery of *AAV2-CNTF-hrGFP* and *AAV2-CNTF-shRhoA-hrGFP* will promote increased RGC survival and axonal regeneration after ONC.

2. Co-administration with Pronase-E will enhance AAV2 transduction efficiency.

5.3 Aims

1. To promote RGC axonal regeneration and survival through the delivery of *AAV2-CNTF-hrGFP* and *AAV2-CNTF-shRhoA-hrGFP*

2. Determine whether co-injection with 0.0002% Pronase-E can increase *AAV2-eGFP* transfection efficiency.

5.4 Results

5.4.1 Design and validation of shRhoA containing constructs

The biological activities of shRNA containing constructs were designed and validated by Dr. Mike Douglas. As well as providing the shRhoA sequence present within the *AAV2-CNTF-shRhoA-hrGFP* plasmid, Dr. Douglas also designed the primers required to determine the orientation of the shRhoA insert. To establish biological activity, Dr. Douglas performed a series of COS-1 cell transfection experiments. Plasmids containing shRhoA

or shGFP were transfected into COS-1 cells that overexpressed rat RhoA. The effectiveness of RhoA gene knockdown was compared against two additional shRhoA sequences (see figure 5.3) – the first of which was designed by Ahmed *et al* (Ahmed, et al. 2005b) and the second by Pillé *et al* (Pillé, et al. 2005). At an appropriate time point, cell lysates were collected and analysed by Western Blotting. The sequence designed by Dr. Douglas showed the greatest level of RhoA gene knockdown and was used in the final construct.

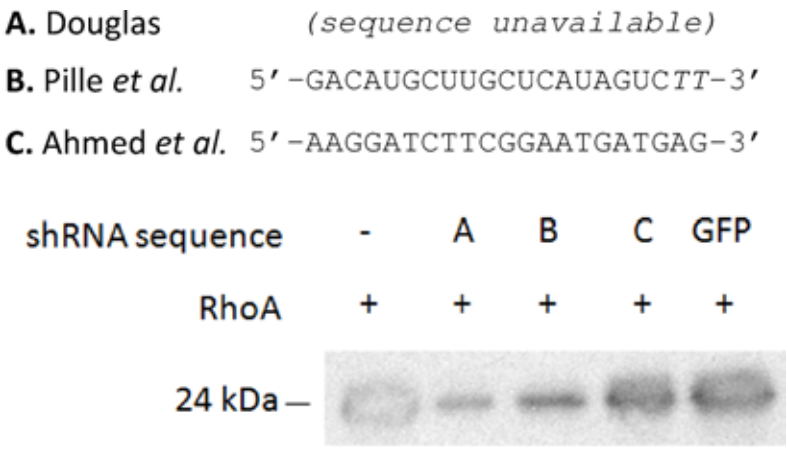

Figure 5.3: Design and validation of shRhoA containing constructs. shRhoA containing constructs were desiged and validated by Dr. Mike Douglas. The effectiveness of RhoA gene knowndown was compared against two previously published sequences, (**B.**) Pillé *et al* and (**C.**) Ahmed *et al*. The sequence designed by Dr. Douglas (**A.**) (sequence unavailable) showed the greatest level of gene knockdown and was used in the final AAV2 construct.

5.4.2 HEK-293 cells transfected with *AAV2-CNTF-hrGFP*, *AAV2-CNTF-shRhoA-hrGFP* and *AAV2-CNTF-FLAG* produced detectable levels of CNTF

An ELISA was performed to determine whether *AAV2-CNTF-hrGFP*, *AAV2-CNTF-shRhoA-hrGFP* or *AAV2-CNTF-FLAG* constructs could produce detectable levels of CNTF 5 d after transfection. Since all CNTF constructs possessed a GFP reporter, transfection efficiencies could be monitored through the use of fluorescence microscopy. Conditioned media

was also collected from untransfected (negative control), lipofectamine treated (reagent control) and *AAV2-eGFP* transfected (transfection control) HEK-293 cells. CNTF was detected in conditioned media obtained from the *AAV2-CNTF-hrGFP*, *AAV2-CNTF-shRhoA-hrGFP* and *AAV2-CNTF-FLAG* transfection groups — although the concentration of CNTF produced varied considerably between each of the treatment groups. The concentration of CNTF in the *AAV2-CNTF-hrGFP* treatment group was approximately 5x the concentration of CNTF in the *AAV2-CNTF-shRhoA-hrGFP* and *AAV2-CNTF-FLAG* groups. As expected, CNTF was not detected in any of the control groups.

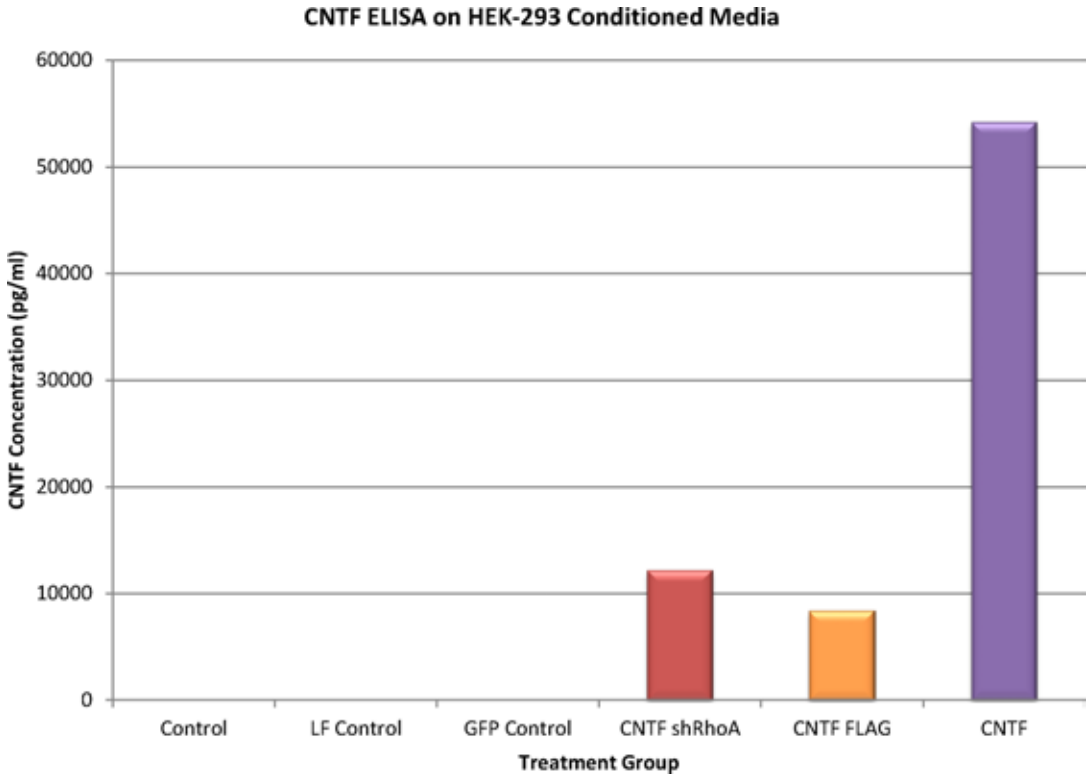

Figure 5.4: CNTF ELISA on HEK-293 Conditioned Media. *AAV2-CNTF-hrGFP*, *AAV2-CNTF-shRhoA-hrGFP* and *CNTF-FLAG* constructs produce biologically relevant levels of CNTF 7 d after transfection. The *AAV2-CNTF-hrGFP* construct produced more CNTF than *AAV2-CNTF-FLAG* or *AAV2-CNTF-shRhoA-hrGFP*, this may have been due to increased toxicity or the presence of the FLAG-tag interfering with secretion.

5.4.3 Co-injection with 0.0002% Pronase-E significantly enhanced *AAV2-eGFP* transduction, but caused some cell death

Co-administration with 0.0002% Pronase-E significantly enhanced RGC GFP transduction compared to *AAV2-eGFP* (1×10^{11} vg/10µl) alone in retinal wholemount preparations 30 d after intravitreal injection (as in section 2.2.6, see figure 5.5). When *AAV2-eGFP* was administered alone 17% of the RGC population was GFP positive, however when delivered in combination with 0.0002% Pronase-E, 52% of the surviving RGC population was GFP positive. Treatment with 0.0002% Pronase-E caused a significant reduction (18%, 192.3 RGC/mm^2 ± 26 RGC/mm^2) in total RGC number. Furthermore GFP expression was significantly weaker in the *AAV2-eGFP* alone treatment group compared to the *AAV2-eGFP* + Pronase-E treatment group (see figure 5.5).

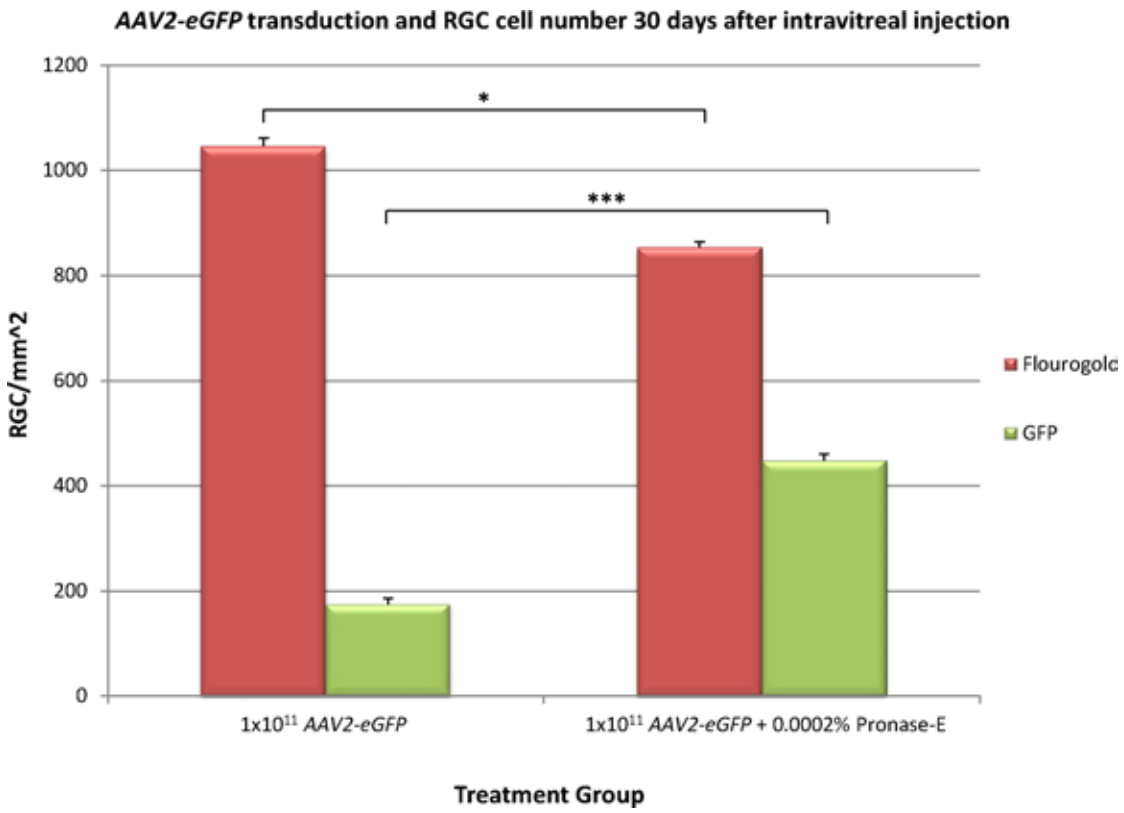

Figure 5.5: AAV2-eGFP transduction. Quantification of RGC survival and GFP transduction 30 d after 1×10^{11} vg/10µl *AAV2-eGFP* intravitreal injection. Co-injection with 0.0002% Pronase-E significantly enhanced RGC GFP transduction in retinal wholemount preparations. However, there was a significant reduction in the number of FG positive RGC. The results represent RGC counts from 3 eyes ± SEM. *p ≤ 0.05, ***p ≤ 0.001. Statistical test = one-way ANOVA.

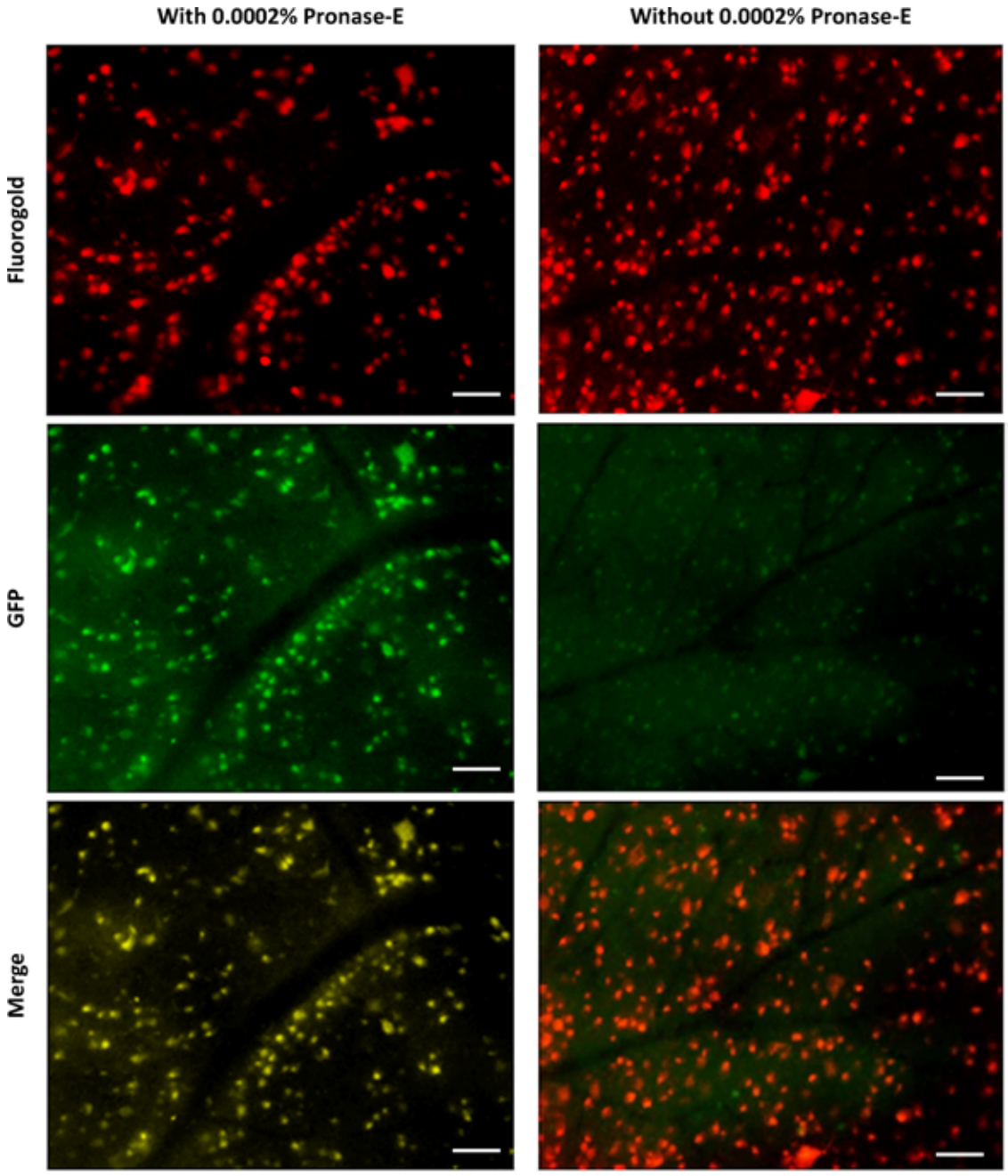

Figure 5.6: AAV2-eGFP transduction representative wholemount images. Representative images of FG-traced (red) and GFP transduced (green) RGC in retinal wholemount preparations (30 days after 1×10^{11} vg/10µl *AAV2-eGFP* intravitreal injection). FG was colourised red so that RGC co-localisation (yellow) could be visualised. Scale bar = 50 µm.

5.4.4 RGC survival was not enhanced by *AAV2-CNTF-hrGFP* + Pronase-E or *AAV2-CNTF-shRhoA-hrGFP* + Pronase-E treatment

Sprague Dawley rats received an intravitreal injection of AAV2 virus 30 d prior to receiving an ONC injury. RGC counts obtained from H&E stained frozen retinal sections 23 d post ONC (see section 2.1.4 for details) demonstrates that all AAV2 treatment groups (1×10^{11} vg/10µl (*AAV2-eGFP* + Pronase-E, *AAV2-CNTF-hrGFP* + Pronase-E and *AAV2-CNTF-shRhoA-hrGFP* + Pronase-E) induced significant (***$p \leq 0.001$) RGC cell death, causing ≈40% reduction in RGC cell number compared to the uninjured/uninjected control group (see figure 5.7). RGC cell loss was accompanied by thinning of the IPL and OPL, this was particularly evident in *AAV2-eGFP* injected animals (see figure 5.8). There was no significant change in mean RGC number between all AAV2 treatment groups. As expected uninjured control retinal sections retained a normal morphological appearance.

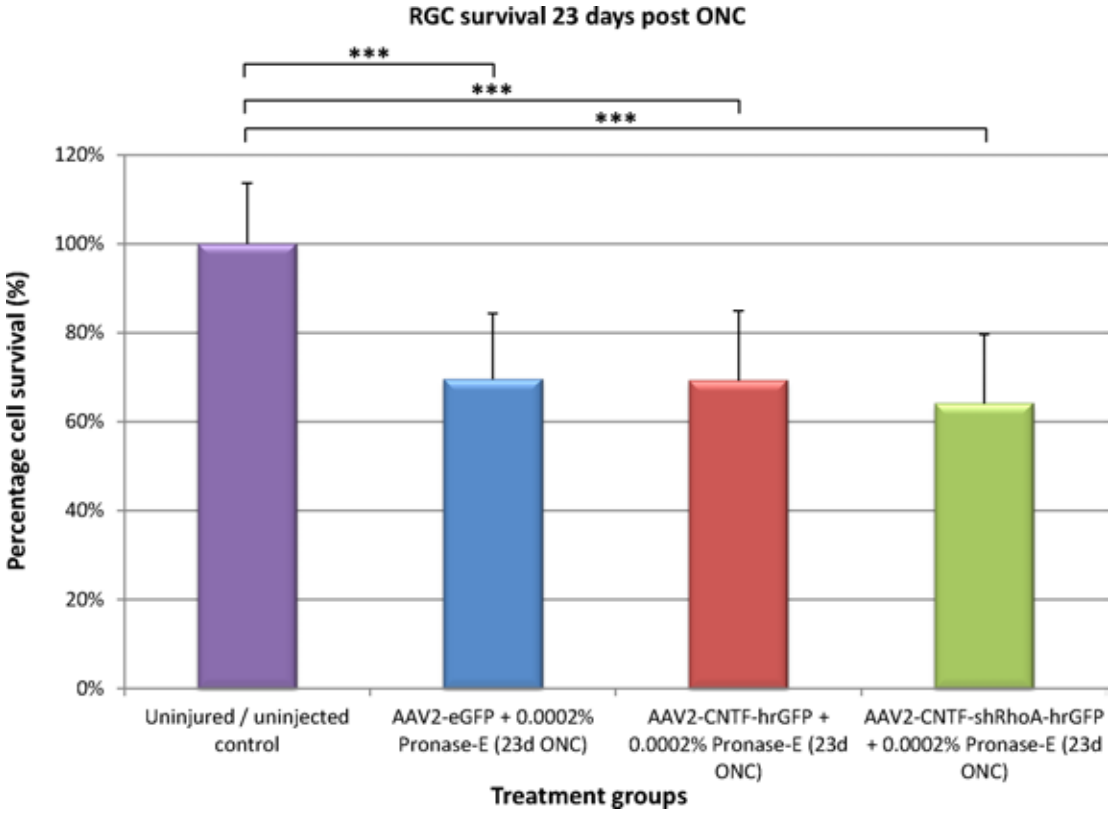

Figure 5.7: RGC Survival was not enhanced by *AAV2-CNTF-hrGFP* or *AAV2-CNTF-sRhoA* Treatment. There was no significant difference in RGC survival between each of the AAV2 treatment groups, however there was a ≈40% reduction in RGC cell number compared to uninjured controls. The results represent RGC counts from 3 eyes ± SEM. ***p ≤ 0.001. Statistical test = one-way ANOVA.

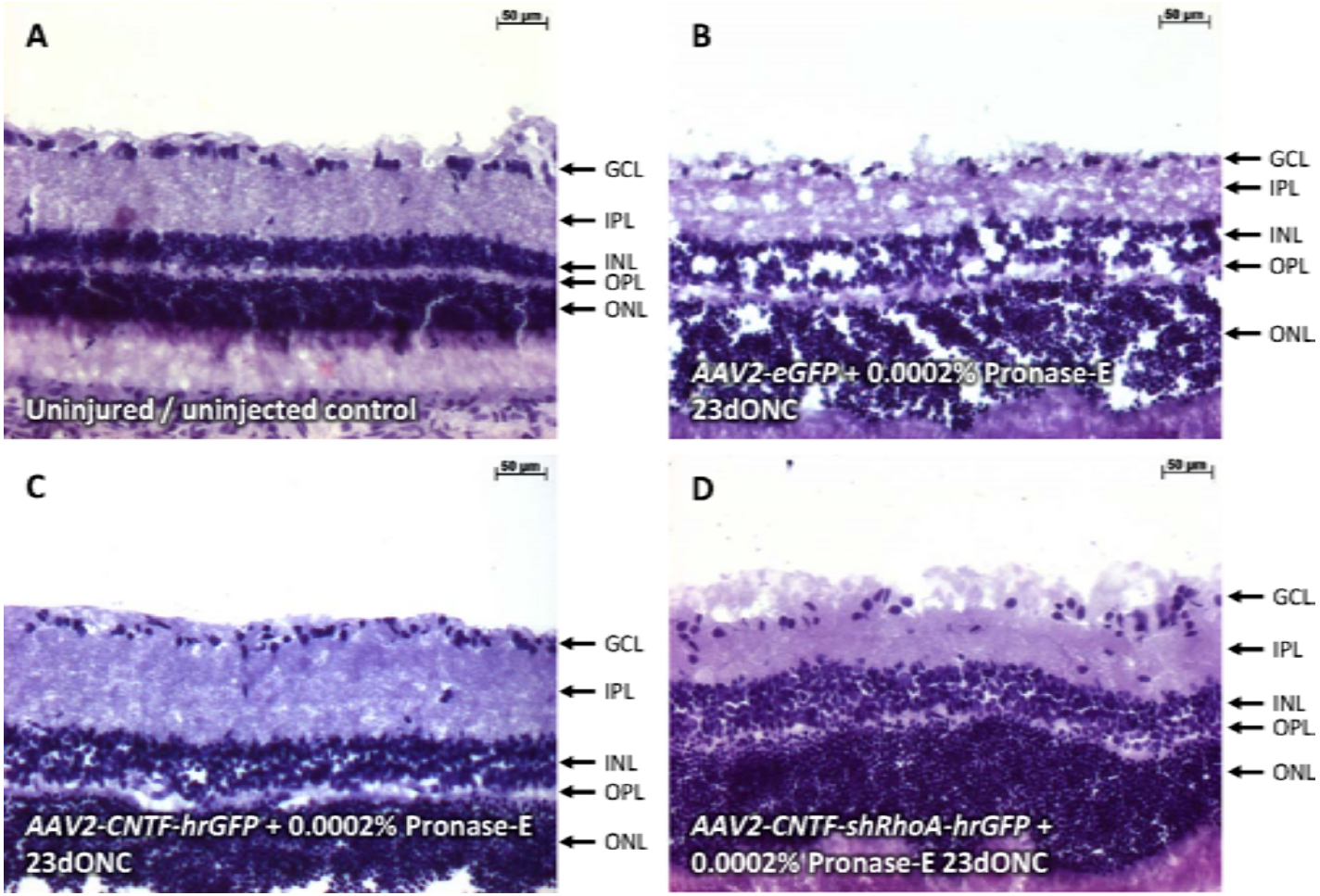

Figure 5.8: Representative images of H&E stained retinal sections. Animals received an injection of AAV2 viruses (*AAV2-eGFP*, *AAV2-CNTF-hrGFP* or *AAV2-CNTF-shRhoA-hrGFP*) 30 d prior to an ON crush injury and were then sacrificed 23 d later. Retinal sections were H&E stained to visualise the all layers of the retina. A reduction of RGC cell number was evident in the GCL 23 d after ONC injury (see figure 5.7). This reduction in RGC cell number was accompanied by thinning of the IPL and OPL, this was particularly evident in the *AAV2-eGFP* (B) treated control, indicating a loss of axonal fibres. Cell loss was also visually apparent in the INL and ONL of the *AAV2-eGFP* treated control group. Scale bar = 50 µm.

5.4.5 *AAV2-CNTF-hrGFP* and *CNTF-shRhoA* did not promote extensive RGC axonal regeneration

Intravitreal injection of *AAV2-CNTF-hrGFP* (1×10^{11} vg/10µl) + 0.0002% Pronase-E or *AAV2-CNTF-shRhoA-hrGFP* (1×10^{11} vg/10µl) + 0.0002% Pronase-E 30 d before ONC failed to promote significant axon regeneration (animals were sacrificed 23 d after ONC injury) when compared to the control (*AAV2-eGFP* + 0.0002% Pronase-E).

Although GAP-43 positive axons (shown in figure 5.11B and 5.12B) entered the crush site (*) in both cases, very few entered the distal stump (D) of the ON (see figures 5.9, 5.11 and 5.12). RGC axons were found, for both treatment groups, to not regenerate beyond 1200 µm (hence why quantification stops at 1200 µm).

A significant difference in the mean number of RGC axons was found at 400 µm for animals treated with *AAV2-CNTF-hrGFP* + 0.0002% Pronase-E when compared to the control (*AAV2-eGFP* + 0.0002% Pronase-E). The mean number of RGC axons was found to be significantly fewer, see figure 5.9 for quantification. There was no significant difference in mean number of RGC axons at all other distances (100 µm, 200 µm, 800 µm and 1200 µm).

When *AAV2-CNTF-shRhoA* + 0.0002% Pronase-E was compared to the control significantly fewer RGC axons (mean of directly counted RGC axons across 3 sections per ON and 3 ON per treatment group) were found at 200 µm from the crush site. There was no significant difference in mean number of RGC axons at all other distances (100 µm, 400 µm, 800 µm and 1200 µm).

Interestingly no GFP was seen in any of the sections (despite the use of polyclonal antibodies to amplify the signal), as a result the lack of regeneration (see figures 5.9, 5.10, 5.11 and 5.12) or survival (see figures 5.7 and 5.8) may have been a consequence of ineffective viral transduction.

AAV2-CNTF-hrGFP + Pronase-E and *AAV2-CNTF-shRhoA-hrGFP* + Pronase-E did not promote extensive RGC axonal regeneration 23 d after ONC (see figure 5.12). Although GAP-43 positive axons entered the crush site (*), very few entered the distal stump (D). From the examples in figure 5.11, it appears that there are more GAP-43 positive axons in the proximal stump compared to the negative control (*AAV2-eGFP* + Pronase-E), suggesting that *AAV2-CNTF-hrGFP* + Pronase-E and *AAV2-CNTF-shRhoA-hrGFP* + Pronase-E could be neuroprotective. This is clearly not the case, since there was no significant difference between RGC number in H&E stained retinal sections (see section 5.4.4). Interestingly no GFP was seen in any of the sections, as a result the lack of regeneration (see figures 5.10, 5.11 and 5.12) or survival (see figure 5.7) may have been a consequence of ineffective viral transduction.

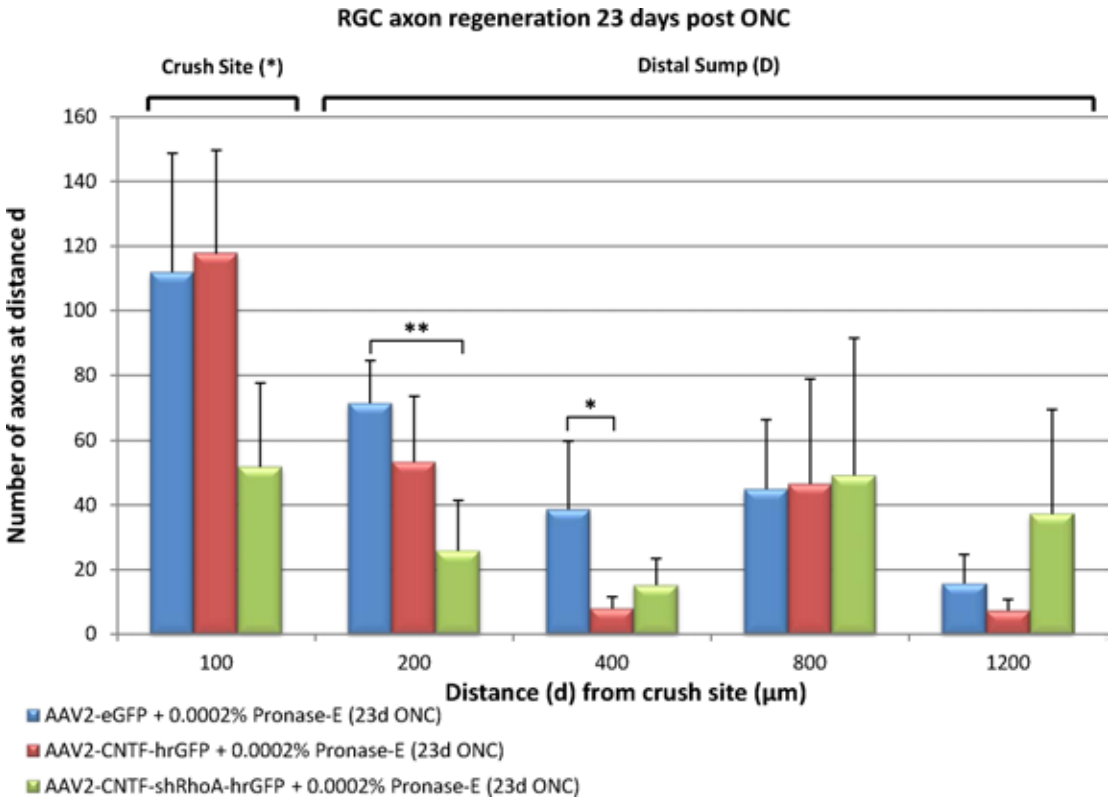

Figure 5.9: Quantification of RGC axon regeneration. Animals received an intravitreal injection of *AAV2-eGFP* + 0.0002% Pronase-E, *AAV2-CNTF-hrGFP* + 0.0002% Pronase-E or *AAV2-CNTF-shRhoA-hrGFP* + 0.0002% Pronase-E; after 30 d the animals were given an ON crush injury and after a further 23 d the animals were sacrificed. Intravitreal injection of *AAV2-CNTF-hrGFP* (1×10^{11} vg/10µl) + 0.0002% Pronase-E or *AAV2-CNTF-shRhoA-hrGFP* (1×10^{11} vg/10µl) + 0.0002% Pronase-E failed to promote significant axon regeneration when compared to the control (*AAV2-eGFP* + 0.0002% Pronase-E). RGC axons were found to not regenerate beyond 1200 µm from the centre of the crush site.

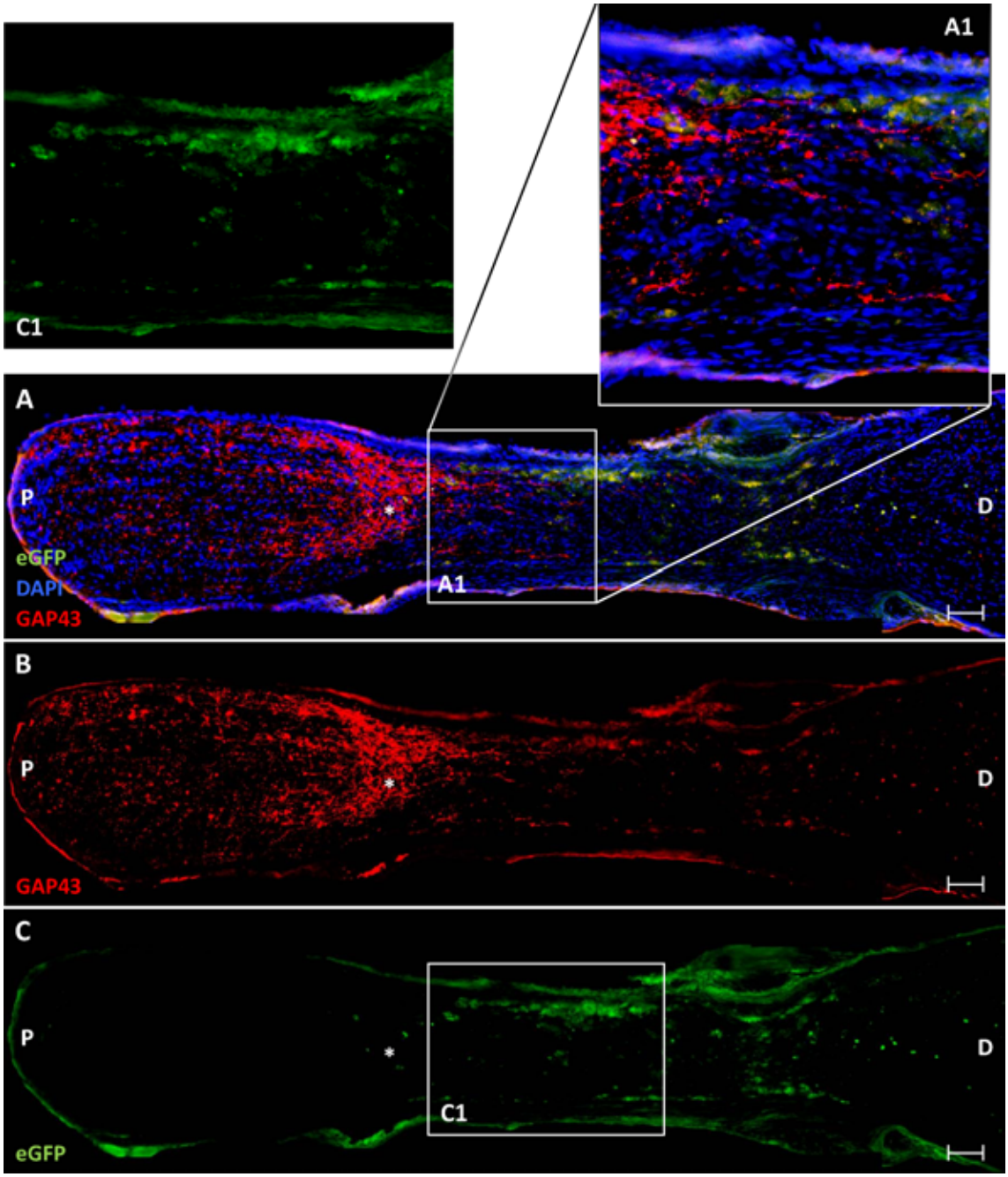

Figure 5.10: Intravitreal injection of *AAV2-eGFP* + 0.0002% Pronase-E did not promote RGC axon regeneration 23 d post-ONC. Although GAP-43 positive (shown in red) axons (see B) entered the crush site (*) very few entered the distal stump (D) of the ON (see A1). **(A.)** Merged image showing GAP-43 (red), eGFP (green) and DAPI (blue) staining. **(A1.)** A magnified section of A showing some GAP-43 positive axons cross the crush site and enter the distal stump of the injured ON. **(B.)** Image showing GAP-43 stained RGC axons only. **(C.)** eGFP immunostaining was not readily apparent, however autofluorescent macrophages (or eGFP positive debris) can be seen **(C1.)** shows a magnified section of C. P = proximal site, * = crush site, D = distal stump. Scale bar = 100 µm

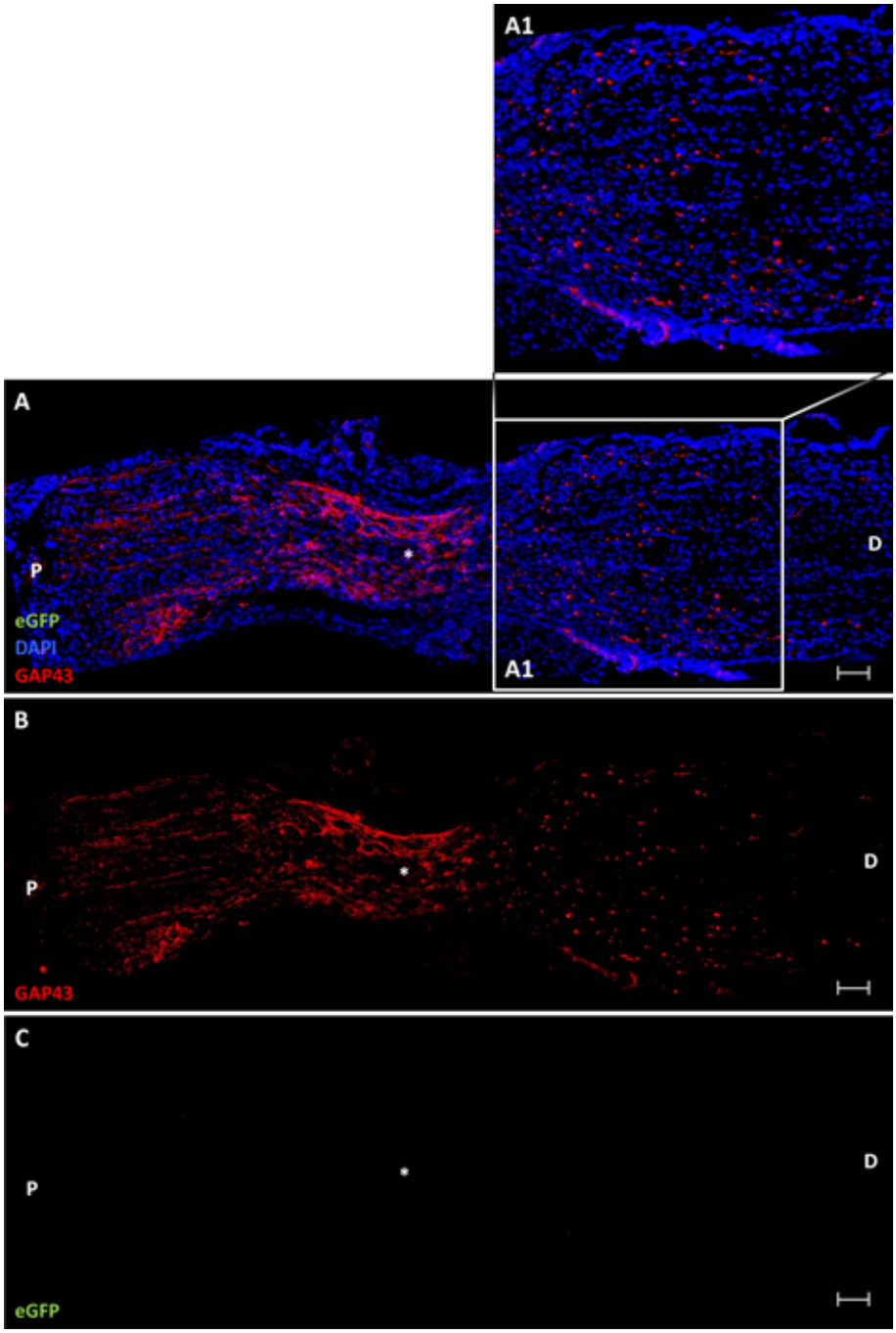

Figure 5.11: Intravitreal injection of *AAV2-CNTF* + 0.0002% Pronase-E did not promote RGC axon regeneration 23 d post-ONC. GAP-43 positive axons (shown in red) are seen to enter the crush site (*), however very few enter the distal stump (D) - as can be seen in the magnified image A1. **(A.)** Merged image showing GAP-43 (red), eGFP (green) and DAPI (blue) staining. **(A1.)** A magnified section of A showing some GAP-43 positive axons cross the crush site and enter the distal stump of the injured ON. **(B.)** Image showing GAP-43 stained RGC axons only. **(C.)** eGFP immunostaining was not readily apparent. P = proximal site, * = crush site, D = distal stump. Scale bar = 100 µm

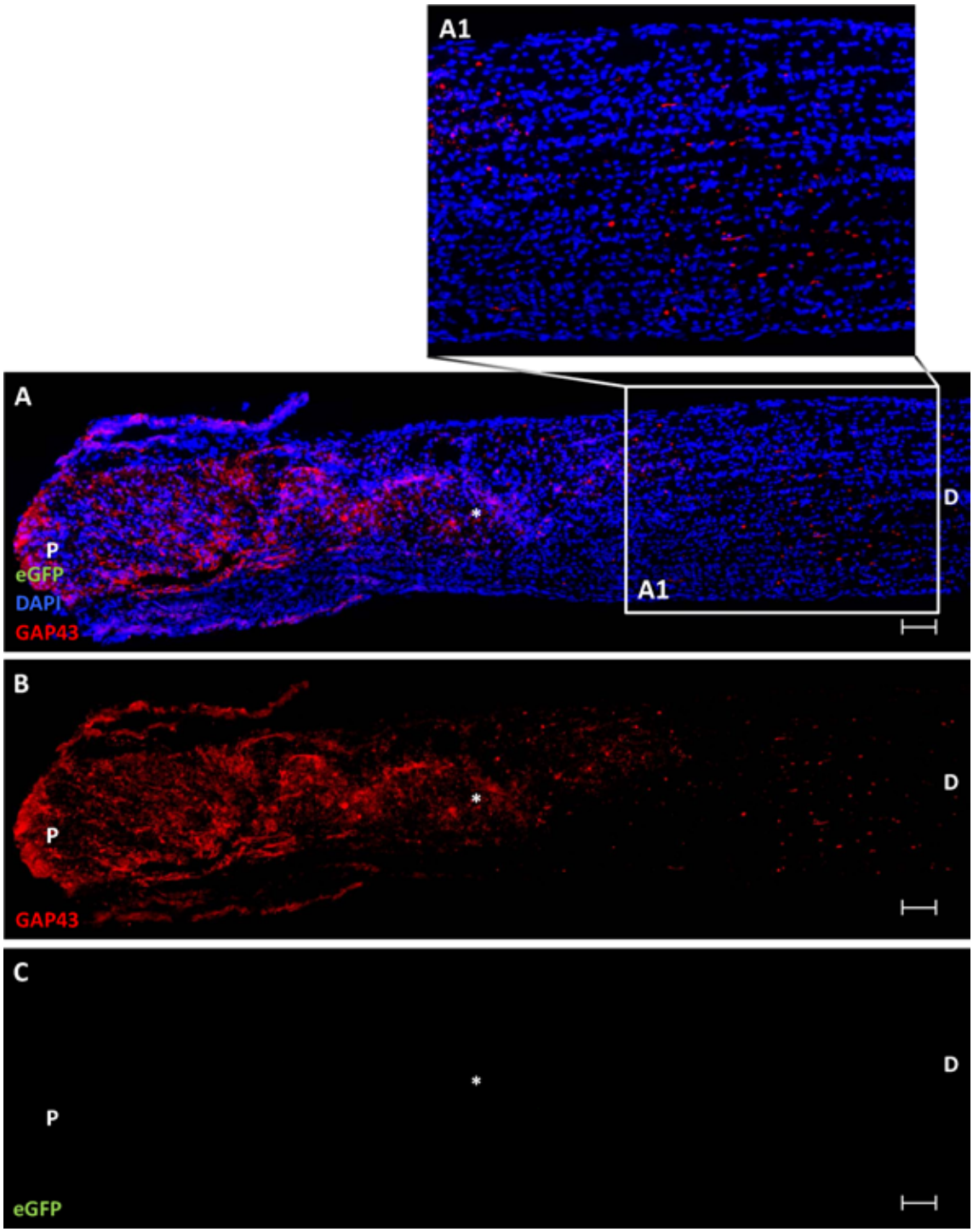

Figure 5.12: Intravitreal injection of *AAV2-CNTF-shRhoA* + 0.0002% Pronase-E did not promote RGC axon regeneration 23 d post-ONC. A shows that although GAP-43 positive axons (red) entered the crush site (*), very few entered the distal stump (D). **(A.)** Merged image showing GAP-43 (red), eGFP (green) and DAPI (blue) staining. **(A1.)** A magnified section of A showing some GAP-43 positive axons cross the crush site and enter the distal stump of the injured ON. **(B.)** Image showing GAP-43 stained RGC axons only. **(C.)** eGFP immunostaining was not readily apparent. P = proximal site, * = crush site, D = distal stump. Scale bar = 100 µm

5.5 Discussion

5.5.1 Conditioned media collected from *AAV2-CNTF-hrGFP*, *AAV2-CNTF-shRhoA-hrGFP* and *AAV2-CNTF-FLAG* transfected HEK-293 cells contained detectable levels of CNTF

Conditioned media was collected from *AAV2-CNTF-hrGFP*, *AAV2-CNTF-shRhoA-hrGFP* and *AAV2-CNTF-FLAG* transfected HEK-293 cells. CNTF ELISAs were performed to determine whether each of the CNTF constructs produced detectable levels of CNTF. Interestingly CNTF levels in the *AAV2-CNTF-shRhoA-hrGFP* and *AAV2-CNTF-FLAG* groups were lower than that of *AAV2-CNTF-hrGFP* alone. Cytotoxicity was apparent in the *AAV2-CNTF-shRhoA-hrGFP* transfected cells, this may have also led to a decrease in CNTF secretion.

5.5.2 *AAV2-eGFP* + Pronase-E significantly enhanced *AAV2-eGFP* transduction

Co-administration with 0.0002% Pronase-E significantly enhanced RGC GFP transduction compared to *AAV2-eGFP* alone in retinal wholemount preparations (see figure 5.5). When *AAV2-eGFP* was administered alone 17% of the RGC population was GFP positive, however, when delivered in combination with 0.0002% Pronase-E 52% of the surviving RGC population was GFP positive. This was probably a direct consequence of digestion of the inner-limiting membrane as in (Dalkara et al. 2009) or due to the degradation or damage of AAV2 receptors laminin or HSPG receptors. It is also possible that the presence

of Pronase-E made the vitreous more permissible, as previously discussed (see section 5.1.1).

5.5.3 *AAV2-eGFP* + Pronase-E significantly reduced RGC number in retinal wholemount preparations

Treatment with 0.0002% Pronase-E caused a significant reduction (18%, 192.3 RGC/mm^2 ± 26 RGC/mm^2) in total RGC number. Furthermore GFP expression was significantly weaker in the *AAV2-eGFP* alone treatment group compared to the *AAV2-eGFP* + Pronase-E treatment group (see figure 5.6). It is possible that the toxicity observed in figure 5.5 was a direct consequence of GFP expression. Several studies (Klein, et al. 2006) have shown a positive correlation between GFP expression and cell death. For example, Klein *et al* has demonstrated that neuronal death in the substantia nigra after AAV8 injection was a direct consequence of GFP expression (Klein et al. 2006). Cell death was attributed to GFP expression, since injection of the AAV8 vector alone (absent the GFP reporter) did not induce cell death (Klein et al. 2006). Moreover, toxicity was ameliorated by a reduction in viral titre, presumably as a consequence of reduced infectivity (Klein et al. 2006). Furthermore, GFP toxicity has also been reported in primary neuronal cultures (Detrait, et al. 2002, Krestel, et al. 2004) and a variety of cell lines (Liu, et al. 1999). Although the mechanism through which GFP causes cell death remains unclear, several proposals have been made: It is possible that GFP affects normal cell functioning through the perturbation of polyubiquitination (Baens, et al. 2006). This post-translational modification is particularly important in modulating p53 tumour suppressor activity as well as other

important signalling events (e.g. NF-κB and JNK signalling) (Baens et al. 2006). Another possibility is that GFP accumulates and prevents retrograde and anterograde transport of essential proteins and nutrients. Furthermore it has been documented that continual stimulation of eGFP can cause cell death through the production of free radicals (cited in (Liu et al. 1999)).

Another potential explanation is that the high viral titre of the *AAV2-eGFP* virus (1×10^{11} vg/10µl) induced RGC cell death. To establish this it would be necessary to perform a dose response experiment. Furthermore it would also be necessary to test different doses of virus using AAV2 vector alone (absent GFP transgene) — this would allow me to differentiate between toxicity induced by viral dose and toxicity induced by eGFP expression. Since an untreated control group wasn't present in the retinal wholemount survival counts I was unable to ascertain whether a dose of 1×10^{11} *AAV2-eGFP* virus caused toxicity.

Perhaps one of the more obvious explanations is that Pronase-E directly caused the death of retinal RGC through protein degradation. To determine whether this was case, a Pronase-E dose response experiment could be performed. Although Dalkara *et al* (Dalkara et al. 2009) reported that 0.0002% Pronase-E did not cause RGC cell death, independent confirmation of this would need to be performed.

Due to time constraints the *AAV2-eGFP* transduction experiments and ON crush experiments were run in parallel. As a result, it was decided to co-inject 0.0002% Pronase-E with each of the AAV2 treatment groups (i.e. *AAV2-eGFP*, *AAV2-CNTF-hrGFP* and *AAV2-CNTF-shRhoA-hrGFP*).

5.5.4 *AAV2-CNTF-hrGFP* and *AAV2-CNTF-shRhoA-hrGFP* did not promote extensive axonal regeneration

AAV2-CNTF-hrGFP and *AAV2-CNTF-shRhoA-hrGFP* did not promote extensive axonal regeneration 23 d post ONC (see figures 5.11 and 5.12). Although quite a few GAP-43 positive axons (red) were present in the proximal stump (of *AAV2-CNTF-hrGFP* and *AAV2-CNTF-shRhoA-hrGFP* injected animals, see figures 5.11 and 5.12), very few axons traversed the crush site and entered the distal stump. Due to the low n number ($n = 1$) RGC axonal regeneration was not quantified.

Interestingly no GFP was seen in any of the ON sections, this may have been due to a number of reasons. It is possible that AAV2 had difficulty reaching the target cell despite co-administration with Pronase-E. Histological examination of the ILM would indicate whether this was the case. Alternatively GFP expression may have been too weak to detect visually, to determine whether this was the case IHC could be performed using an antibody targeted against GFP. This is a possibility since the hrGFP transgene is translated from the IRES – a process which is less efficient and can result in weaker reporter gene expression.

Another possibility is that any virally transduced cells were killed off as a result of viral titre or GFP toxicity (as previously discussed in section 5.5.3). Furthermore, since 0.0002% Pronase-E is toxic to RGC, the presence of this enzyme may have also been a factor, making fewer RGC available for virally mediated transduction.

5.5.5 *AAV2-CNTF-hrGFP* and *AAV2-CNTF-shRhoA-hrGFP* did not protect RGC from cell death

Retinal counts (from H&E stained retinal sections) demonstrate that there was no significant difference in RGC number between each of the AAV2-treatment groups (*AAV2-eGFP* + Pronase-E, *AAV2-CNTF-hrGFP* + Pronase-E and *AAV2-CNTF-shRhoA-hrGFP* + Pronase-E) 23 d post ONC – however significant RGC cell death was exhibited compared to untreated/uninjured controls, with a ≈40% reduction in RGC cell survival. Once more this may have been a consequence of ineffective viral delivery (as previously discussed in section 5.1.1) or the presence of toxic substances (Pronase-E, see figure 5.7). Since GFP expression was not seen in any of the retinal sections examined, the likelihood of GFP mediated toxicity was reduced.

5.6 Conclusions

The ILM appears to be a major barrier to AAV2-mediated gene transduction via intravitreal injection. Although co-administration with Pronase-E could significantly facilitate this process, it also led RGC cell death. Unfortunately I am unable to make any solid conclusions as to the effectiveness of long term CNTF delivery (and/or RhoA knockdown) since the AAV2 delivery technique clearly requires further optimisation.

CHAPTER 6

GENERAL DISCUSSION

6.1 Main Findings and Future Work

The main objective of this investigation was to determine whether CNTF could promote RGC axonal regeneration and survival after ON transection. In order to determine these effects *in vitro*, it was necessary to develop an assay by which neuronal and glial effects could be monitored independently. As described previously (see section 1.1) the retina contains a variety of different cell types. Each of these cell populations can contribute towards any therapeutic outcome through the release of NTF or inhibitory molecules. This makes it difficult to dissect out neuronal and/or glia specific mechanisms. In an effort to try and differentiate between these mechanisms, it was decided to characterise an RGC-5 cell line. This was done primarily to determine whether the RGC-5 cell line could be used as a substitute for primary retinal culture. This would be a particularly effective tool at monitoring the neuronal effects of CNTF since some groups have hypothesized that CNTF acts indirectly through the activation of macrophages (Cen et al. 2007) and/or astrocytes (Müller et al. 2009).

Unfortunately the RGC-5 cell line was not what it was originally reported to be, and is likely derived from a mouse oligodendrocyte progenitor lineage (see chapter 3). As a result of this, it was decided to test our therapeutic agent of interest (e.g. recombinant CNTF) in primary retinal cultures (see chapter 4). Although this assay did not allow for distinction between neuronal and glial specific responses, it allowed me to evaluate the overall functional outcome of CNTF treatment. During the course of this investigation it was established that a dose of 100 ng ml^{-1} CNTF was optimum in terms of RGC neurite outgrowth and survival, and that this dose was capable of disinhibiting RGC neurite out-

growth. Moreover, Forskolin significantly enhanced RGC neurite outgrowth when given alone (or in combination with a low dose of CNTF), but was not required to potentiate the neuritogenic effects of CNTF. To be able to distinguish between neuronal and glial specific responses it would be advantageous to be able to assess the effectiveness of recombinant CNTF on a relatively pure population of RGC — to accomplish this, an immunopanning technique could be used to isolate primary RGC.

6.1.1 Viral Delivery

In agreement with Dalkara *et al* (Dalkara et al. 2009), the ILM was confirmed to be a major barrier to AAV2 mediated gene transduction when administered intravitreally. To address this problem, a series of *in vivo* experiments could be performed to optimise viral transgene delivery. This would involve performing an AAV2 dose response experiment to find an optimal viral concentration. To be an effective therapeutic vector, this dose would need to be capable of reproducibly and efficiently transducing RGC without causing any adverse effects (e.g. RGC toxicity). To determine this, each dose would need to be tested in the presence and absence of a GFP reporter, so that the cause (e.g. viral titre, GFP expression) of any toxicity could be easily assessed. A Pronase-E dose response experiment could also be performed to determine whether 0.0002% Pronase-E was the cause of RGC cell death in chapter 5. To establish this histological examination of the ILM would also be advantageous so that the extent of degradation could be assessed. Although the ILM seems to be a significant structural barrier to AAV2 mediated gene transduction, other potential barriers do exist and it is possible that Pronase-E has affects other than to the

ILM. For example Pronase-E may degrade proteins of the vitreous making the environment more permissible to viral entry.

Since only a single injection of virus was administered to Sprague Dawley rats the effect of multiple injections could also be investigated. Furthermore, the use of slow release devices could be investigated as an alternative to virally mediated gene transfer.

The use of such a device has several advantages:

1. It would eliminate the need of using a virus at all.
2. Therapeutic intervention would be instantaneous (i.e. not necessary to wait up to 30 d for sufficient transgene expression).
3. The implant could be removed if required.

Intravitreal injection of *AAV2-CNTF-hrGFP* + 0.0002% Pronase-E or *AAV2-CNTF-shRhoA-hrGFP* + 0.0002% Pronase-E did not rescue RGC from cell death 23d post ONC. As discussed previously, this was probably a result of defective viral delivery. *AAV2-CNTF-hrGFP* and *AAV2-CNTF-shRhoA-hrGFP* failed to promote significant RGC axon regeneration 23 d after ONC. Furthermore, no GFP was detected in the sections despite the use of antibodies to enhance any signal present. A future experiment would be to replace the *AAV2-eGFP* virus (control) with one containing hrGFP, since hrGFP was used in *AAV2-CNTF-hrGFP* and *AAV2-CNTF-shRhoA-hrGFP* viral vectors.

Furthermore it would be necessary to establish whether the shRNA present in the *AAV2-CNTF-shRhoA-hrGFP* virus was effective at knocking down RhoA expression in primary

RGC. To accomplish this, retinas could be harvested from intravitreally injected animals, and RhoA expression assessed through real time PCR and/or western blot analysis. Furthermore, CNTF over expression could be confirmed using similar techniques.

6.2 Conclusions

The findings of this thesis provide extensive evidence that the RGC-5 cell line was not what it was originally reported to be (R.R.Krishnamoorthy et al. 2000, Agarwal et al. 2007) – and is in fact derived from mouse oligodendrocyte progenitor cells. It was found that recombinant CNTF could promote RGC neurite outgrowth *in vitro*, and could disinhibit Nogo-P4 treated RGC. Although RGC axonal regeneration and survival were not promoted *in vivo* (due to inefficient viral delivery) CNTF and/or shRhoA still has the potential to be an effective therapeutic *in vivo*.

REFERENCES

D. S. Aaronson & C. M. Horvath (2002). `A Road Map for Those Who Don't Know JAK-STAT'. *Science* **296**(5573):1653--1655.

B. A. Adel, et al. (2005). `Ciliary neurotrophic factor protects retinal ganglion cells from axotomy-induced apoptosis via modulation of retinal glia in vivo'. *Journal of Neurobiology* **63**(3).

R. Adler (1993). `Ciliary neurotrophic factor as an injury factor'. *Current Opinion in Neurobiology* **3**(5):785--789.

R. Adler, et al. (1979). `Cholinergic neuronotrophic factors: intraocular distribution of trophic activity for ciliary neurons'. *Science* **204**(4400):1434--6.

A. Agar, et al. (2006). `Retinal ganglion cell line apoptosis induced by hydrostatic pressure'. *Brain Research* **1086**(1):191--200.

R. A. N. Agarwal, et al. (2007). `Comparison of expression profile of neurotrophins and their receptors in primary and transformed rat retinal ganglion cells'. *Molecular Vision* pp. 1311--1318.

A. J. Aguayo (1985). *Axon regeneration from injured neurons in the adult mammalian central nervous system*, pp. 457--84. Guildford Press.

Z. Ahmed, et al. (2005a). `Matrix metalloproteases: degradation of the inhibitory environment of the transected optic nerve and the scar by regenerating axons'. *Mol Cell Neurosci* **28**(1):64--78.

Z. Ahmed, et al. (2005b). `Disinhibition of neurotrophin-induced dorsal root ganglion cell neurite outgrowth on CNS myelin by siRNA-mediated knockdown of NgR, p75NTR and Rho-A'. *Molecular and Cellular Neuroscience* **28**(3):509 -- 523.

B. Alberts (2002). *Molecular Biology of the Cell*. Garland Science, 4th edn.

American Type Culture Collection Standards Development Organization Workgroup ASN-0002 (2010). `Cell line misidentification: the beginning of the end'. *Nat Rev Cancer* **10**(6).

R. W. Atchison, et al. (1965). `Adenovius-Associated Defective Virus Particles'. *Science* **149**:754--6.

M. Baens, et al. (2006). `The Dark Side of EGFP: Defective Polyubiquitination'. *PLoS One* **1**(1):e54.

J. Bain, et al. (2003). `The specificities of protein kinase inhibitors: an update'. *Biochem J* **371**(Pt 1):199--204.

B. A. Barres (2008). `The Mystery and Magic of Glia: A Perspective on Their Roles in Health and Disease'. *Nat Neurosci* **60**(3):430--440.

N. Baumann & D. Pham-Dinh (2001). `Biology of oligodendrocyte and myelin in the mammalian central nervous system'. *Physiol Rev* **81**(2):871--927.

M. F. Bear, et al. (2001). *Neuroscience exploring the brain*. Lippincott Williams and Wilkins, 2nd edn.

N. J. V. Bergen, et al. (2009). `Re-characterisation of the RGC-5 retinal ganglion cell line'. *Investigative Opthalmology & Visual Science* pp. 1--26.

E. Bernstein, et al. (2001). `The rest is silence'. *RNA* **7**(11):1509--21.

A. L. M. Berry (ed.) (1998). *CNS Injuries: Cellular Responses and Pharmacological Strategies*. Informa Healthcare, 1st edn.

M. Berry, et al. (2008). `Regeneration of axons in the visual system'. *Restor Neurol Neurosci* **26**(2--3):147--74.

M. R. Berry, et al. (1986). `Regeneration of axons in the mammalian visual system'. *Experimental Brain Research Supplement* **13**:18--33.

A. U. Bielinska & J. F. Kukowska-Latallo (1997). `The interaction of plasmid DNA with polyamidoamine dendrimers: mechanism of complex formation and analysis of alterations induced in nuclease sensitivity and transcriptional activity of the complexed DNA'. *Biochim Biophys Acta* **1353**(2):180--190.

K. J. Bos, et al. (2001). `Collagen fibril organisation in mammalian vitreous by freeze etch/rotary shadowing electron microscopy'. *Micron* **32**(3):301--6.

T. G. Boulton, et al. (1994). `Ciliary neurotrophic factor/leukemia inhibitory factor/interleukin 6/oncostatin M family of cytokines induces tyrosine phosphorylation of a common set of proteins overlapping those induced by other cytokines and growth factors'. *J Biol Chem* **269**(15):11648--55.

B. B. Boycott & H. Wassle (1974). `The morphological types of ganglion cells of the domestic cat's retina'. *J Physiol* **240**(2):397--419.

E. J. Bradbury, et al. (2002). `Chondroitinase ABC promotes functional recovery after spinal cord injury'. *Nature* **416**(6881):636--640.

D. Cai, et al. (2001). `Neuronal cyclic AMP controls the developmental loss in ability of axons to regenerate'. *J Neurosci* **21**(13):4731--9.

D. Cai, et al. (1999). `Prior Exposure to Neurotrophins Blocks Inhibition of Axonal Regeneration by MAG and Myelin via a cAMP-Dependent Mechanism'. *Neuron* **22**(1):89--101.

S. R. Y. Cajal (1928). `Degeneration and Regeneration of the Nervous System'. *London. Oxford University Press* .

P. Caroni & M. E. Schwab (1988). `Antibody against myelin-associated inhibitor of neurite growth neutralizes nonpermissive substrate properties of CNS white matter'. *Neuron* **1**(1):85--96.

L. P. Cen, et al. (2007). `Chemotactic effect of ciliary neurotrophic factor on macrophages in retinal ganglion cell survival and axonal regeneration'. *Invest Ophthalmol Vis Sci* **48**(9):4257--66.

R. M. Chanock (1974). `Impact of adenoviruses in human disease'. *Preventive Medicine* **3**(4):466 -- 472.

I. Charles, et al. (2005). `Serum deprivation induces apoptotic cell death of transformed rat retinal ganglion cells via mitochondrial signaling pathways'. *Invest Ophthalmol Vis Sci* **46**(4):1330--8.

N. Chaudhry & M. T. Filbin (2006). `Myelin-associated inhibitory signaling and strategies to overcome inhibition'. *J Cereb Blood Flow Metab* **27**(6):1096--1107.

M. S. Chen, et al. (2000). `Nogo-A is a myelin-associated neurite outgrowth inhibitor and an antigen for monoclonal antibody IN-1'. *Nature* **403**(6768):434--9.

R. L. Chow & R. A. Lang (2001). `Early eye development in vertebrates'. *Annu Rev Cell Dev Biol* **17**:255--296.

C. Cogoni, et al. (1996). `Transgene silencing of the al-1 gene in vegetative cells of Neurospora is mediated by a cytoplasmic effector and does not depend on DNA-DNA interactions or DNA methylation'. *EMBO J* **15**(12):3153--63.

Q. Cui, et al. (2008). `Does CNTF mediate the effect of intraocular inflammation on optic nerve regeneration?'. *Brain* **131**(Pt 6):e96; author reply e97.

Q. Cui & A. R. Harvey (2000). `CNTF promotes the regrowth of retinal ganglion cell axons into murine peripheral nerve grafts'. *Neuroreport* **11**(18):3999--4002.

Q. Cui, et al. (2003). `Intraocular elevation of cyclic AMP potentiates ciliary neurotrophic factor-induced regeneration of adult rat retinal ganglion cell axons'. *Mol Cell Neurosci* **22**(1):49--61.

D. Dalkara, et al. (2009). `Inner Limiting Membrane Barriers to AAV-mediated Retinal Transduction From the Vitreous'. *Mol Ther* **17**(12):2096--2102.

S. David & A. J. Aguayo (1981). `Axonal elongation into peripheral nervous system 'bridges' after central nervous system injury in adult rats'. *Science* **214**(4523):931--3.

B. L. Davidson & X. O. Breakefield (2003). `Viral vectors for gene delivery to the nervous system'. *Nat Rev Neurosci* **4**(5):353--364.

B. L. Davidson & P. B. McCray (2011). `Current prospects for RNA interference-based therapies'. *Nat Rev Genet* **12**(5):329--340.

M. E. Davis, et al. (2010). `Evidence of RNAi in humans from systemically administered siRNA via targeted nanoparticles'. *Nature* **464**(7291):1067--1070.

M. R. Dawson & A. Polito (2003). `NG2-expressing glial progenitor cells: an abundant and widespread population of cycling cells in the adult rat CNS'. *Mol Cell Neurosci* **24**(2):476--488.

P. Dergham, et al. (2002). `Rho signaling pathway targeted to promote spinal cord repair'. *J Neurosci* **22**(15):6570--7.

E. R. Detrait, et al. (2002). `Reporter gene transfer induces apoptosis in primary cortical neurons'. *Mol Ther* **5**(6):723--30.

W. G. Dirks, et al. (1999). `ECV304 (endothelial) is really T24 (bladder carcinoma): cell line cross- contamination at source'. *In Vitro Cell Dev Biol Anim* **35**(10):558--9.

W. H. Donovan (2007). `Donald Munro Lecture. Spinal cord injury--past, present, and future'. *J Spinal Cord Med* **30**(2):85--100.

L. Dudus, et al. (1999). `Persistent transgene product in retina, optic nerve and brain after intraocular injection of rAAV'. *Vision Research* **39**(15):2545--2553.

R. Dutta, et al. (2007). `Activation of the ciliary neurotrophic factor (CNTF) signalling pathway in cortical neurons of multiple sclerosis patients'. *Brain* **130**(10):2566--2576.

S. M. Elbashir, et al. (2001). `Duplexes of 21-nucleotide RNAs mediate RNA interference in cultured mammalian cells'. *Nature* **411**(6836):494--498.

S. Ellenbroek & J. Collard (2007). `Rho GTPases: functions and association with cancer'. *Clinical and Experimental Metastasis* **24**(8):657--672.

W. Fan, et al. (2005). `Retinal ganglion cell death and neuroprotection: Involvement of the CaMKIIalpha gene'. *Brain Res Mol Brain Res* **139**(2):306--16.

A. Fasbender & J. Zabner (1997). `Complexes of adenovirus with polycationic polymers and cationic lipids increase the efficiency of gene transfer in vitro and in vivo'. *J Biol Chem* **272**(10):6479--6489.

M. T. Filbin (2003). `Myelin-associated inhibitors of axonal regeneration in the adult mammalian CNS'. *Nat Rev Neurosci* **4**(9):703--713.

A. Fire, et al. (1998). `Potent and specific genetic interference by double-stranded RNA in Caenorhabditis elegans'. *Nature* **391**(6669):806--811.

J. V. Forrester, et al. (2002). *The Eye: Basic Sciences in Practice*. Elsevier, 2nd edn.

A. E. Fournier, et al. (2001). `Identification of a receptor mediating Nogo-66 inhibition of axonal regeneration'. *Nature* **409**(6818):341--346.

L. Frank, et al. (1996). `BDNF down-regulates neurotrophin responsiveness, TrkB protein and TrkB mRNA levels in cultured rat hippocampal neurons'. *Eur J Neurosci* **8**(6):1220--30.

L. J. Frassetto, et al. (2006). `Kinase-dependent differentiation of a retinal ganglion cell precursor'. *Invest Ophthalmol Vis Sci* **47**(1):427--38.

J. Frisen, et al. (1995). `Rapid, widespread, and longlasting induction of nestin contributes to the generation of glial scar tissue after CNS injury'. *J Cell Biol* **131**(2):453--64.

S. Fulda & K. M. Debatin (2006). `Extrinsic versus intrinsic apoptosis pathways in anti-cancer chemotherapy'. *Oncogene* **25**(34):4798--4811.

G. Gallo & P. C. Letourneau (2004). `Regulation of growth cone actin filaments by guidance cues'. *Journal of Neurobiology* **58**(1):92--102.

V. Gallo & R. C. Armstrong (1995). `Developmental and growth factor-induced regulation of nestin in oligodendrocyte lineage cells'. *J Neurosci* **15**(1 Pt 1):394--406.

M. A. Goncalves (2005). `Adeno-associated virus: from defective virus to effective vector'. *Virol J* **2**:43.

T. GrandPre, et al. (2000). `Identification of the Nogo inhibitor of axon regeneration as a reticulon protein'. *Nature* **403**:439--444.

E. Guenther, et al. (1994). `In vitro identification of retinal ganglion cells in culture without the need of dye labeling'. *J Neurosci Methods* **51**(2):177--181.

G. J. Guillemin & B. J. Brew (2003). `Microglia, macrophages, perivascular macrophages, and pericytes: a review of function and identification'. *J Leukoc Biol* **75**(3):388--397.

N. Hagag, et al. (1986). `Inhibition of growth factor-induced differentiation of PC12 cells by microinjection of antibody to ras p21'. *Nature* **319**(6055):680--682.

W. Halfter (1998). `Disruption of the retinal basal lamina during early embryonic development leads to a retraction of vitreal end feet, an increased number of ganglion cells, and aberrant axonal outgrowth'. *J Comp Neurol* **397**(1):89--104.

U. K. Hanisch & H. Ketterman (2007). `Microglia: active sensor and versatile effector cells in the normal and pathologic brain'. *Nat Neurosci* **10**(11):1387--1394.

P. A. Hantzopoulos & C. Suri (1994). `The low affinity NGF receptor, p75, can collaborate with each of the Trks to potentiate functional responses to the neurotrophins'. *Neuron* **13**(1):187--201.

M. M. Harper, et al. (2009). `Brain-derived neurotrophic factor released from engineered mesenchymal stem cells attenuates glutamate- and hydrogen peroxide-mediated death of staurosporine-differentiated RGC-5 cells'. *Experimental Eye Research* **89**(4):538--548.

A. R. Harvey, et al. (2006). `Gene therapy and transplantation in CNS repair: The visual system'. *Progress in Retinal and Eye Research* **25**(5):449 -- 489.

J. D. Houle, et al. (2006). `Combining an autologous peripheral nervous system 'bridge' and matrix modification by chondroitinase allows robust, functional regeneration beyond a hemisection lesion of the adult rat spinal cord'. *J Neurosci* **26**(28):7405--15.

D. W. Huang, et al. (1999). `A therapeutic vaccine approach to stimulate axon regeneration in the adult mammalian spinal cord'. *Neuron* **24**:639--647.

E. J. Huang & L. F. Reichardt (2003). `Trk receptors: Roles in neuronal signal transduction'. *Annual Review of Biochemistry* **72**:609--642.

M. Inoue, et al. (1996). `Activating mechanism of CNTF and related cytokines'. *Mol Neurobiol* **12**(3):195--209.

S. Isenmann, et al. (2001). `Intravitreal adenoviral gene transfer evokes an immune response in the retina that is directed against the heterologous lacZ transgene product but does not limit transgene expression'. *Brain Research* **892**(2):229 -- 240.

S. Isenmann & A. Kretz (2003). `Molecular determinants of retinal ganglion cell development, survival, and regeneration'. *Prog Retin Eye Res* **22**(4):483--543.

E. S. Jang & J. E. Goldman (2011). `Pax6 expression is sufficient to induce a neurogenic fate in glial progenitors of the neonatal subventricular zone'. *PLoS One* **6**(6):e20894.

S. A. Jo, et al. (1999). `Ciliary neurotrophic factor is an axogenesis factor for retinal ganglion cells'. *Neuroscience* **89**(2):579--91.

S. H. Jung, et al. (2010). `Isoquercitrin is the most effective antioxidant in the plant Thuja orientalis and able to counteract oxidative-induced damage to a transformed cell line (RGC-5 cells)'. *Neurochemistry International* **57**(7):713--721.

J. R. Kennerdell & R. W. Carthew (1998). `Use of dsRNA-mediated genetic interference to demonstrate that frizzled and frizzled 2 act in the wingless pathway'. *Cell* **95**(7):1017--26.

R. L. Klein, et al. (2006). `Efficient Neuronal Gene Transfer with AAV8 Leads to Neurotoxic Levels of Tau or Green Fluorescent Proteins'. *Mol Ther* **13**(3):517--527.

R. N. Kolb, H. (1981). `Amacrine cells, bipolar cells and ganglion cells of the cat retina: a Golgi study' **21**(7):1081--1114.

Y. Koriyama, et al. (2009). `Neuroprotective effects of 5-S-GAD against oxidative stress-induced apoptosis in RGC-5 cells'. *Brain Research* **1296**:187--195.

H. E. Krestel, et al. (2004). `Neuronal co-expression of EGFP and beta-galactosidase in mice causes neuropathology and premature death'. *Neurobiol Dis* **17**(2):310--8.

K. S. Lavappa, et al. (1976). `Examination of ATCC stocks for HeLa marker chromosomes in human cell lines'. *Nature* **259**(5540):211--3.

S. G. Leaver, et al. (2006a). `Cooperative effects of bcl-2 and AAV-mediated expression of CNTF on retinal ganglion cell survival and axonal regeneration in adult transgenic mice'. *European Journal of Neuroscience* **24**(12):3323--3332.

S. G. Leaver, et al. (2006b). `AAV-mediated expression of CNTF promotes long-term survival and regeneration of adult rat retinal ganglion cells'. *Gene Ther* **13**(18):1328--1341.

M. Lehmann, et al. (1999). `Inactivation of Rho signaling pathway promotes CNS axon regeneration'. *J Neurosci* **19**(17):7537--47.

S. Leon, et al. (2000). `Lens injury stimulates axon regeneration in the mature rat optic nerve'. *J Neurosci* **20**(12):4615--26.

J. Li, et al. (2011). `Hypoxia induces beta-amyloid in association with death of RGC-5 cells in culture'. *Biochemical and Biophysical Research Communications* **410**(1):40--44.

M. Li, et al. (2000). `Cyclic AMP promotes neuronal survival by phosphorylation of glycogen synthase kinase 3beta'. *Mol Cell Biol* **20**(24):9356--63.

C. J. Lieven, et al. (2007). `Induction of axon and dendrite formation during early RGC-5 cell differentiation'. *Experimental Eye Research* **85**(5):678--683.

H. S. Liu, et al. (1999). `Is green fluorescent protein toxic to the living cells?'. *Biochem Biophys Res Commun* **260**(3):712--7.

B. Lorber, et al. (2005). `Lens injury stimulates adult mouse retinal ganglion cell axon regeneration via both macrophage- and lens-derived factors'. *European Journal of Neuroscience* **21**(7):2029--2034.

L. A. Lowery & D. V. Vactor (2009). `The trip of the tip: understanding the growth cone machinery'. *Nat Rev Mol Cell Biol* **10**(5):332--343.

W. Luo, et al. (2005). `Two types of protease-activated receptors (PAR-1 and PAR-2) mediate calcium signaling in rat retinal ganglion cells RGC-5'. *Brain Research* **1047**(2):159--167.

R. A. MacLeod, et al. (1999). `Widespread intraspecies cross-contamination of human tumor cell lines arising at source'. *Int J Cancer* **83**(4):555--63.

P. Maher & A. Hanneken (2005). `The molecular basis of oxidative stress-induced cell death in an immortalized retinal ganglion cell line'. *Invest Ophthalmol Vis Sci* **46**(2):749--57.

W. J. Mandemakers & B. A. Barres (2005). `Axon Regeneration: It's Getting Crowded at the Gates of TROY'. *Current Biology* **15**(8):302--305.

J. Manns, et al. (2011). `Triggering of a novel intrinsic apoptosis pathway by the kinase inhibitor staurosporine: activation of caspase-9 in the absence of Apaf-1'. *The FASEB Journal* .

J. R. Masters, et al. (2001). `Short tandem repeat profiling provides an international reference standard for human cell lines'. *Proc Natl Acad Sci U S A* **98**(14):8012--7.

P. McConnell & M. Berry (1982). `Regeneration of ganglion cell axons in the adult mouse retina'. *Brain Res* **241**(2):362--5.

L. McKerracher, et al. (1994). `Identification of myelin-associated glycoprotein as a major myelin-derived inhibitor of neurite growth'. *Neuron* **13**(4):805--11.

V. Mester & F. Kuhn (2000). `Internal limiting membrane removal in the management of full-thickness macular holes'. *Am J Ophthalmol* **129**(6):769--77.

S. Mi, et al. (2004). `LINGO-1 is a component of the Nogo-66 receptor/p75 signaling complex'. *Nat Neurosci* **7**(3):221--228.

J. A. Miotke, et al. (2007). `Immunohistochemical localization of CNTFRalpha in adult mouse retina and optic nerve following intraorbital nerve crush: evidence for the axonal loss of a trophic factor receptor after injury'. *J Comp Neurol* **500**(2):384--400.

H. Mizuguchi, et al. (2000). `IRES-Dependent Second Gene Expression Is Significantly Lower Than Cap-Dependent First Gene Expression in a Bicistronic Vector'. *Molecular Therapy* **1**:376--382.

A. Müller, et al. (2009). `Exogenous CNTF stimulates axon regeneration of retinal ganglion cells partially via endogenous CNTF'. *Molecular and Cellular Neuroscience* **41**(2):233--246.

X. Mo & A. Yokoyama (2002). `Rescue of axotomized retinal ganglion cells by BDNF gene electroporation in adult rats'. *Invest Ophthalmol Vis Sci* **43**(7):2401--2405.

P. P. Monnier, et al. (2003). `The Rho/ROCK pathway mediates neurite growth-inhibitory activity associated with the chondroitin sulfate proteoglycans of the CNS glial scar'. *Molecular and Cellular Neuroscience* **22**(3):319--330.

N. T. Monsul, et al. (2004). `Intraocular injection of dibutyryl cyclic AMP promotes axon regeneration in rat optic nerve'. *Exp Neurol* **186**(2):124--33.

C. Moon, et al. (2004). `Upregulation of CD44 expression in the spinal cords of rats with clip compression injury'. *Neuroscience Letters* **367**(1):133--136.

D. A. Morgenstern, et al. (2002). `Chondroitin sulphate proteoglycans in the CNS injury response'. *Prog Brain Res* **137**:313--32.

K. C. Morrison (2011). *Is the Epidermal Growth Factor Receptor involved in visual system regenerative failure?* Ph.D. thesis, University of Birmingham.

G. Mukhopadhyay, et al. (1994). `A novel role for myelin-associated glycoprotein as an inhibitor of axonal regeneration'. *Neuron* **13**(3):757--67.

R. Nelson & E. V. Famiglietti (1978). `Intracellular staining reveals different levels of stratification for on- and off-center ganglion cells in cat retina'. *J Neurophysiol* **41**(2):472--483.

T. Niidome & L. Huang (2002). `Gene Therapy Progress and Prospects: Nonviral vectors'. *Gene Therapy* **9**(24):1647--1652.

R. W. Nims, et al. (1998). `Sensitivity of isoenzyme analysis for the detection of interspecies cell line cross-contamination'. *In Vitro Cell Dev Biol Anim* **34**(1):35--9.

M. Oelgeschlager, et al. (2000). `The evolutionarily conserved BMP-binding protein Twisted gastrulation promotes BMP signalling'. *Nature* **405**(6788):757--763.

J. B. Park, et al. (2005). `A TNF Receptor Family Member, TROY, Is a Coreceptor with Nogo Receptor in Mediating the Inhibitory Activity of Myelin Inhibitors'. *Neuron* **45**(3):345--351.

K. Park, et al. (2004). `Cellular mechanisms associated with spontaneous and ciliary neurotrophic factor-cAMP-induced survival and axonal regeneration of adult retinal ganglion cells'. *J Neurosci* **24**(48):10806--15.

H. F. Paterson, et al. (1990). `Microinjection of recombinant p21rho induces rapid changes in cell morphology'. *Cell Biol* **111**(3):1001--1007.

. Petersén & P. Brundin (1999). `Effects of Ciliary Neurotrophic Factor on Excitotoxicity and Calcium-Ionophore A23187-Induced Cell Death in Cultured Embryonic Striatal Neurons'. *Experimental Neurology* **160**(2):402--412.

J. Y. Pillé, et al. (2005). `Anti-RhoA and anti-RhoC siRNAs inhibit the proliferation and invasiveness of MDA-MB-231 breast cancer cells in vitro and in vivo'. *Mol Ther* **11**(2):267 -- 274.

R. R. Pindzola, et al. (1993). `Putative inhibitory extracellular matrix molecules at the dorsal root entry zone of the spinal cord during development and after root and sciatic nerve lesions'. *Dev Biol* **156**(1):34--48.

R. Prinjha (2000). `Inhibitor of neurite outgrowth in humans'. *Nature* **403**:383--384.

C. Profyris, et al. (2004). `Degenerative and regenerative mechanisms governing spinal cord injury'. *Neurobiology of Disease* **15**(3):415--436.

S. Rabizadeh, et al. (1993). `Induction of apoptosis by the low-affinity NGF receptor'. *Science* **261**(5119):345--348.

R. M. Ransohoff & H. Perry (2009). `Microglial physiology: Unique stimuli, specialised responses'. *Annual Reviews* **27**:119--145.

S. K. Ray (ed.) (2009). *Glioblastoma: Molecular Mechanisms of Pathogenesis and Current Therapeutic Stratagies*. Springer.

B. Reese & R. J. Colello (1992). `Neurogenesis in the retinal ganglion cell layer of the rat'. *Neuroscience* **46**(2):419--428.

L. E. Rivers, et al. (2008). `PDGFRA/NG2 glia generate myelinating oligodendrocytes and piriform projection neurons in adult mice'. *Nat Neurosci* **11**(12):1392--1401.

F. Rousseau, et al. (2008). `Ciliary neurotrophic factor, cardiotrophin-like cytokine, and neuropoietin share a conserved binding site on the ciliary neurotrophic factor receptor alpha chain'. *J Biol Chem* **283**(44):30341--50.

P. P. Roux & P. A. Barker (2002). `Neurotrophin signaling through the p75 neurotrophin receptor'. *Progress in Neurobiology* **67**(3):203 -- 233.

P. A. R.R.Krishnamoorthy, et al. (2000). `Characterisation of a transformed rat retinal ganglion cell line.'. *Molecular Brain Research* **86**:1--12.

T. Sato, et al. (2010). `Effect of hypoxia on susceptibility of RGC-5 cells to nitric oxide'. *Invest Ophthalmol Vis Sci* **51**(5):2575--86.

R. L. Schnaar & P. H. Lopez (2009). `Myelin-associated glycoprotein and its axonal receptors'. *J Neurosci Res* **87**(15):3267--76.

L. Schnell & M. E. Schwab (1990). `Axonal regeneration in the rat spinal cord produced by an antibody against myelin-associated neurite growth inhibitors'. *Nature* **343**:269--272.

M. E. Schwab & H. Thoenen (1985). `Dissociated neurons regenerate into sciatic but not optic nerve explants in culture irrespective of neurotrophic factors'. *J Neurosci* **5**(9):2415--23.

B. R. Schwechter, et al. (2007). `Histone deacetylase inhibition-mediated differentiation of RGC-5 cells and interaction with survival'. *Invest Ophthalmol Vis Sci* **48**(6):2845--57.

E. V. Semina, et al. (2006). `Mutations in laminin alpha 1 result in complex, lens-independent ocular phenotypes in zebrafish'. *Dev Biol* **299**(1):63--77.

E. Sernagor & S. J. Eglen (2001). `Development of Retinal Ganglion Cell Structure and Function'. *Progress in Retinal and Eye Research* **20**(2):139--174.

Z. Shao, et al. (2005). `TAJ/TROY, an orphan TNF receptor family member, binds Nogo-66 receptor 1 and regulates axonal regeneration'. *Neuron* **45**(3):353--9.

Y. Shen, et al. (2009). `PTPσ Is a Receptor for Chondroitin Sulfate Proteoglycan, an Inhibitor of Neural Regeneration'. *Science* **326**(5952):592--596.

M. Simonen, et al. (2003). `Systemic deletion of the myelin-associated outgrowth inhibitor Nogo-A improves regenerative and plastic responses after spinal cord injury'. *Neuron* **38**(2):201--11.

K. Sims, et al. (2009). `In vitro evaluation of a 'stealth' adenoviral vector for targeted gene delivery to adult mammalian neurones'. *The Journal of Gene Medicine* **11**(4):335--344.

M. W. Sleeman, et al. (2000). `The ciliary neurotrophic factor and its receptor, CNTFR[alpha]'. *Pharmaceutica Acta Helvetiae* **74**(2--3):265--272.

S. J. D. Smedt & J. Demeester (2000). `Cationic polymer based gene delivery systems'. *Pharm Res* **17**(2):113--126.

D. M. Snow, et al. (1990). `Molecular and cellular characterization of the glial roof plate of the spinal cord and optic tectum: a possible role for a proteoglycan in the development of an axon barrier'. *Dev Biol* **138**(2):359--76.

E. M. Surace & A. Auricchio (2008). `Versatility of AAV vectors for retinal gene transfer'. *Vision Research* **48**(3):353--359.

T. Tamaoki, et al. (1986). `Staurosporine, a potent inhibitor of phospholipid/Ca++dependent protein kinase'. *Biochem Biophys Res Commun* **135**(2):397--402.

K. T. Tchedre & T. Yorio (2008). `sigma-1 receptors protect RGC-5 cells from apoptosis by regulating intracellular calcium, Bax levels, and caspase-3 activation'. *Invest Ophthalmol Vis Sci* **49**(6):2577--88.

A. F. Thompson & L. A. Levin (2010). `Neuronal differentiation by analogs of staurosporine'. *Neurochemistry International* **56**(4):554--560.

E. W. Thompson, et al. (2004). `LCC15-MB cells are MDA-MB-435: a review of misidentified breast and prostate cell lines'. *Clin Exp Metastasis* **21**(6):535--41.

A. V. Titomirov, et al. (1991). `In vivo electroporation and stable transformation of skin cells of newborn mice by plasmid DNA'. *Biochimica et Biophysica Acta (BBA) - Gene Structure and Expression* **1088**(1):131 -- 134.

J. K. M. Tuszynski (ed.) (2007). *CNS Regeneration: Basic Science and Clinical Advances*. Academic Press, 2nd edn.

Y. M. Ughrin, et al. (2003). `Multiple regions of the NG2 proteoglycan inhibit neurite growth and induce growth cone collapse'. *J Neurosci* **23**(1):175--86.

B. A. van Adel, et al. (2003). `Delivery of ciliary neurotrophic factor via lentiviral-mediated transfer protects axotomized retinal ganglion cells for an extended period of time'. *Hum Gene Ther* **14**(2):103--15.

A. van Bokhoven, et al. (2001). `TSU-Pr1 and JCA-1 cells are derivatives of T24 bladder carcinoma cells and are not of prostatic origin'. *Cancer Res* **61**(17):6340--4.

B. Vanhaesebroeck & J. Guillermet-Guibert (2010). `The emerging mechanisms of isoform-specific PI3K signalling'. *Nat Rev Mol Cell Biol* **11**(5):329--341.

A. Vasileva & R. Jessberger (2005). `Precise hit: adeno-associated virus in gene targeting'. *Nat Rev Micro* **3**(11):837--847.

V. Vereczki, et al. (2006). `Distribution of hypothalamic, hippocampal and other limbic peptidergic neuronal cell bodies giving rise to retinopetal fibers: anterograde and retrograde tracing and neuropeptide immunohistochemical studies'. *Neuroscience* **140**(3):1089--100.

A. Verkhratsky & A. Butt (2007). *Glial Neurobiology*. John Wiley and Sons.

I. M. Verma & M. D. Weitzman (2005). `Gene therapy: twenty-first century medicine'. *Annu Rev Biochem* **74**:711--738.

M. Volosin, et al. (2008). `Induction of proneurotrophins and activation of p75NTR-mediated apoptosis via neurotrophin receptor-interacting factor in hippocampal neurons after seizures'. *J Neurosci* **28**(39):9870--9.

J. D. Vry, et al. (2010). `In vivo electroporation of the central nervous system: A non-viral approach for targeted gene delivery'. *Progress in Neurobiology* **92**(3):227 -- 244.

F. Wang & Y. Zhu (2008). `The interaction of Nogo-66 receptor with Nogo-p4 inhibits the neuronal differentiation of neural stem cells'. *Neuroscience* **151**(1):74--81.

K. C. Wang, et al. (2002). `p75 interacts with Nogo receptor as a co-receptor for Nogo, MAG, and OMgp'. *Nature* **420**:74--78.

S. W. Wang & B. S. Kim (2001). `Requirement for math5 in the development of retinal ganglion cells'. *Genes Dev* **15**(1):24--29.

H. Wassle (2004). `Parallel processing in the mammalian retina'. *Nat Rev Neurosci* **5**(10):747--757.

C. Weigert (1895). `Beiträge zur Kenntnis der normalen menschlichen'. *Frankfurt aum Maim, Weisbrod, Moritz Diesterweg* .

J. Weise, et al. (2000). `Adenovirus-Mediated Expression of Ciliary Neurotrophic Factor (CNTF) Rescues Axotomized Rat Retinal Ganglion Cells But Does Not Support Axonal Regeneration in Vivo'. *Neurobiology of Disease* **7**(3):212--223.

J. S. Werner & L. M. Chalupa (2004). *The visual neurosciences*, vol. 1. MIT Press.

C. Wiese, et al. (2004). `Nestin expression--a property of multi-lineage progenitor cells?'. *Cell Mol Life Sci* **61**(19--20):2510--22.

S. T. Wong, et al. (2002). `A p75(NTR) and Nogo receptor complex mediates repulsive signaling by myelin-associated glycoprotein'. *Nat Neurosci* **5**(12):1302--8.

J. P. Wood, et al. (2010). `A comparison of differentiation protocols for RGC-5 cells'. *Invest Ophthalmol Vis Sci* **51**(7):3774--83.

T. Yamashita, et al. (2002). `The p75 receptor transduces the signal from myelin-associated glycoprotein to Rho'. *J Cell Biol* **157**(4):565--70.

N. Yang, et al. (1998). `Cofilin phosphorylation by LIM-kinase 1 and its role in Rac-mediated actin reorganization'. *Nature* **393**(6687):809--12.

B. Zalc & D. R. Colman (2000). `Origins of vertebrate success'. *Science* **288**(5464):271--2.

C. Zincarelli, et al. (2008). `Analysis of AAV Serotypes 1-9 Mediated Gene Expression and Tropism in Mice After Systemic Injection'. *Mol Ther* **16**(6):1073--1080.

APPENDIX A

CHARACTERISATION OF THE RGC-5 CELL LINE

This appendix contains additional figures from the characterisation of the RGC-5 cell line chapter (chapter 3).

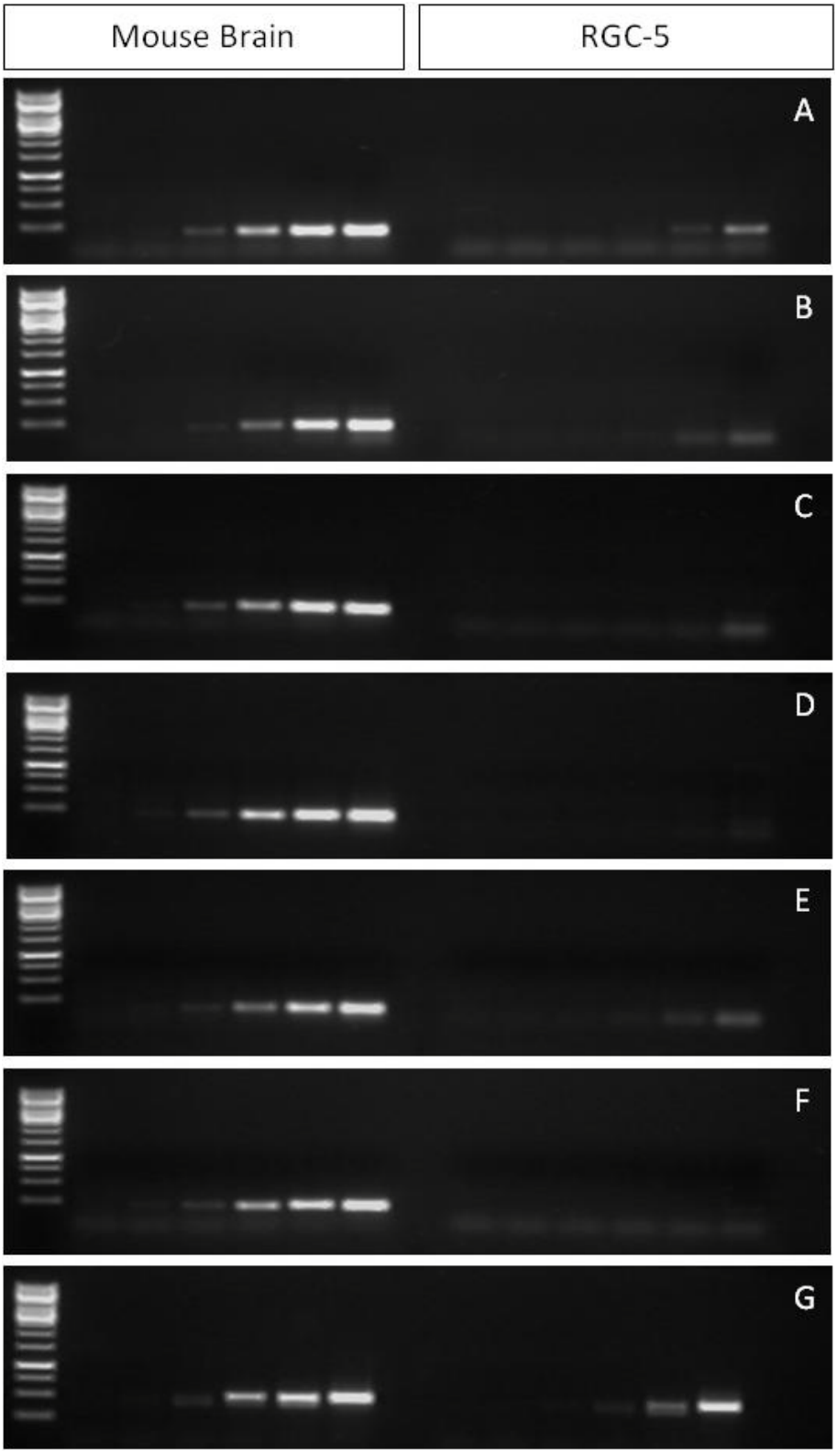

Figure A.1: RGC-5 neuronal marker expression. Complete version of figure 3.9a showing all the bands from the optimisation of the semi-quantitative PCR experiment. RGC-5 cells expressed little or no mRNA for neuronal cell markers including βIII-Tubulin, Neurofilament-H, Neurofilament-L, Neurofilament-M, Tau and Thy-1. (**A.**) βIII Tubulin (**B.**) Neurofilament H (**C.**) Neurofilament L (**D.**) Neurofilament M (**E.**) Tau (**F.**) Thy1 (**G.**) GAPDH

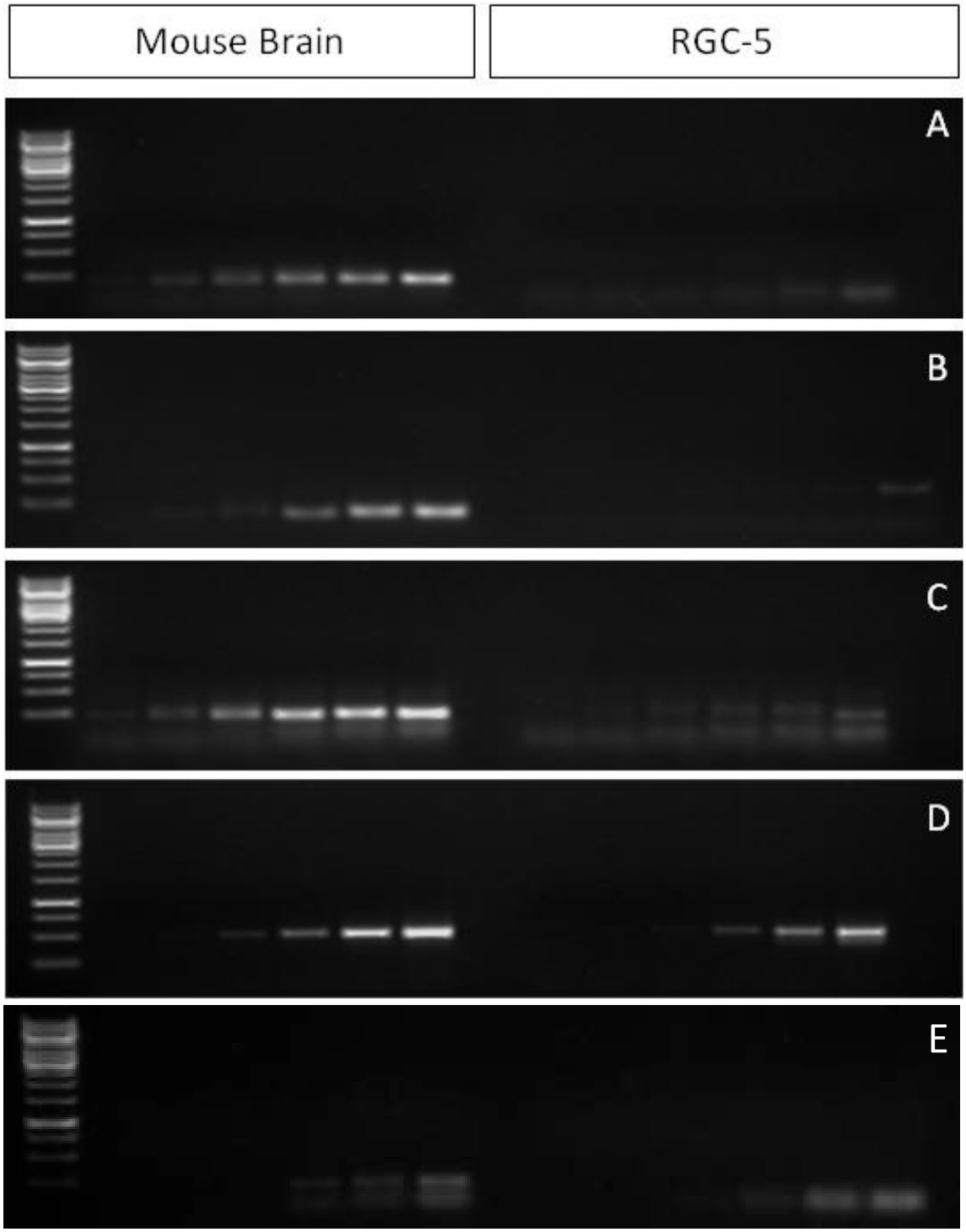

Figure A.2: RGC-5 glial marker expression. Complete version of figure 3.9b showing all the bands from the optimisation of the semi-quantitative PCR experiment. RGC-5 cells did not express mRNAs for the astrocyte marker, GFAP, the fibroblast marker RALDH2, or the activated microglia marker CD11b. (**A.**) RALDH2 (**B.**) CD11b (**C.**) CD68 (**D.**) GAPDH. (**E.**) GFAP.

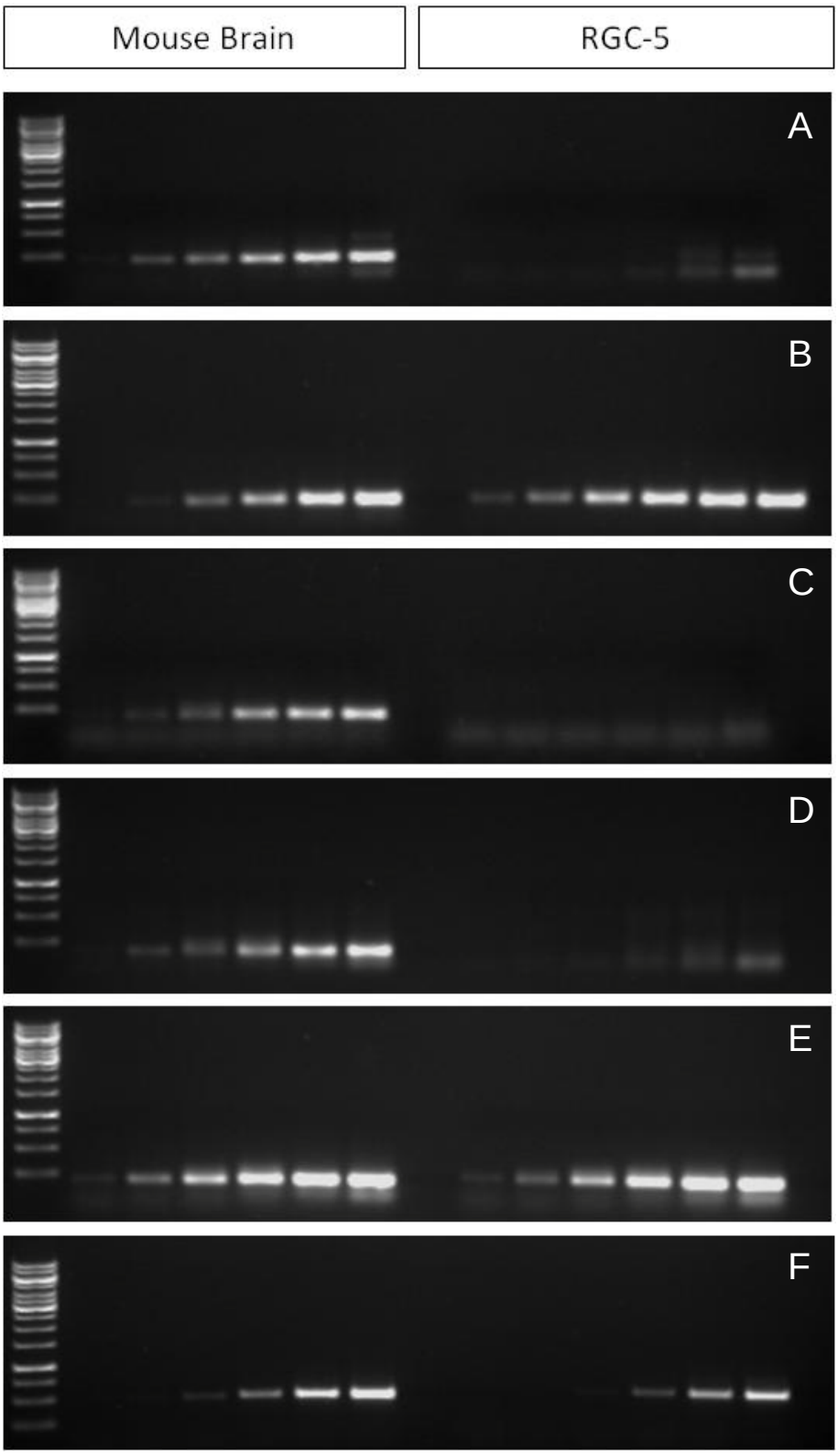

Figure A.3: RGC-5 developmental marker expression. Complete version of figure 3.9c showing all the bands from the optimisation of the semi-quantitative PCR experiment. RGC-5 cells were strongly positive for CD44, Nestin (not shown) and Pax-6 – this was indicative of a early progenitor marker cell lineages. However, RGC-5 cells did not express mRNA for CD133 or ChAT and only very weakly expressed SOX-1. (**A.**) SOX1 (**B.**) CD44 (**C.**) CD133 (**D.**) ChAT (**E.**) PAX6 (**F.**) GAPDH.

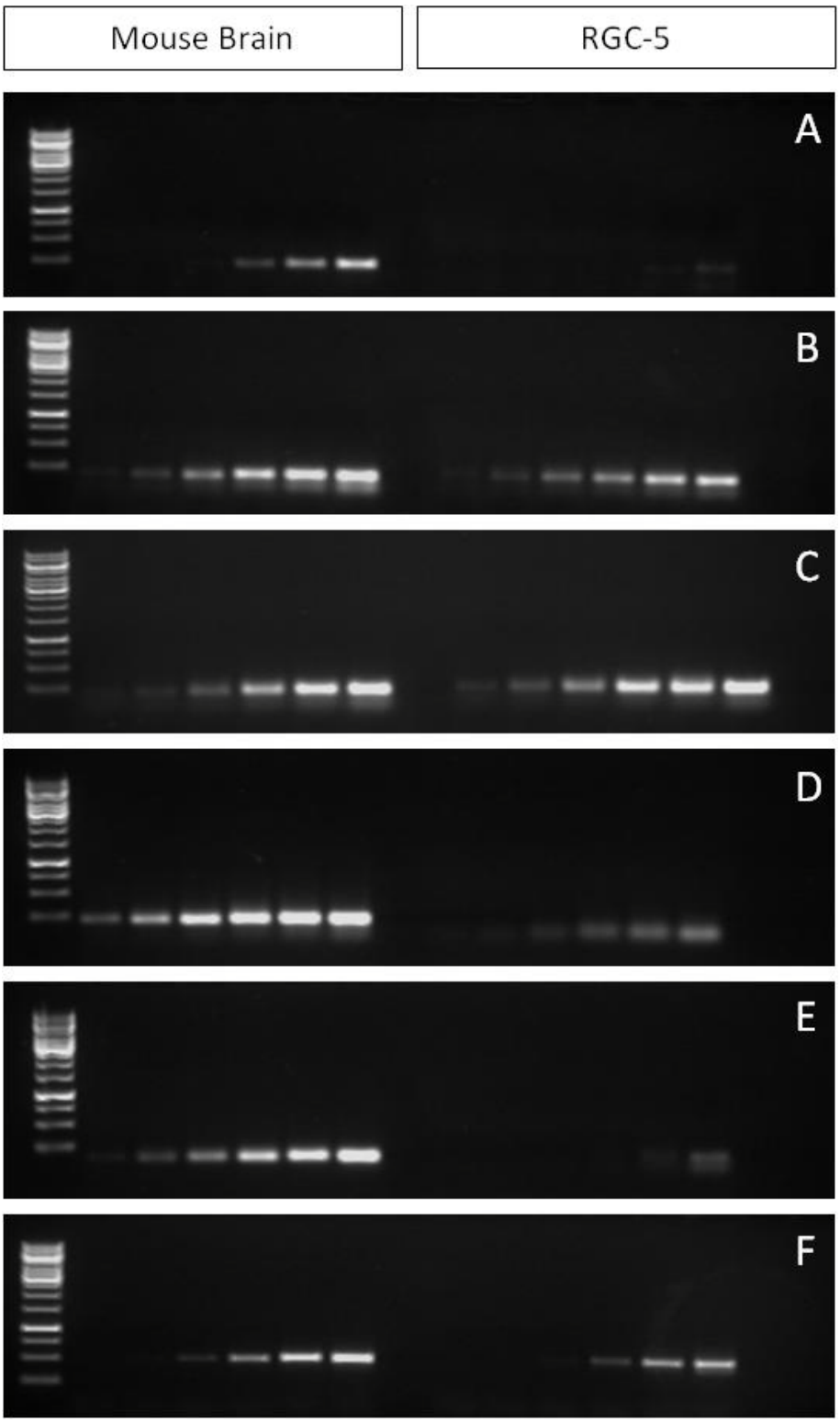

Figure A.4: RGC-5 oligodendroglial lineage marker expression. Complete version of figure 3.10 showing all the bands from the optimisation of the semi-quantitative PCR experiment. Clear bands of the correct size were present in all mouse brain positive control groups for all mRNAs tested. RGC-5 cells expressed mRNA markers of both mature and immature oligodendrocytes (GalC and NG2), but tested negative for Olig-1, Olig-2 and MBP. (**A.**) MBP (**B.**) GalC (**C.**) NG2 (**D.**) Olig-1 (**E.**) Olig-2 (**F.**) GAPDH

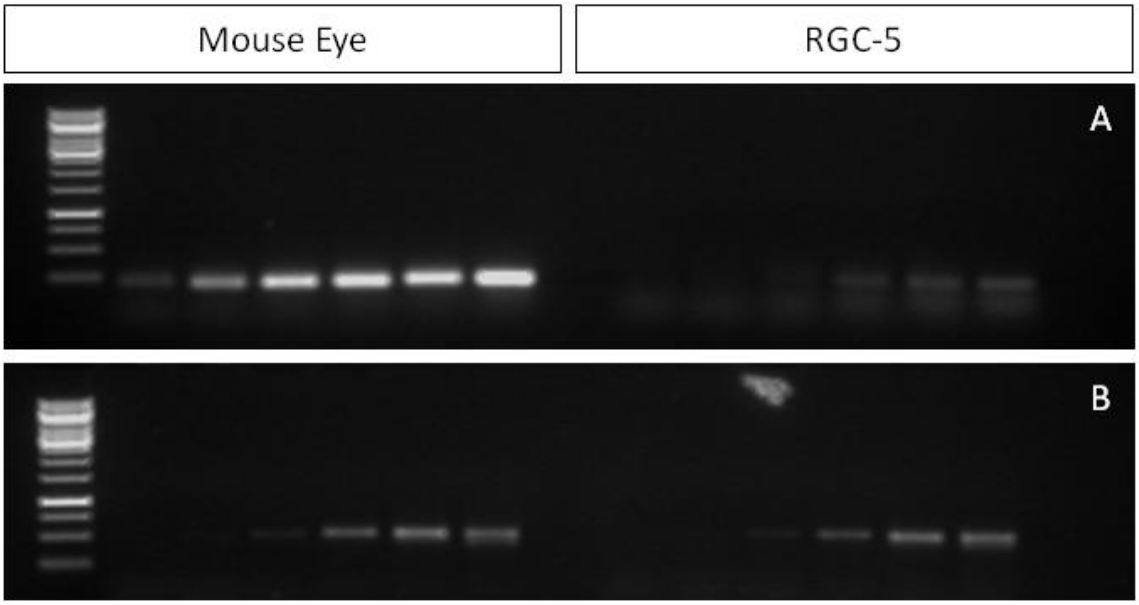

Figure A.5: Blue-sensitive opsin expression. Complete version of figure 3.12 showing all the bands from the optimisation of the semi-quantitative PCR experiment. Semi-quantitative PCR analysis shows that RGC-5 cells did not express blue-sensitive opsin, a marker of cone photoreceptor cells. However, a clear band of the correct size was present in the mouse eye positive control group.